AN ANALYTICAL AND EXPERIMENTAL INVESTIGATION OF THREE PHASE FLOW IN AIRLIFT PUMPS USED FOR DIAMONDIFEROUS MARINE GRAVEL RECLAMATION

by

R RAINER BERG

BSc (Eng.), MSc. (Eng.) in Civil Engineering

A thesis submitted in fulfilment of the requirements for the degree of Doctor of Philosophy

Department of Civil Engineering

University of Cape Town

January 1992

DECLARATION

I, Rolf Rainer Berg, declare that this thesis is essentially my own work and has not been submitted for a degree at another university.

Signed by candidate

R R BERG

January 1992

DEDICATION

To Tracey and my parents.

ABSTRACT

This dissertation covers an investigation on airlift pumps operating in three phase flow. The investigation is specifically geared towards offshore diamond reclamation and the three phases considered are air, water and marine gravels.

The purpose of the research was to develop an analytical technique to simulate mathematically an offshore airlift pump being used in the recovery of diamondiferous marine gravels. This analytical technique is incorporated into computer software which can be used to simulate prototype airlift installations in a CAD (computer aided design) environment.

Extensive laboratory work has been conducted on both a 90 mm and 40 mm diameter airlift pump test facility. This investigation involved the measurement of specific components required for the theoretical simulation. Also monitored were airlift pump delivered outputs and behaviour under various operating conditions. Using this information, the proposed mathematical model was formulated, evaluated and compared with other mathematical models presented in the literature.

The theoretical approach, which is based on a balance of external and internal pressures, proved successful and theoretically predicted solid and liquid output flow rates compared favourably with measured solid and liquid output flow rates. Furthermore, the computer software which was subsequently developed is presently being used in the diamond mining industry to model prototype airlift pumps.

A sensitivity analysis was performed to establish the effect of all the variables used in the mathematical model.

ACKNOWLEDGEMENTS

Professor John Lazarus, for his continuous support, ideas, inspirations and immense knowledge in the hydrotransport field.

The technical and academic staff and postgraduate students of the Department of Civil Engineering for the helpful and stimulating work environment.

Cheryl Wright for her excellent layout, typing and ideas during the documentation.

To Rod Norman, Mike Dingle and other De Beers Marine staff who enabled me to gain "hands-on" prototype exposure and gave valuable input from an engineering perspective.

To André Greyling and Hans Beuster for help and input on the computer generated outputs.

To Ninham Shand Inc for scheduling the time to complete this dissertation.

To Tracey, my family and friends for their support.

For financial and other support :

The Council for Scientific and Industrial Research
The University of Cape Town
De Beers Marine
Anthony Young and Salvalve

CONTENTS

LIST OF FIGURES

LIST OF TABLES

NOMENCLATURE

Symbol	Description	Unit
A	Pipe area	m^2
C_D	Drag coefficient for solids	
C_{vd}	Delivered volumetric concentration of solids	
C_{vt}	*In situ* volumetric concentration of solids	
d	Particle diameter	m
D	Pipe diameter	m
λ	Friction factor (λ = 4f)	
f	Friction factor	
g	Gravitational acceleration (9,81)	m/s^2
Δh	Dilated height	m
k	Pipe roughness	m
ℓ	Length	m
M	Mass	kg
Δp	Pressure change	Pa
P	Absolute pressure	Pa
Q	Flow rate	m^3/s
R	Percentage retained on sieve e.g. (R_1, R_2, R_3 ...)	%
S	Specific gravity	
S_f	Shape factor	
v	Velocity	m/s
Δv	Change in velocity	m/s
V	Volume	m^3
v_{tsph}	Spherical settling velocity	m/s
v_{go}	Relative velocity of gas	m/s
W	Weight	N

ϵ_g	*In situ* volumetric concentration of gas	
ϵ_{go}	Static dilation	
NB	Nominal bore	
PSD	Particle size distribution	
ρ	Density	kg/m^3
τ_o	Shear stress at the pipe wall	Pa
Re	Reynolds number	
ϕ_F	Two phase multiplier for friction	
v'_t	Hindered settling velocity	m/s
ξ_e	entrance loss coefficient	

Subscripts

inc	incremental
B	bubble
g	gas
l	liquid
m	mixture
s	solid
STP	standard temperature and pressure (101300 Pa, 0^0C)
S	suction pipe
D	delivery pipe
F	first
L	last
t	terminal
w	water
P	particle

Superscripts

lg	Liquid-gas
sl	Solid-liquid
slg	Solid-liquid-gas
a	Hindered settling factor (Richardson *et al* 1954)

A NOTE ON TERMINOLOGY

Throughout the literature (Clark 1985, Kytomaa 1986, Dedegil 1982 b, Giot 1982, Weber 1982 etc) the terms gas and air are interchangeably used by prominant authors in the field, when discussing airlift pumping of water and solids. The terms liquid and water are also interchangeably used in many papers.

In the same way, in this dissertation, the terms gas and liquid are synonymous with air and water respectively. Throughout the document, gas and gas flow refer to air and air flow, while any mention of liquid refers to water or sea water. Therefore three phase solid-liquid-gas mixtures are mixtures of solids, water and air; two phase solid-liquid mixtures are mixtures of solids and water and two phase liquid-gas mixtures are mixtures of water and air.

CHAPTER 1

INTRODUCTION

1.1 AIRLIFT PUMP DESCRIPTION

A typical airlift pump arrangement, as used for the reclamation of diamondiferous marine gravels, is shown in Figure 1.1.

It consists of a suction head, a suction pipe, a air injector and a delivery pipe. The suction pipe is normally much shorter than the delivery pipe, thus the air injector is located close to the suction head. A further pipe supplies pressurized air to the air injector from a compressor which is located on board the diamond barge at sea level.

In prototype installations, the suction and delivery pipes are frequently constructed of a ribbed type flexible hose, with a pressure rating suited to the operating conditions.

The suction head is constructed either from steel or aluminium and has a grating covering the inlet. This serves to limit the size of marine gravel entering the suction inlet, thus minimizing the risk of blockages. Various patented devices have been designed for prototypes to release pressures inside the pipe when blockages do occur as failure to do this, could result in the collapsing of the delivery pipe.

The delivery pipe outlet normally discharges onto screens for processing and sorting of the hoisted gravels. Compressed air, which is used to drive the airlift pump, is vented to the atmosphere.

Figure : 1.1
Description : TYPICAL AIRLIFT PUMP ARRANGEMENT

Airlift Pump Investigation

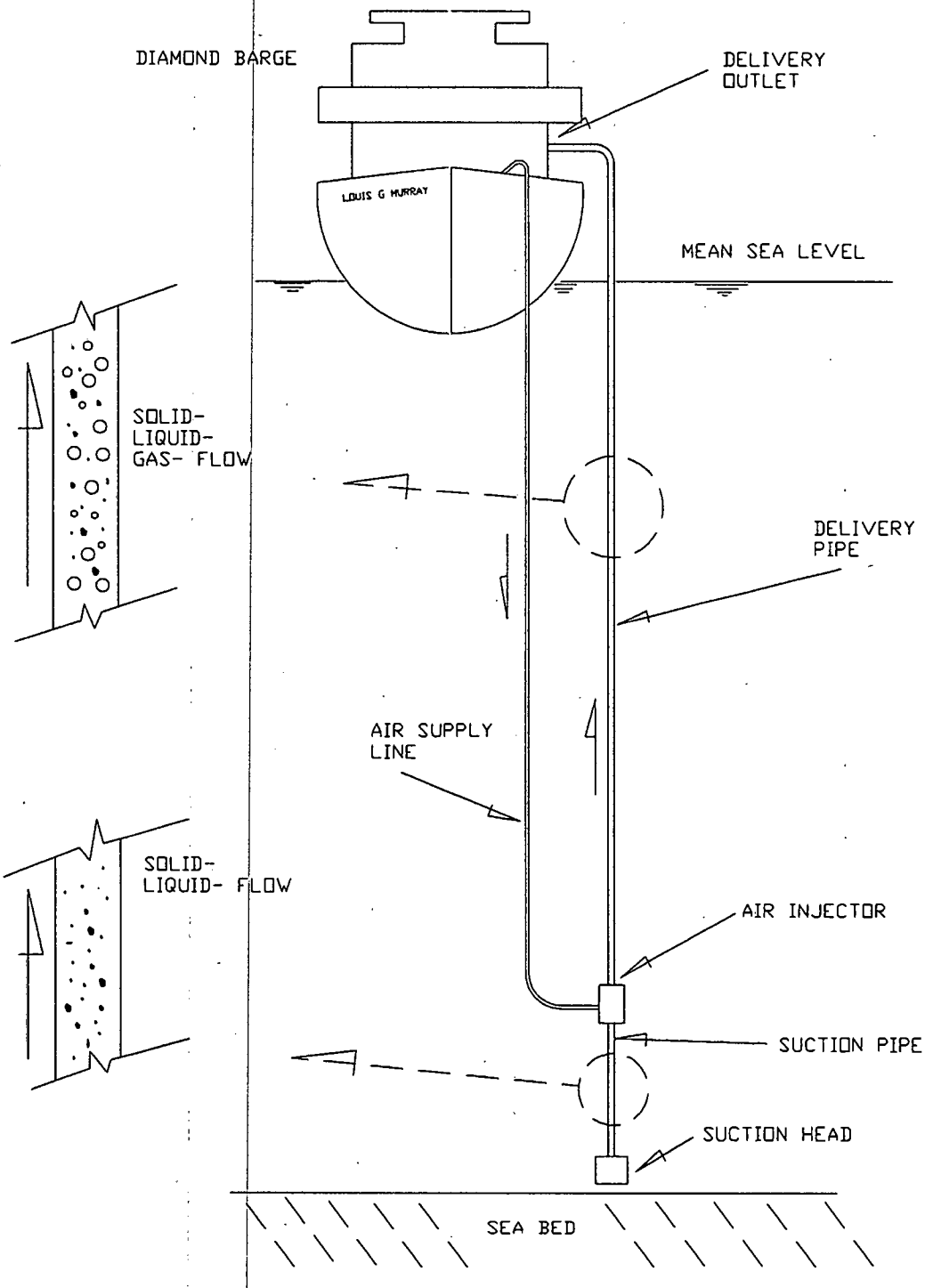

1.2 HISTORY OF AIRLIFT PUMPS

The airlift pump was invented in 1797 by Carl Immanuel Löscher [Gibson (1925), Dedegil (1982)]. An American engineer, Cockford, used the airlift method some 49 years later, in 1846, to pump petroleum out of boreholes in Pennsylvania. However, the first known patent was issued to an R. McGrath in 1865 (AM. Patent Number 47654).

During the 19th century, airlift pumps were successfully used to supply the rapidly growing towns and industries with water which was pumped from wells. However, with the development of the centrifugal pump and other higher efficiency devices for pumping water, the use of the airlift diminished.

Nowadays the airlift pump is used primarily in applications where reliability is more important than efficiency. From the late 19th century until present day the airlift has been used in a variety of applications which are discussed below.

1.3 USES OF AIRLIFT PUMPS

In the late 19th century, the use of airlift pumps shifted from two phase hoisting of liquids, to three phase hoisting of liquids and solids. These applications were for dredging sands and gravels which had been deposited as silt in harbours. The reliability and ease of operation of an airlift pump renders it suitable for marine mining, such as the hoisting of manganese nodules from the bottom of the

Pacific Ocean. These mining operations occurred at depths of up to 4,5 km (Giot, 1982) and took place in the early 1970's.

Further applications of liquid and solid hoisting were for drilling of shafts and wells. This included tunnel drilling and the sinking of bridge piles into river and sea beds (Weber 1976).

In the Soviet Union airlift pumps have been utilized for the hoisting of coal in a coal mines.

Shebatim (1977) reports that one of the applications of airlift pumps is for transporting aluminium hydroxile crystals from vessel to vessel in the aluminium industry. Other such applications in the chemical industry have been to lift erosive and corrosive fluids. In some of those applications the compressed air for driving the airlift pump is integrated into the chemical process (e.g. hydrogeneration of oil in fermenters). In these instances the airlift pump acts as a mixer.

Further applications have been for removing sand during marine salvage operations in the Carribean Sea. In South Africa a small scale airlift pump has been designed, by the author of this dissertation, for the lifting of abelone from the sea bed. The source of the driving compressed air, in this application, has been from the divers' oxygen tanks.

One of the major uses of airlift pumps in South Africa is in the offshore diamond mining industry. Here airlift pumps with pipe diameters ranging from 100 mm to 250 mm have been used over a range of

sea depths. It is primarily for this application of airlift pumps that the research in this dissertation has been conducted.

1.4 ADVANTAGES

Airlift pumps have the advantage of being robust and requiring little maintenance. They have no moving parts and therefore minimum corrosion, erosion and wear can take place making them suitable for pumping of abrasive slurries and corrosive liquids.

The compressor used to provide the pressurized air for driving the airlift pump is located near the surface. This makes it easily accessible should maintenance be required. If this compressor should fail, the system can readily be attached to a backup or even portable compressor. A single compressor can also drive a number of airlift pumps simultaneously.

With airlift pumps, hoisting of solids can take place from great depths without having to perform the operation in stages. Optimization of this operation is achieved by correctly positioning the depth of air injection and by supplying the optimum flow of compressed air.

Depending on the construction of the suction and delivery pipes, airlift pumps are cheap and easy to install. Airlift pumps that operate under conditions where pressure differences between the inside and outside of the delivery pipe are not too large, are often constructed of flexible hose which enhances the handleability of the airlift system.

Airlift pumps have numerous advantages over other pumping systems depending on the priorities of the pumping operation, for example, if the reliability of the system is more important than the efficiency.

1.5 DISADVANTAGES

The major disadvantage of the airlift pump is that its efficiency is lower than most other pumping systems. The efficiency of an airlift is generally between 25 - 35% which is much lower than that of a centrifugal pump. These figures can dramatically affect the costs of a continuous pumping operation. Thus airlift pumps are rarely used for the hoisting and conveying of liquids only, as other pumps are far more economical.

Another disadvantage of the airlift pump is the pulsating flow at the delivery outlet due to the rising air bubbles. Furthermore, at the delivery outlet the individual velocity components of the pumped phases are very high, thus additional energy has to be dissipated before the hoisted slurry can be processed. In the marine diamond recovery industry, the airlift pump discharge impinges on large chains which are placed opposite the delivery outlet for the purpose of energy dissipation.

1.6 SCOPE OF RESEARCH

It was mentioned previously that this research into airlift pumps was sponsored by the offshore marine diamond mining industry in South Africa. Most of the laboratory test work was conducted using slurries which were pumped at similar concentrations and with similar particles to those encountered in prototype marine diamond mining

installations, i.e. solid delivered volumetric concentrations of up to 15% and particle size distributions ranging between 2 mm and 15 mm.

Because of the difficulty and high costs attached to offshore prototype tests, two vertical research installations were constructed in the laboratory. These were used to measure specific components and monitor general airlift pump behaviour for the purpose of developing the mathematical model. With this model, prototype airlift pumps operating in three phase flow can be calculated and simulated. The mathematical model, in its basic form, consists of numerous variables. These had to be restricted to the most fundamental which could be analysed with the aid of the research installations. For example, the mathematical model does not take into account additional prototype variables such as non-vertical delivery pipes, complex suction inlet configurations, delivery outlet and air injection configurations.

The final output of the research was to incorporate the mathematical model into a highly interactive, user friendly computer program. This software provides the offshore diamond mining industry with the ability to design and optimize prototype airlift pumps which are used for reclamation of diamondiferous marine gravels.

1.7 CONTRIBUTIONS TO THE FIELD OF THREE PHASE AIRLIFT PUMPS

The author's contributions to the subject are :

- presentation of a theoretical procedure which can be used to calculate solid *in situ* volumetric concentrations in airlift pump suction pipes. Allowance is made for hindered particle

settling, shape factors and particle size distributions. The theoretical procedure is tested and verified using experimental data.

- evaluation of various theoretical procedures for calculating airlift pump suction pipe friction head losses with the aid of measured experimental data (two phase solid-liquid flow).

- presentation of a mathematical model for evaluating pressure changes in the airlift pump suction pipe (two phase solid-liquid flow). This model is verified using experimental laboratory tests.

- measurement and investigation of particle settling and hindered settling velocities in air-water mixtures, for a range of gas *in situ* volumetric concentrations.

- presentation of a theoretical calculating procedure for calculating gas and solid *in situ* volumetric concentrations in vertically moving three phase mixtures, specific to airlift pump delivery pipes. This procedure and other procedures presented in the literature, are evaluated using experimental test data from two test facilities.

- presentation of a theoretical procedure for calculating shear stresses of three phase vertically moving mixtures at the pipe wall. This procedure and other theoretical procedures are evaluated using measured experimental data.

- presentation of a complete mathematical model for calculating pressure changes in airlift pump delivery pipes (three phase, solid-liquid-gas flow). This model is verified using experimental tests in the laboratory.

- observation and measurement of airlift pumps operating :
  - at a range of delivered concentrations
  - with various particle size distributions
  - at a range of annular air injection areas
  - at a range of submergence ratios
  - with a high percentage of finer material (d_{50} = 1 000 μm).

- designing and programming highly user interactive computer software to aid designers of prototype installations in the offshore diamond mining industry. This software allows evaluation of a range of airlift pump configurations for the purpose of testing and optimizing prototype systems.

- evaluation of the sensitivity of all the variables in the three phase solid-liquid-gas mathematical model using the developed user friendly software.

1.8 USER FRIENDLY SOFTWARE (AIRLIFT)

With the development of sophisticated and advanced computer systems, engineering has seen many programs written to aid design. These programs vary from drafting packages through to urban stormwater system design tools and are collectively called Computer Aided Design packages (CAD).

To aid engineers in the design of prototype airlift pumps, the contents of this dissertation was integrated into a design package (AIRLIFT).

Considerable care was taken to write the software to suit the industrial design engineering environment by liaising with engineers who would benefit. Tabular data input is used, with numerous error handlers and help screens to make the software interactive and user friendly. Ten different airlift pump layouts are allowed for the purpose of a sensitivity analysis. Output from the program is a series of useful graphs summarising the information that the engineer requires for further system design.

A comprehensive user manual for the AIRLIFT program is given in Appendix A.

CHAPTER 2

AIRLIFT PUMP PRINCIPLE

2.1 STATIC CONDITIONS

Figure 2.1 shows an airlift pump immersed to a depth ($\ell 1 + \ell 2$) below the free water surface. Air is injected at a depth of $\ell 1$. Above the water surface, the airlift pump rises to a height ($\ell 3 - \ell 1$) which is termed the static lift height.

In Figure 2.1a, no air is injected, thus no flow can take place and the water inside the airlift pump is at the same level as the surrounding water surface. Disregarding minor pressure fluctuations, the pressure inside the system at any level is equal to the outside pressure at the same level. Similarly, densities inside and outside the system are the same at all levels.

2.2 HOISTING OF LIQUID

Figure 2.1b shows compressed air introduced at the gas injector. The liquid inside the airlift pump dilates by Δh . The height of dilation depends on the amount of air that is allowed to enter the airlift pump.

In the literature, this dilation (Δh) is explained as a pressure disequilibrium between the lower density liquid - gas mixture inside the airlift pump pipe, and the higher density liquid surrounding the airlift pump pipe. (Weber 1976, 1982, Clark *et al* 1986, Gibson 1925 and others).

Figure : 2.1
Description : AIRLIFT PUMP PRINCIPLE

Airlift Pump
Investigation

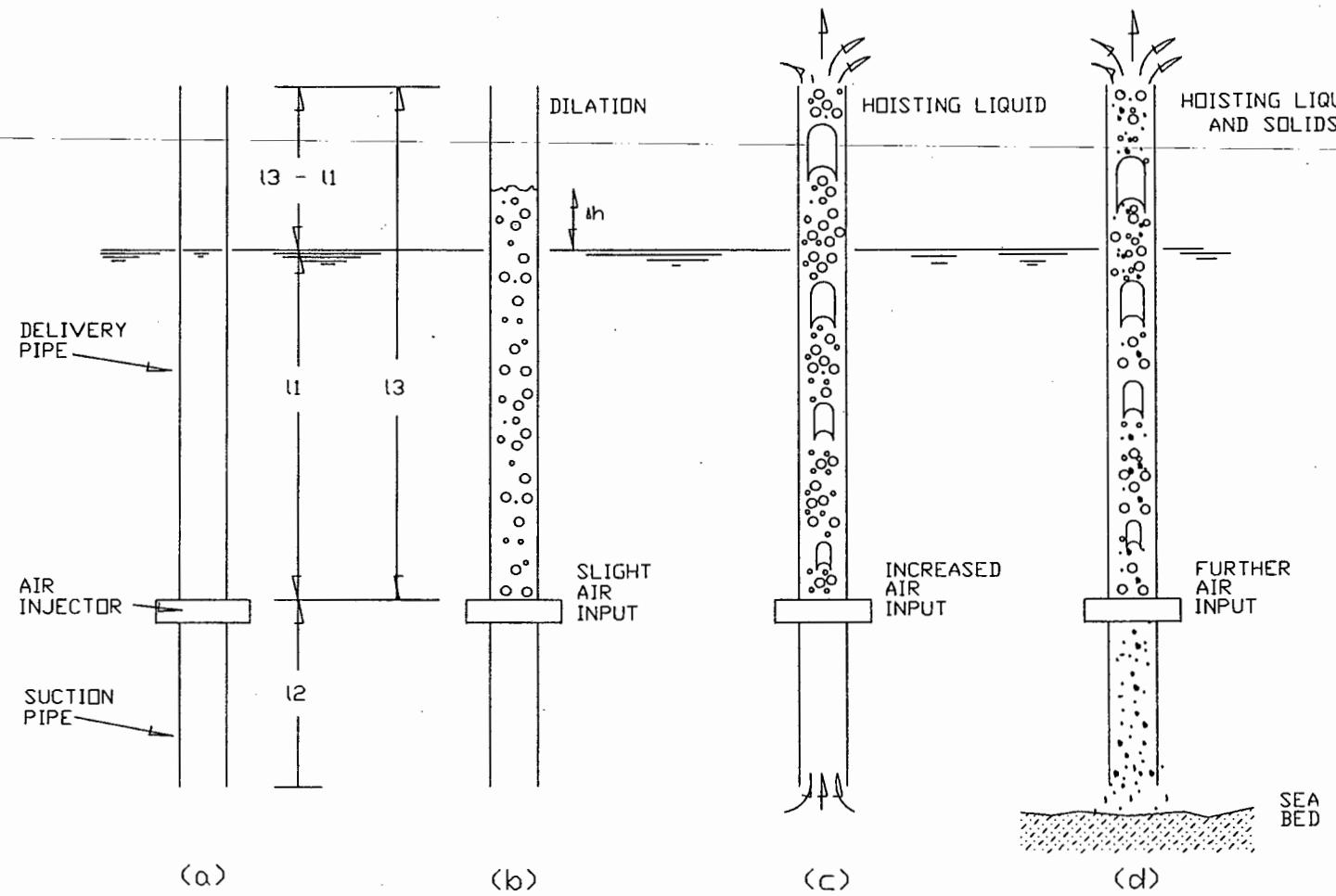

Pressure is a function of density, gravity and height, thus the lower density of the liquid-gas mixture is compensated by an increase in height (Δh) to regain the same pressure as the surrounding liquid.

A further explanation is given by Halde *et al* (1981), Stenning *et al* (1968) and Chisholm (1983) who also consider the effect of the rising air bubbles on the dilation. Assuming that the air enters the airlift pump as a single incompressible bubble, this bubble would displace the column of liquid above it, momentarily, by its own diameter. As the bubble rises, the liquid flows downward between the bubble and the pipe wall. When the bubble emerges at the top, the displaced liquid drops back to its original height. Allowing for the compressibility of the air, and a steady stream of bubbles, the liquid level would remain at the same displaced height (Δh). In the literature this effect is termed as "liquid hold up".

Should the dilated height (Δh) exceed the lift height ($\ell 3 - \ell 1$), liquid would flow out of the top of the airlift pump (Figure 2.1c). The quantity of liquid that flows out of the top is replenished at the lower end, at depth ($\ell 1$ & $\ell 2$). If the input air flow rate is maintained, a conveying system is established whereby liquid is "sucked" in at the bottom and "discharged" at the top of the airlift pump. This conveying system attains a state of dynamic equilibrium. In this dynamic state, the external static pressures are in equilibrium with the weight of the liquid-gas mixture inside the pipe (divided by the pipe area), the pressure changes due to the friction of the moving liquid-gas mixture with the pipe wall and other pressure changes due to isothermal expansion, momentum changes, inlet and outlet losses.

At this stage, the volume of air allowed to enter the airlift is sufficient to allow only liquid to be hoisted.

2.3 HOISTING OF SOLIDS AND LIQUIDS

If the bottom of the airlift pump is in close proximity to the sea bed, and the volume flow rate of air is increased, the sea bed material will also be "sucked up" (see Figure 2.1d).

The volume of material that will be hoisted is dependent on the :

1. size of the solid particles
2. density of the solid particles
3. proximity of the particles to the suction inlet
4. shape of the solid particles
5. volume of air allowed to enter the airlift pump
6. settling velocity of the solid particles
7. depth of air injection
8. height of the delivery outlet above the free water surface (lift height)
9. depth of the suction inlet.

An increase in the volume of air input will, at first, cause a rapid increase in the output of the solid and liquid phases. An optimum throughput is reached when an increase in the volume of air input will not increase the output of solids and liquids. This effect results in the typical airlift pump operating curve shown in Figure 2.2.

Figure : 2.2
Description : TYPICAL AIRLIFT PUMP OPERATING CURVE

Airlift Pump Investigation

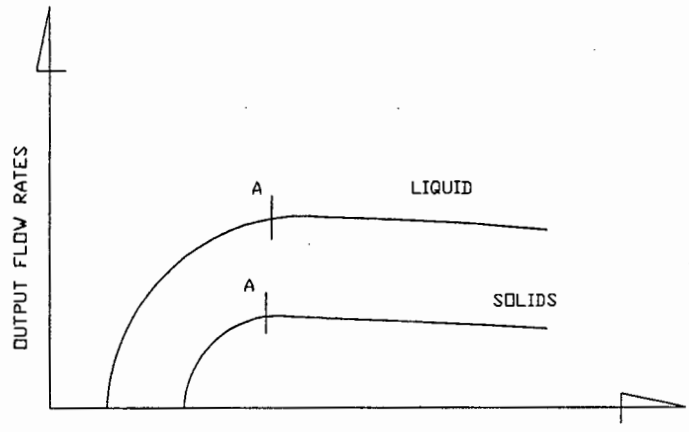

The reason for the drop in output flow rates at high air flow rates is primarily the increased conveyance velocity with the increased air input. This results in high shear stresses at the pipe wall, and thus the larger pressure losses result in a decrease of the conveyed mixture.

From the above, it is important to establish the air flow rate (A) at which the optimum solid and liquid output from a particular airlift pump configuration is obtained. More air input than required for optimum conditions, not only increases the power costs unnecessarily, but can also result in a decreased delivered output.

CHAPTER 3

LITERATURE REVIEW

3.1 INTRODUCTION

This chapter is a review of airlift pump analysis techniques which have been presented in the literature. The analysis techniques discussed are those, which deal specifically with airlift pumps that are used for the hoisting of coarse solids in a three phase heterogeneous mixture.

Generally literature on the subject is scarce and authors presenting the literature originate from Japan, Russia, Sweden, England, USA and West Germany. The majority of the sources were technical and scientific journals. An international "DIALOG" literature search was used to locate literature.

The most prominent contributions to the subject were made by Weber, Dedegil, Kato and Giot. Other analysis techniques in the literature are often case specific (e.g. apply to low air flow rates only) or are highly empirical and are therefore not considered suitable for general marine diamond reclamation.

Significant literature is presented on two phase liquid-gas and solid-liquid flow. Although this literature was evaluated, it is not discussed.

3.2 REVIEW

Airlift pumps are analysed in the literature using a balance of internal conditions, with external conditions. Weber (1976 a and b, 1982) and Dedegil (1974, 1982) use an energy flux balance to calculate

Figure : 3.1
Description : WEBER (1976) - ENERGY FLUX BALANCE.

Airlift Pump Investigation

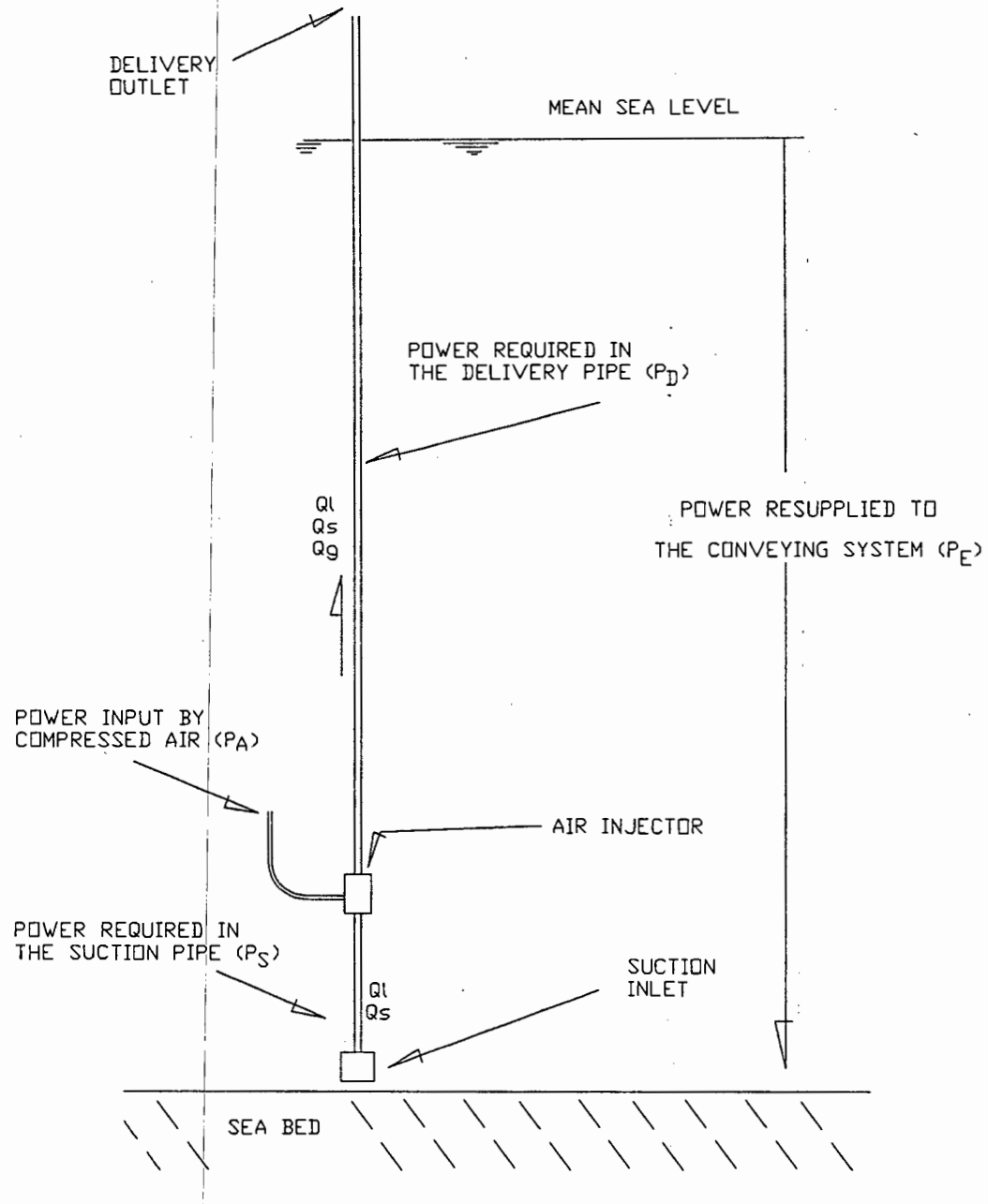

the conveying characteristics of airlift pumps operating in a three phase heterogeneous environment, while Kato (1975) and Giot (1982) suggest a balance of momentum.

To analyse airlift pump behaviour, the two phase solid-liquid flow below the air injection point is treated separately from the solid-liquid-gas flow above the air injection point.

Referring to Figure 3.1, Weber (1976, 1982) and Dedegil (1974, 1982) give their energy flux balance as :

$$P_A = P_D + P_S - P_E \qquad (3.1)$$

where P_A = power input by compressed air

P_S = power requirement in the suction pipe section before air injection

P_D = power requirement in the delivery pipe section after air injection

P_E = energy flux resupplied to the conveying system by the water flow rate entering the system from the outside.

In contrast to this, Giot (1982) and Kato (1975) give their momentum balance as :

Momentum at the
suction inlet = Momentum at the delivery outlet
+ Mixture weight in the suction and delivery pipe
+ Friction, in the suction and delivery pipe.

(3.2)

The above two equations are essentially the same. Rearranging and multiplying Equation 3.2 by the respective phase flow rates will result in power terms and consequently Equation 3.1.

The next task in the analysis is to calculate the various components required for the above equations. For the suction pipe, the weight and shear stresses of the vertically moving two phase solid-liquid mixture has to be evaluated while for the delivery pipe, in addition to the weight and shear stress, the acceleration of the three phase solid-liquid-gas mixture has to be evaluated.

Mixture weights

TWO PHASE

In the literature, there is agreement that the weight of the two phase solid-liquid mixture in the suction pipe (W_S) is expressed as :

$$W_S = \ell_S \, g \, (\, (1 - C_{vt}^{s\ell}) \, \rho_\ell + C_{vt}^{s\ell} \, \rho_s) \, A_S \qquad (3.3)$$

where ℓ_S = length of suction pipe

A_S = suction pipe cross-sectional area

ρ_ℓ and ρ_s = density of liquid and solid phases respectively

$C_{vt}^{s\ell}$ = solid *in situ* volumetric concentration.

It is in the evaluation of the two phase solid in situ volumetric concentration ($C_{vt}^{s\ell}$) that the theories in the literature differ.

Weber (1976 a and b) initially suggests that the upward velocity of the solids in a vertically moving two phase mixture is the difference between the upward velocity of the liquid and the settling velocity of the solid particles.

$$v_s = v_l - v_t \tag{3.4}$$

where v_s = velocity of solids

v_l = velocity of the liquid

v_t = settling velocity of solids.

From Equation 3.4, with suitable substitution of continuity equations, Weber obtains from first principles :

$$\frac{Q_l}{A}\left[\frac{1}{(1 - C_{vt}^{sl})} - \frac{C_{vd}^{sl}}{(1 - C_{vd}^{sl})\,(C_{vt}^{sl})}\right] = \sqrt{\frac{\frac{4}{3}\, d\, g\, (\rho_s - \rho_l)}{C_D\, \rho_l}} \tag{3.5}$$

where C_D = drag coefficient of solids

d = particle diameter

C_{vd}^{sl} = solid delivered volumetric concentration.

Equation 3.5 can be solved implicitly to yield the *in situ* volumetric concentration of solids (C_{vt}^{sl}) in a solid-liquid mixture.

In a later approach however, Weber (1982) suggests that Equation 3.4 be replaced by the following equation :

$$v_s = v_m^{s\ell} - v_t \qquad (3.6)$$

In this equation, Weber now suggests that the upward velocity of solids is the difference between the mean mixture velocity and the settling velocity of the solid particles.

This expression has the same form as the hold up equation first presented by Behringer in 1936 and subsequently used by Zuber and Findley (1965), Govier and Aziz (1972) and Chisholm (1983) for vertical two phase solid-liquid flow.

The term v_t in Equation 3.6 is evaluated by Weber with an empirical approach, based on work by Dedegil. Along with this approach, substitution of continuity equations, and suitable transformation Weber obtains :

$$C_{vt}^{s\ell} = \frac{\frac{v_t}{v_m^{s\ell}} - 1 + \sqrt{\left(\frac{v_t}{v_m^{s\ell}} - 1\right)^2 + 4\left(2{,}8\,\frac{v_t}{v_m^{s\ell}}\,C_{vd}^{s\ell}\right)}}{2\left(2{,}8\,\frac{v_t}{v_m^{s\ell}}\right)} \qquad (3.7)$$

The empirical factor 2,8 is the result of *hindered* settling considerations also based on Dedegil's research (valid for $192 < Re_s <$ 7445 and $C_{vt}^{s\ell} < 0{,}2$).

Kato (1975) relies largely on experimental results and empirical correlations for solutions to phase *in situ* volumetric concentrations, while Giot (1982) suggests using the Zuber and Findley (1965) hold up equation given in Equation 3.6. This equation can be rewritten as :

$$\frac{Q_s}{C_{vt}^{s\ell} A} = C_{s\ell} \frac{Q_m^{s\ell}}{A} - v_t \qquad (3.8)$$

where $C_{s\ell}$ = distribution coefficient.

Giot suggests that the value of the distribution coefficient is "close to unity" and that v_t can be estimated as the terminal settling velocity of particles.

THREE PHASE

Due to the isothermal expansion of the injected gas there is agreement in the literature that the delivery pipe has to be analysed in increments. These increments are consequently integrated for the total delivery pipe length. In each increment, the weight, friction and acceleration of the solid-liquid-gas mixture has to be calculated.

Considering the weight (W_{inc}) in a typical delivery pipe increment, the literature agrees that this component in each increment can be expressed as :

$$W_{inc} = \ell_{inc}\, g \left[(1 - C_{vt}^{s\ell g} - \epsilon_g^{s\ell g})\, \rho_\ell + C_{vt}^{s\ell g}\, \rho_s + \epsilon_g^{s\ell g}\, \rho_g \right] A_{inc} \qquad (3.9)$$

where $C_{vt}^{s\ell g}$ = solid *in situ* volumetric concentration (solid-liquid-gas mixture)

$\epsilon_g^{s\ell g}$ = gas *in situ* volumetric concentration (solid-liquid-gas mixture)

ℓ_{inc} = length of delivery pipe increment

A_{inc} = incremental pipe cross-sectional area.

As before, it is in the evaluation of the solid and gas in situ volumetric concentration that the authors in the literature differ.

To calculate the solid and gas *in situ* volumetric concentrations, Weber (1976 a and b) suggests using an iterative procedure. He presents a technique for obtaining the *in situ* concentration of gas ($\epsilon_g^{\ell g}$) in a liquid-gas mixture, based on a relationship between the static dilation of a water column ($\epsilon_{go}^{\ell g}$) and the gas superficial velocity ($\frac{Q_g}{A}$).

In this technique, Weber (1976 a and b) suggests that the absolute velocity of the gas phase (v_g) is the sum of the relative velocity (v_{go}) between gas and liquid and the absolute velocity of liquid (v_ℓ). Thus

$$v_g = v_{go} + v_\ell \tag{3.10}$$

The relative velocity (v_{go}) between gas and liquid is expressed as :

$$v_{go} = \frac{Q_g}{\epsilon_{go}^{\ell g} A} \tag{3.11}$$

$$\text{also} \quad v_\ell = \frac{Q_\ell}{\epsilon_g^{\ell g} A} \tag{3.12}$$

By transforming and applying continuity equations, Weber shows that :

$$\epsilon_g^{lg} = \frac{1}{2}\left[1 + \epsilon_{go}^{lg}\left(\frac{Q_g + Q_l}{Q_l}\right)\right] - \sqrt{\left(1 + \epsilon_{go}^{lg}\frac{Q_g + Q_l}{Q_g}\right)^2 - 4\,\epsilon_{go}^{lg}} \qquad (3.13)$$

In a later paper Weber (1978), after researching airlift pumps operating under "extreme conditions" corrects Equation 3.9 and suggests that the absolute velocity of the gas phase (v_g) is the sum of the relative velocity (v_{go}) and the superficial velocity of liquid ($\frac{Q_l}{A}$).

Thus

$$v_g = v_{go} + \frac{Q_l}{A} \qquad (3.14)$$

Weber therefore shows that :

$$\epsilon_g^{lg} = \frac{1}{\frac{1}{\epsilon_{go}^{lg}} + \frac{Q_l}{Q_g}} \qquad (3.15)$$

In his 1982 paper, Weber supersedes Equation 3.15 by Equation 3.27 which Dedegil (1982) suggests after investigating "relatively high - coalescent systems of air and water".

Having evaluated the solid and gas *in situ* volumetric concentrations in their respective two phase environments, Weber's iteration procedure is as follows :

Figure : 3.2
Description : WEBER (1976) - ITERATION METHOD

Airlift Pump Investigation

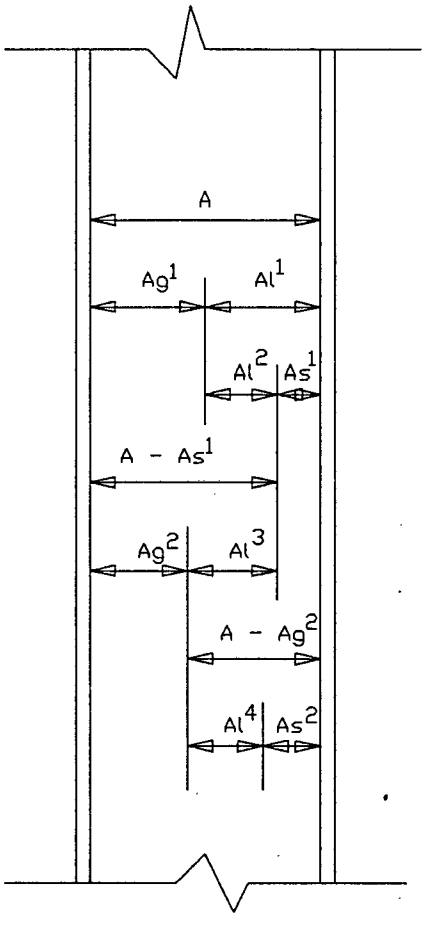

Referring to Figure 3.2 :

1. It is first assumed that the entire pipe cross-sectional area (A) is occupied by the liquid and gas phases only. Equation 3.15 is applied and the *in situ* concentration of gas (ϵ_g^{lg}) is calculated. From this the areas occupied by the gas and the liquid phase are calculated using :

$$A_g^{(1)} = A\,\epsilon_g^{lg} \tag{3.16}$$

$$A_l^{(1)} = A\,(1 - \epsilon_g^{lg}) \tag{3.17}$$

2. It is then assumed that the area of liquid ($A_l^{(1)}$), calculated in Equation 3.17 above, is occupied by liquid and solids phases only. Equation 3.7 is applied and the *in situ* volumetric concentration of solids (C_{vt}^{sl}) is calculated. From this the area occupied by the solids and a <u>new</u> area occupied by the liquid is calculated using :

$$A_s^{(1)} = A_l^{(1)}\,C_{vt}^{sl} \tag{3.18}$$

$$A_l^{(2)} = A_l^{(1)}\,(1 - C_{vt}^{sl}) \tag{3.19}$$

also $A_g^{(1)} + A_s^{(1)} + A_l^{(2)} = A$

$$\therefore \quad A_g^{(1)} + A_g^{(2)} = A - A_s^{(1)} \tag{3.20}$$

3. It is now assumed that the total pipe cross-sectional area minus the area of solids ($A - A_s^{(1)}$) is occupied by the liquid and gas. Thus item 1 above is repeated and a new area of gas and liquid is calculated.

$$A_g^{(2)} = (A - A_s^{(1)})\,\epsilon_g^{lg} \tag{3.21}$$

$$A_l^{(3)} = (A - A_s^{(1)})\,(1 - \epsilon_g^{lg}) \tag{3.22}$$

4. In the same way as item 3 above, it is assumed that the total pipe cross-sectional area minus the area of gas ($A = A_g^{(2)}$) is occupied by the liquid and solids. Thus item 2 above is repeated and a new area of liquid and solid is calculated.

$$A_s^{(2)} = (A - A_g^{(2)})\, C_{vt}^{sl} \tag{3.23}$$

$$A_l^{(4)} = (A - A_g^{(2)})\, (1 - C_{vt}^{sl}) \tag{3.24}$$

5. Items 3 and 4 above are now alternatively repeated until the adjustment to the areas from one iteration process to the next prove to be negligible. At this stage the *in situ* volumetric concentrations of the solids (C_{vt}^{slg}) and gas (ϵ_g^{slg}) in a solid-liquid-gas mixture can be calculated using :

$$C_{vt}^{slg} = \frac{A_s^{(n)}}{A} \tag{3.25}$$

$$\epsilon_g^{slg} = \frac{A_g^{(n)}}{A} \tag{3.26}$$

where $A_s^{(n)}$ and $A_g^{(n)}$ = the areas of liquid and gas respectively after the nth iteration.

Dedegil (1974) agrees with this iterative technique and all the equations that are initially presented by Weber.

After more research, however, Dedegil (1982) suggests that a better approximation to calculate solid *in situ* volumetric concentrations in a solid-liquid mixture is obtained with Equations 3.6 and 3.7.

He also suggested an empirical equation, which is based on his own research, to evaluate the gas *in situ* volumetric concentration in a gas-liquid mixture. This equation he presents as :

$$\epsilon_g^{lg} = \frac{\frac{Q_s}{A}}{v_B + K\frac{Q_s}{A} + \frac{Q_l}{A}} \qquad (3.27)$$

where v_B = 0,41 is the rise velocity of a single bubble (for D > 50 mm)

and K = 1,081 is an empirical constant.

The above equations are then iterated as before.

Kato (1975) performed a series of tests to monitor the *in situ* volumetric concentrations of the solid and gas phases in a three phase mixture. His assumptions were that all the solids are located in the liquid phase and his tests were performed in a 19 mm plexiglass tube using glass spheres. The final conclusion was, that three phase flow can be analysed by applying the empirical two phase flow theory presented by Akagawa in 1957.

Akagawa, for two phase liquid-gas flow, suggests that the gas *in situ* concentration in two phase liquid-gas flow is evaluated using :

$$\frac{1 - (1 - \epsilon_g^{lg})}{(1 - \epsilon_g^{lg})} = C \frac{(\frac{Q_g}{A})^N}{(\frac{Q_l}{A})^M} \qquad (3.28)$$

Table 3.1 below gives Akagawa's factors N, M and C.

Figure 3.3 shows the results of Kato's (1975) experimental measurements. From these, he concludes that the decrease in $(1 - \epsilon_g^{lg})$ is equal to the increase in C_{vt}^{sl}. Furthermore, he concludes that $\left[(1 - \epsilon_g^{lg}) + C_{vt}^{sl} \right]$ is constant, and can be expressed by the solid lines in the figure. The constants intercepts with the y axis on Figure 3.3 are calculated using Equation 3.28, i.e. for the case where $C_{vt}^{sl} = 0$ in Equation 3.29. Kato thus suggests expanding on Equation 3.28 by including the solid *in situ* volumetric concentration :

$$\frac{1 - ((1 - \epsilon_g^{lg}) + C_{vt}^{sl})}{(1 - \epsilon_g^{lg}) + C_{vt}^{sl}} = C \frac{(\frac{Q_g}{A})^N}{(\frac{Q_l}{A})^M} \qquad (3.29)$$

$\frac{Q_l}{A}$ m/s	N	M	C
< 0,5	0,96	0,69	0,82
> 0,5	0,78	0,69	0,67

TABLE 3.1 : Akagawa's empirical factors (Kato 1975)

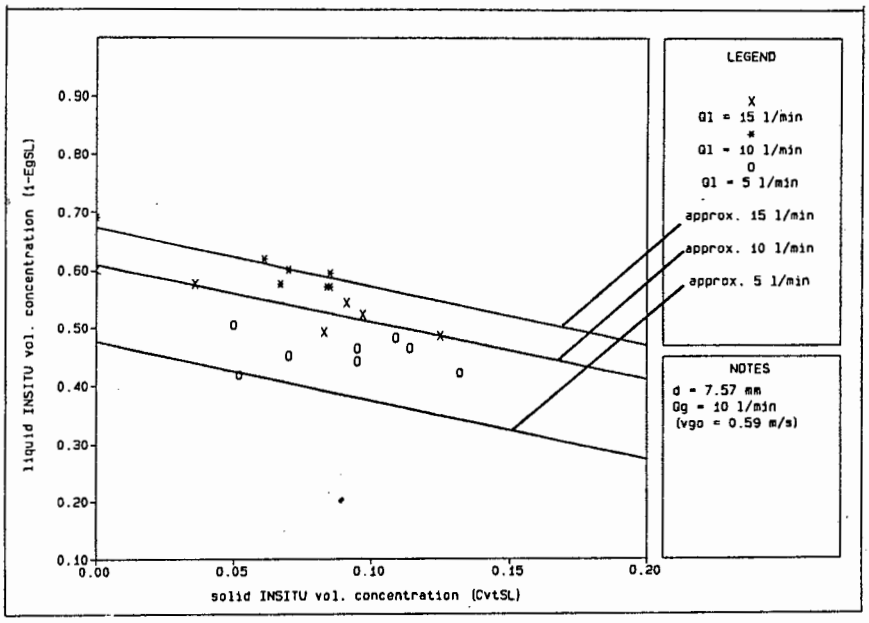

Figure 3.3 : Kato (1975) - phase *in situ* concentration measurements

Giot (1982) expands on the two phase liquid-gas hold up equation of Zuber and Findley (1965), and suggests that the solid *in situ* volumetric concentration in a solid-liquid-gas mixture is calculated from :

$$v_s = C_{lg}\, v_m^{slg} - v_t^{lg} \tag{3.30}$$

Thus, by substitution of continuity equations, Giot shows :

$$\frac{Q_s}{C_{vt}^{slg}\, A} = C_{lg}\, \frac{Q_g + Q_l + Q_s}{A} - v_t^{lg} \tag{3.31}$$

Likewise, for predicting the *in situ* concentration of gas in a solid-liquid-gas mixture Giot uses :

$$v_g = C_{sl}\, v_m^{slg} + v_B^{sl} \tag{3.32}$$

Thus obtaining

$$\frac{Q_g}{\epsilon_g^{s\ell g} A} = C_{s\ell} \frac{Q_g + Q_\ell + Q_s}{A} + v_B^{s\ell} \qquad (3.33)$$

Giot suggests that the terminal settling velocity of particles in a gas-liquid mixture ($v_t^{\ell g}$) can be readily predicted. In the same way, the terminal rise velocity of the bubbles in solid-liquid mixtures ($v_B^{s\ell}$) is not affected by the presence of the low concentration of solids.

In his article, Giot compares his own calculations against the calculation techniques of Weber and Kato, but does not compare them with experimental data. Furthermore, he assumes that the distribution parameters $C_{\ell g}$ and $C_{s\ell}$ have a value of 1 in his comparison.

Mixture shear stress

Weber (1976 a and b) calculates the two phase solid-liquid and solid-liquid-gas mixture shear stresses using a separated flow model.

In the separated flow model it is assumed that each phase is in contact with the pipe wall (perimeter) for a fraction of the total pipe perimeter. Each phase is also assumed to flow separately with no entrainment taking place. The contact fraction of each phase is related to its phase *in situ* concentration. Therefore it can be shown that for solid-liquid-gas mixtures :

$$\tau_{om}^{s\ell g} \frac{\pi D \ell_{inc}}{A} = \left[\epsilon_g^{s\ell} \tau_g + (1 - \epsilon_g^{s\ell g} - C_{vt}^{s\ell g}) \tau_\ell + C_{vt}^{s\ell g} \tau_s \right] \frac{\pi D \ell_{inc}}{A} \quad (3.34)$$

where $\tau_g = \frac{1}{2} f_g \rho_g v_g^2$ (3.35)

$$\tau_\ell = \frac{1}{2} f_\ell \rho_\ell v_\ell^2 \quad (3.36)$$

$$\tau_s = \frac{1}{2} f_s \rho_s v_s^2 \quad (3.37)$$

f_g, f_ℓ, f_s = phase friction factors.

If the gas term in Equation 3.34 is allowed to tend to zero, this equation can be used to calculate the shear stress of a solid-liquid mixture with the pipe wall.

In discussing the separated flow model for liquid-gas flow, Chisholm (1983) notes that a major assumption is :

$$f_\ell = f_g \quad (3.38)$$

Likewise, Weber assumes that

$$f_g = f_s = f_\ell \quad (3.39)$$

To calculate f_ℓ , Weber uses the Fanning friction factor for fully rough turbulent flow (i.e. dependent on pipe wall roughness, not Re) as in the case of pure liquids and smooth pipes,

$$\frac{1}{\sqrt{f_\ell}} = 4 \log (3.7 D/k) \quad (3.40)$$

By substituting Equations 3.35 to 3.37 into Equation 3.34, Weber obtains :

$$\tau_{om}^{s\ell g} = \tfrac{1}{2} f_\ell \left[\epsilon_g^{s\ell g} \rho_g v_g^2 + (1 - \epsilon_g^{s\ell g} - C_{vt}^{s\ell g}) \rho_\ell v_\ell^2 + C_{vt}^{s\ell g} \rho_s v_s^2 \right] \quad (3.41)$$

In his 1974 article, Dedegil also uses the separated flow model to calculate the shear stress of the solid-liquid and solid-liquid-gas mixture with the pipe wall. In a later article, however, Dedegil (1982), suggests treating the solid and liquid phases as a suspension, behaving as a liquid of higher density. Dedegil then applies the *homogeneous theory* together with the suspension density to calculate the solid-liquid friction component. The homogeneous theory assumes no slip between the solid and liquid phases.

$$\tau_{om}^{s\ell} = \tfrac{1}{2} f \rho_m^{s\ell} \left[\frac{Q_m^{s\ell}}{A} \right]^2 \quad (3.42)$$

where $\rho_m^{s\ell} = \rho_s C_{vt}^{s\ell} + \rho_\ell (1 - C_{vt}^{s\ell})$

Dedegil expresses the friction factor (f) as a function of the mixture Reynolds number :

$$Re = \frac{D v_m^{s\ell}}{\nu} \quad (3.43)$$

The friction factor, Dedegil (1982), calculates according to Blasius for hydraulically smooth pipes which he gives in his paper as :

$$f = \frac{1}{4} (0,316 (Re)^{-0,25}) \tag{3.44}$$

For the calculation of the three phase solid-liquid-gas shear stress, Dedegil (1982) uses :

$$\tau_{om}^{s\ell g} = \frac{1}{2} f \rho_m^{s\ell} (1 - \epsilon_g^{s\ell g}) \left(\frac{Q_g + Q_\ell}{A}\right)^2 \tag{3.45}$$

The friction factor in this case is evaluated with Equation 3.40 by assuming fully rough turbulent flow.

To calculate the friction pressure drop of the three phase mixture with the pipe wall, Kato (1975) uses the empirical relationship suggested by Akagawa for two phase liquid-gas flow.

Akagawa uses a two phase multiplier to calculate the friction pressure drop of a two phase liquid-gas mixture from the friction pressure drop of single phase liquid flow.

$$\tau_{om}^{\ell g} = \tau_o \phi_{F\ell}^2 \tag{3.46}$$

Akagawa's empirical relationship for the two phase multiplier is given as :

$$\phi^2_{Fl} = (1 - \epsilon_g^{lg})^{-1,51} \qquad (3.47)$$

where ϕ^2_{Fl} = two phase multiplier.

also $$\tau_o^l = \tfrac{1}{2} f_l \rho_l (\frac{Q_l}{A})^2 \qquad (3.48)$$

where τ_o^l = shear stress of liquid with the pipe wall

$$f_l = f_n (Re^l) \qquad (3.49)$$

$$= f_n (\frac{Q_l}{A} D)$$

Giot (1982) suggests calculating the three phase shear stress with the pipe wall *either* by using the same technique as Weber (separated flow model) or Kato (Akagawa's empirical technique). In later literature, Giot (1986) concerned himself with the airlift pumping of clay-water mixtures (non-settling slurries). Here he uses two phase multipliers which were presented by Martinelli and co-workers (Chisholm 1983).

In his paper, he states the following about friction pressure drops (shear stresses) :

"Experimental evidence is still too scarce to point to a best design method. However, the friction pressure drops are usually not the most important resistance factor for three phase flow and inaccuracy in these terms entail no major consequence" (Giot 1986).

Mixture acceleration

To evaluate the mixture acceleration in the delivery pipe increment, the authors all use the average momentum in the delivery pipe increment.

The phases are all considered seaprately and the average momentum pressure is expressed as :

$$\text{Momentum pressure} = \tfrac{1}{2}\left[(1 - C_{vt}^{s/g} - \epsilon_g^{s/g})\, \rho_l\, \Delta v_l^2 + C_{vt}^{s/g}\, \rho_s\, \Delta v_s^2 + \epsilon_g^{s/g}\, \rho_g\, \Delta v_g^2 \right] \qquad (3.50)$$

where Δv_l, Δv_g, Δv_s = changes in phase velocities from the bottom to the top of the delivery pipe increment.

To test the validity of the theories presented, tests are conducted. In these tests, experimental results are compared with the theories discussed.

CHAPTER 4

PROPOSED ANALYTICAL APPROACH

4.1 INTRODUCTION

In Chapter 3, three phase airlift pump analysis techniques presented in the literature are investigated and discussed. Detailed reference is made to the calculation of specific variables and the methods used by the authors to evaluate them.

This chapter gives a proposed analytical approach in its entirety. The evaluation of each variable in the analytical approach is described in detail. Aspects of the proposed analytical approach are similar to methods discussed in the literature. However, certain important refinements are made. In the refinements, specific variables are evaluated in different ways. In other refinenents additional variables are introduced to increase the accuracy of the analysis.

4.2 THREE PHASE ANALYSIS TECHNIQUE

When operating under conditions of a constant steady air input flow rate, airlift pumps rapidly reach a state of dynamic equilibrium. This equilibrium is a balance of static pressure gains outside the airlift pump and conveying pressure losses inside the airlift pump.

To analyse airlift pumps operating in three phase flow it is therefore necessary to evaluate various pressure changes.

Figure : 4.1
Description : PROPOSED 3 PHASE ANALYSIS TECHNIQUE

Airlift Pump Investigation

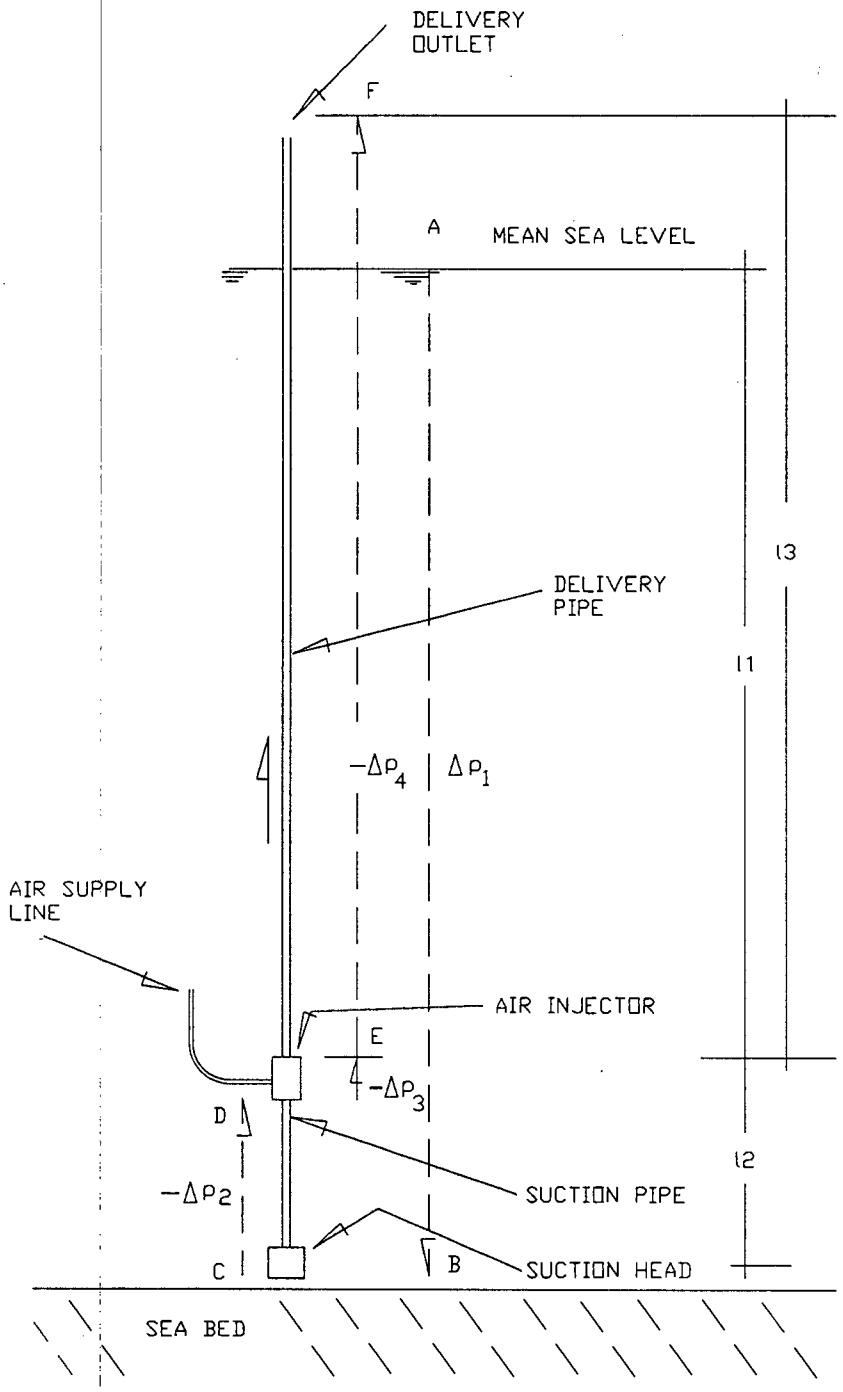

Referring to the airlift pump in Figure 4.1, the pressure changes are :

1. Δp_1 = the pressure differential from point A to C in the surrounding liquid

   cause : increase in depth in the surrounding liquid
   entrance loss and entrance acceleration

2. Δp_2 = the pressure drop from point C to point D in the suction pipe

   causes : friction and weight of two-phase solid-liquid mixture

3. Δp_3 = the pressure drop from point D to point E across the air injector

   cause : momentum of two-phase solid-liquid and three-phase solid-liquid-gas mixture

4. Δp_4 = the pressure drop from point E to point F in the delivery pipe

   cause : friction, weight and momentum of three-phase solid-liquid-gas mixture.

Analogous to the analysis techniques in the literature (Chapter 3), a pressure balance is performed. In this case the pressures are balanced as follows :

$$\Delta p_1 - \Delta p_2 - \Delta p_3 - \Delta p_4 = 0 \qquad (4.1)$$

Using Equation 4.1 to calculate the mixture output flow rates for a given air input, the following iterative procedure is adopted :

1. an output mixture flow rate (Q_m^{sl}) and solid delivered volumetric concentration (C_{vd}^{sl}) is assumed.

2. the above pressure changes (Δp_1, Δp_2, Δp_3 and Δp_4) are calculated using the assumed conditions from item 1.

3. the pressures are balanced in Equation 4.1.

Should the pressures not balance and Equation 4.1 is not satisfied, then a new adjusted mixture flow rate is chosen. This procedure is iterated until the pressures in Equation 4.1 balance. The resulting mixture output flow rates correspond to the air input flow rate and the system is in dynamic equilibrium. Thus the output flow rates for an air input flow rate have been calculated. Repeating this procedure at a range of air input flow rate yields the operating curve for a particular airlift pump configuration, pumping at the assumed solid delivered volumetric concentration.

4.3 STATIC PRESSURE GAIN PARAMETERS (Δp_1)

4.3.1 Summary of variables

Referring to Figure 4.1, the first requirement of the pressure balance is the pressure differential Δp_1 , from point A to C. Point C is located inside the suction inlet to the airlift pump, while point A is at mean sea level where atmospheric conditions prevail.

The pressure differential, which is evaluated using Bernoulli's energy equation comprises a static pressure gain, an entrance acceleration and entrance loss component:

$$\text{static pressure gain component} = \rho_{\ell} g \, (\ell_1 + \ell_2) \tag{4.2a}$$

$$\text{entrance loss and entrance acceleration component} = \rho_m^{s\ell} g \left[\frac{(v_m^{s\ell})^2}{2g} + \xi_e \frac{(v_m^{s\ell})^2}{2g} \right] \tag{4.2b}$$

Combining these two components, the pressure differential (Δp_1) from point A to point C inside the suction pipe can be written as

$$\Delta p_1 = \rho_{\ell} g \, (\ell_1 + \ell_2) - \rho_m^{s\ell} g \left[\frac{(v_m^{s\ell})^2}{2g} + \xi_e \frac{(v_m^{s\ell})^2}{2g} \right] \tag{4.3}$$

where ρ_{ℓ} = density of the liquid

ℓ_1, ℓ_2 = refer to figure 4.1

$\rho_m^{s\ell}$ = density of solid-liquid mixture in the suction pipe

$v_m^{s\ell}$ = average velocity of solid-liquid mixture in suction pipe

g = gravitational acceleration = 9.81 m/s^2

ξ_e = entrance loss coefficient

The variables $\rho_m^{s\ell}$ and $v_m^{s\ell}$ in Equation 4.3 will be discussed in Section 4.4 below. All other variables are readily obtained.

4.4 SUCTION PIPE PARAMETERS (Δp_2)

4.4.1 Summary of variables

The next requirement in the pressure balance Equation 4.1 is to calculate the pressure drop in the suction pipe (Δp_2), moving from point C to D in Figure 4.1. Point C is inside the suction inlet,

while point D is at the base of the air injectors. To calculate this, pressure drop, the momentum force equation is applied.

$$\therefore \quad \left[(P + \rho_m^{s\ell} (v_m^{s\ell})^2) A \right]^{\text{at C}} \uparrow = \left[(P + \rho_m^{s\ell} (v_m^{s\ell})^2) A \right]^{\text{at D}} \downarrow + W_m^{s\ell} \downarrow + \tau_{om}^{s\ell} \pi D \ell \downarrow \tag{4.4}$$

where P = absolute pressure

$\rho_m^{s\ell}$ = density of the solid-liquid mixture in the suction pipe

$v_m^{s\ell}$ = average velocity of the solid-liquid mixture in the suction pipe

$W_m^{s\ell}$ = weight of the solid-liquid mixture in the suction pipe

$\tau_{om}^{s\ell}$ = shear stress at the pipe wall due to the vertically moving solid-liquid mixture

D = pipe diameter

ℓ = pipe length = ℓ_2

A = pipe cross-sectional area

Assuming that the mixture velocity and density in the suction inlet is the same as at the base of the air injectors, the two momentum force terms $[\rho_m^{s\ell}(v_m^{s\ell})^2 A]$ cancel out. (It must be mentioned, that the momentum force terms are an approximation of the average of the momentum forces of the two phases.) Thus dividing by the pipe area, Equation 4.4 is rewritten as :

$$\Delta p_2 = P_C - P_D = \frac{W_m^{s\ell}}{A} + \tau_{om}^{s\ell} \frac{\pi D \ell_2}{A} \qquad (4.5)$$

4.4.2 Solid-liquid mixture weight ($W_m^{s\ell}$)

With reference to Equation 4.5, the weight of the solid-liquid mixture in the suction pipe can be expressed as :

$$W_m^{s\ell} = \rho_m^{s\ell} g \ell_2 A \qquad (4.6)$$

where $\rho_m^{s\ell}$ = the density of the solid-liquid mixture.

Solid-liquid mixture density ($\rho_m^{s\ell}$)

The density of the solid-liquid mixture in the suction pipe can be expressed as :

$$\rho_m^{s\ell} = \rho_s C_{vt}^{s\ell} + \rho_\ell (1 - C_{vt}^{s\ell}) \qquad (4.7)$$

where ρ_s and ρ_ℓ = the density of solid and liquid phases

$C_{vt}^{s\ell}$ = *in situ* concentration of the solids in the solid-liquid mixture.

Equations 4.6 and 4.7 can be combined to give the weight of the solid-liquid mixture in the airlift pump suction pipe as :

$$W_m^{s\ell} = \left[\rho_s C_{vt}^{s\ell} + \rho_\ell (1 - C_{vt}^{s\ell})\right] g \ell_2 A \qquad (4.8)$$

This equation is identical to Equation 3.3 which is used throughout the literature.

Solid *in situ* volumetric concentration - 2 phase ($C_{vt}^{s\ell}$)

To evaluate Equation 4.8, it is necessary to calculate the *in situ* concentration of solids ($C_{vt}^{s\ell}$) in the solid-liquid mixture. This variable is defined as the ratio of volume of solids being transported in the pipe to the volume of mixture being transported in the pipe.

$$C_{vt} = \frac{V_s}{V_m^{s\ell}} \tag{4.9}$$

where V_s = volume of transported solids

$V_m^{s\ell}$ = volume of transported solid-liquid mixture.

For a cross-sectional area, Equation 4.9 becomes

$$C_{vt} = \frac{A_s}{A_m^{s\ell}} \tag{4.10}$$

where A_s = area of transported solids

$A_m^{s\ell}$ = area of transported solid-liquid mixture.

As mentioned in Section 4.2, one of the independent assumed variables in the analysis of airlift pumps is the solid delivered volumetric concentration ($C_{vd}^{s\ell}$) . This, unlike the *in situ* volumetric concentration of solids ($C_{vt}^{s\ell}$), is defined as the ratio of solid volume flow rate to solid- liquid mixture volume flow rate discharged at the delivery outlet.

$$C_{vd}^{sl} = \frac{Q_s}{Q_m^{sl}} = \frac{v_s A_s}{v_m^{sl} A_m^{sl}} \tag{4.11}$$

where v_s = velocity of solids

v_m^{sl} = average velocity of the solid-liquid mixture.

Substituting Equation 4.10 into 4.11, the relationship between solid *in situ* and delivered volumetric concentration becomes :

$$C_{vd}^{sl} = \frac{v_s}{v_m^{sl}} C_{vt}^{sl} \tag{4.12}$$

Considering the vertically upward moving mixture flow in the suction pipe, the mean velocity of the solids (v_s) is equal to the mean solid-liquid mixture velocity (v_m^{sl}) minus the hindered terminal settling velocity of the solids (v_t')

$$v_s = v_m^{sl} - v_t' \tag{4.13}$$

This equation is identical to Equation 3.6 and is presented in the literature by Zuber and Findley (1965), Govier and Aziz (1972) and Chisholm (1983). It is furthermore used by Weber (1982) and Giot (1982).

Substituting Equation 4.13 into 4.12, the relationship between solid *in situ* and delivered volumetric concentrations for solid-liquid mixtures becomes :

$$C_{vd}^{s\ell} = \frac{(v_m^{s\ell} - v_t')}{v_m^{s\ell}} C_{vt}^{s\ell}$$

$$\therefore \quad C_{vd}^{s\ell} = \frac{\left[\frac{Q_s + Q_\ell}{A} - v_t'\right]}{\left[\frac{Q_s + Q_\ell}{A}\right]} C_{vt}^{s\ell} \qquad (4.14)$$

Settling velocity of spherical solids (v_t)

The terminal settling velocity of particles in liquid is evaluated from first principles. Furthermore, consideration is given to the hindered settling effect, particle shape and particle size distributions.

The settling velocity of spheres in liquid from first principles (Lazarus, 1982) is given as :

$$v_{tsph} = \sqrt{\frac{4}{3}\frac{gd}{C_D}\frac{(\rho_s - \rho_\ell)}{\rho_\ell}} \qquad (4.15)$$

where v_{tsph} = single particle terminal settling velocity

d = diameter of the sphere

C_D = drag coefficient of the sphere.

Using dimensional analysis, the drag coefficient (C_D) can be shown to be a function of the particle Reynold's number (R_{ep}).

Experimental results have made it possible to obtain three well accepted emperical correlations of the drag coefficient to the particle Reynolds number (Lazarus 1982). These three laws are applicable over three particle Reynolds number ranges as follows :

Stokes Law : $C_D = {}^{24}/_{Re}$ valid within 15%

(Laminar Regime) for $0 < R_{ep} < 0,8$ (4.16)

Intermediate Law : $C_D = {}^{14}/_{(Re)^{\frac{1}{2}}}$ valid within 15%

for $6 < R_{ep} < 1,00$ (4.17)

Newton's Law : $C_D = 0,44$ valid within 15%

(Turbulent Regime) for $1000 < R_{ep} < 10^5$ (4.18)

where $R_{ep} = \frac{v_{tsph} d}{\nu}$ (4.19)

Marine gravels larger than 2 mm in diameter have particle Reynold's number greater than 1000 and thus Newton's law (turbulent regime) is applicable.

Substituting Equation 4.18 into Equation 4.15, the settling velocities of single spherical particles in a liquid are :

$$v_{tsph} = 0,981\ d^{\frac{1}{2}} \sqrt{(\rho_s - \rho_l)\ g\ \pi/\rho_l} \quad (4.20)$$

Non-spherical particles

Equation 4.20, has to be corrected for *nonspherical particles*. The correction applied, is to multiply the settling velocity of an equivalent diameter sphere as the particle, by a shape factor (S_f).

$$v_t = S_f \times v_{tsph} \quad (4.21)$$

Shape factors are determined experimentally and typical values for marine gravels are between 0,7 and 0,8.

Hindered settling

Furthermore, the settling velocity of individual particles is reduced by the presence of other particles. An increase in the concentration of particles reduces the settling velocity of the solitary particle. This effect is termed the *hindered settling velocity*. It can be shown that the relationship of hindered settling velocity to solitary particle velocity is (Lazarus, 1982) :

$$v'_t = v_t \, (1 - C_{vt}^{s\ell}) \tag{4.22}$$

Richardson and Zaki (1954b) used the following relationship between hindered and solitary particle settling velocities :

$$v'_t = v_t \, (1 - C_{vt}^{s\ell})^{\alpha} \tag{4.23}$$

The variable α is a function of Re_p and are shown to have the values listed in Table 4.1. For the purpose of an upper limit in equation 4.23, it must be noted that generally *in situ* concentrations $C_{vt}^{s\ell}$ in airlift pumps are low (less than 20%).

factor α	Valid Re_p region
4,65	$Re_p < 0,2$
$4,35 \, R_{ep}^{-0,03}$	$0.2 < Re_p < 1$
$4,45 \, R_{ep}^{-0,1}$	$1 < Re_p < 500$
2,29	$Re_p > 500$

TABLE 4.1 : Hindered settling factor (α)

For typical marine gravels, larger than 2 mm diameter, Equations 4.20, 4.21 and 4.23 are combined to yield the hindered settling velocity of a non-spherical particle to be :

$$v'_t = 0,7 \times \left[0,981\, d^{\frac{1}{2}} \sqrt{(\rho_s - \rho_l)\, g\, \pi/\rho_l}\right] (1 - C_{vt}^{sl})^{2.4} \qquad (4.24)$$

Allowance for particle sizes

A marine gravel sample consists of a particle size distribution (PSD). Thus it is necessary to calculate the contribution to the solid *in situ* volumetric concentration by each particle size present.

A sieve analysis of the sample would show the amount and sizes of particles present in a sample. For each particle size, the non-spherical hindered settling velocity is calculated.

From Equations 4.12, 4.13, 4.21 and 4.23, the relationship between the *in situ* concentration, the delivered concentration, the mixture velocity and the hindered settling velocity for *one* particle size is given by the implicit equation :

$$C_{vt}^{sl} = \left[\frac{v_m^{sl}}{v_m^{sl} - S_f\, v_{tsph}\, (1 - C_{vt}^{sl})^a}\right] C_{vd}^{sl} \qquad (4.25)$$

For a range of particle sizes, Equation 4.25 is applied for each particle size and multiplied by its "percentage present" (R). The "percentage present" is obtained from the sieve analysis (percentage retained on each sieve).

$$C_{vt}^{sl} = C_{vd}^{sl} v_m^{sl} \left[\frac{R_1}{v_m^{sl} - S_f v_{t_1} (1 - C_{vt}^{sl})^a} + \right. \tag{4.26}$$

$$\left. \frac{R_1}{v_m^{sl} - S_f v_{t_2} (1 - C_{vt}^{sl})^a} + \ldots \right]$$

Equation 4.26 is solved implicitly, to yield the *in situ* concentration for a range of particle sizes in a vertically moving solid-liquid mixture.

4.4.3 Shear stress of the solid-liquid mixture (τ_{om}^{sl})

Apart from the weight, the other component required for predicting the pressure loss in the suction pipe (Equation 4.5) is the shear stress of the solid-liquid mixture at the pipe wall (τ_{om}^{sl}).

In a vertically moving solid-liquid mixture consisting of marine gravels, it is expected that the particles move to the centre of the pipe resulting in predominantly liquid being in contact with the pipe wall. If the amount of fines in the liquid are sufficiently low, as not to change the viscosity, the clear water friction factor is used.

Thus the shear stress is expressed as :

$$\tau_{om}^{sl} = \tfrac{1}{2} \rho_l (v_m^{sl})^2 f^{sl} \tag{4.27}$$

The clear water friction factor is evaluated according to Churchill (Chisholm, 1983) for all Reynolds numbers (refer Figure 8.9).

Thus $f^{sl} = f^{l}$ = clear water friction factor

$$f^{l} = 2\left[\left(\frac{8}{Re}\right)^{12} + \left(\frac{1}{A+B}\right)^{3/2} \right]^{1/12} \qquad (4.28)$$

where $A = \left(2{,}457 \times \log\left(\frac{1}{\left(\frac{7}{Re}\right)^{0,9}} + 0{,}27\,\frac{k}{D} \right)\right)^{16}$

$B = \left(\frac{37\,530}{Re}\right)^{16}$

Re = Equation 3.43 .

4.5 AIR INJECTOR PARAMETERS (Δp_3)

4.5.1 Summary of variables

The effect of the air injector has been omitted in most literature. This pressure drop (Δp_3) is calculated by applying the momentum force equation to a control volume between points D and E on Figure 4.1.

$$\left[(P + \rho_m^{sl} (v_m^{sl})^2)\, A \right]^{\text{at D}} \uparrow = \left[(P + \rho_m^{slg} (v_m^{slg})^2)\, A \right]^{\text{at E}} \downarrow + W_m^{slg} \downarrow + \tau_{om}^{slg}\, \pi\, D\, l \downarrow \qquad (4.29)$$

where P = absolute pressure

ρ_m^{sl} = density of the solid-liquid mixture before air injection

ρ_m^{slg} = density of the solid-liquid-gas mixture after air injection

v_m^{sl} = average velocity of the solid-liquid mixture before air injection

v_m^{slg} = average velocity of the solid-liquid-gas mixture after air injection

A = pipe cross-sectional area

$W_m^{s\ell g}$ = weight of the solid-liquid-gas mixture

$\tau_{om}^{s\ell g}$ = shear stress at the pipe wall due to the vertically moving solid-liquid-gas mixture.

It is assumed that the control volume between points D and E is small compared with the total airlift pump suction and delivery pipe lengths. Therefore, the weight ($W_m^{s\ell g}$) and shear stress ($\tau_{om}^{s\ell g}$) are assumed to have a negligible effect on the pressure drop and Equation 4.26 can be rewritten as :

$$\Delta p_3 = P_D - P_E = - \left[\rho_m^{s\ell} \, (v_m^{s\ell})^2 \right]^{\text{at D}} + \left[\rho_m^{s\ell g} \, (v_m^{s\ell g})^2 \right]^{\text{at E}} \qquad (4.30)$$

A separated flow model is now assumed, and the momentum terms in Equation 4.30 are expanded as follows :

Momentum pressure ***before*** air injection

$$\left[\rho_m^{s\ell} \, (v_m^{s\ell})^2 \right]^{\text{at D}} = \rho_s \, C_{vt}^{s\ell} \, v_s^2 + \rho_\ell \, (1 - C_{vt}^{s\ell}) \, v_\ell^2 \qquad (4.31)$$

where ρ_s and ρ_ℓ = density of the solids and liquid respectively

$C_{vt}^{s\ell}$ = solid *in situ* volumetric concentration in the solid-liquid mixture

v_s and v_ℓ = velocity of the solids and liquid respectively.

Momentum pressure *after* air injection

$$\left[\rho_m^{s/g} \, (v_m^{s/g})^2 \right]^{\text{at E}} = \rho_s \, C_{vt}^{s/g} \, v_s^2 + \rho_l \, (1 - C_{vt}^{s/g} - \epsilon_g^{s/g}) \, v_l^2 + \rho_g \, \epsilon_g^{s/g} \, v_g^2 \qquad (4.32)$$

where $C_{vt}^{s/g}$ = solid *in situ* volumetric concentration in the solid-liquid-gas mixture

ρ_g = density of the gas

$\epsilon_g^{s/g}$ = gas *in situ* volumetric concentration in the solid-liquid-gas mixture

v_g = velocity of the gas.

To evaluate the pressure drop across the air injector (Δp_3) using Equations 4.31 and 4.32, the following parameters have to be calculated :

1. $C_{vt}^{s/l}$ - solid *in situ* volumetric concentration in the solid-liquid mixture

2. $C_{vt}^{s/g}$ - solid *in situ* volumetric concentration in the solid-liquid-gas mixture

3. $\epsilon_g^{s/g}$ - gas *in situ* volumetric concentration in the solid-liquid-gas mixture.

Evaluation of the two phase solid *in situ* volumetric concentration ($C_{vt}^{s/l}$) has been discussed in Section 4.4.2 in detail.

Evaluation of the three phase solid and gas in situ volumetric concentrations (C_{vt}^{slg} and ϵ_g^{slg}) will be discussed in Section 4.6 under the heading "delivery pipe parameters". The reason being that these variables are also required here and the calculation procedure is the same.

4.6 DELIVERY PIPE PARAMETERS (Δp_4)

4.6.1 Summary of variables

Moving vertically up the delivery pipe from points E to F on Figure 4.1, the pressure decreases, resulting in isothermal expansion of the gas phase.

To model this effect, ideal gas conditions are assumed and Boyle's Law is applied :

$$Q_{gx} = \frac{Q_{gSTP}\, P_{STP}}{P_x}$$

where Q_{gx} = gas flow rate at any level x in the airlift pump delivery pipe

P_x = absolute pressure at the same level x

Q_{gSTP} = gas flow rate at standard atmospheric conditions

P_{STP} = absolute pressure at standard atmospheric conditions.

The isothermal expansion effect results in a nonlinear pressure change, and consequently pressures are analysed over small increments up the delivery pipe. These increments are then integrated over the entire airlift pump delivery pipe length. Govier (1972) suggests that for liquid-gas flow each increment length pressure change should not exceed the upstream pressure by more than 10 percent.

To calculate the pressure change in one such increment in the delivery pipe, the momentum force equation is again applied.

$$\left[(P + \rho_m^{s\ell g} (v_m^{s\ell g})^2) A \right]^{Bottom} \uparrow = \left[(P + \rho_m^{s\ell g} (v_m^{s\ell g})^2) A \right]^{Top} \downarrow + W_m^{s\ell g} \downarrow + \tau_{om}^{s\ell g} \pi D \ell \downarrow \quad (4.33)$$

where Top and Bottom refer to the incremental step and

P = absolute pressure

$\rho_m^{s\ell g}$ = density of the solid-liquid-gas mixture

$v_m^{s\ell g}$ = average velocity of the solid-liquid-gas mixture

$W_m^{s\ell g}$ = weight of the solid-liquid-gas mixture in the delivery pipe increment

$\tau_{om}^{s\ell g}$ = shear stress on the pipe wall due to the solid-liquid-gas mixture

D = pipe diameter

ℓ = incremental pipe length.

Dividing by the pipe area and rearranging, Equation 4.33 can be expressed as :

$$\Delta p_{inc} = P_{Bottom} - P_{Top} = - \left[\rho_m^{s\ell g} (v_m^{s\ell g})^2 \right]^{Bottom} + \left[\rho_m^{s\ell g} (v_m^{s\ell g})^2 \right]^{Top} + \frac{W_m^{s\ell g}}{A} + \tau_{om}^{s\ell g} \frac{\pi D \ell_{inc}}{A} . \quad (4.34)$$

where Δp_{inc} is the pressure loss across one increment in the delivery pipe.

These increments are consequently summed up as shown in Equation 4.35.

$$\Delta p_4 = \sum_{E}^{F} \Delta p_{inc} \qquad (4.35)$$

4.6.2 Solid-liquid-gas mixture weight (W_m^{slg})

The weight of the solid-liquid-gas mixture (W_m^{slg}) in Equation 4.34 can be expressed as :

$$W_m^{slg} = \rho_m^{slg}\, g\, l_{inc}\, A \qquad (4.36)$$

To calculate the solid-liquid-gas mixture weight using Equation 4.36 it is first necessary to evaluate the solid-liquid-gas density (ρ_m^{slg}).

Solid-liquid-gas mixture density (ρ_m^{slg})

The density of the solid-liquid-gas mixture in the delivery pipe can be expressed as the sum of the densities of each of the phases multiplied by their *in situ* volumetric concentrations. Thus :

$$\rho_m^{slg} = \rho_s\, C_{vt}^{slg} + \rho_l\, (1 - C_{vt}^{slg} - \epsilon_g^{slg}) + \rho_g\, \epsilon_g^{slg} \qquad (4.37)$$

where C_{vt}^{slg} = solid *in situ* volumetric concentration in the 3 phase solid-liquid-gas mixture

ϵ_g^{slg} = gas *in situ* volumetric concentration in the 3 phase solid-liquid-gas mixture.

Substitution of Equation 4.37 into 4.36 will result in an equation identical to Equation 3.9 which is used throughout the literature.

Solid *in situ* volumetric concentration - three phase ($C_{vt}^{s/g}$)

The solid *in situ* volumetric concentration in the three phase mixture is calculated using a modified Equation 4.25 :

As before (Section 4.4.2) the solid *in situ* volumetric concentration is defined as the ratio of volume of solids to volume of mixture. In the case of three phase flow this is expressed as :

$$C_{vt}^{s/g} = \frac{v_s}{v_m^{s/g}} = \frac{A_s}{A_m^{s/g}} \tag{4.38}$$

Likewise, the solid delivered volumetric concentration is defined as the flow of solids to the flow of mixture.

$$C_{vd}^{s/g} = \frac{Q_s}{Q_m^{s/g}} = \frac{v_s\ A_s}{v_m^{s/g}\ A_m^{s/g}} \tag{4.39}$$

Combining Equations 4.39 and 4.38 and including the non-spherical, hindered settling velocities for each particle size in a similar manner as described in Section 4.4.2, it can be shown that the solid *in situ* volumetric concentration in a three phase mixture is given by :

$$C_{vt}^{s/g} = C_{vd}^{s/g}\ v_m^{s/g} \left[\frac{R_1}{v_m^{s/g} - S_f\ v_{tsph1}} + \frac{R_2}{v_m^{s/g} - S_f\ v_{tsph2}} + \ldots \right] \tag{4.40}$$

The settling velocity of particles in a liquid-gas mixture have been extensively researched (refer to Chapter 8, Section 8.2) and it was observed that no particle interaction took place, hence the hindered settling correction $(1 - C_{vt}^{s\ell})^a$ has been omitted in Equation 4.40.

Gas *in situ* volumetric concentration - three phase ($\epsilon_g^{s\ell g}$)

To calculate the gas *in situ* concentration in the solid-liquid-gas mixture the technique presented by Zuber and Findlay (1965), verified by Berg (1988a) for calculating the *in situ* concentration of gas in a liquid-gas mixture is expanded to include the solid phase.

Zuber and Findlay suggest that the vertical mean upward velocity of the gas (v_g) is the sum of the mean mixture velocity $v_m^{s\ell g}$ and the rise velocity of a single bubble. An empirical factor $C_{s\ell}$ is used to correct for the central position of the gas bubbles in the pipe cross-section. Hence :

$$v_g = C_{s\ell} (v_m^{s\ell g}) + v_B^{s\ell} \qquad (4.41)$$

Using continuity relationships, Equation 4.41 can be rewritten as :

$$\frac{1}{\epsilon_g^{s\ell g}} \left(\frac{Q_g}{A}\right) = C_{s\ell} \left(\frac{Q_s}{A} + \frac{Q_\ell}{A} + \frac{Q_g}{A}\right) + v_B^{s\ell} \qquad (4.42)$$

This equation is also presented by Giot (1982). For the distribution parameter ($C_{s\ell}$) it is suggested that the same value be used as for liquid-gas flow (i.e. $C_{s\ell} = 1.2$). The bubble rise velocity ($v_B^{s\ell}$)

would be expected to remain unchanged due to the low concentration of solids. This variable can be expressed using the drift velocity of a Taylor bubble (Berg 1988a).

$$v_B^{sl} = 0,35\ (gd)^{\frac{1}{2}} \qquad (4.43)$$

4.6.3 Shear stress of the solid-liquid-gas mixture (τ_{om}^{slg})

Analogous to the shear stress of a solid-liquid mixture (Section 4.4.3), the shear stress of the solid-liquid-gas mixture with the pipe wall (τ_{om}^{slg}) can be expressed as :

$$\tau_{om}^{slg} = \tfrac{1}{2}\ \rho\ (v_m^{slg})^2\ f^{slg} \qquad (4.44)$$

where f^{slg} = friction factor of solid-liquid-gas mixture.

It is proposed that two phase liquid-gas shear stress assumptions are used to calculate the shear stress of the three phase mixture with the pipe wall. This assumption is based on the argument that the solid *in situ* volumetric concentrations are low with respect to the other two phases. It is also assumed that the solids are largely located towards the centre of the pipe in the faster moving section.

To calculate the shear stress of a two phase liquid-gas mixture, with the pipe wall, Berg (1987) obtained favourable approximations using a modification to the theory presented by Clark (1986).

Clark (1986) uses the Lockhart and Martinelli two phase multiplier to relate the shear stress of a liquid-gas mixture with the pipe wall, to the shear stress if a single phase liquid was flowing under the same conditions.

$$\tau_{om}^{lg} = \left[\tfrac{1}{2} \rho_l \, (v_m^{lg})^2 \, f^l \right] \phi_{Fl}^2 \qquad (4.45)$$

where v_m^{lg} = mean liquid-gas mixture velocity

ρ_l = density of the liquid

f_l = friction factor of the liquid

ϕ_{Fl}^2 = Lockhart and Martinelli two phase multiplier.

For the two phase multiplier, Clark suggests using a Maclaurin expansion truncated to the second term of an empirical correlation presented by Orikizewski (Clark 1985).

$$\phi_{Fl}^2 = (1 + 1.8 \, \epsilon_g^{lg}) \qquad (4.46)$$

where ϵ_g^{lg} = gas *in situ* volumetric concentration in the liquid-gas mixture.

Clark however concludes that, for slug flow, a factor of 1,5 instead of 1,8 in Equation 4.46 is a better approximation. Thus,

$$\phi_{Fl}^2 = (1 + 1,5 \, \epsilon_g^{lg}) \qquad (4.47)$$

The <u>modification</u> that is proposed involves using the liquid velocity (v_l) instead of the mixture velocity (v_m^{sl}) in Equation 4.45. The liquid velocity in a three phase mixture would be :

$$v_l = \frac{Q_l}{(1 - C_{vt}^{slg} - \epsilon_g^{slg}) \, A} \qquad (4.48)$$

It is furthermore proposed to use the same two phase multiplier as suggested by Clark. The shear stress of the solid-liquid-gas mixture with the pipe wall can thus be evaluated using :

$$\tau_{om}^{s\ell g} = \left[\tfrac{1}{2} \rho_{\ell} (v_{\ell})^2 f^{\ell} \right] (1 + 1{,}5\ \epsilon_g^{s\ell g}) \qquad (4.49)$$

4.6.4 Solid-liquid-gas momentum pressure

The momentum pressure at the top and bottom of the increment are the terms $\left[\rho_m^{s\ell g} (v_m^{s\ell g})^2 \right]^{Bottom}$ and $\left[\rho_m^{s\ell g} (v_m^{s\ell g})^2 \right]^{Top}$ in Equation 4.34. These two terms can be expanded and expressed using the separated flow model and the method discussed in Section 4.5 and Equation 4.31 previously.

4.7 SUMMARY OF ALL VARIABLES

Table 4.2 lists all equations used in the proposed 3 phase analysis technique. The equation numbers given in the tables correspond to this chapter.

ANALYSIS ITEM	EQUATION NO

1. $\Delta p_1 - \Delta p_2 - \Delta p_3 - \Delta p_4 = 0$ (4.1)

2. $$\Delta p_1 = (\ell_1 + \ell_2)\,\rho_\ell g - \rho_m^{s\ell}\, g \left[\frac{(v_m^{s\ell})^2}{2g} + \xi_e \frac{(v_m^{s\ell})^2}{2g}\right]$$ (4.3)

3. $$\Delta p_2 = \frac{W_m^{s\ell}}{A} + \tau_{om}^{s\ell} \frac{\pi D\, \ell_2}{A}$$ (4.5)

$$W_m^{s\ell} = \left[\rho_s C_{vt}^{s\ell} + \rho_\ell (1 - C_{vt}^{s\ell})\right] g\, \ell_2\, A$$ (4.8)

$$C_{vt}^{s\ell} = C_{vd}^{s\ell}\, v_m^{s\ell} \left[\frac{R_1}{v_m^{s\ell} - S_f\, v_{t_1} (1 - C_{vt}^{s\ell})^a} + \frac{R_2}{v_m^{s\ell} - S_f\, v_{t_2} (1 - C_{vt}^{s\ell})^a} + \ldots\right]$$ (4.26)

$$\tau_{om}^{s\ell} = \tfrac{1}{4}\, \rho\, (v_m^{s\ell})^2\, f^{s\ell}$$ (4.27)

4. $$\Delta p_3 = -\left[\rho_m^{s\ell}\, (v_m^{s\ell})^2\right]^{\text{Before}} + \left[p_m^{s\ell g}\, (v_m^{s\ell g})^2\right]^{\text{After}}$$ (4.30)

$$\left[\rho_m^{s\ell}\, (v_m^{s\ell})^2\right]^{\text{Before}} = \rho_s C_{vt}^{s\ell}\, v_s^2 + \rho_\ell (1 - C_{vt}^{s\ell})\, v_\ell^2$$ (4.31)

$$\left[p_m^{s\ell g}\, (v_m^{s\ell g})^2\right]^{\text{After}} = \rho_s C_{vt}^{s\ell g}\, v_s^2 + \rho_\ell (1 - C_{vt}^{s\ell g} - \epsilon_g^{s\ell g})\, v_\ell^2 + \rho_g\, \epsilon_g^{s\ell g}\, v_g^2$$ (4.32)

$C_{vt}^{s\ell}$ = in Equation (4.26)

$C_{vt}^{s\ell g}$ = in Equation (4.40)

$\epsilon_g^{s\ell g}$ = in Equation (4.42)

5. $$\Delta p_{inc} = -\left[\rho_m^{s\ell g}\, (v_m^{s\ell g})^2\right]^{\text{Bottom}} + \left[\rho_m^{s\ell g}\, (v_m^{s\ell g})^2\right]^{\text{Top}} + \frac{W_m^{s\ell g}}{A} + \tau_{om}^{s\ell g} \frac{\pi D \ell}{A}$$ (4.34)

$\rho_m^{s\ell g}\, (v_m^{s\ell g})^2\big]^{\text{Bottom and Top}}$ = as in Equation (4.31)

$$W_m^{s\ell g} = \left[\rho_s C_{vt}^{s\ell g} + \rho_\ell (1 - C_{vt}^{s\ell g} - \epsilon_g^{s\ell g}) + \rho_g\, \epsilon_g^{s\ell g}\right] g\, \ell_3\, A$$ (4.36) and (4.37)

$$C_{vt}^{s\ell g} = C_{vd}^{s\ell g}\, v_m^{s\ell g} \left[\frac{R_1}{v_m^{s\ell g} - S_f\, v_{tsph1}} + \frac{R_2}{v_m^{s\ell g} - S_f\, v_{tsph2}} + \ldots.\right]$$ (4.40)

$$\frac{1}{\epsilon_g^{s\ell g}} \left(\frac{Q_g}{A}\right) = 1{,}2 \left(\frac{Q_s}{A} + \frac{Q_\ell}{A} + \frac{Q_g}{A}\right) + v_B^{s\ell}$$ (4.42)

$$\tau_{om}^{s\ell g} = \tau_o^{\ell g} = \tfrac{1}{4}\, f_\ell\, \rho_\ell\, v_\ell^2 (1 + 1.5\, \epsilon_g^{s\ell g})$$ (4.49)

TABLE 4.2 : Equations for proposed theory

CHAPTER 5

TEST FACILITIES

5.1 INTRODUCTION

Tests are conducted to evaluate :

1. the theories in Chapters 3 and 4 which are used to predict fundamental variables required for the analysis of 3 phase flow in airlift pumps,
2. the complete analysis technique presented in Chapter 4,
3. the operation of airlift pumps under a range of different conditions.

Some of the variables in item 1 above are best observed in installations other than airlift pumps, where only the required component is measured. Other variables however need to be measured in prototype or model airlift pump installations.

For this purpose, tests are performed in the following experimental installations :

1. two-phase solid-liquid pipeline test facility
2. settling tube
3. 40 mm airlift pump
4. 90 mm airlift pump.

In this chapter, the above test installations are described. Specific measurements taken on these installations are discussed in Chapter 6.

5.2 TWO PHASE PIPELINE TEST FACILITY

5.2.1 Introduction

The Hydrotransport Research pipeline test facility at the University of Cape Town consists of two pipelines. This test facility is primarily used to examine the behaviour of conveyed solid-liquid two-phase mixtures. Effects of varying concentration, densities and particle sizes can be measured for a range of mixture velocities.

The use of this test facility in the airlift pump investigation is to measure variables which would be encountered in the airlift pump suction pipe. The vertical limbs of this test installation are ideal for this purpose.

5.2.2 Description

A schematic of the pipe test loop facility is shown in Figure 5.1. It consists, amongst others, of :

1. a small and large diameter pipeloop
2. a centrifugal slurry pump (B)
3. a feed hopper (A)
4. a weigh tank (G)
5. computer data logging equipment (H,I,J)
6. various other measurement devices (C,D,E).

Table 5.1 below gives the dimensions of the two pipelines in which the tests were conducted.

Figure : 5.1
Description : TWO PHASE PIPELINE TEST FACILITY

Airlift Pump
Investigation

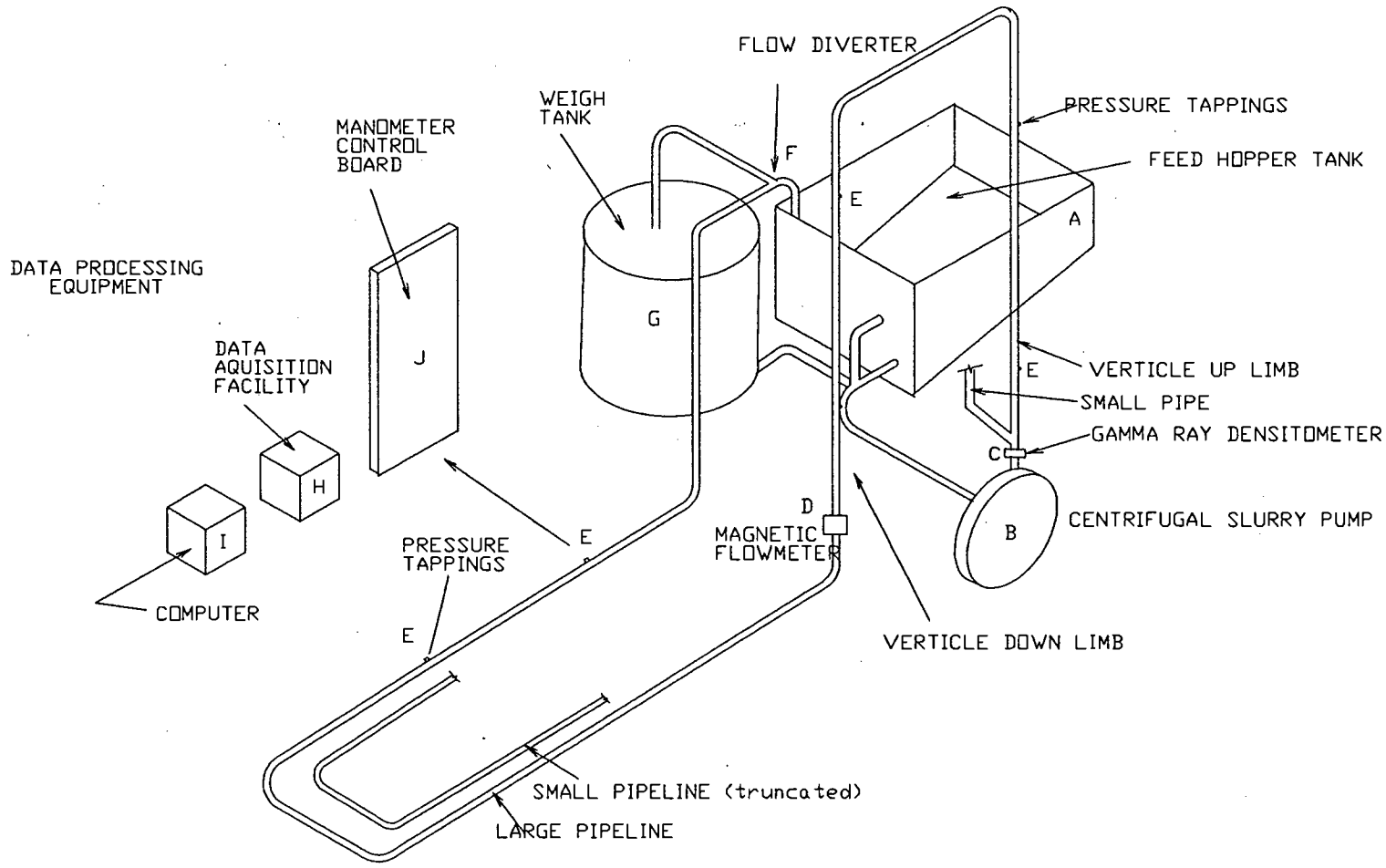

Nominal Diameter (mm)	Actual Inside Diameter (mm)	Pipe Class	Wall Thickness (mm)
90	79,715	12	5
160	139,3	12	10

TABLE 5.1 : Two phase pipeline dimensions

During operation, the test material is pumped along either of the pipelines by switching valves located near the pump outlet.

Referring to Figure 5.1, the test material is loaded into the feed hopper tank (A). From here it is pumped with the centrifugal slurry pump (B) along the desired pipeline.

At first the pipeline rises vertically for approximately 3 metres. Located in this uplimb is a gamma ray densitometer (C) which records the solid *in situ* volumetric concentration in the two phase slurry. After a short horizontal limb at the top, the material is pumped through the downlimb back to ground level. A magnetic flow meter (D) is located near the bottom of the downlimb to monitor mixture velocity in the pipe.

The flow then continues in a long horizontal limb back to the feed hopper.

Various pressure tappings (E) are provided along the pipe length for measuring pressure changes in the up, down and horizontal pipeline limbs.

A flow diverter valve (F) is located near the delivery outlet of the horizontal limb. This is to divert flow into the weigh tank (G) for the calibration of the magnetic flow meter.

The output from all measurement equipment is relayed via a data acquisition facility (H) to a computer (I) where the output is continuously monitored with the aid of inhouse computer software.

A manometer control board (J) is used to monitor pressure fluctuations from the pressure tappings. The fluctuations are also relayed via transducers to the data acquisition facility. The manometer control board serves to calibrate the transducers and to provide a constant check on pressures during operation.

Note : A more detailed description of the test equipment is available in the operator's manual for this equipment (Sive 1988).

5.3 SETTLING TUBE

5.3.1 Introduction

A 12 m high settling tube exists in the hydraulics tower at the University of Cape Town. This tube is used to monitor settling and hindered settling behaviour of particles in liquid only.

Alterations to this equipment allowed air to be injected at the base of the settling tube.

The use of this test facility in the airlift pump investigation is to measure particle settling behaviour in liquid-gas mixtures.

5.3.2 Description

Figure 5.2 shows a schematic of the settling tube. It consists of 0,15 m diameter transparent perspex sections, which are flanged together to form the 12 m high standpipe.

Referring to the Figure 5.2 , a catch box (B) is located underneath a gate valve (C). This allows the test particles to be retrieved without having to drain the standpipe.

For the purpose of measuring the settling and hindered settling behaviour of solids in a two-phase liquid-gas mixture, air is allowed to bubble into the catch box (B) through a 25,4 mm nozzle located at (A). The input air flow rate is regulated with a ball valve and is measured with two pressure tappings from an orifice plate.

A range of measurement sections (D) and (E) are demarcated along the settling tube length. Pressure tappings located at these sections lead to manometers via isolation pods, to allow absolute pressure measurement.

During operation, the particles are released into the top of the standpipe, and their settling velocities are measured using stopwatches.

Figure : 5.2
Description : SETTLING TUBE

Airlift Pump
Investigation

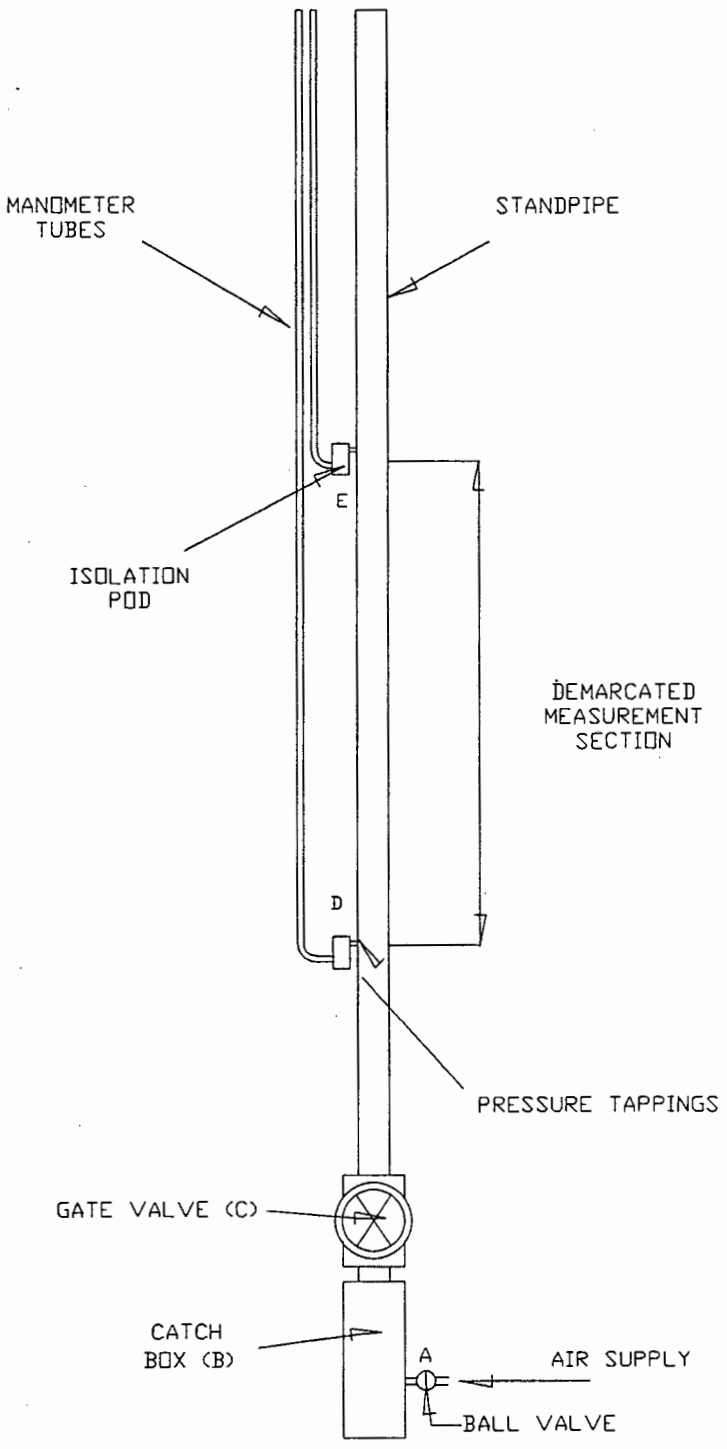

5.4 AIRLIFT PUMPS

5.4.1 Introduction

For the purpose of monitoring and measuring specific variables used to predict airlift pumps and their performance under a range of operating conditions, two research installations were designed and constructed.

The two airlift pumps differ essentially in scale with delivery pipe and test section lengths as long as possible to minimise the possibility of imperfect flow development. The delivery pipe diameters and length over diameter ratios (ℓ/D) are :

A. 40 mm nominal bore (ℓ/D = 45)

B. 90 mm nominal bore (ℓ/D = 105)

The 40 mm nominal bore airlift pump was later replaced with a 50 mm nominal bore delivery pipe.

Both airlift pumps are recirculating systems constructed of transparent PVC pipe, to facilitate vizual observation during testing.

5.4.2 Description - 40 mm NB airlift pump

Figure 5.3 shows a schematic of the 40 mm airlift pump research apparatus.

The apparatus is constructed of 36 mm internal diameter clear PVC pipe throughout. Referring to the schematic in Figure 5.3 , a constant head tank (A) is used to provide a static pressure at the air injection points (B). During operation, the test material is loaded into this constant head tank through the air vent (C) located at the top.

Figure : 5.3
Description : 40mm AIRLIFT PUMP EXPERIMENTAL APPARATUS

Airlift Pump Investigation

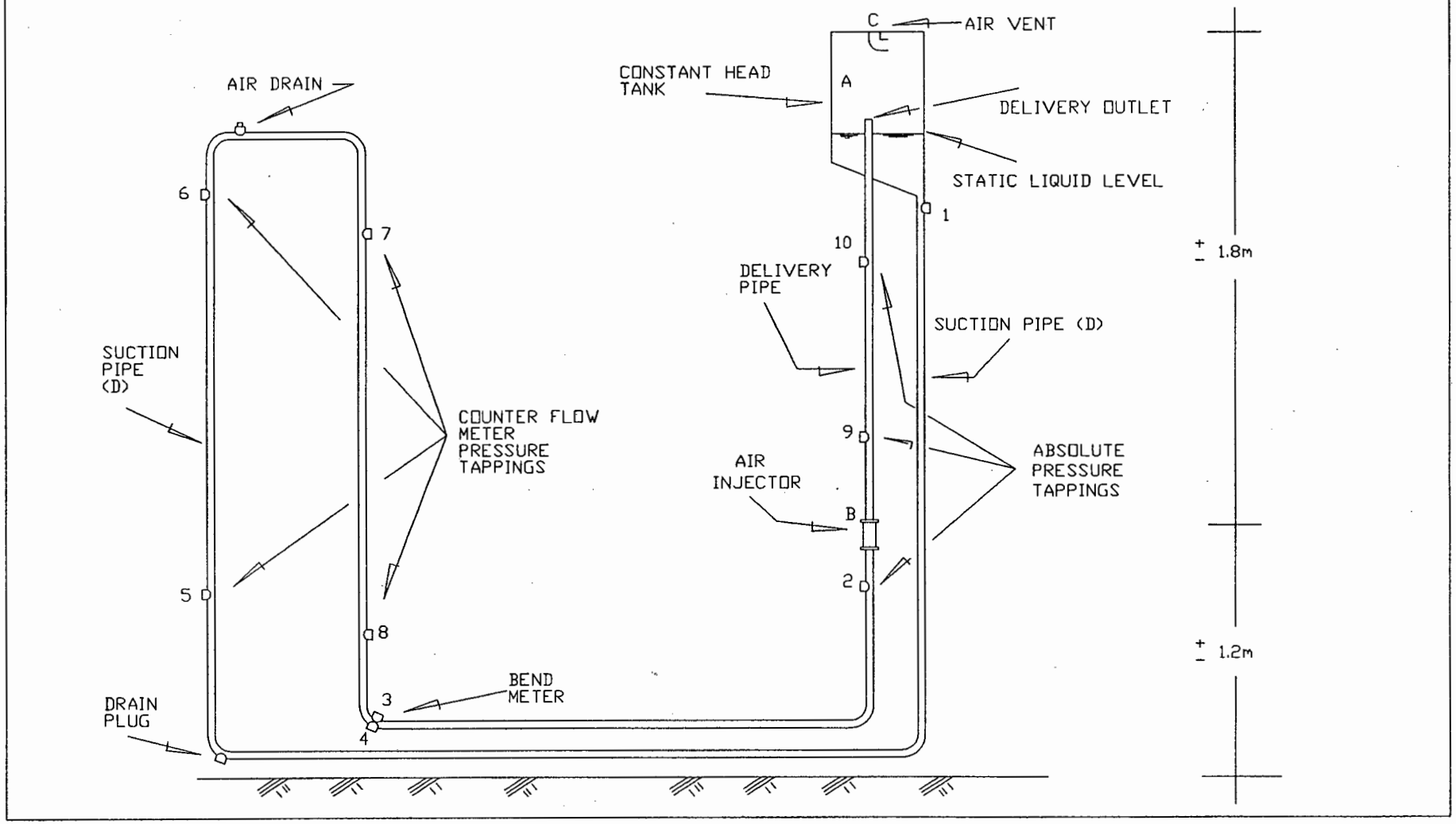

The constant head tank outlet is connected to the suction pipe (D), which ends at the base of the air injectors.

Most of the measurements in the 40 mm airlift pump takes place in the suction pipe, which also forms the return line for the recirculating systems. These measurements are in the form of pressure tappings for measuring pressure fluctuations.

Pressure tapping points 1 and 2 are used to monitor absolute pressures before air injection. Tapping points 3 and 4 are located on the inside and outside radius of an elbow which form a bendmeter for measuring mixture velocities and flows.

Four further pressure tappings, two of which are located in the uplimb (5 and 6), and two are located in the downlimb (7 and 8) are used to measure solid-liquid delivered concentrations. These tappings form a counterflow meter.

The 40 mm airlift pump is fitted with an inline air injector.

Air is allowed to enter the airlift pipe through holes in a horizontal direction (refer to Figure 5.4). The injector consists of a 40 mm nominal bore pipe surrounded by a 50 mm nominal bore pipe which has blanked off annular openings at either end. Air is injected into the annular chamber and enters the airlift pump via holes drilled at regular intervals into the inner 40 mm nominal bore pipe. The injector is easily dismantled for cleaning purposes.

Figure : 5.4
Description : 40mm AIRLIFT PUMP AIR INJECTOR

Airlift Pump
Investigation

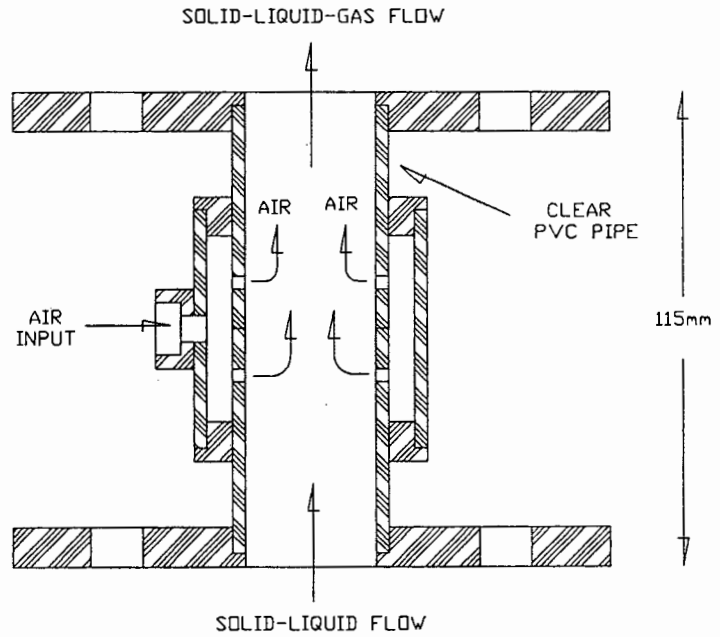

Referring to Figure 5.3 the delivery pipe starts at the top of the air injectors and rises vertically for ± 1,8 m entering into the constant head tank through its base. The delivery outlet is located ± 0,25 m inside the constant head tank which is vented to atmopshere through air vent (C) mentioned before.

Pressure tappings 9 and 10 are used to measure absolute pressures after air injection.

The static pressure and lift height are adjusted by altering the level in the constant head tank. This is achieved by adding or draining liquid from the system.

5.4.3 Description - 40 mm airlift pump with a 50 mm NB delivery pipe

For the purpose of measuring solid, liquid and gas phase *in situ* volumetric concentrations in the airlift pump delivery pipe, two inline knife gate valves were installed. During operation, the knife gate valves are shut off simultaneously, trapping a sample of the pumped slurry between them.

To prevent significant pressure losses across these valves, it was required to match the valve internal diameter with that of the airlift delivery pipe. The 40 mm nominal bore delivery pipe was therefore replaced with a 50 mm nominal bore delivery pipe.

Figure 5.5 shows a schematic of the altered airlift pump delivery pipe.

The knife gate valves are pneumatically activated and synchronized using a series of pneumatic switch valves to ensure instantaneous closure of both valves at the same time.

Three pressure tappings are provided along the delivery pipe to monitor absolute pressures during testing. Tapping 1 is used to measure pressures before air injection, while tappings 2 and 3 give the pressure changes across the *in situ* volumetric concentration measurement section between the two knife gate valves.

A 50 mm nominal bore ball valve is provided below the lower knife gate valve to allow removal of the trapped sample without having to drain the system.

Figure : 5.5
Description : 40mm AIRLIFT PUMP with 50mm DELIVERY PIPE

Airlift Pump Investigation

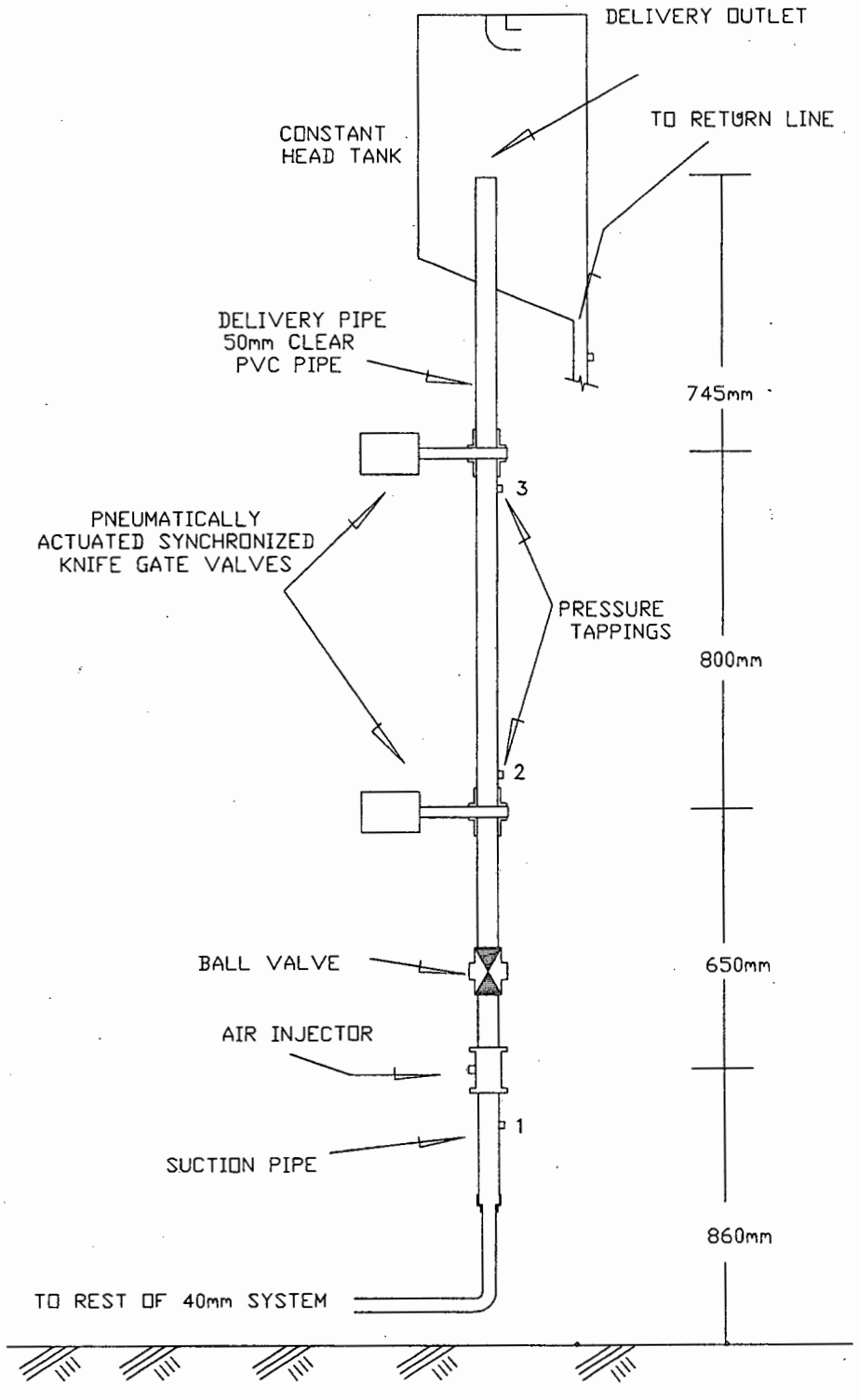

5.4.4 Description - 90 mm NB airlift pump

A schematic of the 90 mm nominal bore airlift pump is shown in Figure 5.6. Referring to the figure, the constant head tank (A) discharges into a pressure vessel (B). The pressure vessel is located ± 4,5 m below the constant head tank, to provide a static head. The discharge is through a 75 mm flexible hose which splits into 2 hoses and enters the pressure vessel on either side of the suction pipe inlet (C). This allows the material to accumulate back in the pressure vessel in a uniform way before being pumped out through the suction pipe located in the centre.

The airlift pump suction inlet (C) is located inside the pressure vessel (B) and exits the vessel via a flanged outlet at the top. Inside the pressure vessel, the suction pipe consists of a 90 mm nominal bore PVC pipe which houses a 75 mm nominal bore PVC pipe. The 75 mm pipe is connected to two push rods which exit the pressure vessel at the top through gland seals. Using the push rods, the 75 mm pipe can be moved telescopically inside the 90 mm PVC pipe. This allows the suction pipe to be extended and retracted.

After exiting the pressure vessel, the suction pipe is joined to the annular air injector (D). A schematic of the air injector is shown in Figure 5.7. It consists of an inner sleeve which can be moved relative to a tapered outer sleeve using a hand wheel. This movement results in a varying annular apperture. Air is injected equally at four points around the circumference of the outer sleeve. This air enters the annular chamber and enters the airlift pump delivery pipe in a vertical direction.

Figure : 5.6
Description : 90mm AIRLIFT PUMP EXPERIMENTAL APPARATUS

Airlift Pump Investigation

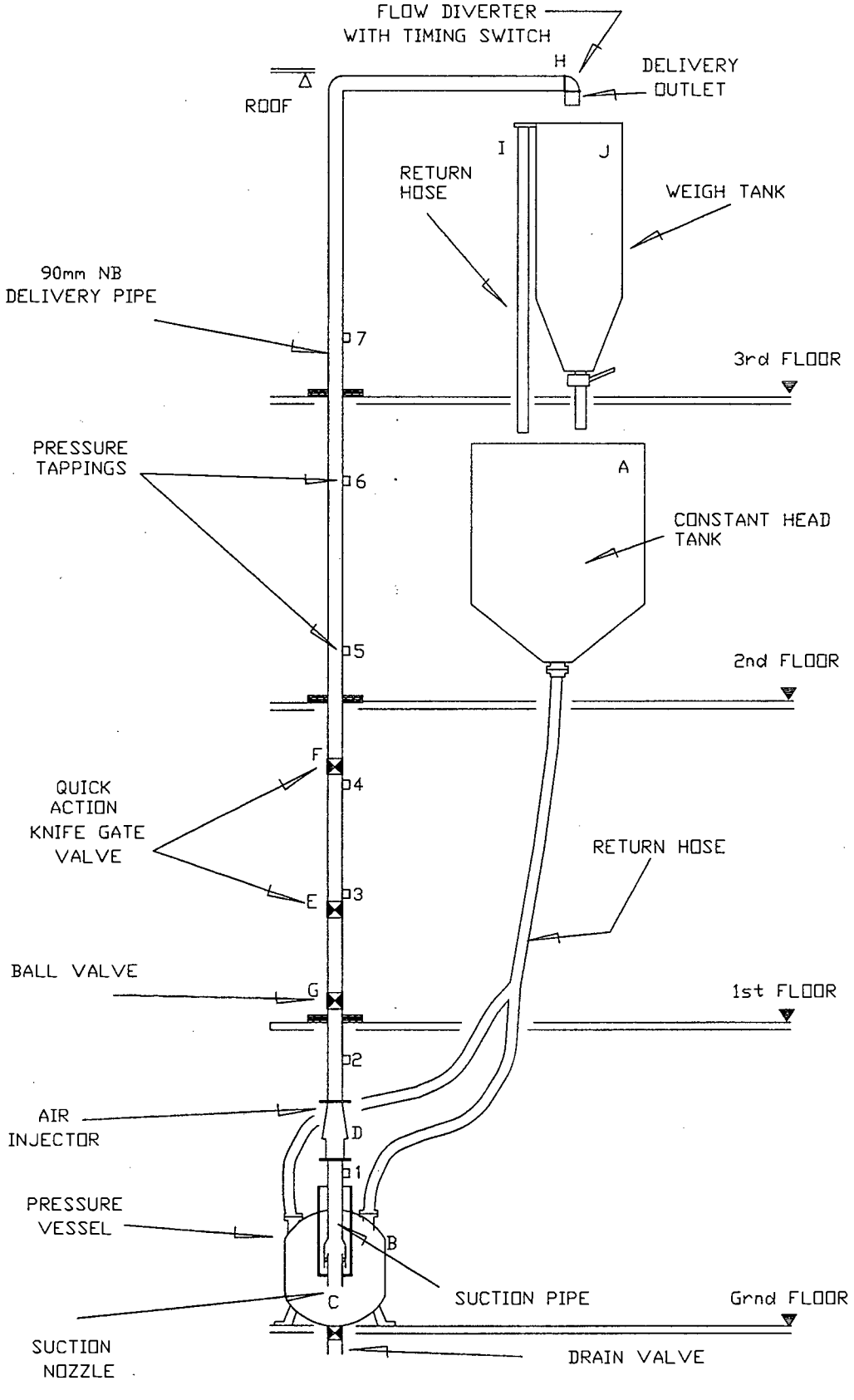

Figure : 5.7
Description : 90mm AIRLIFT PUMP AIR INJECTOR

Airlift Pump
Investigation

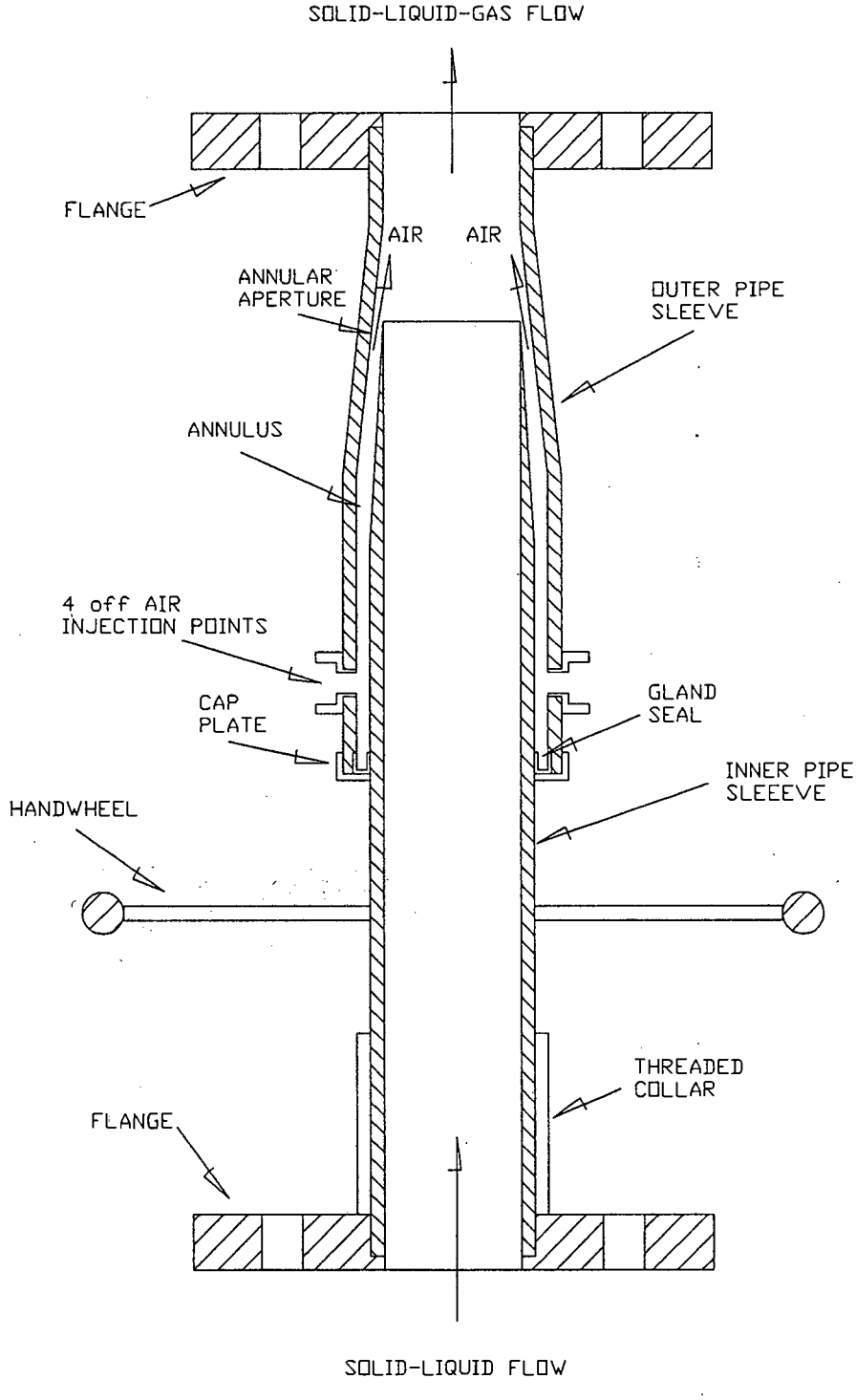

Referring back to Figure 5.6 , the delivery pipe is attached to the top of the air injector. This pipe is constructed of 90 mm nominal bore clear PVC.

Two 90 mm nominal bore pneumatically activated knife gate valves (E and F) are located ± 1,1 m apart for measuring *in situ* concentrations during testing as described before (Section 5.4.3). A further 90 mm nominal bore ball valve (G) is provided below the bottom knife gate valve to allow for the removal of the sample without having to drain the system.

A range of pressure tappings (1 to 7) are located at intervals up the delivery pipe to monitor pressures during operation.

At the top of the delivery pipe, the flow enters a gooseneck flow diverter (H), which is pneumatically activated. Using the diverter, flow can be diverted either to a return hose (I) which discharges back into the constant head tank (A), or to a weigh tank (J) which is used to monitor output flow rates and concentrations. A microswitch connected to a stopwatch is activated halfway through the travel of the gooseneck, for time measurement during sampling. The weigh tank also discharges back into the constant head tank.

CHAPTER 6

MEASUREMENT, CALIBRATION AND ERRORS

6.1 INTRODUCTION

This chapter discusses the measurements, calibration procedures and highest expected error for the variables measured on the facilities described in Chapter 5. Although voluminous literature (e.g. HETSRONI, 1982) is available on three phase flow metering, it was apparent that this equipment would be too expensive in the scope (and budget) of this investigation. Thus use was made of standard techniques.

6.2 DETERMINATION OF MEASUREMENT ERRORS

The highest expected errors of each measured variable is calculated using the following method outlined by Brinkworth (1968).

Considering the quantity, X , to be a function of a range of measured variables, i.e.

$$X = fn\ (a, b, c, \ldots\ldots n) \tag{6.1}$$

The highest expected error is defined as

$$\left(\frac{\delta X}{X}\right) = \sum_{a}^{n} \left(\frac{\partial X}{\partial u}\right)^2 \left(\frac{u}{X}\right)^2 \left(\frac{\partial u}{u}\right)^2 \tag{6.2}$$

where X = measured quantity

δX = expected measurement error in quantity

u = measured variable

∂u = measurement error of variable (u).

For each measurement, the variables required in Equation 6.2 are tabulated while, where applicable, the trend in error is shown graphically for the measurement range.

6.3 TWO PHASE SOLID-LIQUID PIPELINE TEST FACILITY

Table 6.1 summarizes the variables measured on this test facility, and the instruments used for measurement.

No	Variable	Symbol	Units	Instrument
1	Solid-liquid mixture volume flow rate and velocity	Q_m^{sl} & v_m^{sl}	m^3/s & m/s	Magnetic flow meter
2	Solid delivered volumetric concentration	C_{vd}^{sl}	%	Counterflow meter
3	Pressure changes	Δp	Pa	Pressure tappings and transducers
4	Solid *in situ* volumetric concentration	C_{vt}^{sl}	%	Gamma Ray densitometer
5	Particle density and size distributions	ρ_s & PSD	kg/m^3	Sampling and sieving

TABLE 6.1 : Two phase pipeline measurements

6.3.1 Solid-liquid mixture volume flow rate and velocity [Q_m^{sl} & v_m^{sl}]

Measurement

Both pipelines are fitted with inline Magnetic flow meters for measuring solid-liquid mixture velocities and flow rates. The Magnetic flow meters consist of a detection head and signal processor. This provides a direct current output which is proportional to the mean flow velocity through the detection head.

During operation, the current output is relayed via a data acquisition facility to a personal computer. Here it is continuously monitored using inhouse computer software.

Calibration

The Magnetic flow meters are calibrated with clear water using the following procedure :

1. The system is set to run at a low flow rate with clear water.
2. A velocity measurement is recorded with the instrument.
3. The flow is diverted into a weigh tank for a predetermined sample time.
4. The sample mass in the weigh tank and the time of sampling is measured.
5. Items 3 to 4 are repeated for 2 further samples at this flow rate in order to obtain an average reading.
6. Items 2 to 5 are repeated for a range of different flow rates.
7. The calibration equation constants are obtained using linear regression.

Errors

Sive (1988) did extensive tests on the pipeline test facility.

Figures 6.1 a & b show his calculated experimental errors in velocity measurement for the 90 and 160 mm nominal bore pipelines.

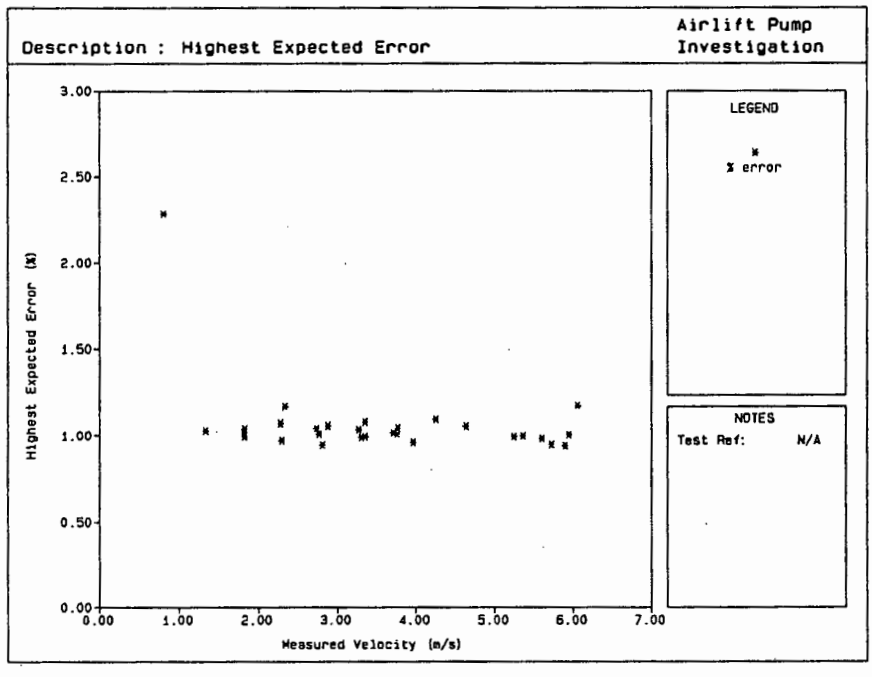

Figure 6.1 a : Sive (1988) - 90 mm NB pipeline velocity measurement errors

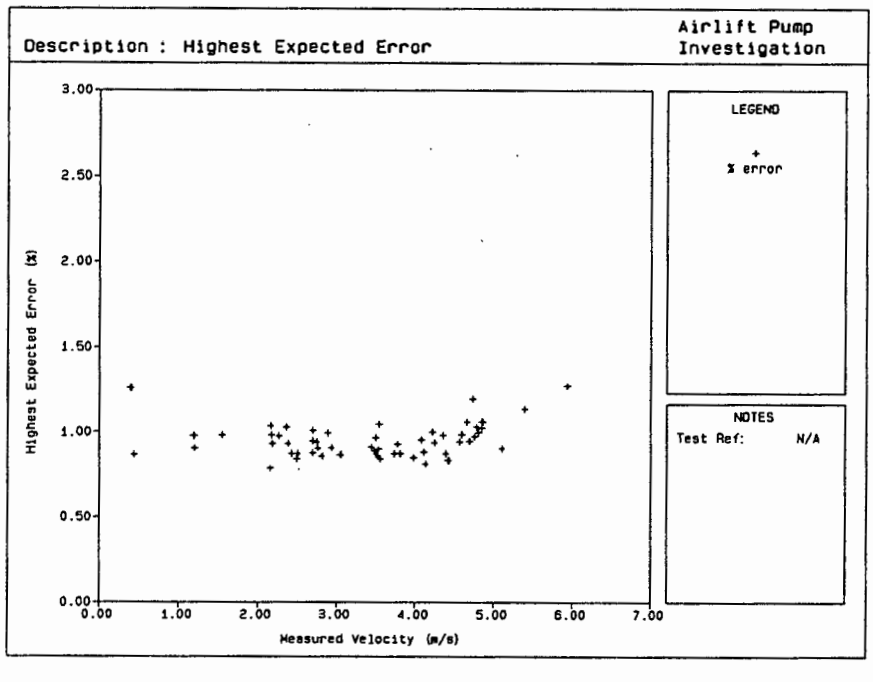

Figure 6.1 b : Sive (1988) - 160 mm NB pipeline velocity measurement errors

6.3.2 Solid delivered volumetric concentration [$C_{vd}^{s\ell}$]

Measurement

A counterflow meter is provided on both pipelines for measuring two-phase solid delivered volumetric concentrations. For the counterflow meter, two differential pressures obtained from four pressure tappings are required. Two of these tappings are located in the uplimb and the other two are located in the downlimb of the pipeline.

The pressures from the tappings are recorded with pressure transducers and manometer tubes. Each pressure transducer provides a voltage output which is monitored with the data acquisition facility and personal computer.

The equation used for converting the differential pressures to the solid-liquid delivered concentration is given by Einstein (1966) as :

$$C_{vd}^{s\ell} = \frac{\Delta h_{UP} - \Delta h_{DOWN}}{2\ L\ (S_s - 1)} \qquad (6.3)$$

Where $C_{vd}^{s\ell}$ = solid delivered volumetric concentration in the two-phase mixture

Δh_{UP} = differential pressure in the uplimb

Δh_{DOWN} = differential pressure in the downlimb

S_w = specific gravity of water

S_s = specific gravity of the solids

L = length of pipeline between the up and down limb pressure tappings. [NOTE: equal lengths between up and down limb pressure tappings].

The relationship between the delivered volumetric concentration ($C_{vd}^{s\ell}$) and the delivered relative density ($S_m^{s\ell}$) is :

$$C_{vd}^{s\ell} = \frac{S_m^{s\ell} - S_w}{S_s - S_w} \qquad (6.4)$$

Thus by suitable substitution and assuming $S_w = 1$, the following equation can be used to convert the two differential pressures to the delivered relative density ($S_m^{s\ell}$).

$$S_m^{s\ell} = \left[\frac{\Delta h_{up} - \Delta h_{down}}{2L} \right] + 1 \qquad (6.5)$$

Calibration

The calibration procedure of differential pressure transducers is discussed in Section 6.3.3.

Errors

Figures 6.2 a and 6.2 b show the experimental errors for the counterflow meter calculated by Sive (1988). The errors are in terms of the delivered relative density ($S_m^{s\ell}$) of the mixture.

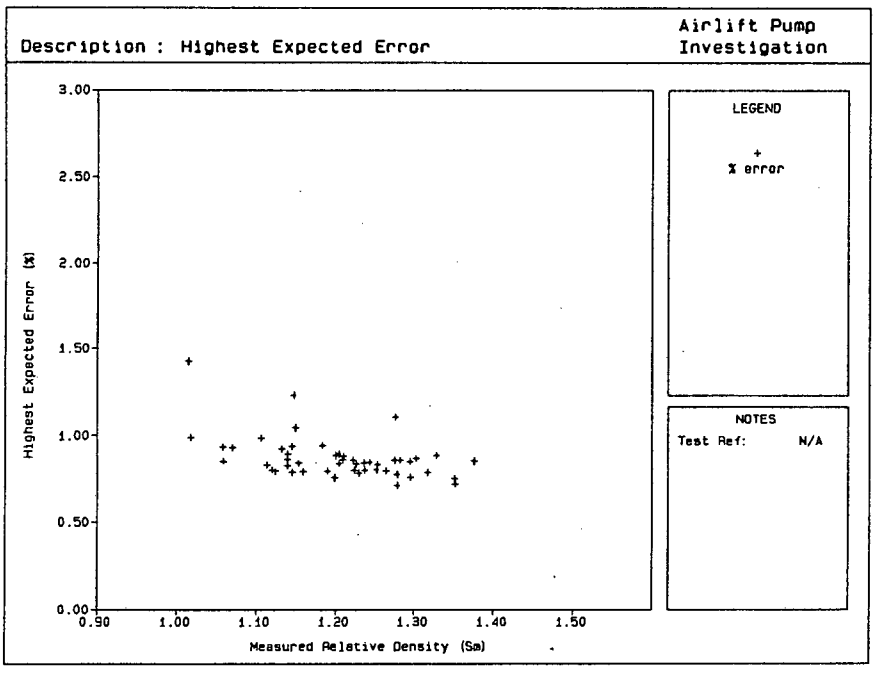

Figure 6.2 a : Sive (1988) - 90 mm NB pipeline experimental error in density measurement

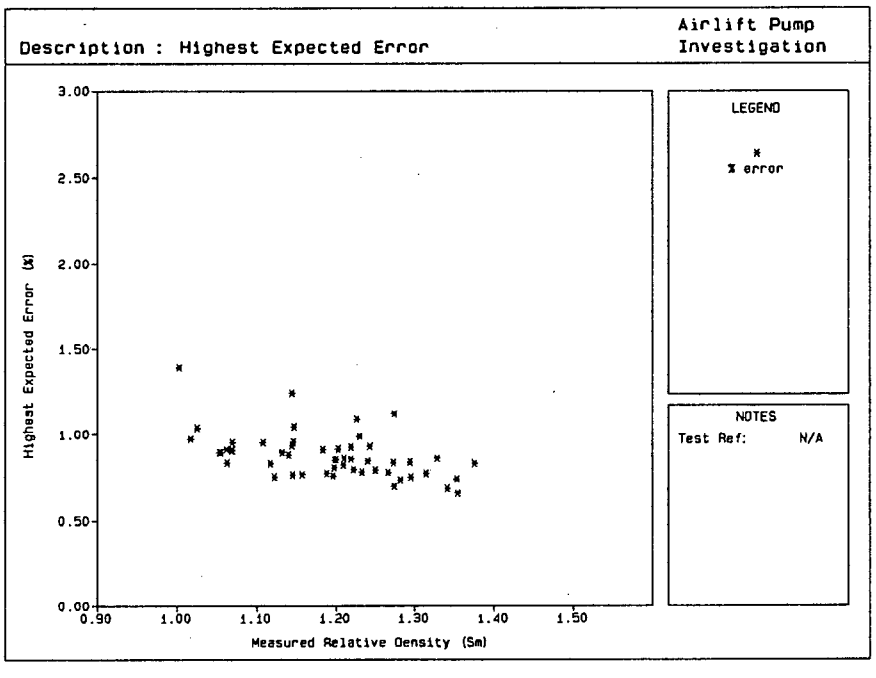

Figure 6.2 b : Sive (1988) - 160 mm NB pipeline experimental error in density measurement

6.3.3 Differential pressures (Δp)

Measurement

Differential pressures on the pipeline test facility are measured using static pressure tappings located in the pipe wall. Each pressure measurement is obtained from two adjacent pressure tappings which lead to manometer tubes and pressure transducers. The tappings are 3 mm diameter holes which are drilled into the pipe wall.

The separation pod or solids trap shown in Figure 6.3 is provided to prevent the pumped slurry from entering the air over clear water manometers.

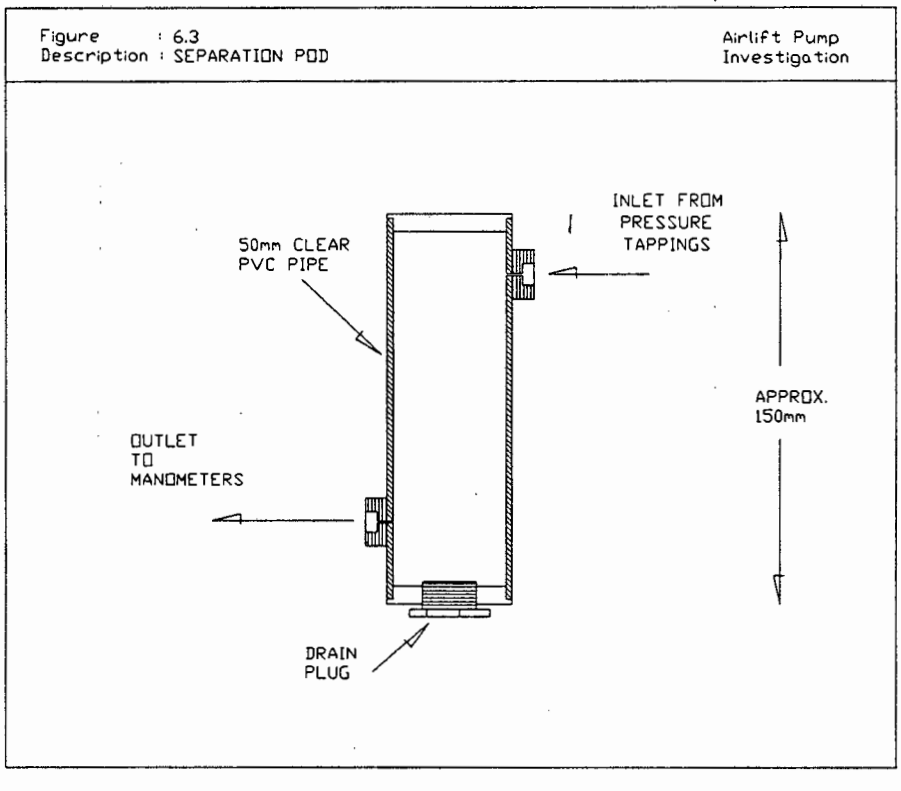

The pressures measured using the differential pressure transducers transmit electrical signals which are logged on the personal computer.

Calibration

The calibration procedure for the differential pressure transducers is as follows :

For each pair of manometers,

1. Bleed all manometers of air by flushing the measurement system with clear water.
2. Using compressed air, at ± 150 kPa pressure, adjust the level of the meniscus in one of the two manometer pipes to half the manometer pipe length.
3. Adjust the level in the second of the two manometer pipes to any level by introducing compressed air.
4. Read the differential heights in the manometer tubes. At the same time read the output from the pressure transducers using the data logger and personal computer.
5. Re-adjust the height in the second manometer tube by adding or releasing compressed air.
6. Repeat items 4 to 5 for a range of differential pressure readings.
7. Plot the differential height versus the pressure transducer output and obtain the equation constants using linear regression.

Errors

Figure 6.4 shows a graph of the highest expected error for the differential pressure transducers as calculated by Sive (1988).

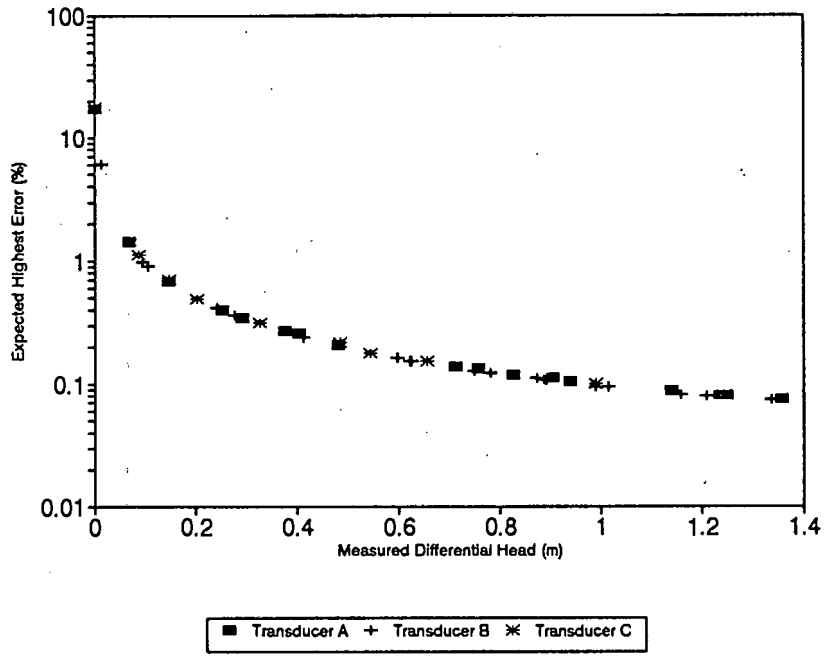

Figure 6.4 : Sive (1988) - expected error in pressure transducer measurement

6.3.4 Solid *in situ* volumetric concentration [C_{vt}^{sl}]

Measurement

Solid *in situ* volumetric concentration on the pipeline test facility is measured using an inline Gamma Ray Densitometer. This instrument is installed in the uplimbs of both diameter pipelines and measures the *in situ* volumetric concentration of the pumped mixture using a nuclear source and a detection head. The output from the instrument is relayed via an amplifier to the data acquisition facility and personal computer.

Calibration

The Gamma-Ray densitometer is calibrated using zinc chloride [Zn Cl_2]. The advantage of zinc chloride is its ability to raise the average mixture density without the particles settling out of the solution.

The density of the zinc chloride used for the calibration is 2 860 kg/m^3.

The calibration procedure is as follows :

1. Blank off a pipe section with the inline Gamma Ray Densitometer.
2. Accurately establish the volume of the blanked pipe section with clear water.
3. Add a massed quantity of zinc chloride to the pipe section filled with clear water.
4. Calculate the *in situ* concentration of the mixture in the pipe section using the measured quantities in items 2 and 3 above.
5. Measure the current output from the instrument.
6. Repeat by adding more zinc chloride to the solution and raising its concentration.

Errors

The manufacturer claims an accuracy "of between 0,7 and 2,5% of the measuring range depending on the measuring range and measuring length." (Krohne Handbook).

6.4 SETTLING TUBE

Table 6.2 summarizes the variables measured and instruments used for measurement in the settling tube :

Variable	Symbol	Units	Instrument
Absolute pressure	P	Pa	Manometers
Gas flow rate (STP)	Q_g^{STP}	m^3/s	Orifice plate and manometers
Settling velocity	v_T and v'_T	m/s	Timing with stop-watches

TABLE 6.2 : Settling tube measurements

6.4.1 Absolute pressure (P)

Measurement

Absolute pressures in the settling pipe are measured using standpipe manometers. The absolute pressures are required in order to relate gas flow rates at standard temperature and pressure (STP) to *in situ* gas flow rates at various points in the delivery pipe. The tappings which consist of 3 mm holes are placed at the beginning and end of a demarcated measurement section which is located along the settling tube length.

Referring to Figure 6.5, the manometer tubes are linked to the pressure tappings via separation pods (refer Figure 6.3) which prevent the pumped gas-liquid mixture from entering the air over clear water manometers.

Measurements are converted into pressures using :

$$P = P_{STP} + \rho_\ell \, g \, h \qquad (6.6)$$

where P_{STP} = atmospheric pressure (Pa)

ρ_ℓ = density of the liquid in the manometer tube

h = height of the liquid measured in the manometer tube (m)

P = absolute pressure (Pa).

Calibration

No calibration is required.

Errors

From Equation 6.6, pressures are calculated using :

$$P = \rho_\ell \, g \, h \qquad (6.7)$$

Thus the highest expected error is given by :

$$\left[\frac{\partial P}{P}\right]^2 = \left[\frac{\partial P}{\partial h}\right]^2 \left[\frac{h}{P}\right]^2 \left[\frac{\partial h}{h}\right]^2 \qquad (6.8)$$

where $\frac{\partial P}{2h} = \rho_\ell g$

Thus

$$\frac{\partial P}{P} = \sqrt{\left[\rho_\ell \, g\right]^2 \left[\frac{h}{P}\right]^2 \left[\frac{\partial h}{h}\right]} \qquad (6.9)$$

Table 6.3 lists the variables required for Equation 6.9.

Variable	Units	Value/Range
∂h	m	0,050
h	m	1,3 - 5,5
P	Pa	12753 - 53955

TABLE 6.3 : Variables for Equation 6.9

Figure 6.5 shows the trend in error with absolute pressure measurement.

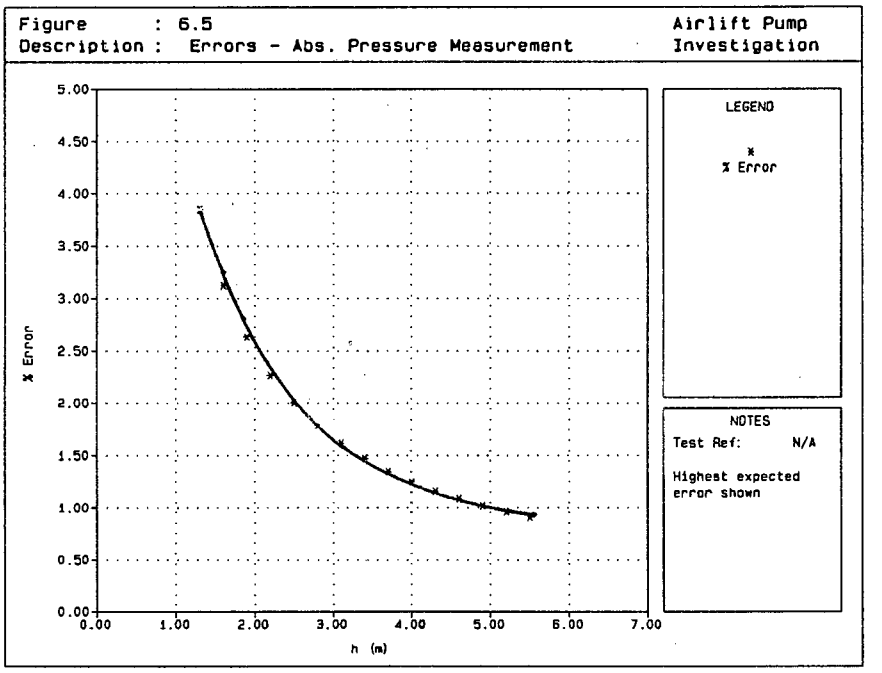

6.4.2 Gas flow rate (STP) (Q_g^{STP})

Measurement

The input air flow rates or gas flow rates are measured using an orifice plate which was designed according to British standards (BS 1042). Table 6.4 lists the orifice design data.

Item	Units	Value/Range
Orifice diameter	mm	20,6474
Pipe diameter	mm	28,7
β		0,727
Max flow (STP) - Q_{MAX}	m^3/hr	170
Deflection at Max. flow	m	1
Operating temperature	^0C	35
Operating gauge pressure	kPa	200

TABLE 6.4 : Orifice design data (settling tube)

The pressure tappings from the orifice plate lead to manometer tubes. A pressure regulator is used to ensure a constant operating pressure during measurement.

The differential pressure readings from the manometer are converted to gas flow rates at STP using :

$$Q_{gSTP} = Q_{gMAX} \sqrt{\frac{\Delta h}{1000}} \qquad (6.10)$$

where Δh = head difference (mm)

Q_{gSTP} = gas flow rate STP (m^3/hr)

Q_{gMAX} = max. flow (STP).

The average *in situ* gas flow rate (Q_g) is calculated from the standard gas flow rate (Q_{gSTP}) by assuming ideal gas behaviour. Using Boyles Law, it is assumed that the change in the *in situ* gas flow rate across the demarcated measurement section is small. An average *in situ* gas flow rate is therefore calculated using :

$$Q_{gSTP} = \left[\frac{Q_{go} \; P_{STP}}{P_{TOP}} + \frac{Q_{go} \; P_{STP}}{P_{BOTTOM}} \right] / 2 \qquad (6.11)$$

where Q_{gSTP} = gas flow rate at S.T.P. (m^3/hr)

P_{STP} = atmospheric pressure

P_{TOP} = absolute pressure at the top of the delivery pipe increment

P_{BOTTOM} = absolute pressure at the bottom of the delivery pipe increment

Q_g = average *in situ* gas flow rate (m^3/hr).

Calibration

No calibration is required.

Errors

The gas flow rate at standard conditions (STP) is calculated using Equation 6.10.

From this equation, the highest expected error is :

$$\left[\frac{\partial Q_{gSTP}}{Q_{gSTP}}\right]^2 = \left[\frac{\partial Q_{gSTP}}{\partial \Delta h}\right]^2 \left[\frac{\Delta h}{Q_{gSTP}}\right]^2 \left[\frac{\partial \Delta h}{\Delta h}\right]^2 \qquad (6.12)$$

where $$\frac{\partial Q_{gSTP}}{\partial \Delta h} = \frac{Q_{gMAX}}{2\sqrt{\Delta h}}$$

Thus $$\frac{\partial Q_{gSTP}}{Q_{gSTP}} = \sqrt{\left[\frac{Q_{gMAX}}{2\sqrt{\Delta h}}\right]^2 \left[\frac{\Delta h}{Q_{gSTP}}\right]^2 \left[\frac{\partial \Delta h}{\Delta h}\right]^2} \qquad (6.13)$$

Table 6.5 lists the variables required for Equation 6.13 while Figure 6.6 shows the trend in error for increasing head difference Δh .

Variable	Units	Value/Range
Q_{gMAX}	m^3/s	0,047222
Δh	m	0,003 to 0,300
Q_{gSTP}	Pa	0,0021 to 0,0259
$\partial \Delta h$	m	0,001

TABLE 6.5 : Variables for Equation 6.13

Referring to Figure 6.6, the error is large (± 16%) at low gas flow rates and consequently only 1 or 2 measurements are taken in this region. For Δh measurements larger than 50 mm, errors reduce to less than 1%.

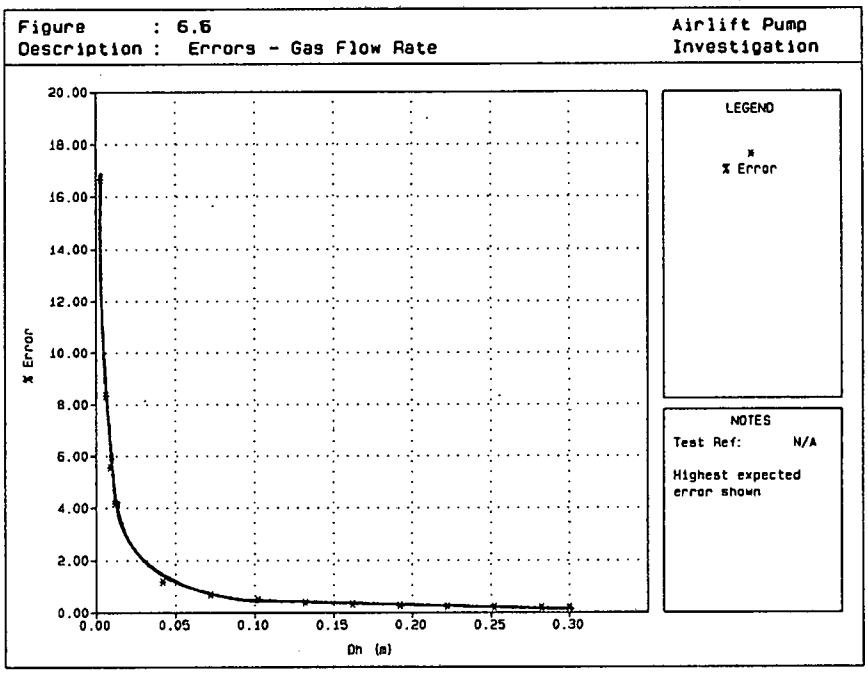

6.4.3 Single particle settling velocity (v_T)

Measurement

Referring to Figure 5.2, a 3 m measurement length is provided along the standpipe. Settling velocities are measured by timing the fall of a particle through 2 consecutive 1,5 m lengths, using a stopwatch. The operator activates two stopwatches when the particle reaches the start of the demarcated measurement length. After the particle has fallen 1,5 m, the first stopwatch is stopped and after a further 1,5 m fall the second stopwatch is stopped. Both times are recorded. The settling velocity is calculated using :

$$v_T = \frac{1,5}{T_1} + \frac{3}{T_2} \qquad (6.14)$$

where T_1 = the time after 1,5 m fall length (stopwatch 1)

T_2 = the time after 3 m fall length (stopwatch 2)

v_T = settling velocity.

Calibration

No calibration is required.

Errors

Single particle settling velocities are calculated by averaging the fall of a particle through 1,5 m and 3 m. Considering the fall through 1,5 m to give the worst scenario, the highest expected error is given as :

$$\left[\frac{\partial v_T}{v_T}\right]^2 = \left[\frac{\partial v_T}{\partial T}\right]^2 \left[\frac{T}{v_T}\right]^2 \left[\frac{\partial T}{T}\right]^2 \qquad (6.15)$$

where $\frac{\partial v_T}{\partial T} = -\frac{1,5}{T^2}$

Thus $$\frac{\partial v_T}{v_T} = \sqrt{\left[-\frac{1,5}{T^2}\right]^2 \left[\frac{T}{v_T}\right]^2 \left[\frac{\partial T}{T}\right]^2} \qquad (6.16)$$

Table 6.6 lists the variables required for Equation 6.16.

Variable	Units	Value/Range
∂T	s	0,01
T	s	3 - 1
v_T	m/s	0,5 - 1,5

TABLE 6.6 : Variables for Equation 6.16

Figure 6.7 shows the trend in error with velocity measurement.

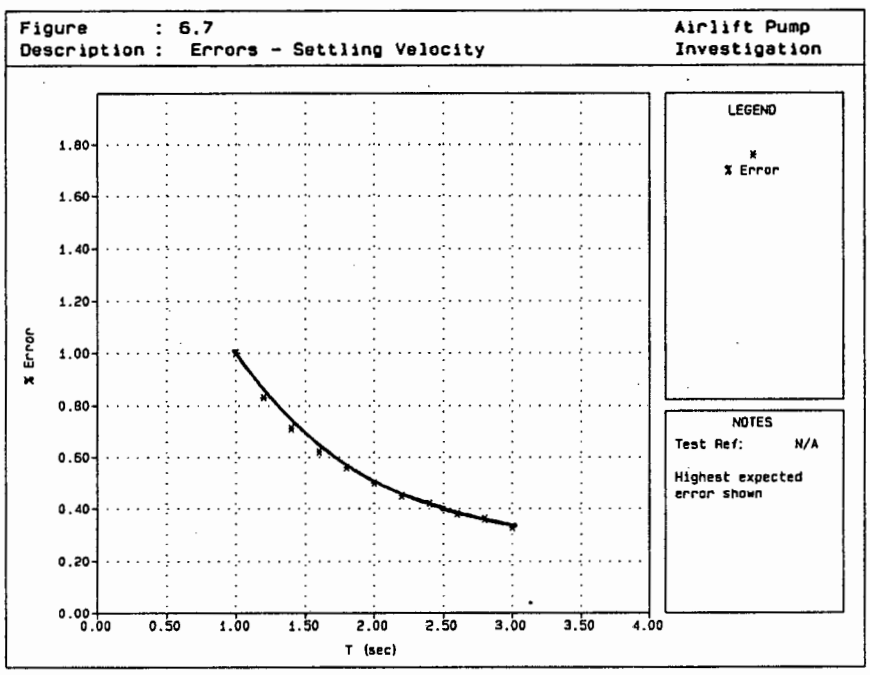

6.4.4 Multiple particle settling velocity (v'_T)

Measurement

Referring to Figure 5.2, a 4,015 m measurement section is provided along the standpipe. Settling velocities are measured as described in Section 6.4.3.

After releasing a cluster of particles, at the top of the standpipe, a stopwatch is activated as the first particle of the cluster of particles reach the beginning of the demarcated measurement section. As the last of the cluster of particles reaches the beginning of the demarcated measurement section, a second stopwatch is activated. After the particles fall through the 4,015 m measurement length, the first stopwatch deactivated (T_F) as the first particle of the cluster reach the end of the demarcated measurement section. The second stopwatch is subsequently deactivated (T_L) as the last of the cluster of particles reach the demarcated measurement section. The settling velocity for an "average particle" located in the centre of the cluster is given by :

$$v'_t = \left(\frac{4,015}{T_F} + \frac{4,015}{T_L} \right) / 2 \qquad (6.17)$$

where T_F and T_L = the time when the first and last particles reach the end of the demarcated measurement section

v'_t = settling velocity of an "average particle" located in the centre of the cluster of particles.

Calibration

No calibration is required.

Errors

Refer to Section 6.4.3.

6.5 AIRLIFT PUMPS

Table 6.7 is a summary of the instruments used and the variables measured on both airlift pump installations. Quantities calculated using other measured variables are also listed.

Variable	Airlift Pump Installation	Instrument	Symbol	Units
Gas Flow Rate (STP)	40 mm & 90 mm	Orifice Plate	Q_g^{STP}	m^3/s
Mixture Flow Rate	40 mm 90 mm	Bend Meter Sample Tank	Q_m^{sl}	m^3/s
Mixture Density	40 mm 90 mm	Calculated using C_{vd}^{sl} Sample Tank	ρ_m^{sl}	kg/m^3
Solid Delivered Concentration	40 mm 90 mm	Counterflow Meter Calculated Using ρ_{vd}^{sl}	C_{vd}^{sl}	%
Solid and Gas Volumetric Concentration (*in situ*)	40 mm & 90 mm	Twin Valve Shut Off	C_{vt}^{slg} ϵ_g^{slg}	%
Pressures	40 mm & 90 mm	Pressure Tappings	P & Δp	Pa
Gas Flow Rate (*in situ*)	40 mm & 90 mm	Calculation using Q_g^{STP}	Q_g	m^3/s
Phase Flow Rates	40 mm & 90 mm	Calculation using Q_m^{sl}	Q_s & Q_l	m^3/s
Solid Mass Flow Rates	40 mm & 90 mm	Calculation using Q_s, Q_l	M_s	kg/s

TABLE 6.7 : Airlift pump measurements.

6.5.1 Gas flow rate (S.T.P.) (Q_{gSTP})

Measurement

The input air flow rates or gas flow rates are measured using an orifice plate as discussed in Section 6.4.2. Table 6.8 gives the design data for the orifices used on all the airlift pump installations.

ITEM	UNIT	AIRLIFT PUMP INSTALLATION		
		40 mm	50 mm	90 mm
Orifice diameter	mm	6,549	8,950	20,647
Orifice pipe diameter	mm	17	17	28,7
β		0,385	0,524	0,727
Max. flow (m^3/hr at STP)	m^3/hr	17	36	170
Deflection at Max. flow	m	1	1	1
Operating temperature	^{0}C	35	35	35
Operating gauge pressure	kPa	300	300	200

TABLE 6.8 : Orifice design data (airlift pumps)

Calibration

No calibration is required.

Errors

Refer to Section 6.4.2 and Figure 6.6.

6.5.2 Solid-liquid mixture flow rate ($Q_m^{s\ell}$)

6.5.2.1 40 mm airlift pump

Measurement

Solid-liquid mixture flow rates are monitored using the calibrated bend meter. Pressure differences are recorded on a differential pressure manometer. From the calibration, the mixture flow is given by :

$$Q_m^{s\ell} = 5.738 \times 10^{-3} + 9.091 \times 10^{-2} \sqrt{\Delta h} \qquad (6.18)$$

where $Q_m^{s\ell}$ = solid-liquid mixture flow rate (ℓ/s)

Δh = head difference on the manometer (mm).

Calibration

The calibration procedure is as follows :

1. The bend meter is connected between a continuous regulated clear water supply and a sample tank.
2. A flow rate is set through the bend meter.
3. The bend meter manometer differential head is measured.
4. The flow is diverted into the sample tank for a predetermined sample time.
5. The sample mass and time is recorded.
6. Items 4 to 5 are repeated for two further samples.
7. Items 2 to 6 are repeated for a range of flow rates.
8. The calibration equations constants are obtained using regression.

Figure 6.8 shows the calibration curve obtained for the bend meter.

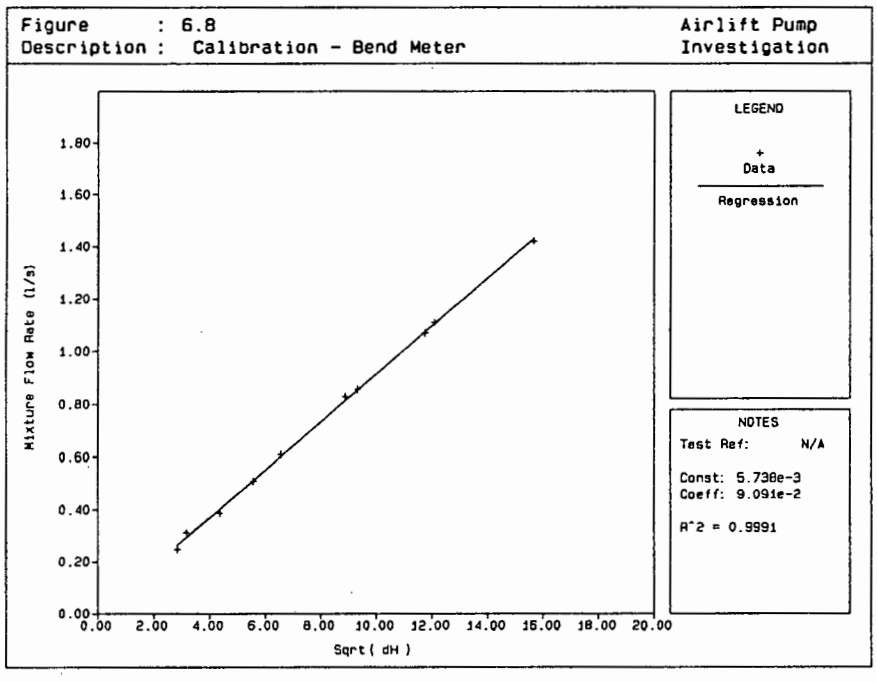

Errors

The mixture flow rate on the 40 mm airlift pump is calculated using Equation 6.18. From this equation, the highest expected errors are :

$$\left[\frac{\partial Q_m^{s\ell}}{Q_m^{s\ell}}\right]^2 = \left[\frac{\partial Q_m^{s\ell}}{\partial \Delta h}\right]^2 \left[\frac{\Delta h}{Q_m^{s\ell}}\right]^2 \left[\frac{\partial \Delta h}{\Delta h}\right]^2 \qquad (6.19)$$

where $\dfrac{\partial Q_m^{s\ell}}{\partial \Delta h} = \dfrac{C}{2\sqrt{\Delta h}}$

$C = 9{,}091 \times 10^{-2}$

Thus $$\frac{\partial Q_m^{s\ell}}{Q_m^{s\ell}} = \sqrt{\left[\frac{C}{2\sqrt{\Delta h}}\right]^2 \left[\frac{\Delta h}{Q_m^{s\ell}}\right]^2 \left[\frac{\partial \Delta h}{\Delta h}\right]^2} \qquad (6.20)$$

Table 6.9 lists the variables required for Equation 6.20 while Figure 6.9 shows the trend in error for increasing head difference Δh.

Variable	Units	Value/Range
$Q_m^{s\ell}$	ℓ/s	0,209 - 0,959
Δh	mm	5 - 110
$\partial\ \Delta h$	mm	1

TABLE 6.9 : Variables for Equation 6.20

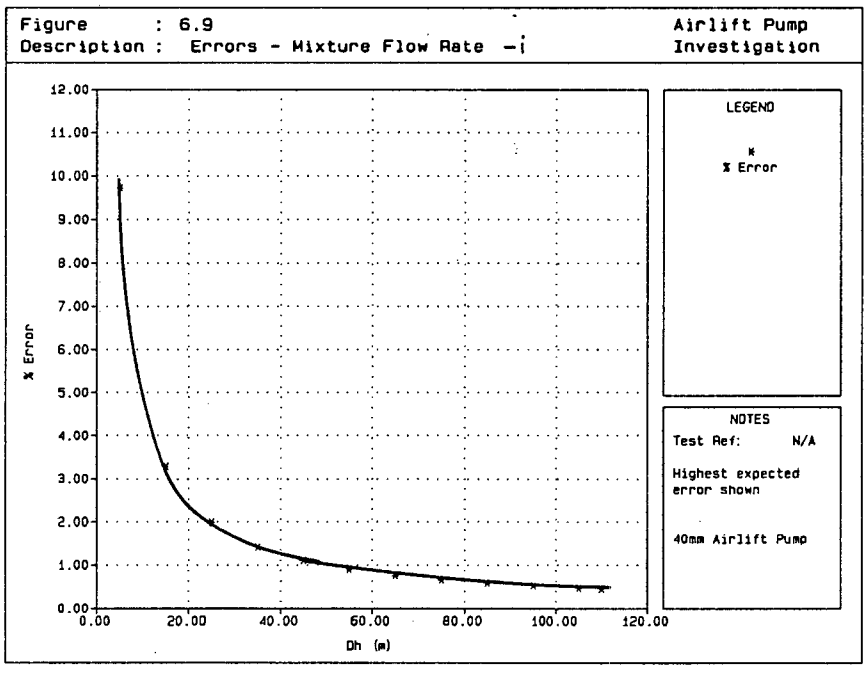

6.5.2.2 90 mm airlift pump

Measurement

Solid-liquid mixture flow rates are measured using a calibrated sample tank and a micro-switch timing facility. As the goose-neck flow diverter at the delivery outlet is swung from a return hose to the

sample tank, the micro-switch is activated which starts a stop-watch. Swinging the goose-neck back to the return hose reactivates the switch and the stopwatch is stopped. The time recorded, combined with the volume of the solid-liquid mixture in the sample tank, yields the solid-liquid mixture flow rate (Q_m^{sl}) :

$$Q_m^{sl} = V_m^{sl}/t \qquad (6.21)$$

where V_m^{sl} = volume of solid-liquid mixture in sample tank (l)

t = time of sample (s)

Q_m^{sl} = solid-liquid mixture flow rate (l/s).

Calibration

In the calibration process, accurately measured volumes of clear water are added to the sample tank. The cumulative volumes and height on the standpipe mounted to the side of the tank are recorded. From this, the relationship between sample tank volume and height on the mounted standpipe is given as :

$$V = 29{,}560899 + 0{,}116741\ H \qquad (6.22)$$

where V = volume in sample tank (l)

H = measured standpipe height (mm)

Errors

The solid mixture flow rate on the 90 mm airlift pump is calculated using Equation 6.21 and 6.22.

From Equation 6.21, the highest expected error is expressed as :

$$\left[\frac{\partial Q_m^{sl}}{Q_m^{sl}}\right]^2 = \left[\frac{\partial Q_m^{sl}}{\partial V_m^{sl}}\right]^2 \left[\frac{V_m^{sl}}{Q_m^{sl}}\right]^2 \left[\frac{\partial V_m^{sl}}{V_m^{sl}}\right]^2 + \left[\frac{\partial Q_m^{sl}}{\partial t}\right]^2 \left[\frac{t}{Q_m^{sl}}\right]^2 \left[\frac{\partial t}{t}\right]^2 \quad (6.23)$$

where $\frac{\partial Q_m^{sl}}{\partial V_m^{sl}} = \frac{1}{t}$

$$\frac{\partial Q_m^{sl}}{\partial t} = -\frac{V_m}{t^2}$$

However, from the calibration of the sample tank (Equation 6.22) the highest expected error in volume measurement is given by :

$$\left[\frac{\partial V_m^{sl}}{V_m^{sl}}\right]^2 = \left[\frac{\partial V_m^{sl}}{\partial H}\right]^2 \left[\frac{H}{V_m^{sl}}\right]^2 \left[\frac{\partial H}{H}\right]^2 \quad (6.24)$$

where $\left[\frac{\partial V_m^{sl}}{\partial H}\right] = 0{,}116741.$

The highest expected error in the mixture flow rate measurement is thus found by substituting the sample tank calibration error into Equation 6.23.

Table 6.10 lists the variables required for Equations 6.23 and 6.24 while the trend in mixture flow rate error is shown in Figure 6.10 for increasing time. For this calculation the highest expected error in volume flow rate is used (i.e. 0,33%).

Variable	Units	Value/Range
∂H	mm	1
H	mm	50 - 200
$V_m^{s\ell}$	ℓ	35,39 - 52,91
Highest error in $V_m^{s\ell}$	%	0,33
$\partial V_m^{s\ell}$	ℓ	0,12
∂t	s	0,01
t	s	10 - 20
$Q_m^{s\ell}$	ℓ/s	3,54 - 1,77

TABLE 6.10 : Variables for Equations 6.23 and 6.24

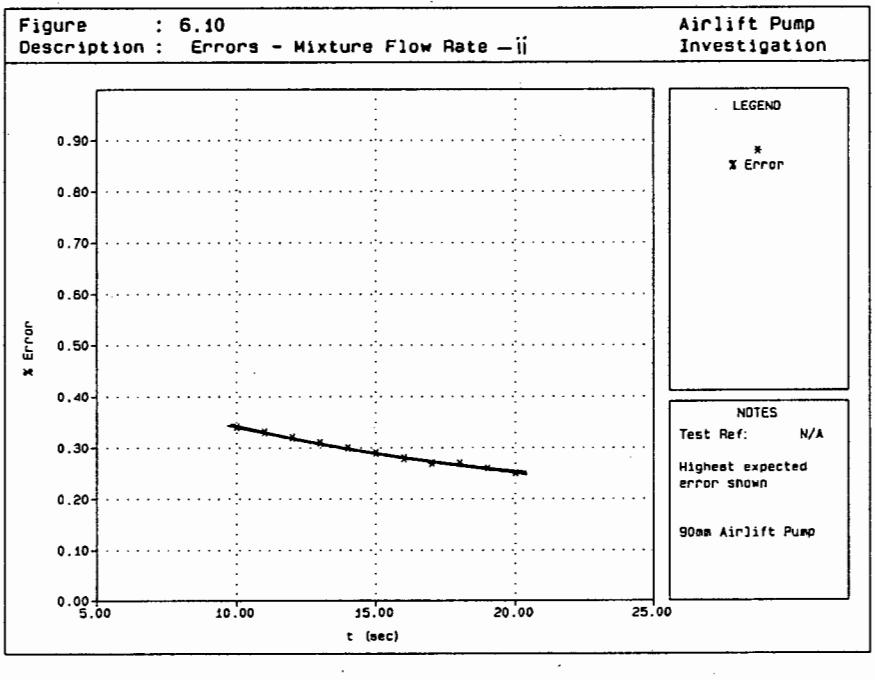

6.5.3 Solid-liquid mixture density (ρ_m^{sl})

6.5.3.1 40 mm airlift pump

Measurement

Mixture densities are calculated from the solid delivered volumetric concentration (refer Section 6.5.4),

$$S_m^{sl} = C_{vd}^{sl} (S_s - S_w) + S_w \tag{6.25}$$

and,

$$\rho_m^{sl} = S_m^{sl} \rho_w \tag{6.26}$$

where ρ_m^{sl} = density of solid-liquid mixture (kg/m^3)

S_m^{sl} = specific gravity of solid-liquid mixture

ρ_w = density of water

S_s = specific gravity of solids

S_w = specific gravity of water.

Calibration

No calibration is required.

Errors

From Equations 6.25 and 6.26, the highest expected error is expressed as :

$$\left[\frac{\partial \rho_m^{sl}}{\rho_m^{sl}}\right]^2 = \left[\frac{\partial \rho_m^{sl}}{\partial C_{vd}^{sl}}\right]^2 \left[\frac{C_{vd}^{sl}}{\rho_m^{sl}}\right]^2 \left[\frac{\partial C_{vd}^{sl}}{C_{vd}^{sl}}\right]^2 \tag{6.27}$$

where $\frac{\partial \rho_m^{sl}}{\partial C_{vd}^{sl}} = (S_s - S_w) \rho_w$.

Table 6.11 lists the variables required for Equation 6.27 while the highest expected error in solid-liquid mixture density calculation is 0,07%.

Variable	Units	Value/Range
$C_{vd}^{s\ell}$	%	1,4 - 4,3
error in $C_{vd}^{s\ell}$	%	3,16 - 1,03
$\rho_m^{s\ell}$	mm	1

TABLE 6.11 : Variables for Equation 6.27

6.5.3.2 90 mm airlift pump

Measurement

Mixture densities are monitored using the calibrated sample tank. After taking a sample, as described in Section 6.5.2 above, the mass of the solid-liquid sample is recorded. The mass of the sample together with the volume of the sample yields the mixture density as follows :

$$\rho_m^{s\ell} = \frac{M_m^{s\ell}}{V_m^{s\ell}} \qquad (6.28)$$

where $M_m^{s\ell}$ = mass of solid-liquid sample (kg)

$\rho_m^{s\ell}$ = density of solid-liquid mixture (kg/m^3).

Calibration

No calibration required.

Errors

From Equation 6.28, the highest expected error is expressed as :

$$\left[\frac{\partial \rho_m^{sl}}{\rho_m^{sl}}\right]^2 = \left[\frac{\partial \rho_m^{sl}}{\partial M_m^{sl}}\right]^2 \left[\frac{M_m^{sl}}{\rho_m^{sl}}\right]^2 \left[\frac{\partial M_m^{sl}}{M_m^{sl}}\right]^2 + \left[\frac{\partial \rho_m^{sl}}{\partial V_m^{sl}}\right]^2 \left[\frac{V_m^{sl}}{\rho_m^{sl}}\right]^2 \left[\frac{\partial V_m^{sl}}{V_m^{sl}}\right]^2 \quad (6.29)$$

where $\dfrac{\partial \rho_m^{sl}}{\partial M_m^{sl}} = \dfrac{1}{V_m^{sl}}$

$$\frac{\partial \rho_m^{sl}}{\partial V_m^{sl}} = -\frac{M_m^{sl}}{(V_m^{sl})^2} .$$

Table 6.12 lists the variables required for Equation 6.29 while Figure 6.11 shows the trend in solid-liquid mixture density error with increasing sample tank mass. For this calculation, the highest expected error in volume flow rate measurement is used (refer to Section 6.5.2.2).

Variable	Units	Value/Range
Highest error in $V_m^{s\ell}$	%	0,33
$\partial M_m^{s\ell}$	kg	0,25
$M_m^{s\ell}$	kg	35,39 - 45,30
$V_m^{s\ell}$	ℓ	35,39
$\rho_m^{s\ell}$	kg/m^3	1 000 - 1 280

TABLE 6.12 : Variables for Equation 6.29

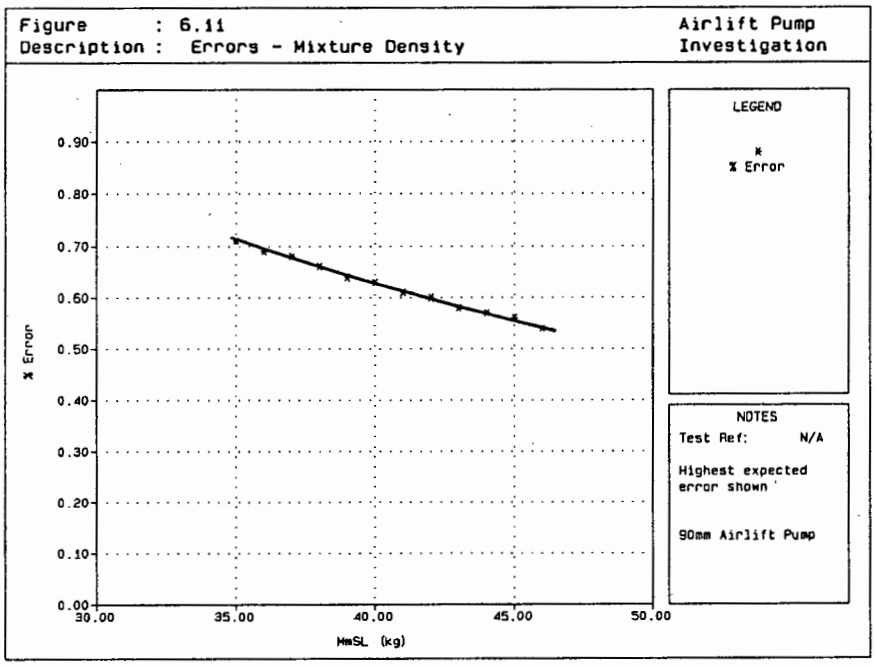

6.5.4 Solid delivered volumetric concentration ($C_{vd}^{s\ell}$)

6.5.4.1 40 mm airlift pump

Measurement

Solid-liquid delivered concentrations are measured using a counterflow meter as described in Section 6.3.2. Pressures from the four pressure tappings are monitored with two air over clear water manometers. The delivered concentration of the solid-liquid mixture is then calculated using Equation 6.3.

Calibration

No calibration is required.

Errors

From Equation 6.3 the highest expected error is given by :

$$\left[\frac{\partial C_{vd}^{s\ell}}{C_{vd}^{s\ell}}\right]^2 = \left[\frac{\partial C_{vd}^{s\ell}}{\partial \Delta h_{UP}}\right]^2 \left[\frac{\Delta h_{UP}}{C_{vd}^{s\ell}}\right]^2 \left[\frac{\partial \Delta h_{UP}}{\Delta h_{UP}}\right]^2 + \left[\frac{\partial C_{vd}^{s\ell}}{\partial \Delta h_{DOWN}}\right]^2 \left[\frac{\Delta h_{DOWN}}{C_{m}^{s\ell}}\right]^2 \left[\frac{\partial \Delta h_{DOWN}}{\Delta h_{DOWN}}\right]^2 \quad (6.30)$$

where $\dfrac{\partial C_{vd}^{s\ell}}{\partial \Delta h_{UP}} = \dfrac{1}{2L\ (S_s - 1)}$

$\dfrac{\partial C_{vd}^{s\ell}}{\partial \Delta h_{DOWN}} = -\dfrac{1}{2L\ (S_s - 1)}$.

Table 6.13 lists the variables required for Equation 6.30 while Figure 6.12 shows the trend in error with respect to the measured delivered volumetric concentration.

Variable	Units	Value/Range
L	m	1
S_s	-	2,6
$\partial\ \Delta h_{UP}$	m	0,001
Δh_{UP}	m	0,050 - 0,180
$\partial\ \Delta h_{DOWN}$	m	0,001
Δh_{DOWN}	m	0,005 - 0,040
$C_{vd}^{s\ell}$	%	1,4 - 4,3

TABLE 6.13 : Variables for Equation 6.30

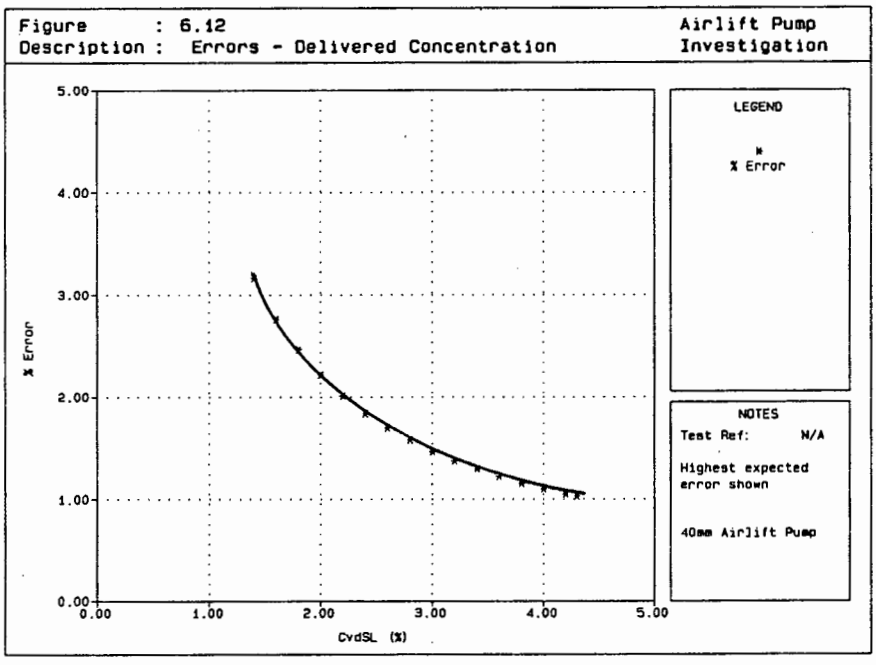

6.5.4.2 90 mm airlift pump

Measurement

Delivered concentrations are calculated from the solid-liquid mixture density. The solid-liquid mixture specific gravity is calculated using :

$$S_m^{sl} = \frac{\rho_m^{sl}}{\rho_w} \tag{6.31}$$

where ρ_w = density of water

S_m^{sl} = solid-liquid mixture specific gravity.

Substitution of Equation 6.31 into Equation 6.25 results in the solid-liquid delivered volumetric concentration :

$$C_{vd}^{sl} = \frac{S_m^{sl} - S_w}{S_s - S_w} \tag{6.32}$$

Calibration

No calibration is required.

Errors

From Equation 6.32, the highest expected error is expressed as :

$$\left[\frac{\partial C_{vd}^{sl}}{C_{vd}^{sl}}\right]^2 = \left[\frac{\partial C_{vd}^{sl}}{\partial S_m^{sl}}\right]^2 \left[\frac{S_m^{sl}}{C_{vd}^{sl}}\right]^2 \left[\frac{\partial S_m^{sl}}{S_m^{sl}}\right]^2 \tag{6.33}$$

where $\frac{\partial C_{vd}^{sl}}{\partial S_m^{sl}} = \frac{1}{S_s - S_w}$

$S_m^{sl} = \frac{\rho_m^{sl}}{\rho_w}$.

Table 6.14 lists the variables required for Equation 6.33, while Figure 6.13 shows the trend in error with increasing solid-liquid mixture relative density. For this calculation the highest expected error in solid-liquid mixture density is assumed (refer to Section 6.5.3.2 and Figure 6.11).

Variable	Units	Value/Range
Highest error		
in $\rho_m^{s\ell}$	%	0,7
$S_m^{s\ell}$	-	1,03 - 1,28
$C_{vd}^{s\ell}$	%	1,04 - 11,67

TABLE 6.14 : Variables for Equation 6.33

Also shown on Figure 6.13 is the increase in solid delivered volumetric concentration. Most tests on the 90 mm airlift pump are conducted at solid delivered volumetric concentrations greater than 5% resulting in errors less than 5%.

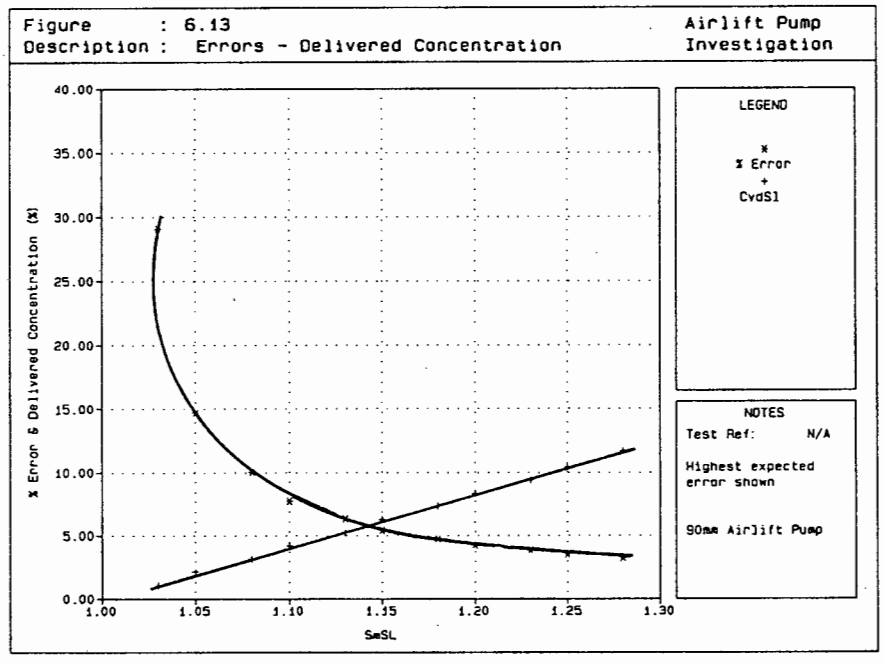

6.5.5 Solid and gas *in situ* volumetric concentration ($C_{vt}^{s\ell g}$, $\epsilon_g^{s\ell g}$)

Measurement

In situ concentrations of the solid, liquid and gas phases are measured using two pneumatically operated inline knife gate valves. The valves are placed ± 0,8 m apart in the 50 mm, and ± 1 m apart in the 90 mm airlift pump delivery pipe. During operation, the two pneumatically linked valves are shut off simultaneously, trapping a sample of solid, liquid and gas. Once the solid-liquid mixture and the gas have separated, the *in situ* concentration of gas in a solid-liquid-gas mixture is calculated using :

$$\epsilon_g^{s\ell g} = \left[K_1 - [K_2 + K_3 L] \right] / K_1 \qquad (6.34)$$

where L = length measured on tape adhered to the clear pipe section between the two valves (m)

$K_{1..3}$ = calibration constants. These are given in Table 6.15 (K_3 = total volume of pipe section (ℓ)).

Calibration Constant	40 mm Airlift Pump	90 mm Airlift Pump
K_1	1,518	6,780
K_2	0,088	0,501
K_3	1,739	5,900

TABLE 6.15 : *In situ* concentration calibration constants

The sample of solid and liquid trapped between the knife gate valves is then drained and weighed. The volume of the solid-liquid mixture is given by :

$$V_m^{sl} = (K_2 + K_3 L) / 1000 \quad (m^3) \tag{6.35}$$

The mass together with the volume of the sample yields the sample density.

$$\rho_m^{sl} = \frac{M_m^{sl}}{V_m^{sl}} \tag{6.36}$$

From this, the *in situ* concentration of the solids is

$$C_{vt}^{slg} = \frac{\frac{\rho_m^{sl}}{\rho_w} - S_w}{S_s - S_w} \tag{6.37}$$

where S_s = specific gravity of the solids

S_w = specific gravity of the water (1 000 kg/m^3).

Calibration

In the calibration of the pipe section between the knife gate valves, the height on a measuring tape adhered to the side of the pipe is related to the volume inside the pipe. The curves in Figure 6.14 for the 50 mm and Figure 6.15 for the 90 mm airlift pump delivery pipes show this relationship.

Errors

From Equation 6.34, the highest expected error in gas *in situ* volumetric concentration measurement is given by :

$$\left[\frac{\partial\, \epsilon_g^{s/g}}{\epsilon_g^{s/g}}\right]^2 = \left[\frac{\partial\, \epsilon_g^{s/g}}{\partial\, L}\right]^2 \left[\frac{L}{\epsilon_g^{s/g}}\right]^2 \left[\frac{\partial\, L}{L}\right]^2 \qquad (6.38)$$

where $\dfrac{\partial\, \epsilon_g^{s/g}}{\partial\, L} = -\dfrac{K_3}{K_1}$.

Table 6.16 lists the variables required for Equation 6.38. The highest expected error trend in 3 phase gas *in situ* volumetric concentration is shown in Figure 6.16.

This trend is shown for the 40 mm airlift pump only as it represents the worst scenario compared to the 90 mm airlift pump.

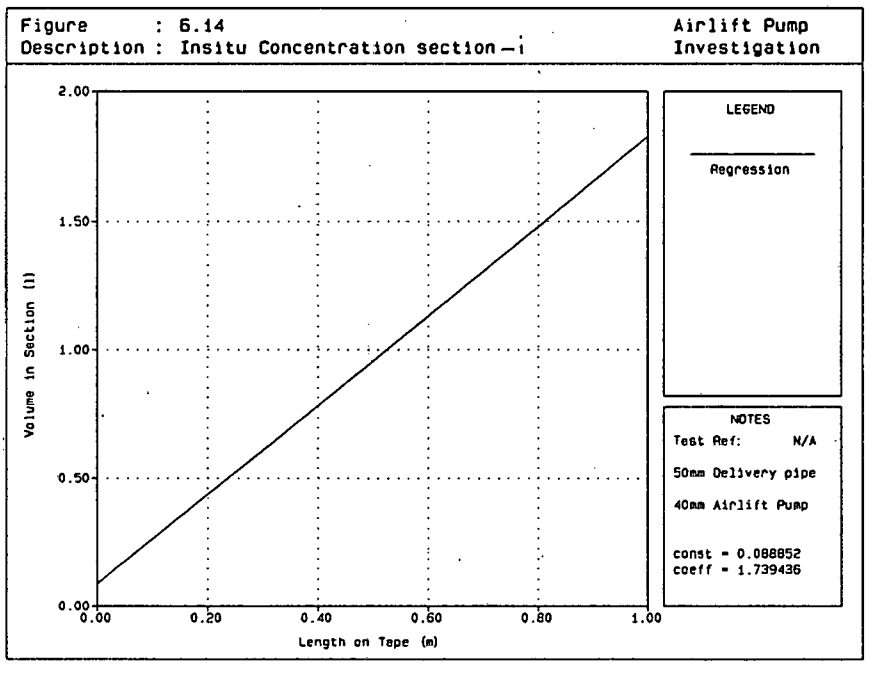

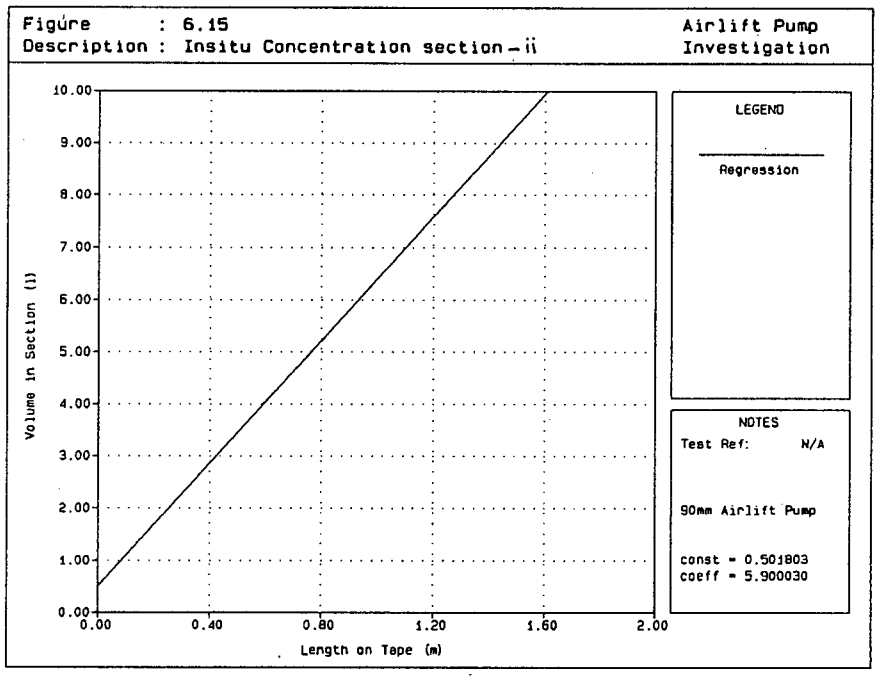
Figure : 6.15
Description : Insitu Concentration section - ii
Airlift Pump Investigation
Volume in Section (l)
Length on Tape (m)
LEGEND
Regression
NOTES
Test Ref: N/A
90mm Airlift Pump
const = 0.501803
coeff = 5.900030

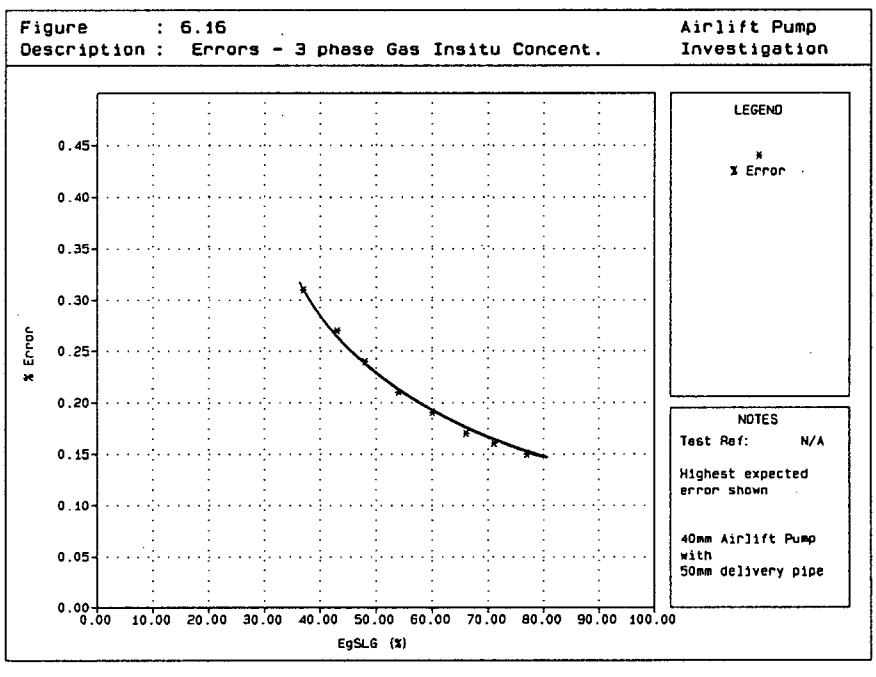
Figure : 6.16
Description : Errors - 3 phase Gas Insitu Concent.
Airlift Pump Investigation
% Error
EgSLG (%)
LEGEND
% Error
NOTES
Test Ref: N/A
Highest expected error shown
40mm Airlift Pump with 50mm delivery pipe

Variable	Units	Value/Range
∂ L	m	0,001
L	m	0,150 - 0,500
$\epsilon_g^{s\ell g}$	%	76,9 - 36,8

TABLE 6.16 : Variables for Equation 6.38

From Equation 6.35 the highest expected error in volume measurement ($V_m^{s\ell}$) is given by :

$$\left[\frac{\partial V_m^{s\ell}}{V_m^{s\ell}}\right]^2 = \left[\frac{\partial V_m^{s\ell}}{\partial L}\right]^2 \left[\frac{L}{V_m^{s\ell}}\right]^2 \left[\frac{\partial L}{L}\right]^2 \qquad (6.39)$$

where $\frac{\partial V_m^{s\ell}}{\partial L} = \frac{K_3}{1\,000}$.

Table 6.17 lists the variables required for Equation 6.39. The trend in highest expected error in solid-liquid volume measurement is shown in Figure 6.17 for the 40 mm airlift pump with the 50 mm delivery pipe.

Variable	Units	Value/Range
L	m	0,15 - 0,500
∂ L	m	0,001
$V_m^{s\ell}$	ℓ	0,35 - 0,96

TABLE 6.17 : Variables for Equation 6.39

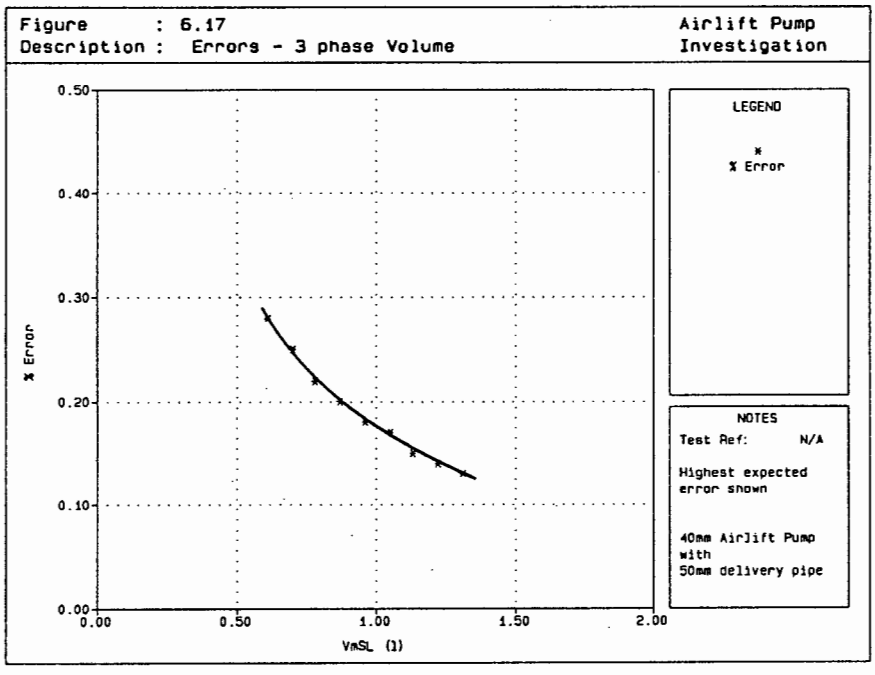

From Equations 6.34 and 6.37, the highest expected error in solid *in situ* concentration measurement is given by :

$$\left[\frac{\partial C_{vt}^{sl_g}}{C_{vt}^{sl_g}}\right]^2 = \left[\frac{\partial C_{vt}^{sl_g}}{\partial M_m^{sl}}\right]^2 \left[\frac{M_m^{sl}}{C_{vt}^{sl_g}}\right]^2 \left[\frac{\partial M_m^{sl}}{M_m^{sl}}\right]^2 + \left[\frac{\partial C_{vt}^{sl_g}}{\partial V_m^{sl}}\right]^2 \left[\frac{V_m^{sl}}{C_{vt}^{sl_g}}\right]^2 \left[\frac{\partial V_m^{sl}}{V_m^{sl}}\right]^2 \qquad (6.40)$$

where $$\frac{\partial C_{vt}^{sl_g}}{\partial M_m^{sl}} = \frac{1}{V_m^{sl}\,\rho_w}$$

$$\frac{\partial C_{vt}^{sl_g}}{\partial V_m^{sl}} = -\frac{M_m^{sl}}{\rho_w\,(S_s - S_w)\,(V_m^{sl})^2} \quad .$$

Table 6.18 lists the variables required for Equation 6.40, while the trend in highest expected error in the three phase solid *in situ* volumetric concentration measurement is shown in Figure 6.18.

Variable	Units	40 mm airlift pump Value/Range	90 mm airlift pump Value/Range
$\partial\ M_m^{sl}$	kg	0,0001	0,00001
M_m^{sl}	kg	0,613 - 1,316	2,023 - 5,031
C_{vt}^{slg}	%	0,24 - 0,56	1 - 3,6
V_m^{sl}	l	0,61 - 1,31	1,98 - 4,63
$\partial\ V_m^{sl}$	%	0,28 - 0,13	0,30 - 0,13

TABLE 6.18 : Variables for Equation 6.40

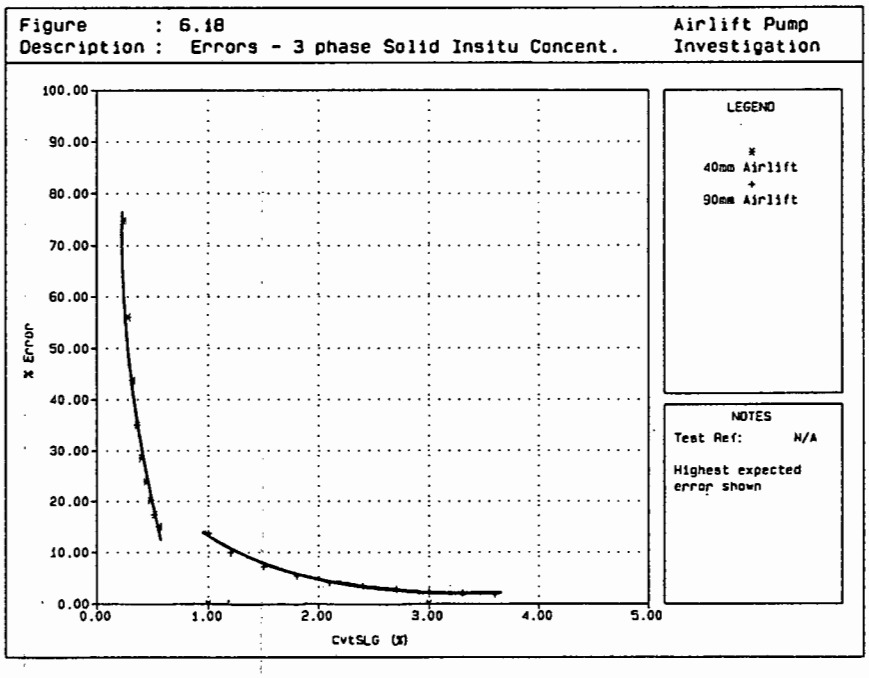

Referring to Figure 6.18, because of the exceptionally high expected errors on the 40 mm airlift pump solid *in situ* volumetric concentration measurement, these measurements are treated with circumspection. On the 90 mm airlift pump the measurements are deemed acceptable, especially at higher solid *in situ* volumetric concentrations where errors are generally less than 2%.

6.5.6 Absolute pressures (P)

Measurement

Absolute pressure tappings are provided at intervals up the airlift pump pipe to monitor pressure changes. Measurement using these tappings are discussed in Section 6.4.1.

Calibration

No calibration is required.

Errors

Refer to Section 6.4.1.

6.5.7 Phase volume flow rates calculation (Q_l & Q_s)

Using the mixture flow rate (Section 6.5.2) and the solid delivered volumetric concentration (Section 6.5.4), the liquid volume flow rate (Q_l) is calculated using :

$$Q_l = (1 - C_{vd}^{sl})\, Q_m^{sl} \qquad (6.41)$$

Likewise, the solid volume flow rate (Q_s) is calculated using :

$$Q_s = C_{vd}^{s\ell}\, Q_m^{s\ell} \tag{6.42}$$

6.5.8 Solid mass flow rate calculation (M_s)

Solid mass flow rates are obtained using :

$$M_s = Q_s\, \rho_s$$

$$M_s = \rho_s\, C_{vd}^{s\ell}\, Q_m^{s\ell} \tag{6.43}$$

where ρ_s = density of solids $\left[\frac{kg}{m^3} \right]$

M_s = solid mass flow rate (kg/s).

CHAPTER 7

EXPERIMENTS, PROCEDURES AND TEST MATERIAL

7.1 INTRODUCTION

This chapter describes the experiments conducted, procedures and test materials used on the experimental equipment discussed in Chapter 5. The general purpose of the tests are to measure specific variables required for the analysis of 3 phase flow in airlift pumps and to monitor airlift pump operation under a range of conditions. Table 7.1 summarizes the experimental tests conducted.

7.2 VERTICAL TWO PHASE PIPELINE TESTS

Summary of experiments conducted

Experiments are conducted in both the 90 mm and 160 mm NB pipelines for a range of mixture velocities and delivered volumetric concentrations. Table 7.2 below summarizes the tests conducted.

Procedures

To measure vertical 2 phase solid-liquid shear stresses and solid *in situ* volumetric concentrations, the experimental procedure adopted for each pipeline (after loading the test material) is as follows :

No	Test	Purpose
1	vertical 2 phase solid-liquid pipeline tests	Measure vertical 2 phase solid-liquid shear stresses and solid *in situ* volumetric concentrations
2	Single particle settling velocity tests (air-water mixtures)	Measure the effect of gas-water mixtures on single spherical particle settling velocities
3	Multiple particle settling velocity tests (air-water mixtures)	Observe the effect of other particles on single spherical particle settling velocities in gas-water mixtures
4	vertical 3 phase *in situ* volumetric concentration tests	Measure solid and gas *in situ* volumetric concentrations in vertically moving 3 phase solid-liquid-gas mixtures
5	Airlift pump operating tests	Measure and observe the effect of a range of variables on airlift pump delivered output
5 a	Particle size tests	Measure the effect of particle size
5 b	Submergence ratio tests	Measure the effect of submergence ratio
5 c	Solid delivered volumetric concentration tests	Measure the effect of solid delivered volumetric concentration
5 d	Annular air injector tests	Measure the effect of the annular air injector aperture
5 e	Fines tests	Measure the effect of fine particle sizes

TABLE 7.1 : Experimental tests conducted

Test Number	Pipeline Diameter (mm NB)	Approximate Delivered Volumetric Concentration - C_{vd}^{sl} (%)
DL001305	160	0
DL051807	160	5
DL111907	160	10
DL201207	160	15
DS001605	90	0
DS040801	90	4
DS080208	90	8

TABLE 7.2 : Two phase pipeline test numbers

1. The system is set to pump at a constant average solid-liquid mixture velocity and solid delivered volumetric concentration.

2. The solid-liquid mixture velocity, solid *in situ* concentration and all pressure tappings are measured using the computer software and data loggers.

3. The mixture velocity is changed using the centrifugal pump. All measurements are repeated after the system has stabilized at a new mixture velocity.

4. Items 1 to 3 above are repeated for a range of velocities up to ± 5 m/s.

5. More test material is added to the feed hopper to raise the solid delivered volumetric concentration and items 1 to 4 are repeated.

Test material

The test material used for the experiments is marine gravel tailings with particle sizes of 2 to 15 mm. Average densities are around 3 400 kg/m^3. The particle size distributions of the test material are given in Appendix B.

7.3 SINGLE PARTICLE SETTLING VELOCITY TESTS (AIR-WATER MIXTURES)

Summary of experiments conducted

Table 7.3 below summarizes the tests conducted.

Test Number	Sphere Size (mm)
Vt-15-8s	15,8
Vt-24-5s	24,5

TABLE 7.3 : Settling velocity test numbers

Procedure

To measure single particle settling velocities, in air-water mixtures, the following experimental procedure is adopted :

1. The standpipe is filled with water and gas is allowed to bubble into its base. The rate of gas flow entering is measured using the gas flow manometers.

2. Pressures at the demarcated measurement sections are measured using the absolute pressure manometers.

3. The test particles are individually dropped and the fall times are measured.

4. A different gas flow rate is adjusted and items 2 to 3 are repeated.

5. Items 2 to 4 are repeated until the fall velocities for a range of gas flow rates are obtained.

Test material

Experiments are conducted using two sizes of glass spheres covered in black paint for visibility. Table 7.4 lists the properties and theoretical single spherical particle settling velocity (in water) of the two glass sphere sizes. This settling velocity is calculated using Equations 4.15 to 4.19.

Particle	Diameter (mm)	Relative Density	Theoretical Settling Velocity (m/s)
Small sphere	15,8	2,535	0,848
Large sphere	24,5	2,455	1,028

TABLE 7.4 : Settling velocity test particle properties

7.4 MULTIPLE PARTICLE SETTLING VELOCITY TESTS (AIR-WATER MIXTURES)

Summary of experiments conducted

Only one test was conducted with the 15,8 mm spheres. The number of this test is Vt-15-8m.

Procedure

To observe and measure the effect of hindered settling due to the presence of other particles in air-water mixtures, the following experimental procedures are used :

1. The fall behaviour of a cluster of particles is observed under conditions of no gas flow.

2. The fall behaviour of a cluster of particles is observed, however, in the presence of a single released air bubble.

3. Item 2 is repeated, however with a continuous gas flow behind a single bubble.

4. Item 3 is repeated, however with a continuous stream of rising gas bubbles.

Tests are consequently conducted at a range of continuous gas flow rates as described in Section 7.3.

Test material

The 15,8 mm diameter spheres (small) shown in Table 7.4 (refer to Section 7.3), are used for the tests.

7.5 *IN SITU* VOLUMETRIC CONCENTRATION TESTS (3 PHASE)

(40 and 90 mm airlift pumps)

Summary of experiments conducted

Experiments are conducted in both the 90 mm and 40 mm NB airlift pump installations for a range of gas flow rates and delivered volumetric concentrations.

Table 7.5 below summarizes the tests conducted.

Test Number	Airlift Pump (mm NB)	Approximate Delivered Volumetric Concentration C_{vd}^{sl} (%)
DB042203	90	4
DB070803	90	7
DB101303	90	10
DBOS0589	40	4
DBOL0589	40	4

TABLE 7.5 : *In situ* concentration test numbers

Procedure

Tests to measure solid and gas *in situ* volumetric concentrations are conducted in both the 40 mm and 90 mm diameter airlift pump installations. As discussed in Section 5.3.2, the 40 mm airlift pump test installation is fitted with a 50 mm delivery pipe to match the inline knife gate valves used for these tests.

The experimental procedures are similar on both the 40 mm and 90 mm test facilities excepting for the measurement techniques which are unique to either installation.

The experimental procedure adopted is as follows :

1. The system is set to pump steady at a predetermined solid delivered volumetric concentration.

2. The following items are measured :
   - injector depths
   - lift heights
   - material type
   - suction pipe lengths
   - material density
   - material particle size distribution.

3. The head difference on the gas flow manometers is measured.

4. Three samples of sample tank height, sample time and mass are taken (90 mm test facility only).

5. The head difference on the two counterflow meter and bend meter manometers are recorded (40 mm test facility only).

6. Before shutting off the knife gate valves, all absolute pressure manometers are recorded.

7. The two inline knife gate valves are shut instantaneously and simultaneously trapping a gas, liquid and solids sample. The gas flow rate is deactivated, halting the system. After the phases between the knife gate valves have separated, the sample height is measured. The sample is drained and weighed. This procedure is repeated 10 times.

8. The gas flow rate is reactivated, and items 3 to 6 are re-recorded.

9. A different gas flow rate is adjusted and the system is allowed to stabilize.

10. Items 4 to 8 are repeated for a range of gas flow rates.

Test material

40 mm airlift pump

Two sets of tests are conducted in the 40 mm delivery pipe airlift pump. In each of these, a different sized particle is used, however, both sets of particles are quartz filter grits with specifications given in Table 7.6. Particle size distributions are given in Appendix B.

Ref No	Effective Size (mm)	Density (kg/m^3)
4/10	2,46	2 630
16/30	0,62	2 532

TABLE 7.6 : *In situ* volumetric concentration test particles (40 mm airlift pump)

90 mm airlift pump

In the 90 mm airlift pump, marine gravels are used with particle sizes ranging from 2 to 15 mm. Particle densities are approximately 3 400 kg/m^3. Typical particle size distributions are given in Appendix B.

7.6 AIRLIFT PUMP OPERATING TESTS

7.6.1 Particle size tests (40 mm airlift pump)

Summary of experiments conducted

The results of the particle size tests and submergence ratio tests (see Section 7.6.2) are extracted from the range of experiments listed in Table 7.7 below.

Test Number	Material Size (mm)	Submergence ratio (%)
DS011087	2,46	88
DS021087	2,46	96
DS031087	1,42	88
DS041087	1,42	96
DS051087	0,62	88
DS061087	0,62	96

TABLE 7.7 : Airlift pump operating test numbers

Procedure

For the purpose of monitoring the effect of particle size on airlift pump operating curves, tests are conducted using 3 particle sizes. Throughout the tests, it is attempted to maintain the solid delivered volumetric concentration at a constant 4%. In order to achieve this constant delivered concentration at higher gas flow rates, additional test material has to be added to the system.

For each particle size the experimental procedure is as follows :

1. The system is set to pump steady at the predetermined solid delivered volumetric concentration (4%).

2. The following items are measured :
   - injector depth
   - lift height
   - suction pipe length
   - material type
   - material density
   - material particle size distribution.

3. The head difference on the gas flow manometers is recorded.

4. The head difference on the bend meter manometers is recorded.

5. The head differences on the two counterflow meter manometers are recorded.

6. All absolute pressure manometers are recorded.

7. A different gas flow rate is adjusted and the system is allowed to stabilize.

8. Items 3 to 7 are repeated for a range of gas flow rates.

Test material

The tests are conducted with the two quartz filter grits described in Table 7.3, (Section 7.5). An additional set of tests is conducted using the particle size shown in Table 7.8.

Ref No	Effective Size (mm)	Density (kg/m^3)
7/16	1,42	2 634

TABLE 7.8 : Additional 40 mm airlift pump operating test particles

The particle size distribution is shown in Appendix B.

7.6.2 Submergence ratio tests (40 mm airlift pump)

Summary of experiments conducted

Refer to Section 7.6.1.

Procedure

The submergence ratio (SR) is defined as :

$$SR = \frac{\text{injector depth}}{\text{vertical delivery pipe height}}$$

where :

injector depth = depth from surrounding free water surface to the point of gas injection

vertical delivery pipe height = length from gas injection point to the delivery outlet.

For the purpose of monitoring the effect of submergence ratio on airlift pump operating curves, tests are conducted at the two submergence ratios listed in Table 7.9.

Lift Height (mm)	Injector Depth (mm)	Delivery Pipe Height (mm)	Submergence Ratio (%)
240	1 755	2 015	88
80	1 935	2 015	96

TABLE 7.9 : Submergence ratio test settings

The experimental procedure is described in Section 7.6.1.

Test material

The tests were conducted using the three quartz filter grits described in Tables 7.6 and 7.8.

7.6.3 Solid delivered volumetric concentration tests (90 mm airlift pump)

Summary of experiments conducted

Experiments are conducted for a range of gas flow rates and delivered volumetric concentrations.

Table 7.10 below summarizes the experimental tests conducted.

Test Number	Approximate Delivered Volumetric Concentration $C_{vd}^{s\ell}$ (%)
DB041310	4
DB081510	8
DB111810	11

TABLE 7.10 : Solid delivered volumetric concentration test numbers

Procedure

In order to maintain a constant solid delivered concentration, the suction nozzle is raised or lowered with respect to the level of the material in the pressure vessel. For each concentration the experimental procedure is as follows :

1. The system is set to pump steady at the chosen solid delivered volumetric concentration.

2. The following items are measured :
   - injector depth
   - lift height

- suction pipe length
- material type
- material density
- material particle size distribution.

3. The head difference on the gas flow manometer is recorded.

4. Three samples of sample tank height, sample time and mass are taken.

5. All absolute pressure manometers are recorded.

6. A different gas flow rate is adjusted and the system is allowed to stabilize.

7. Items 3 to 6 are repeated for a range of gas flow rates.

Test material

The solid delivered volumetric concentration tests are conducted using marine gravels described in Section 7.5. Particle size distributions are given in Appendix B.

7.6.4 Annular air injector tests (90 mm airlift pump)

Summary of experiments conducted

Experiments are conducted for a range of gas flow rates and aperture areas.

Table 7.11 below summarizes the experimental tests conducted.

Test Number	Aperture Number
DB091910	4
DB092010	6
DB092410	8

TABLE 7.11 : Annular air injector test numbers

Procedure

For the purpose of monitoring the effect of annular air injector aperture, tests are conducted at a range of aperture areas. These areas are summarized in Table 7.12.

Aperture No	Annular Gap Distance (mm)	Aperture Area (mm^2)
4	4,5	1335,2
6	7	1766,36
8	9,0	2770,9

TABLE 7.12 : Aperture settings and areas

During all tests, the solid delivered volumetric concentrations are kept constant at approximately 6%. For each of the aperture areas, the experimental procedure is described in Section 7.6.3.

Test material

The annular aperture tests are conducted using the marine gravels described in Section 7.5. Particle size distributions are given in Appendix B.

7.6.5 Fines tests (90 mm airlift pump)

Summary of experiments conducted

Experiments are conducted for a range of gas flow rates with two batches of fines material. Table 7.13 below summarizes the experimental tests conducted.

Test Number	Material
DBF60726 DBL60789	fines fines and lime

TABLE 7.13 : Fines test numbers

Procedure

Most experiments conducted with the 90 mm airlift pump involve particle sizes of between 2 mm and 15 mm with an approximate d_{50} = 6,5 mm. To monitor the effect of smaller particles on airlift pump operation, tests are conducted with material of less than 3,3 mm (i.e. d_{50} of 1 mm).

Tests are conducted using two materials :

1. Large percentage fines (d_{50} = 1 000 μm)

2. Fines (d_{50} = 1 000 μm) plus large percentage building lime (10 μm - 15 μm).

For each test, the experimental procedure is described in Section 7.6.3.

Test material

Particle size distributions of each test material are given in Appendix B. The d_{50} and density of the materials are summarized in Table 7.14.

Test No	Material	d_{50} mm	Density (kg/m^3)
1	fines	1	2 930
2	fines and lime	0,9	2 927

TABLE 7.14 : Fines test material properties

CHAPTER 8

RESULTS AND DISCUSSION

8.1 INTRODUCTION

This chapter discusses the results of the experiments conducted to evaluate the mathematical models discussed in Chapters 3 and 4. The mathematical models are compared to the experimental results and the proposed model is verified. Also discussed in this chapter are results of experiments conducted to measure specific variables required for the mathematical models.

Further discussion covers the results of experiments conducted to observe and report on airlift pump behaviour under a range of operating conditions.

Comparison of test results and theoretical approaches

Considerable time and effort is required to obtain each measured data point. For example, measurement of the gas and solid phase *in situ* concentration in the airlift pump installations, involves a repetitive task of sampling numerous times to obtain a meaningful average. For this reason, the number of data points in each experiment varies between 9 and 15.

A large variety of statistical parameters are available for comparing theoretical approaches with measured data (correlation coefficients, determination coefficient, efficiency coefficient etc). These parameters, however, are usually only meaningful for larger data samples. One statistical parameter that may be used, is the log

standard error (Lazarus *et al* 1978). However, Sive (1988) and Cooke (1991) both note that this parameter should be treated with circumspection, as it may be weighted by the number of data points.

Because of the above, comparison of theoretical approaches to measured data in this dissertation is done primarily with deviation graphs. Figure 8.1. b shows a typical deviation graph. Measured data is plotted on the x axis against the theoretical prediction on the y axis. Should the theory agree with the data, a point will be plotted on the 45^0 line (diagonal from x_{min}, y_{min} to x_{max}, y_{max}). Additional lines can be drawn on the graph to show a 10%, 20% etc. deviation from the line representing 100% agreement of data (100% agreement line). The proximity of the plotted point to these deviation lines is used to evaluate the theoretical approach.

In some cases, where sufficient data points are available the log standard error is tabulated. The log standard error is calculated as follows :

$$S = 1 - \sqrt{\frac{\sum_{i=1}^{u} [\log (obs) - \log (th)]^2}{u - 1}}$$

where obs = observed or measured data

th = theoretically predicted data

u = number of data points.

In these cases, average error values above 98% should be considered the lower limit for a good correlation (Sive, 1988).

8.2 VERTICAL TWO PHASE SOLID-LIQUID PIPELINE TESTS

Purpose :

Measurement of two phase solid-liquid shear stress and two phase solid in situ volumetric concentrations.

8.2.1 Vertical two phase solid-liquid shear stress (τ_{om}^{sl})

The measured shear stress is evaluated from the measured total head loss (ΔH_T) and the measured *in situ* volumetric concentration (C_{vt}^{sl}).

From Equation 4.5 and Figure 4.1, the shear stress is expressed as :

$$\tau_{om}^{sl} \frac{\pi D l_2}{A} = (P_C - P_D) - \frac{W_m^{sl}}{A} \qquad (8.1)$$

In terms of absolute manometer levels at points C and D, Equation 8.1 is rewritten as :

$$\tau_{om}^{sl} \frac{\pi D l_2}{A} = \rho g (l_2 + \Delta H_T) - \frac{W_m^{sl}}{A} \qquad (8.2)$$

where l_2 = distance between pressure tappings = 1 m

ΔH_T = total head loss or differential head.

Furthermore, the term $\frac{W_m^{sl}}{A}$ is expanded using Equations 4.6 and 4.7. Division of Equation 8.2 by $\frac{A}{\pi D l_2}$ allows the shear stress (τ_{om}^{sl}) to be evaluated in terms of measured quantities, thus the "measured" shear stress is obtained.

The shear stress, compared to the weight of the two phase mixture, generally contributes a small portion to the total pressure loss (Δp_2) in the suction pipe. For velocities from 2 m/s to 6 m/s and for delivered volumetric concentrations up to 15%, Figure 8.8 shows the contribution of the shear stress and the weight to the total pressure drop (Δp_2) per meter in the airlift pump suction pipe.

Table 8.1 lists the shear stress theories evaluated.

Author/Theory	Shear Stress Equation	Friction Factor Equation
Proposed Theory	4.27	4.28
Weber and Giot	3.34	3.40
Dedegil	3.42	3.44
Homogeneous	3.42	4.28
High Velocity	4.27 with $v_m^{s\ell} = v^{\ell}$	4.28

TABLE 8.1 : Two phase shear stress theories evaluated

The Homogeneous theory in Table 8.1 is the same as Dedegil's equation, however, the friction factor has been evaluated using Churchill's approximation (Chisholm 1983) applicable for all Reynolds number ranges (refer Figure 8.9).

The High Velocity theory arises from the argument, that the presence of the solids cause the liquid velocity to be higher due to a reduced flow area. From definitions of *in situ* and delivered volumetric concentrations (Equations 4.9 and 4.11) the increased velocity can be expressed as

$$v_l = \left[\frac{1 - C_{vd}^{sl}}{1 - C_{vt}^{sl}} \right] v_m \qquad (8.3)$$

This theory has been included for interest.

Figures 8.1 (a and b) and 8.5 (a and b) show the result of clear water tests performed to evaluate the validity of Churchill's friction factor equation (Equation 4.28) and to determine the pipe roughnesses of both test pipelines. The evaluation is achieved by comparing a graph of the calculated and measured shear stresses for a range of mixture velocities (Figure 8.1 a). A further evaluation is performed by considering a deviation graph (Figure 8.1 b) where the measured shear stress is plotted against the calculated shear stress.

The figures show clearly that the calculated shear stresses are predicted with adequate accuracy by all authors excepting Dedegil. Dedegil's (1982) friction factor equation (Equation 3.44) is shown to under-predict by 15%. This under-prediction is explained by an under-prediction of the Blasius smooth pipe friction factor for Reynolds numbers above 10^5 (Weber 1971). The Reynolds numbers for the clear water tests conducted in both test pipelines range from $1,5 \times 10^5$ to $8,5 \times 10^5$. Thus better agreement of Dedegil's shear stress, with the data, is observed at lower velocities where Reynolds numbers are lower and are closer to the Blasius friction factor range of applicability.

Using the test results, the pipeline roughnesses are calculated and listed in Table 8.2.

Pipeline NB mm	Roughness (k) mm
160	0,0001
90	0,015

TABLE 8.2 : Two phase pipeline roughnesses

Figures 8.2 a & b to 8.7 a & b show comparisons of the shear stress theories with measured data. The comparisons are both on graphs of shear stress versus mixture velocity and on deviation graphs of measured versus calculated shear stresses.

At 5% delivered volumetric concentration ($C_{vd}^{s\ell}$) in the 160 mm NB pipeline (Figures 8.2 a and b), the Homogeneous theory, Weber and Giot's shear stress theories tend to predict higher shear stresses than the Proposed theory, Dedegil's and the Higher Velocity theory. All simulated shear stresses, however, compare to a 10% accuracy at velocities above 2 m/s.

At a similar delivered volumetric concentration (4%) in the 90 mm NB pipeline (Figures 8.6 a and b), Dedegil simulates the shear stress much lower than the other authors. The Proposed theory slightly under-predicts, while Weber, Giot and the Homogeneous theory over-predict. All theories again compare to within 10% of the measured data.

Test results at higher delivered volumetric concentrations (10% to 15%) in the 160 mm NB pipeline (Figures 8.3 a & b, 8.4 a & b respectively) show measured mixture shear stresses to be less than the clear water shear stresses (Proposed theory). This is not considered possible, and is explained by the influence of the solid *in situ* volumetric concentration measurement. This variable is used to evaluate the "measured" shear stress in Equations 8.2, 4.6 and 4.7. Because of the much larger contribution of the weight to the total pressure loss at higher concentrations (refer Figure 8.3), a very small change in the solid *in situ* volumetric concentration measurement will have a large effect in the calculation of the "measured" shear stress. Typically it can be shown that if the solid *in situ* volumetric concentration measurement were 2-4% lower, acceptable comparisons of the Proposed and Dedegil's shear stress theories with measured data would be obtained in Figure 8.3. The over-prediction of shear stresses at the higher solid *in situ* volumetric concentrations will, however, have little effect on the total solid-liquid pressure loss prediction required for the airlift pump suction pipe.

Referring to Figures 8.3 a & b, 8.4 a & b, the Proposed theory, however, compares more favourably to the "measured" shear stresses than the other authors.

At higher delivered volumetric concentrations (9%) in the 90 mm NB pipeline (Figures 8.7 a & b), favourable agreement with the measured data is obtained by the Proposed, Dedegil and Higher Velocity theories while the Homogeneous, Giot and Weber's theories over-predict the solid-liquid shear stresses.

With exception of the tests conducted in the 160 mm NB pipeline at higher delivered volumetric concentrations (10% and 15%), all theories evaluated predict the solid-liquid shear stresses to within a 15% accuracy compared with "measured" data. Weber, Ciot and the Homogeneous theory generally result in higher solid-liquid shear stress predictions compared to the other authors. Generally, the closest prediction of the "measured" shear stress data is obtained with the Proposed theory.

For the test conducted at the higher delivered volumetric concentration (10% and 15%), a very small change in the *in situ* volumetric concentration results in a large effect in the calculation of the "measured" shear stress.

However, the shear stress compared with the weight of the two phase mixture contributes a small portion of the total pressure loss in the airlift pump section pipe. Therefore a slight inaccuracy in the prediction of this shear stress will have a small effect on the prediction of the total pressure loss.

8.2.2 Vertical two phase solid *in situ* volumetric concentration (C_{vt}^{sl})

The solid *in situ* volumetric concentration (C_{vt}^{sl}) is a function of the delivered volumetric concentration (C_{vd}^{sl}) as shown in Equation 4.14 below. For small particle sizes (3-15 mm) at high velocities, the settling velocity term in Equation 4.14 is small and thus the solid *in situ* volumetric concentration (C_{vt}^{sl}) is only slightly larger than the delivered volumetric concentration (C_{vd}^{sl}).

$$C_{vd}^{s\ell} = \frac{(v_m^{s\ell} - v_t')}{v_m^{s\ell}} C_{vt}^{s\ell} \qquad (4.14)$$

Because the delivered volumetric concentration ($C_{vd}^{s\ell}$) is an input variable in the airlift pump analysis, the solid *in situ* volumetric concentration ($C_{vt}^{s\ell}$) is obtained with reasonable accuracy. Consequently, most theories are expected to result in similar two phase solid *in situ* volumetric concentration predictions, provided the calculation procedure uses the delivered volumetric concentration as a variable.

Table 8.3 lists the solid *in situ* volumetric concentration theories evaluated.

Author/Theory	Equation
Proposed Theory	4.9 - 4.26
Weber (1976)	3.5
Weber (1982) and Dedegil	3.7
Giot	3.8

TABLE 8.3 : Two phase *in situ* volumetric concentration theories evaluated

Figures 8.10 to 8.14 show comparisons of *in situ* volumetric concentration theories with measured data. The comparisons are on deviation graphs of measured versus calculated *in situ* volumetric concentrations.

Figure 8.10 shows the results of tests conducted at 5% delivered volumetric concentration (C_{vd}^{sl}) in the 160 mm NB pipeline. Noticeably predictions by all the authors are similar. Weber's (1976) approach shows slight over-prediction, while his later approach (1982) agrees favourably with the Proposed theory and the calculation procedure presented by other authors. Predictions at higher velocities are more accurate because of the diminishing influence of the solid settling velocity variable in Equation 4.14.

Figure 8.11 shows the results of tests conducted at a higher delivered volumetric concentration (10%) in the 160 mm NB pipeline. All predictions compare mostly within 10 to 15% of the measured data. At 15% delivered volumetric concentration (Figure 8.12), all theories again predict the solid *in situ* volumetric concentration to within 10% of the measured data.

The severe over-predictions shown in Figure 8.13 on the 90 mm NB pipeline are the result of the level of accuracy attainable in the solid *in situ* volumetric concentration measurement. At the low delivered volumetric concentration (1-4%), at which this set of tests was conducted, measurement with a gamma ray densitometer becomes exceedingly difficult. At higher concentrations, however, (Figure 8.14) all authors again predict the measured solid *in situ* concentrations favourably (within 10 to 15% deviation of the measured data).

For all the tests conducted the Proposed theory agrees well with the measured data and theories presented by other authors. The advantage of this theory, however, compared with other theories, is the ability to predict solid in situ volumetric concentrations (C_{vt}^{sl}) *for a wide range of particle sizes, particle size distributions and particle shapes. This is achieved by considering each particle size, fraction and characteristics during the evaluation of solid in situ volumetric concentrations. Furthermore, allowance is made for the effect of hindered settling caused by the presence of other solids. This ability makes the Proposed theory more favourable for evaluating solid in situ concentrations in the marine gravel environment, where a large diversity of particle characteristics are encountered.*

8.2.3 Vertical two phase solid-liquid total pressure loss (Δp_2)

Having evaluated both the two phase shear stress and the two phase solid *in situ* volumetric concentration, the total vertical pressure loss in the airlift pump suction pipe can be calculated.

Table 8.4 summarizes the final theories evaluated.

Author	Shear Stress Equation	Friction Factor Equation	*in situ* Concentration Theory
Proposed Theory	4.27	4.28	4.9 to 4.26
Weber (1976)	3.34	3.40	3.5
Weber (1982)	3.34	3.40	3.7
Dedegil	3.42	3.44	3.7
Giot	3.34	3.40	3.8

TABLE 8.4 : Two phase pressure theories evaluated

Figures 8.15 to 8.21 show the two phase total pressure loss theories compared with measured two phase total pressure losses. The comparisons are on a deviation graph of measured total pressure loss versus calculated total pressure loss.

The figures show that good approximations of the total pressure loss are achieved by all theories evaluated.

Figures 8.15 to 8.21 show that the total pressure loss is predicted to within 5% deviation of the measured data for all tests conducted at a range of solid *in situ* volumetric concentrations and for two pipe sizes. On closer examination of the figures, the theories presented by Weber (1976 & 1982), Dedegil and Giot result in slightly higher predicted total pressure losses than the Proposed theory. Furthermore, the total pressure loss approximations with the Proposed theory tend to plot closer to the 100% agreement line than the presented theories by the other authors.

For all the tests, the Proposed theory results in slightly more favourable total pressure drop predictions than the other theories evaluated.

Figure : 8.1a
Description : Solid/Liquid Shear Stress Theories

Airlift Pump Investigation

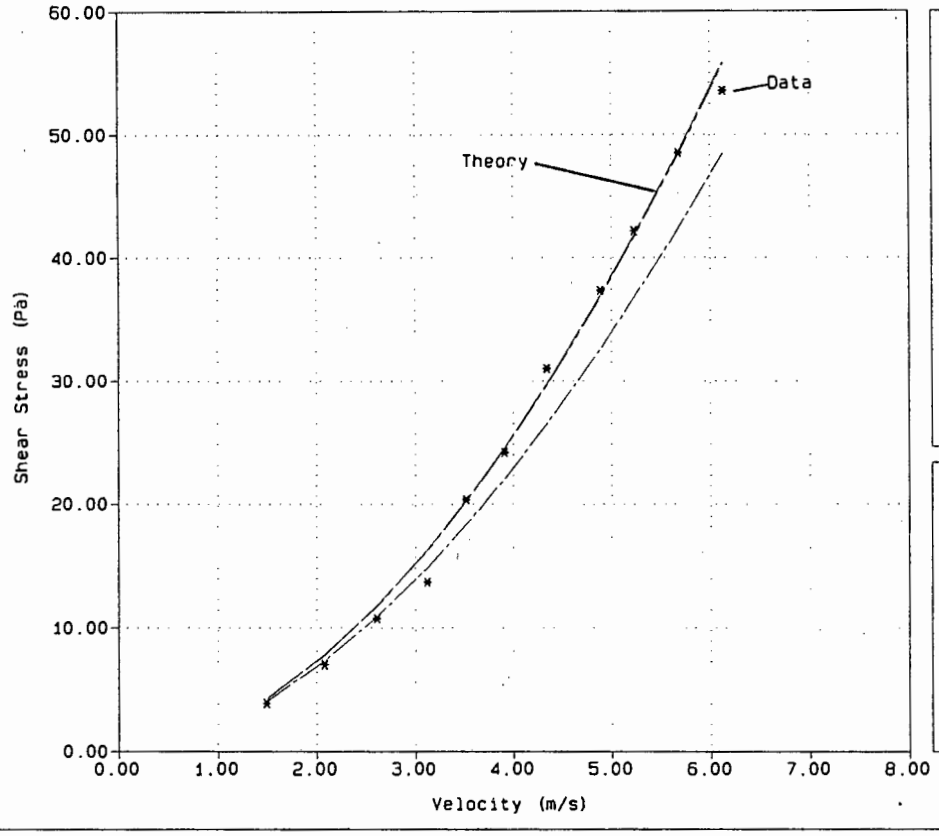

LEGEND

*
Data

Proposed Theory

Weber & Giot

Dedegil

Homogeneous

Higher vel.

NOTES
Test Ref: DL001305
Apparatus: PipeLine
Pipe Diam: 150mm NB
Material : Cl.Water

apprx Cvd: 0 %

Figure : 8.1b
Description : Solid/Liquid Shear Stress Theories

Airlift Pump Investigation

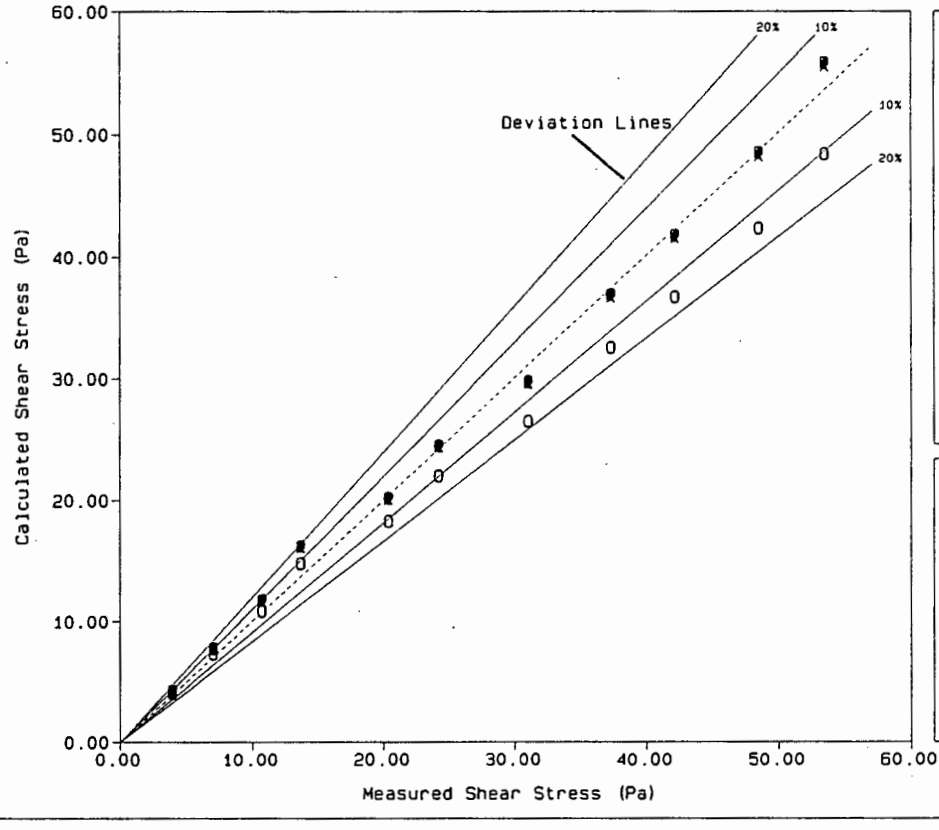

LEGEND

\+
Proposed Theory
@
Weber & Giot
D
Dedegil
X
Homogeneous
#
Higher vel.

100% Agreement Line

NOTES
Test Ref: DL001305

Apparatus: PipeLine
Pipe Diam: 150mm NB
Material : Cl.Water

apprx Cvd: 0 %

Figure : 8.2a
Description : Solid/Liquid Shear Stress Theories

Airlift Pump Investigation

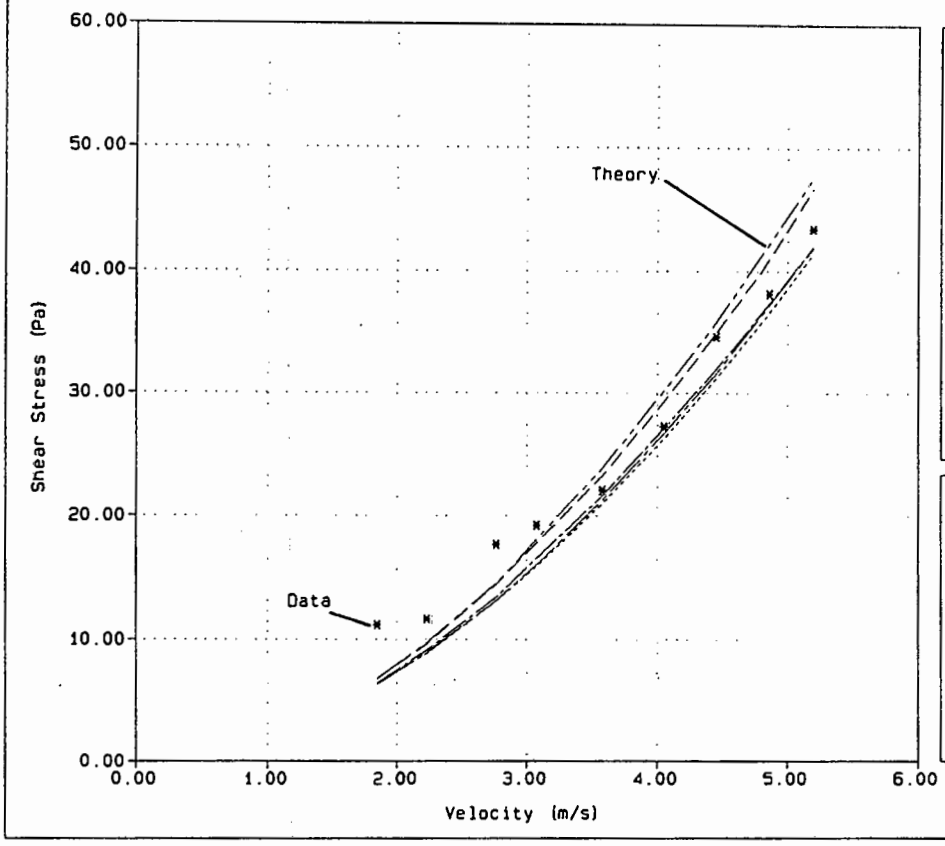

LEGEND

*
Data
Proposed Theory
Weber & Giot
Dedegil
Homogeneous
Higher vel.

NOTES
Test Ref: DL051807
Apparatus: PipeLine
Pipe Diam: 160mm NB
Material : Mar.Grav

apprx Cvd: 5 %

Figure : 8.2b
Description : Solid/Liquid Shear Stress Theories

Airlift Pump Investigation

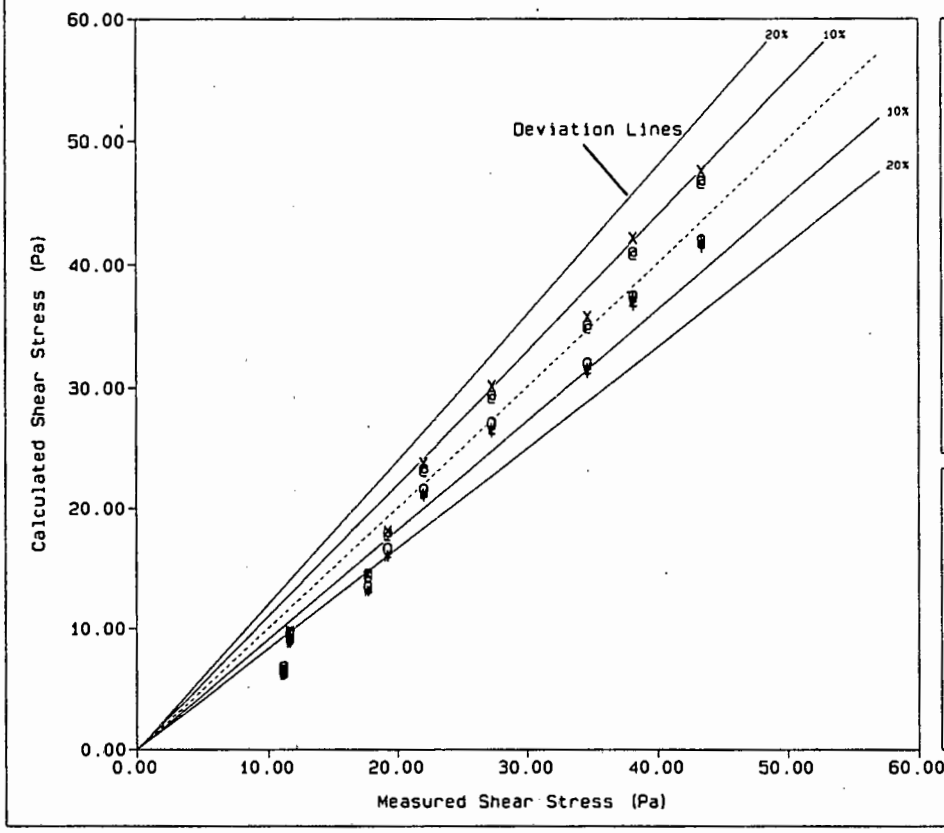

LEGEND

\+
Proposed Theory
e
Weber & Giot
D
Dedegil
X
Homogeneous
#
Higher vel.
100% Agreement Line

NOTES
Test Ref: DL051807

Apparatus: PipeLine
Pipe Diam: 160mm NB
Material : Mar.Grav

apprx Cvd: 5 %

Figure : 8.3a
Description : Solid/Liquid Shear Stress Theories

Airlift Pump Investigation

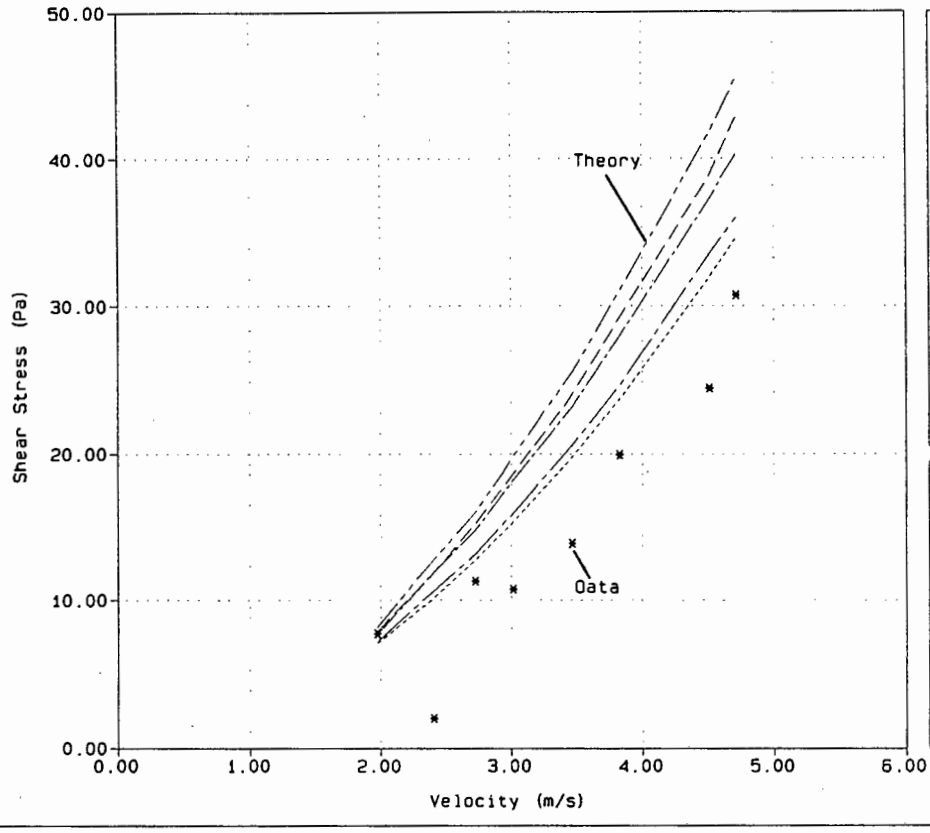

Figure : 8.3b
Description : Solid/Liquid Shear Stress Theories

Airlift Pump Investigation

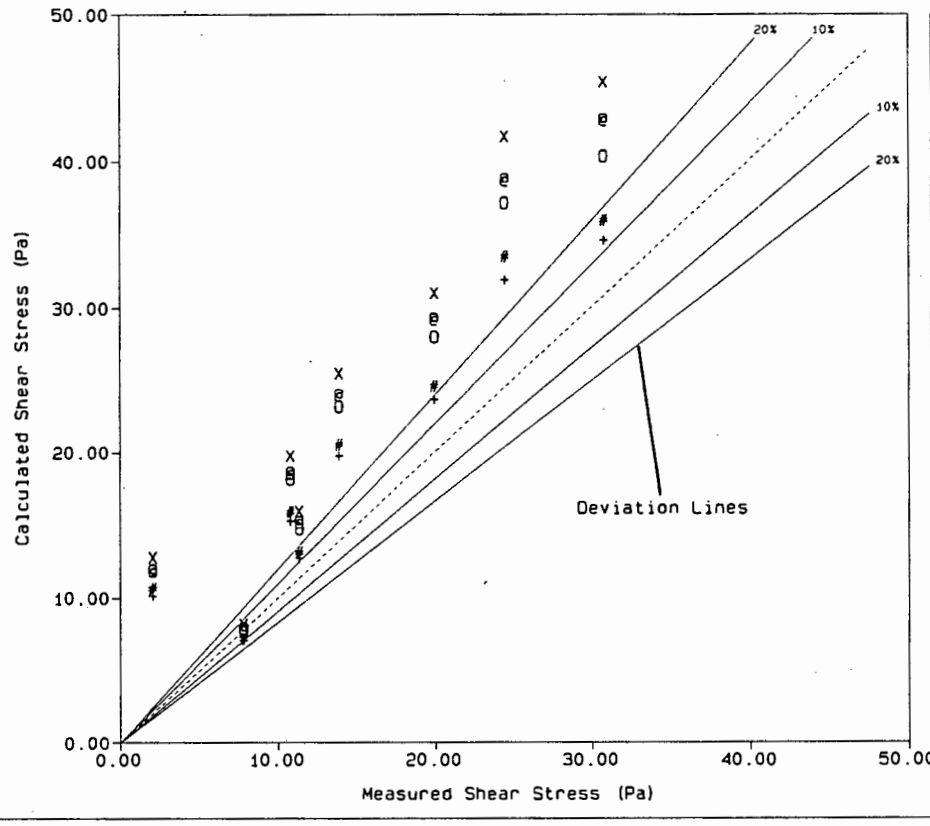

Figure : 8.4a
Description : Solid/Liquid Shear Stress Theories

Airlift Pump Investigation

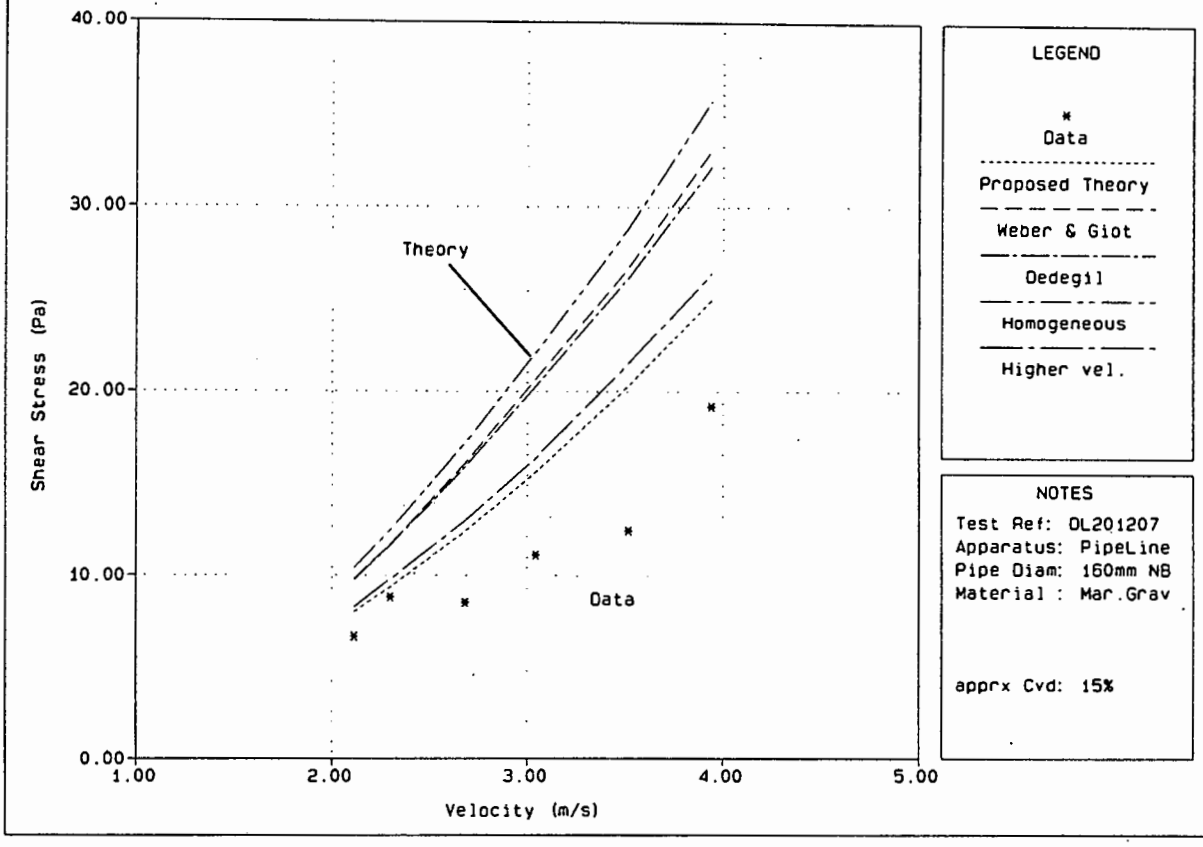

Figure : 8.4b
Description : Solid/Liquid Shear Stress Theories

Airlift Pump Investigation

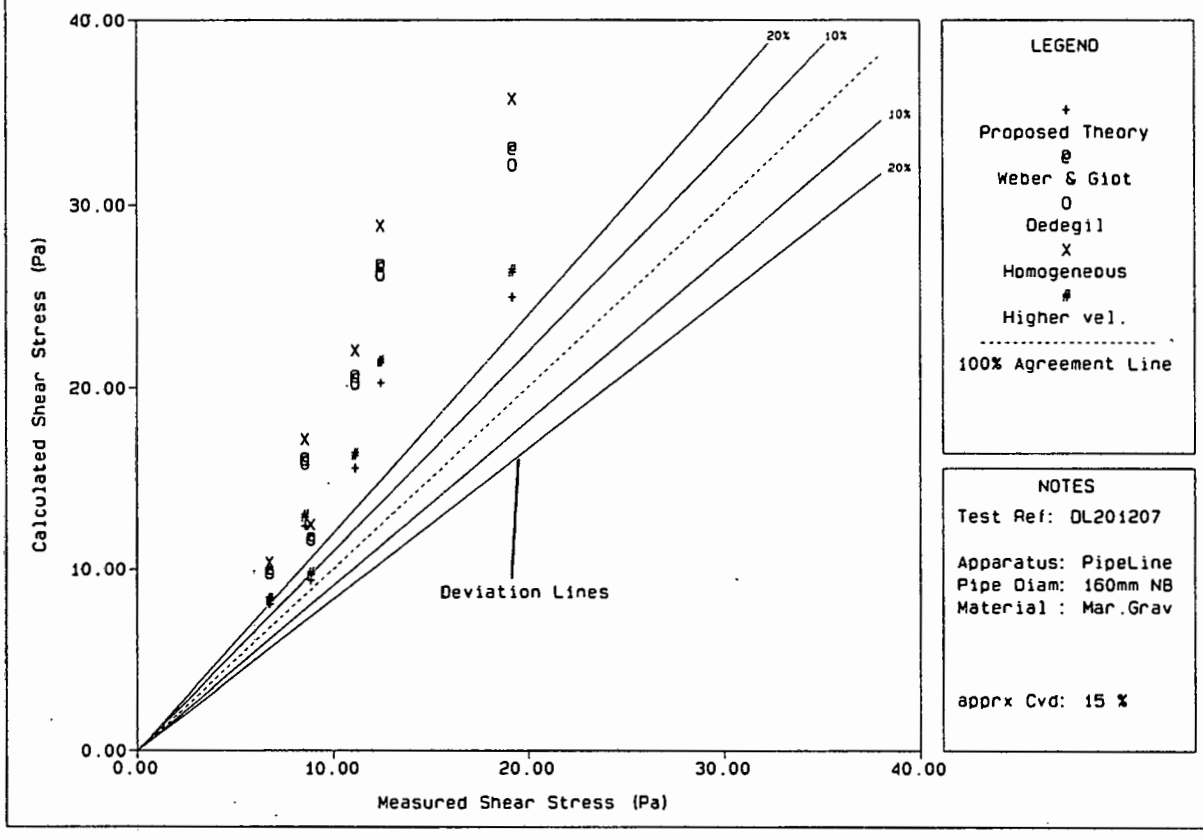

Figure : 8.5a
Description : Solid/Liquid Shear Stress Theories

Airlift Pump Investigation

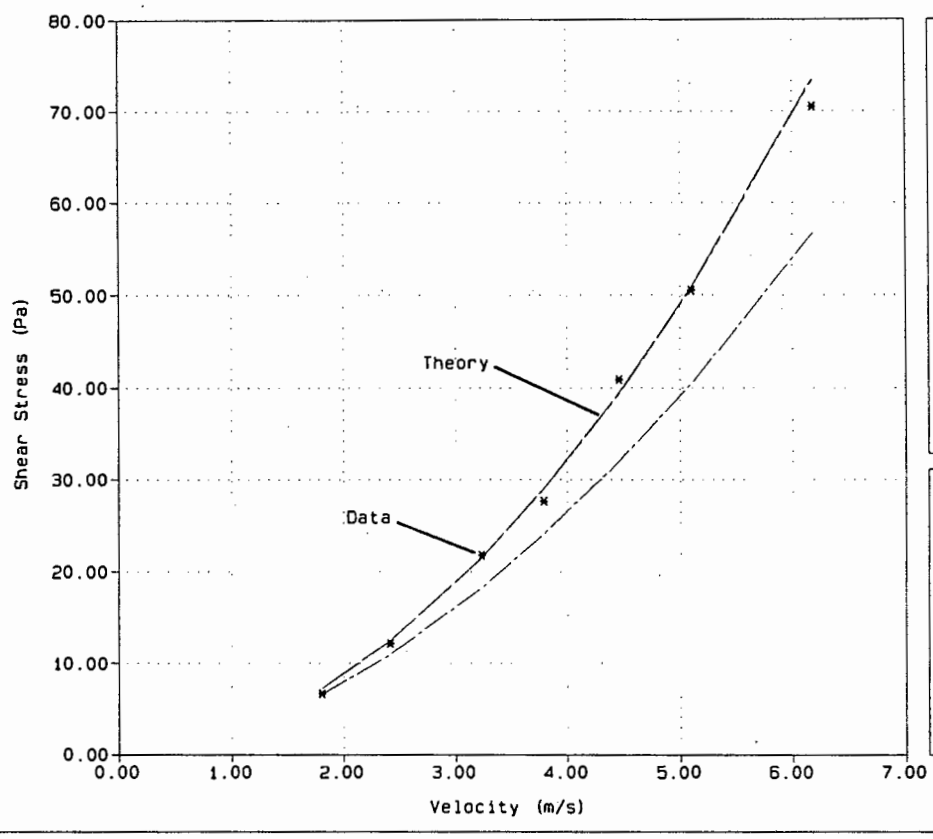

LEGEND

*
Data

Proposed Theory

Weber & Giot

Dedegil

Homogeneous

Higher vel.

NOTES

Test Ref: DS001605
Apparatus: PipeLine
Pipe Diam: 90mm NB
Material : Cl.Water

apprx Cvd: 0 %

Figure : 8.5b
Description : Solid/Liquid Shear Stress Theories

Airlift Pump Investigation

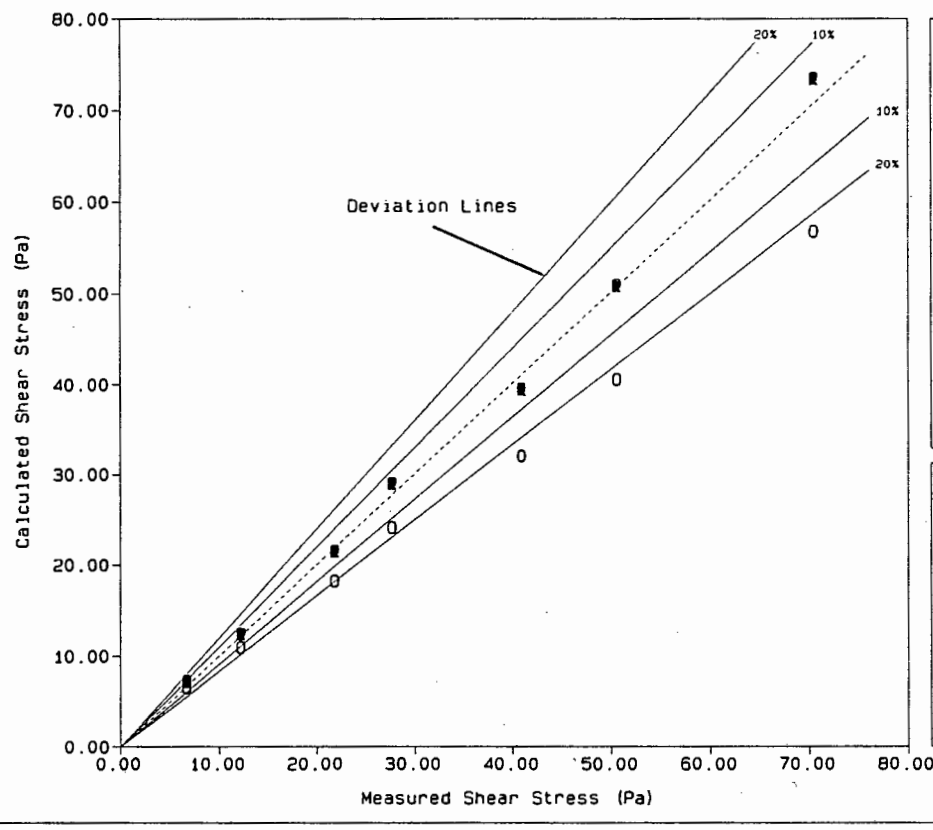

LEGEND

\+
Proposed Theory
@
Weber & Giot
O
Dedegil
X
Homogeneous
#
Higher vel.

100% Agreement Line

NOTES

Test Ref: DS001605

Apparatus: PipeLine
Pipe Diam: 90mm NB
Material : Cl.Water

apprx Cvd: 0 %

Figure : 8.6a
Description : Solid/Liquid Shear Stress Theories

Airlift Pump Investigation

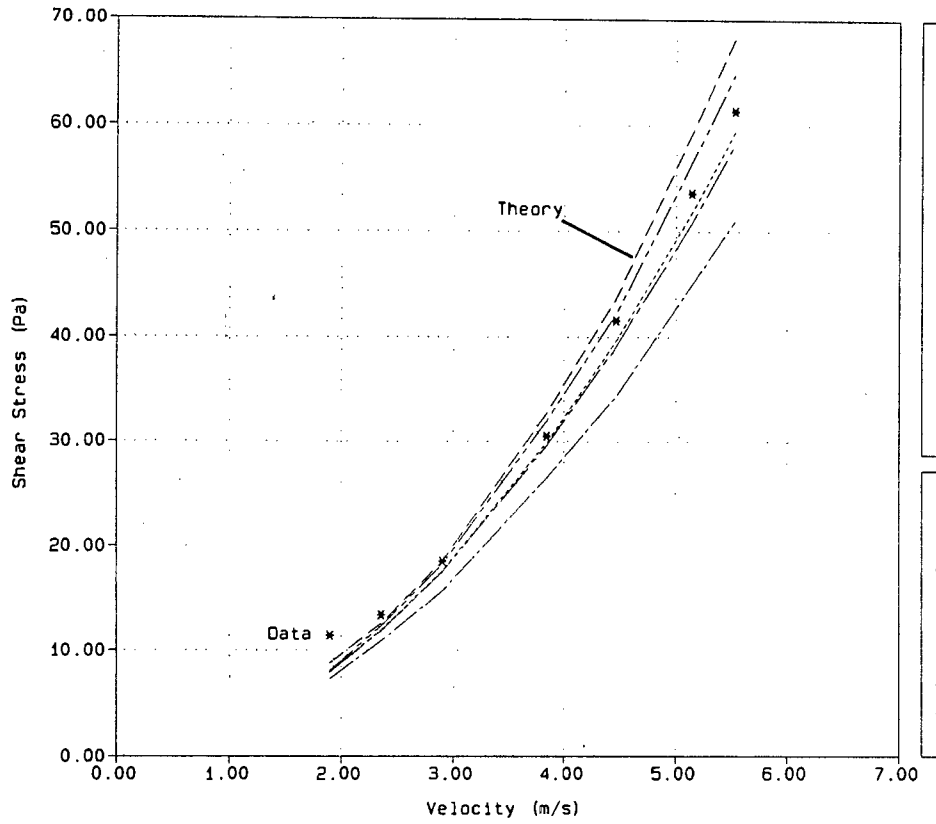

LEGEND

*
Data

Proposed Theory

Weber & Giot

Dedegil

Homogeneous

Higher vel.

NOTES
Test Ref: DS040801
Apparatus: Pipeline
Pipe Diam: 90mm NB
Material : Mar.Grav

apprx Cvd: 4 %

Figure : 8.6b
Description : Solid/Liquid Shear Stress Theories

Airlift Pump Investigation

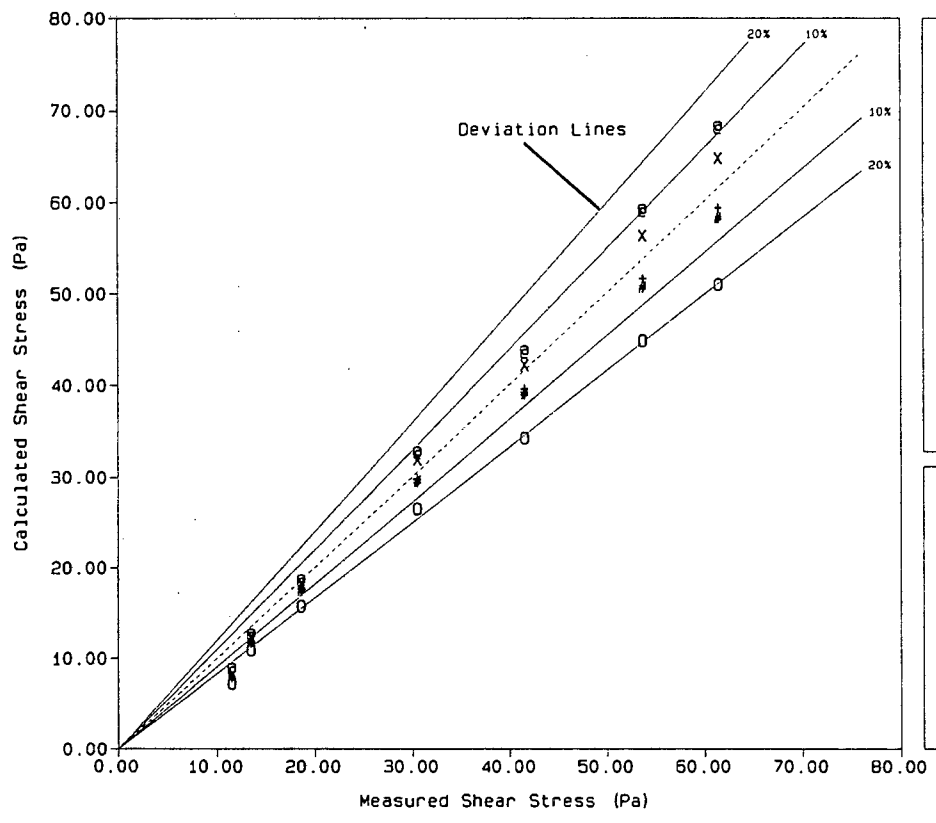

LEGEND

\+
Proposed Theory
@
Weber & Giot
D
Dedegil
X
Homogeneous
#
Higher vel.

100% Agreement Line

NOTES
Test Ref: DS040801

Apparatus: PipeLine
Pipe Diam: 90mm NB
Material : Mar.Grav

apprx Cvd: 4 %

Figure : 8.7a
Description : Solid/Liquid Shear Stress Theories

Airlift Pump Investigation

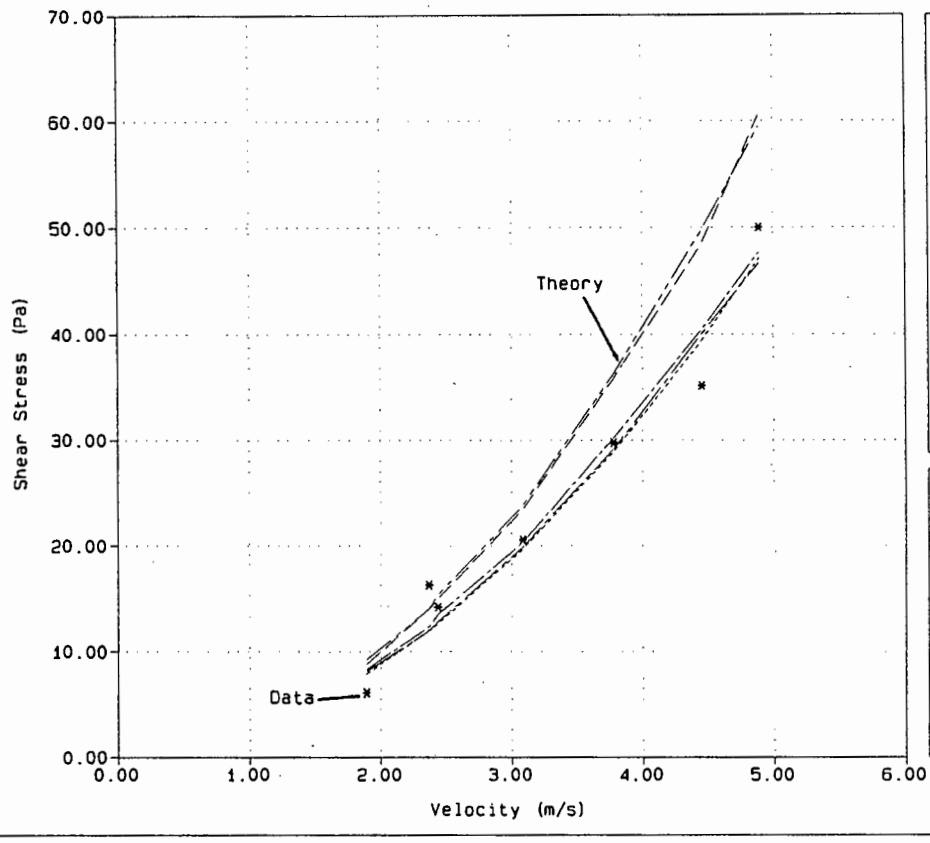

Figure : 8.7b
Description : Solid/Liquid Shear Stress Theories

Airlift Pump Investigation

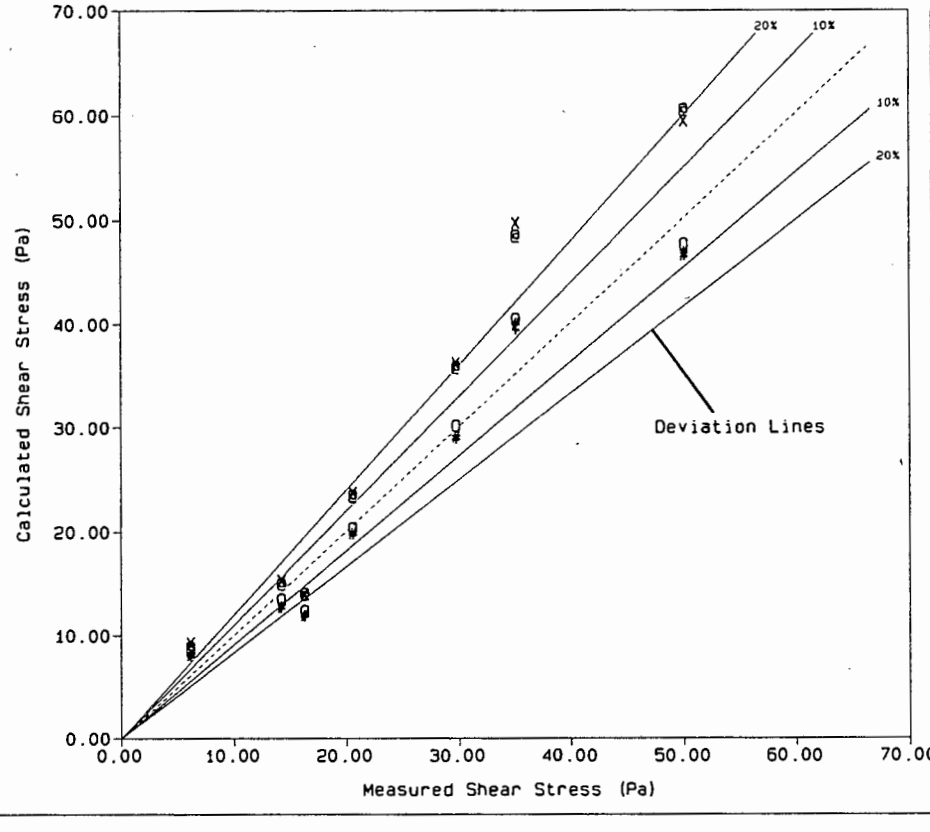

Figure : 8.8
Description : 2 Phase Shear Stress, Weight Contribution

Airlift Pump Investigation

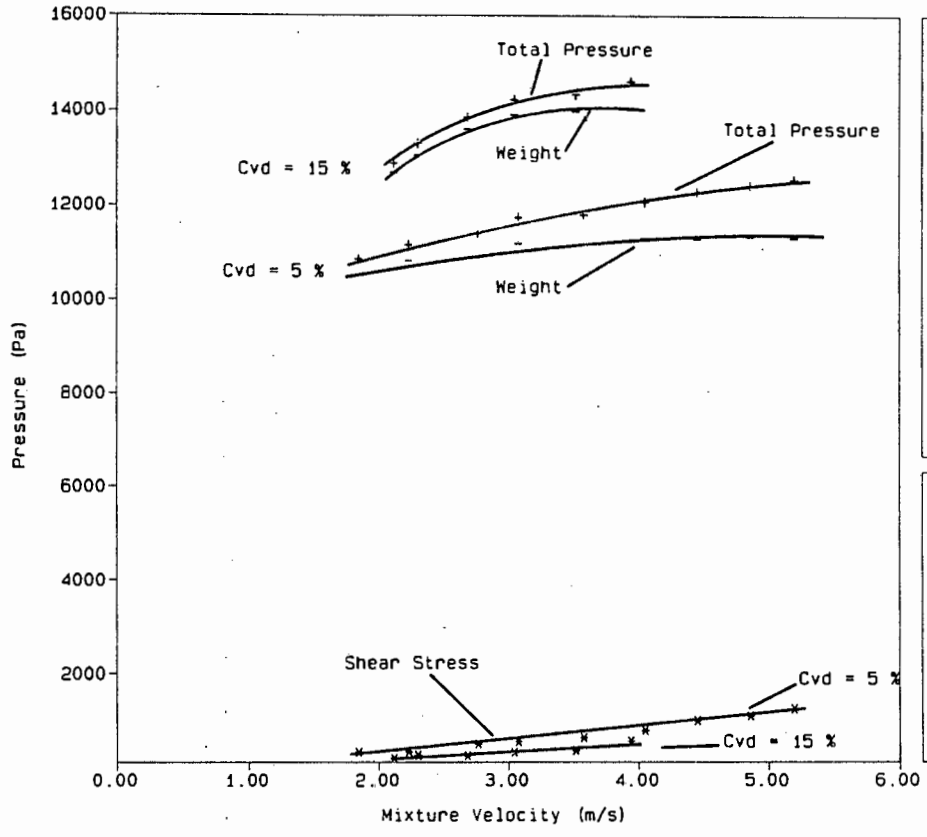

LEGEND

+ Total Pressure

* Shear Stress

- Weight

NOTES

Test Ref: -

Figure : 8.9
Description : Churchill, s Friction Factor Equation

Airlift Pump Investigation

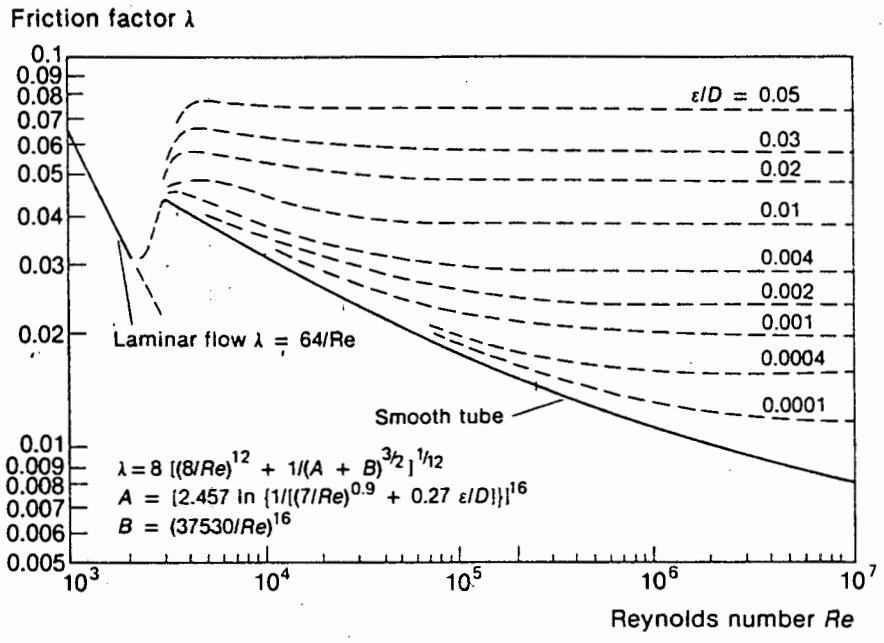

LEGEND

NOTES

Test Ref: -

Ref: Chisholm (1983)

Figure : 8.10
Description : Solid/Liquid Cvt Theories

Airlift Pump Investigation

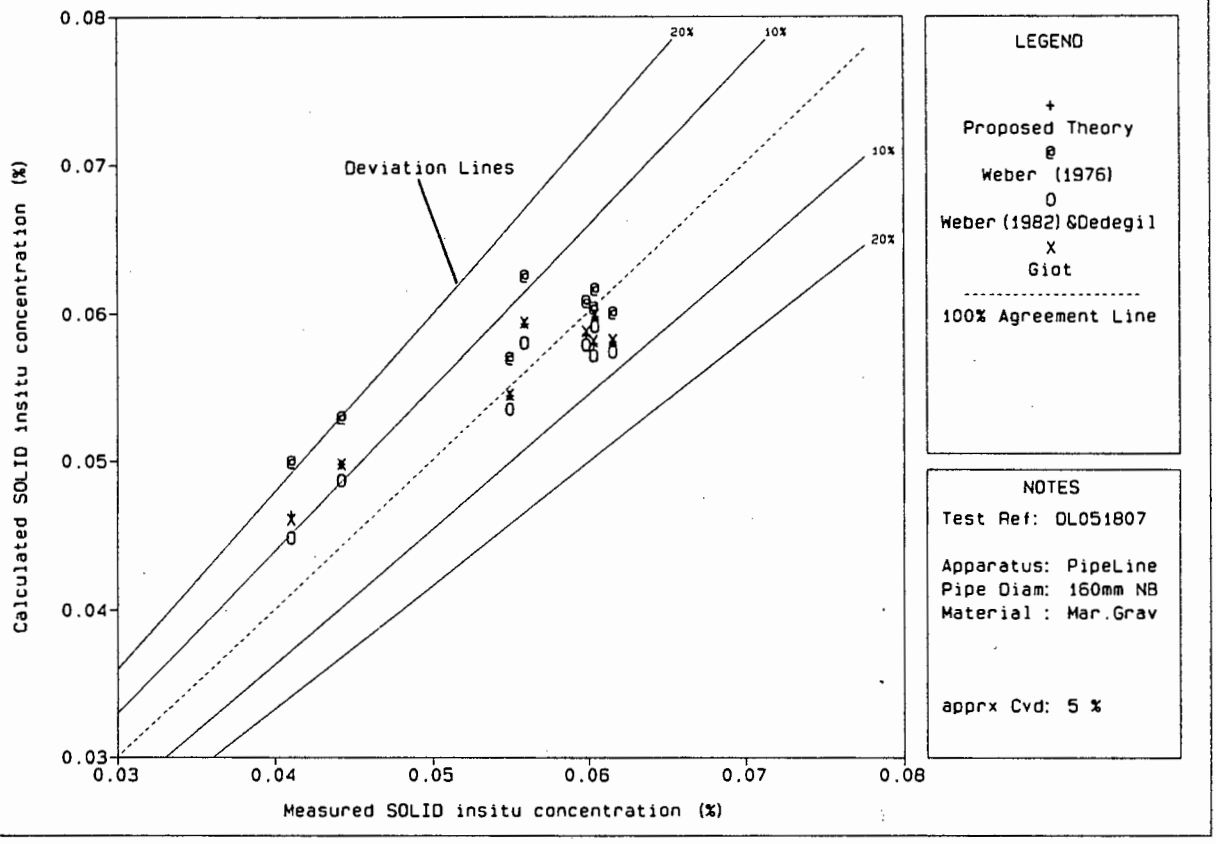

Figure : 8.11
Description : Solid/Liquid Cvt Theories

Airlift Pump Investigation

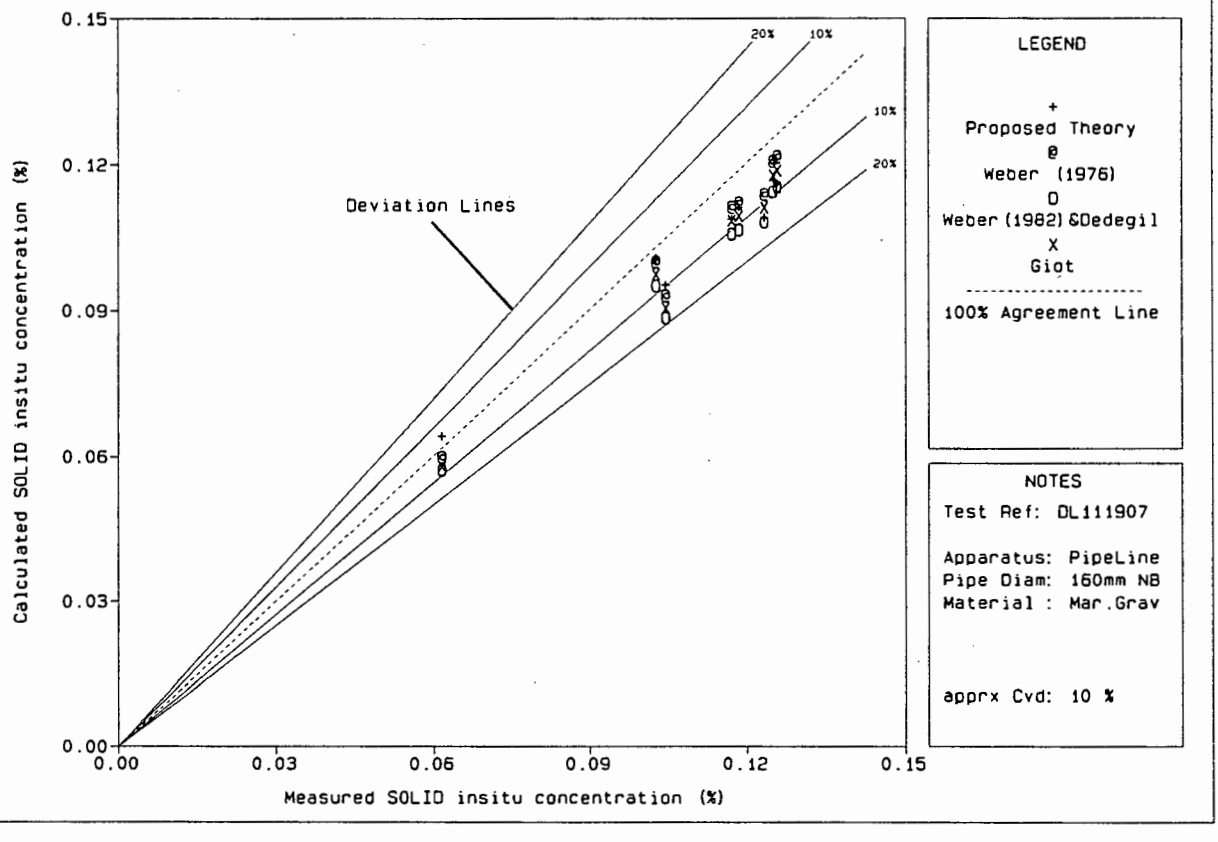

Figure : 8.12
Description : Solid/Liquid Cvt Theories

Airlift Pump Investigation

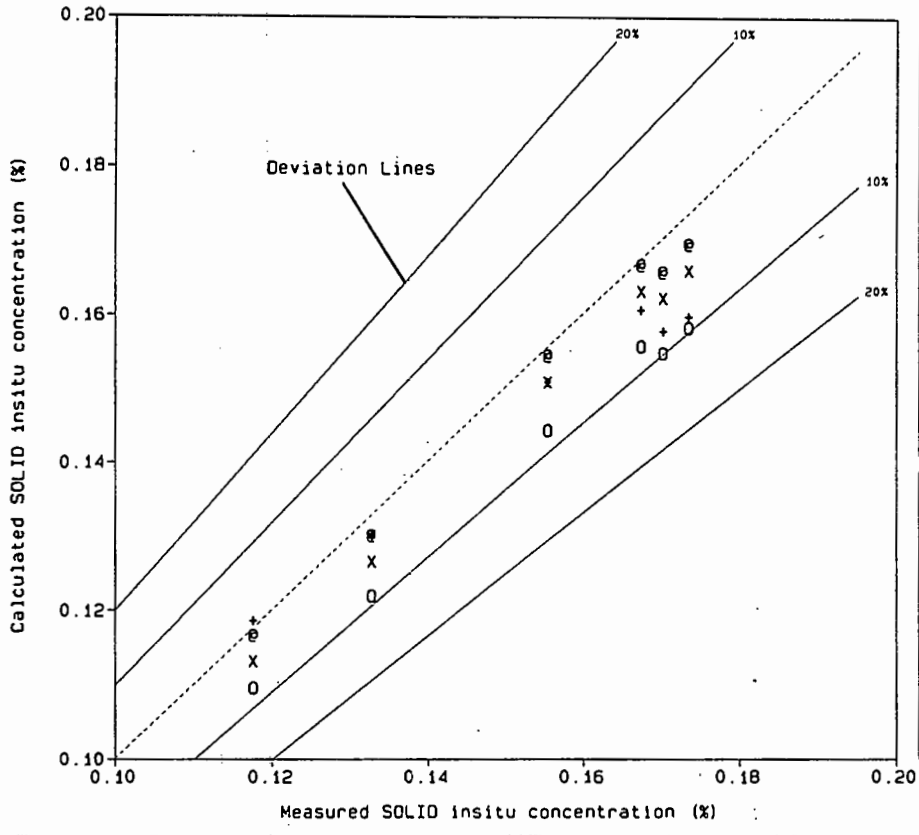

Figure : 8.13
Description : Solid/Liquid Cvt Theories

Airlift Pump Investigation

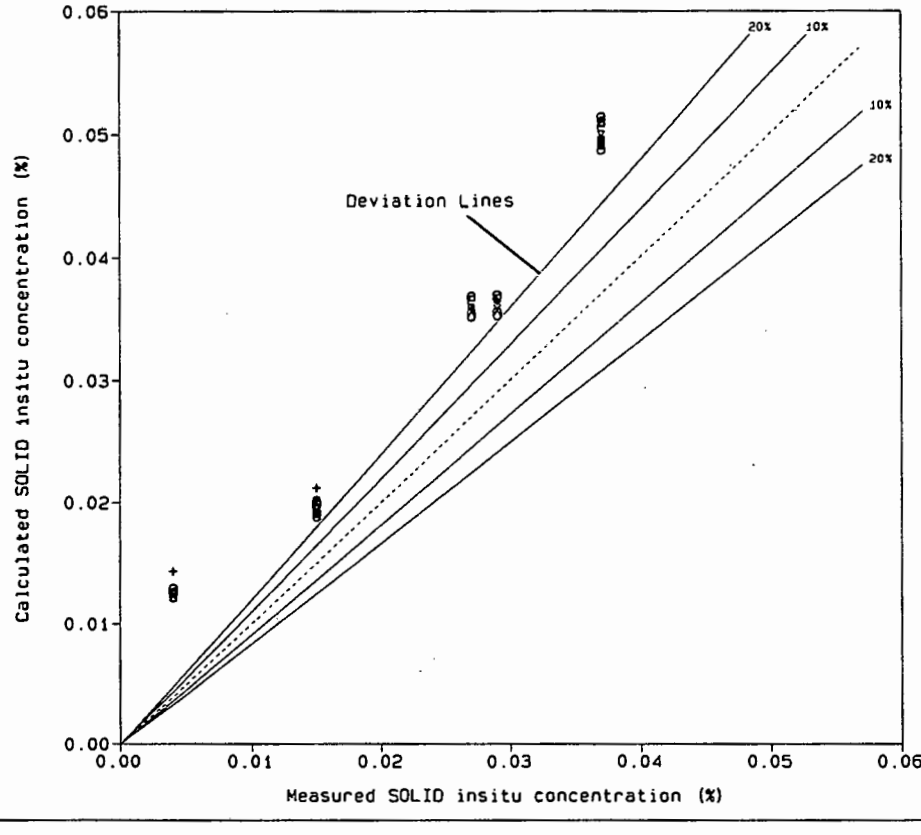

Figure : 8.14
Description : Solid/Liquid Cvt Theories

Airlift Pump Investigation

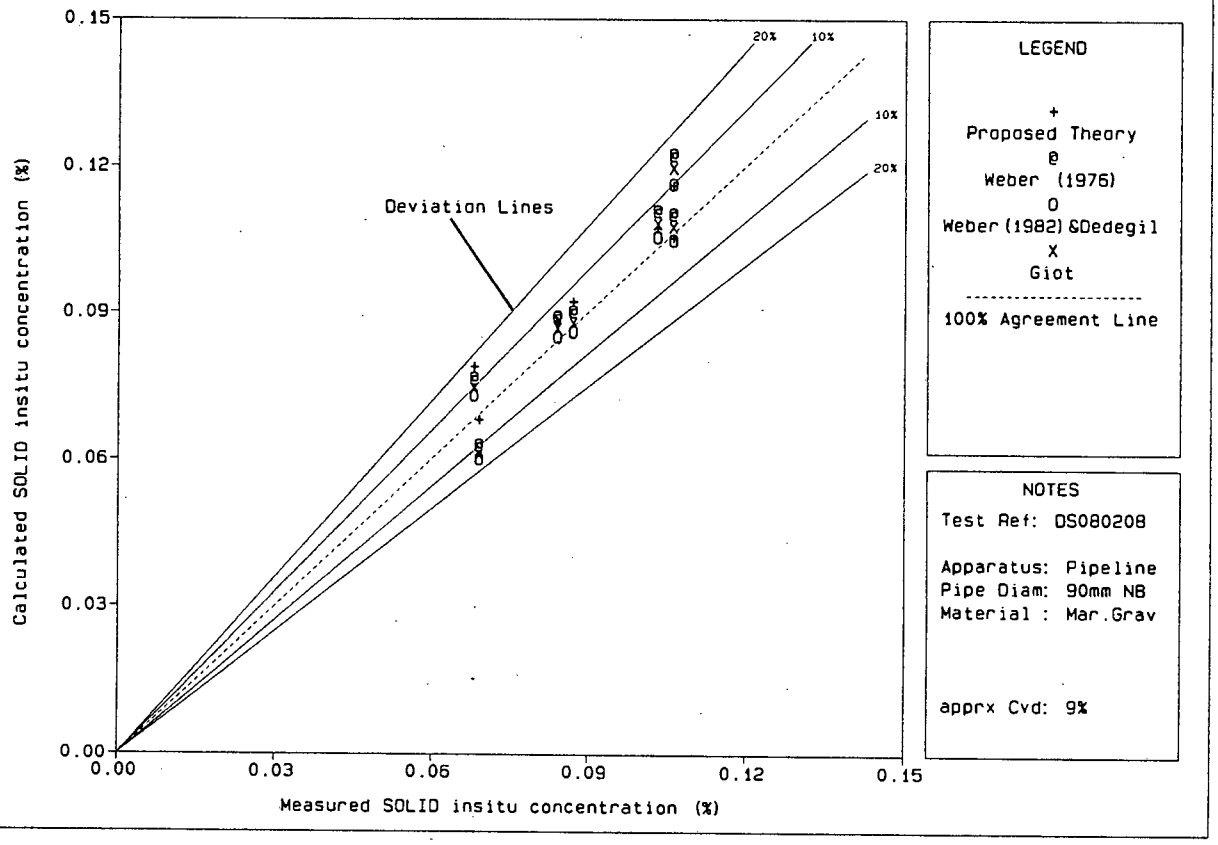

Figure : 8.15
Description : Solid/Liquid Total Pressure Loss Theories

Airlift Pump Investigation

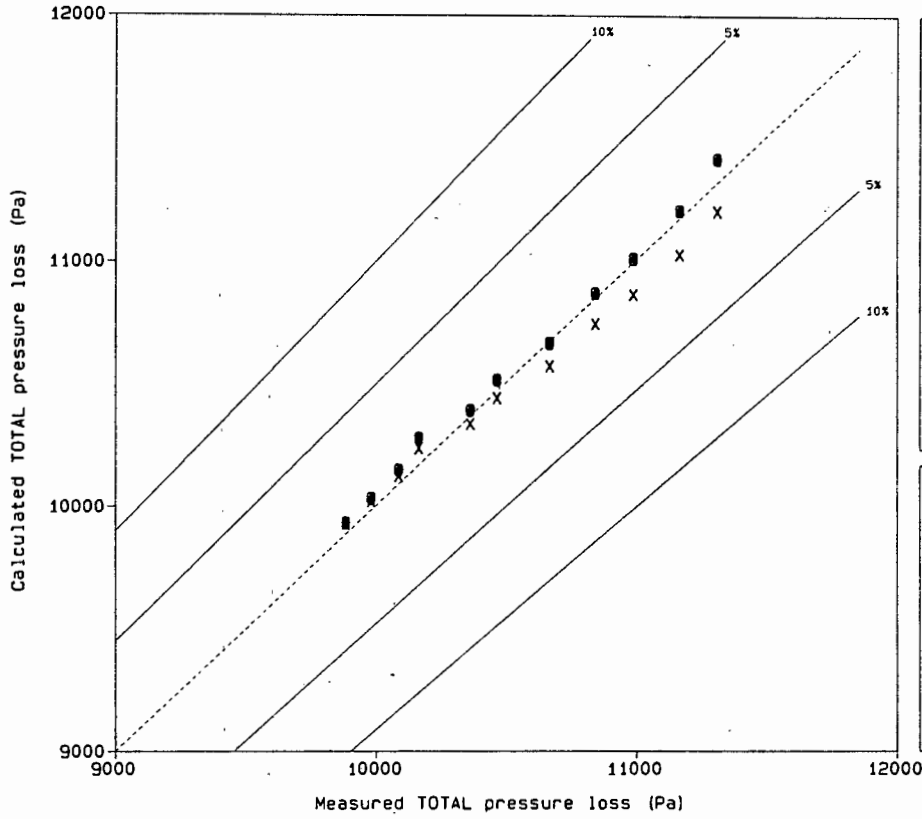

Figure : 8.16
Description : Solid/Liquid Total Pressure Loss Theories

Airlift Pump Investigation

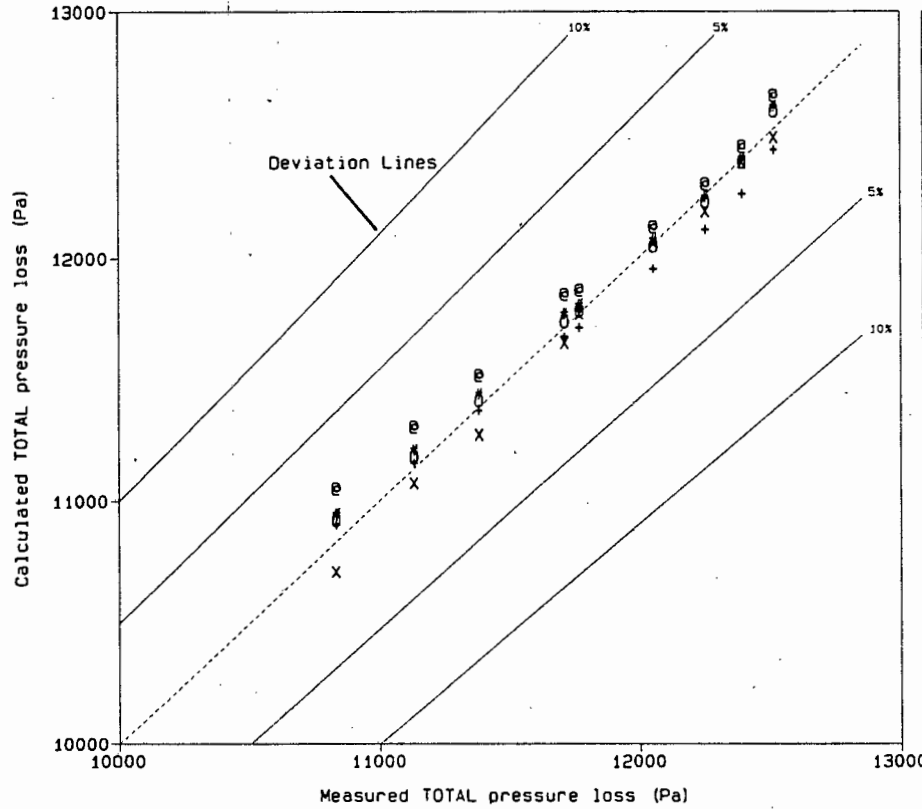

Figure : 8.17 Airlift Pump
Description : Solid/Liquid Total Pressure Loss Theories Investigation

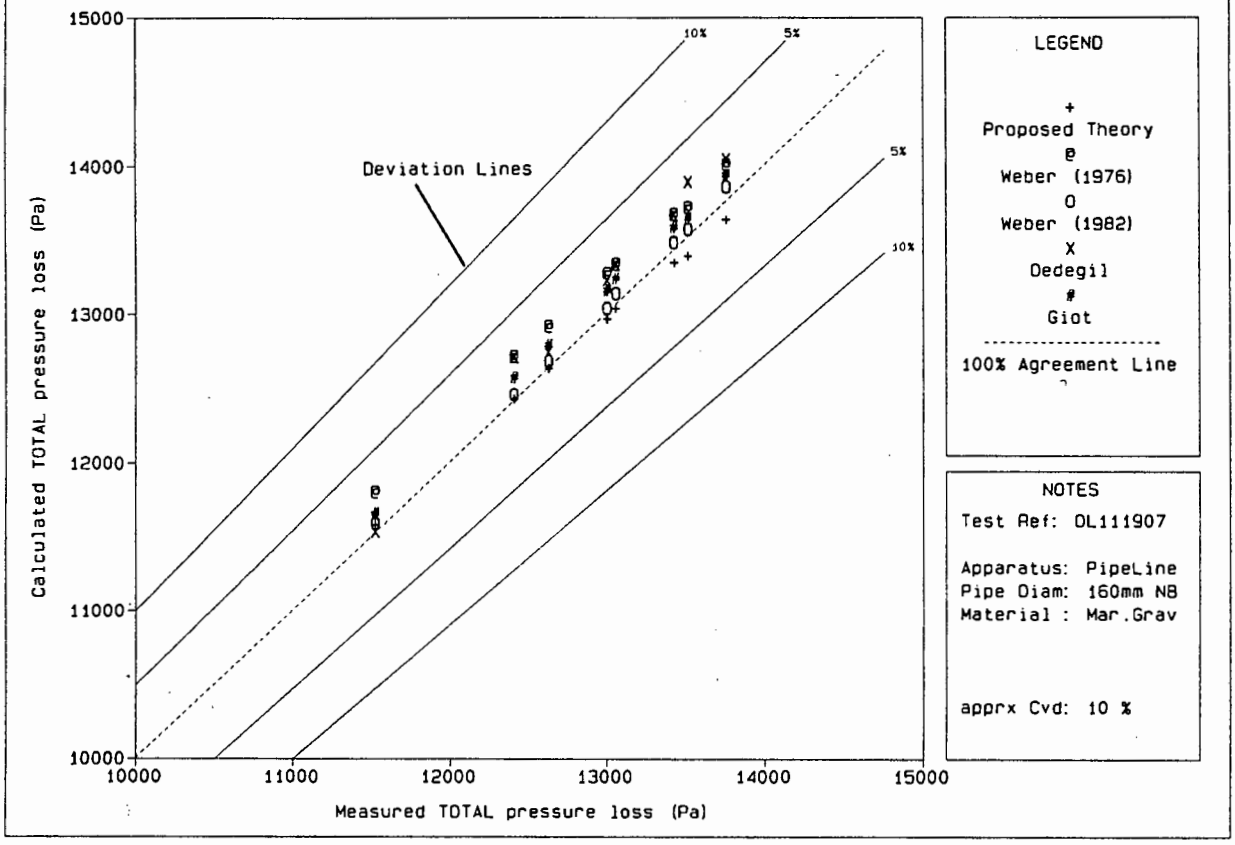

Figure : 8.18 Airlift Pump
Description : Solid/Liquid Total Pressure Loss Theories Investigation

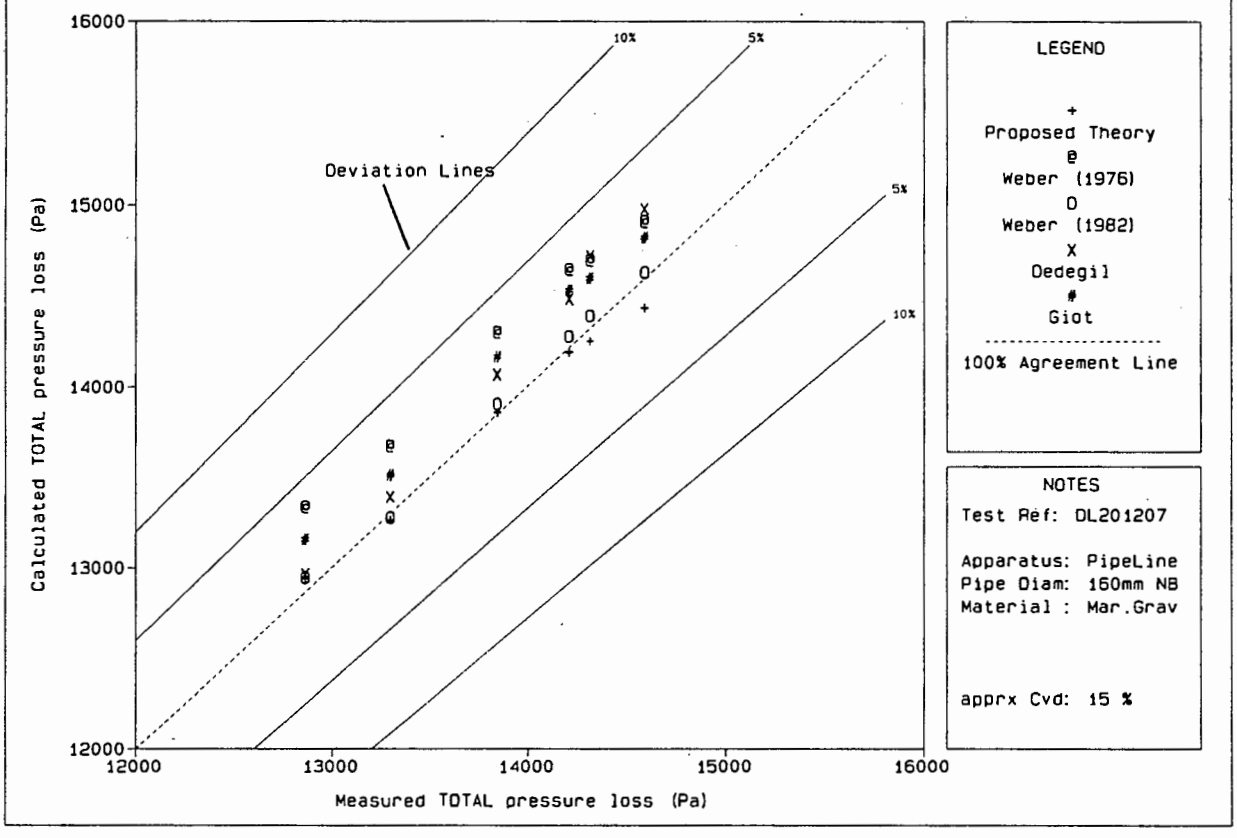

Figure : 8.19
Description : Solid/Liquid Total Pressure Loss Theories
Airlift Pump Investigation

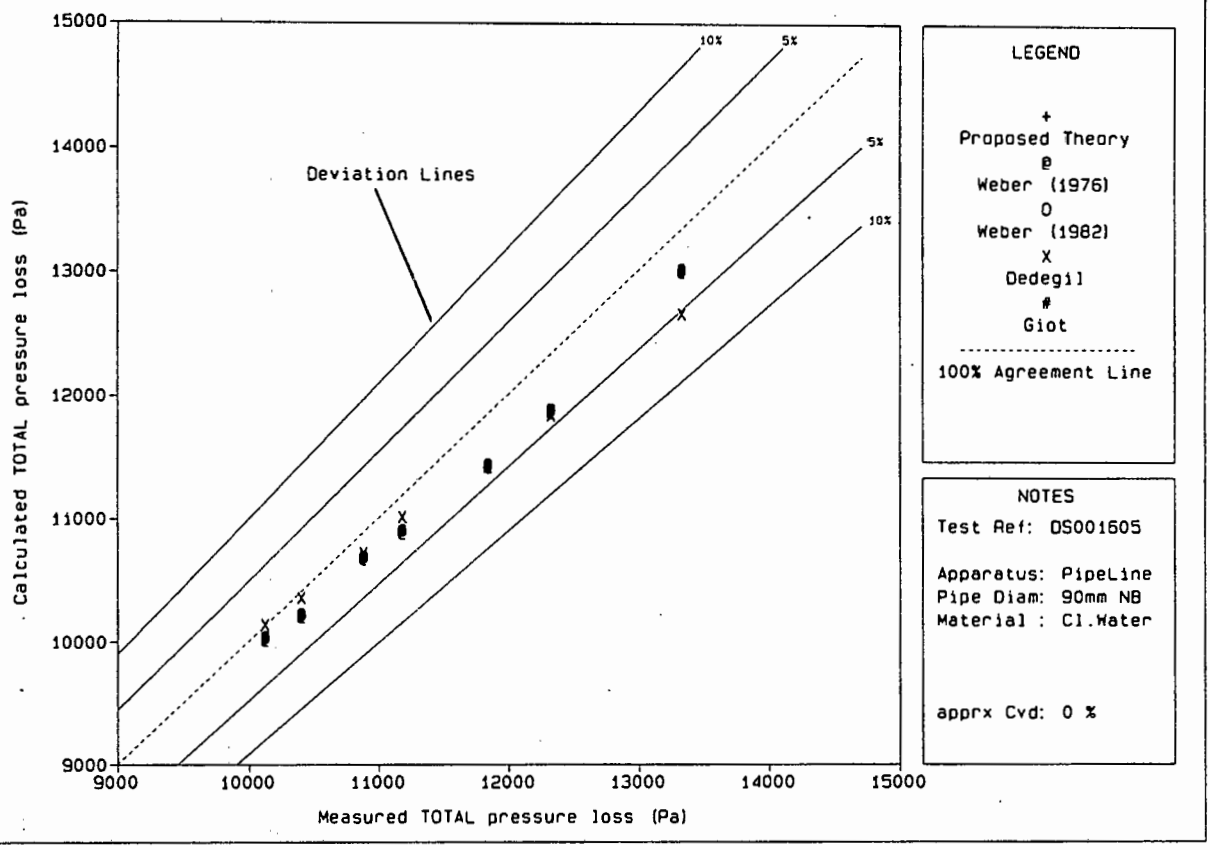

Figure : 8.20
Description : Solid/Liquid Total Pressure Loss Theories
Airlift Pump Investigation

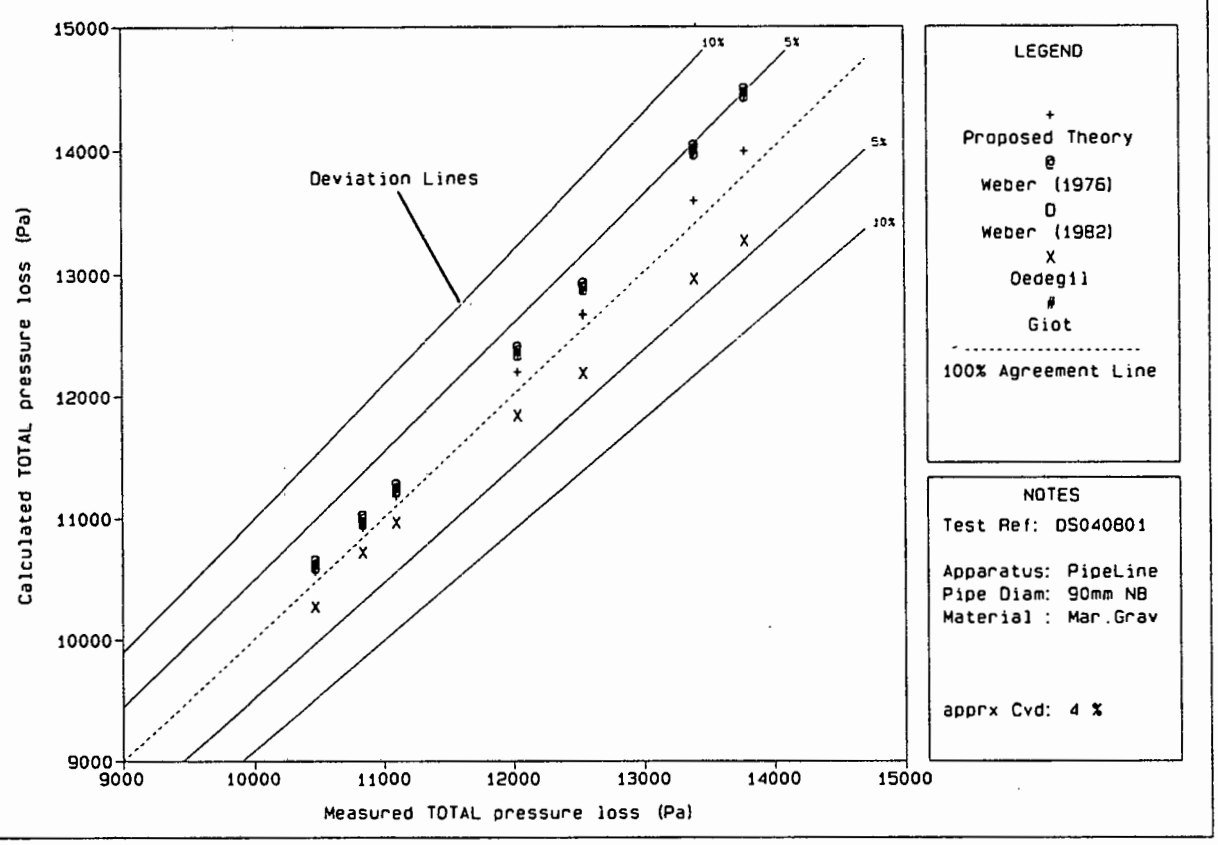

Figure : 8.21 Airlift Pump
Description : Solid/Liquid Total Pressure Loss Theories Investigation

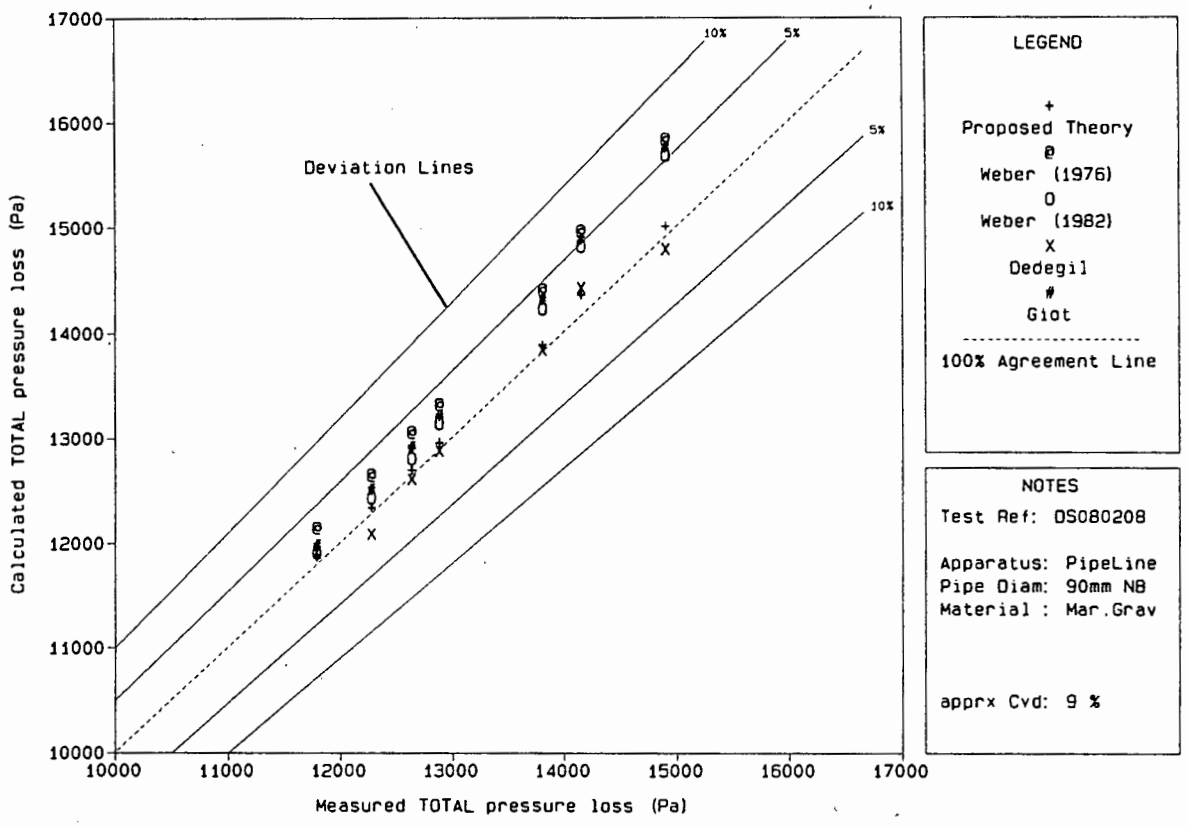

8.3 SINGLE PARTICLE SETTLING VELOCITY TESTS (AIR-WATER MIXTURES)

Purpose :

Measurement of the effect of gas-liquid mixtures on single spherical particle settling velocities.

Figure 8.22 shows the results of the experiments conducted using 15,8 mm diameter spheres while Figure 8.23 shows the same for the 24,5 mm diameter spheres.

In both figures, the settling velocities are shown for a range of gas *in situ* volumetric concentrations. The gas *in situ* volumetric concentration is calculted using Zuber and Findlay's (1965) drift flux model, (verified by Berg (1987)).

$$v_g = C_{lg}\, v_m^{lg} + v_B^{l} \tag{8.4}$$

Using continuity relationships, Equation (8.4) is rewritten as :

$$\frac{1}{\epsilon_g^{lg}} \left(\frac{Q_g}{A}\right) = C_{lg} \left(\frac{Q_l}{A} + \frac{Q_g}{A}\right) + v_B^{l} \tag{8.5}$$

where ϵ_g^{lg} = gas *in situ* volumetric concentration in a two phase liquid-gas mixture

$Q_{g,l}$ = gas and liquid flow rates

A = pipe cross-sectional area

v_B^{l} = bubble rise velocity

C_{lg} = distribution parameter.

Considering no liquid flow in the standpipe and evaluating the bubble rise velocity as the Taylor bubble drift velocity with the distribution parameter set to 1,2 (Berg 1987), the gas *in situ* concentration in the standpipe is expressed as :

$$\frac{1}{\epsilon_g}\left(\frac{Q_g}{A}\right) = 1{,}2\left(\frac{Q_g}{A}\right) + 0{,}35\sqrt{gd} \qquad (8.6)$$

From Figure 8.22 a 5% increase in the particle settling velocity for gas *in situ* concentrations less than 40% is observed compared with the theoretical clear water settling velocity. This response is caused by the particles falling through the rising gas bubbles in the gas-liquid mixture. Furthermore, minor oscillations in the mixture are observed, when compared to large gas flow rates with gas *in situ* volumetric concentrations above 40%. The increased mixture oscillations in this region results in the particles stalling or being carried upwards for short distances before falling through or around the gas bubbles. The result is erratic particle fall paths and the trumpet shaped scatter of particle settling velocities shown. The extended fall paths significantly reduce the settling velocity of some particles while other particles which missed the gas bubbles exhibited accelerated settling velocities. On average, the particle settling velocities are scattered about the theoretical particle settling velocity in clear water calculated with Equation (4.20) and shown by the horizontal line.

Referring to Figure 8.23, the increased size and weight of the larger particles resulted in an average 5% higher settling velocities for all gas flow rates when compared to the theoretical clear water settling

velocities. Furthermore, the particles are observed to be less susceptible to the oscillatory motion of the rising gas bubbles at higher gas flow rates and gas *in situ* volumetric concentrations. The particles are no longer carried upwards by the rising gas bubbles, however, they are observed to stall for brief periods of time, thus resulting in the trumped shaped data scatter shown. The 5% higher settling velocities occur at all gas flow rates and gas *in situ* volumetric concentrations.

Because of the erratic fall behaviour of the particles, no terminal settling velocity is defined. However, globally, the results indicate that the settling velocity of particles in gas-liquid mixtures consisting of a range of gas concentrations does not deviate significantly from the theoretical particle settling velocity in clear water calculated with Equation 4.20.

Considering only a 5-7% increase in settling velocity when comparing the 15,8 mm to the 24,5 mm diameter spheres, it is deemed acceptable to extrapolate the theoretical spherical particle settling equation for clear water (Equation 4.20) for use in a gas-liquid mixture environment.

8.4 MULTIPLE PARTICLES SETTLING VELOCITY TESTS (AIR-WATER MIXTURES)

Purpose :

Observe the effect of other particles on single spherical particle settling velocities in gas-water mixtures.

The diagrams in Figure 8.24 show the *observed* fall behaviour of a cluster of particles for the following range of conditions :

- no gas flow (clear water)
- single rising gas bubbles
- single rising gas bubble with continuous stream of gas flow behind
- continuous stream of rising gas bubbles.

Referring to Figure 8.24 a, it is observed that as the cluster of particles settles under conditions of no gas flow, there is a slight vertical spread of the particles as they move down the standpipe. However, this spread does not significantly to stop particle interactions and thus reduces the settling velocity of a single particle located in the cluster.

Referring to Figure 8.24 b, as the cluster of falling particles reach a single rising gas bubble, most of the particles are forced outwards and fall around the bubble, with a few of the particles falling through the bubble. The gas bubble, as well as an area of turbulence behind the rising bubble, significantly spread the cluster out thereby reducing the particle interaction.

The spreading out of the cluster is even more significant when the rising gas bubble is followed by a stream of continuous gas flow as shown in Figure 8.24 c. For the case of continuous gas flow shown in Figure 8.24 d, the cluster of spherical particles is spread out soon after being released at the top of the standpipe. Thus no particle

interaction is observed with no effect on the single particle settling velocities. These observations are verified from the experimental results shown in Figure 8.25.

In Figure 8.25, the settling velocity of an "average" particle located in the middle of a cluster is super-imposed on the settling velocity of single particles at four gas *in situ* volumetric concentrations. Tests are conducted using 15,8 mm spheres, and the gas *in situ* volumetric concentration is evaluated as in Section 8.3 with Equation 8.6.

The settling velocity of the "average" particle within the cluster is shown with a cross (x) in the figure. Under conditions of no gas flow (gas *in situ* concentration = 0%), the particle interaction plays a significant role in reducing the settling velocities. In the experiments, a reduction of ± 15% was measured.

As soon as gas is released, and the particles are spread out by the rising gas bubbles, the experimental results indicate that the "average" particle settling velocity is similar to the single particle settling velocity because it plots centrally within the trumpet shaped scatter of the single particle settling velocity measurements. Thus no effect of reducing settling velocity of a solitary particle due to particle interaction is measured, under conditions of a steady gas input flow.

Figure : 8.22
Description : Liquid/Gas Settling Velocities

Airlift Pump Investigation

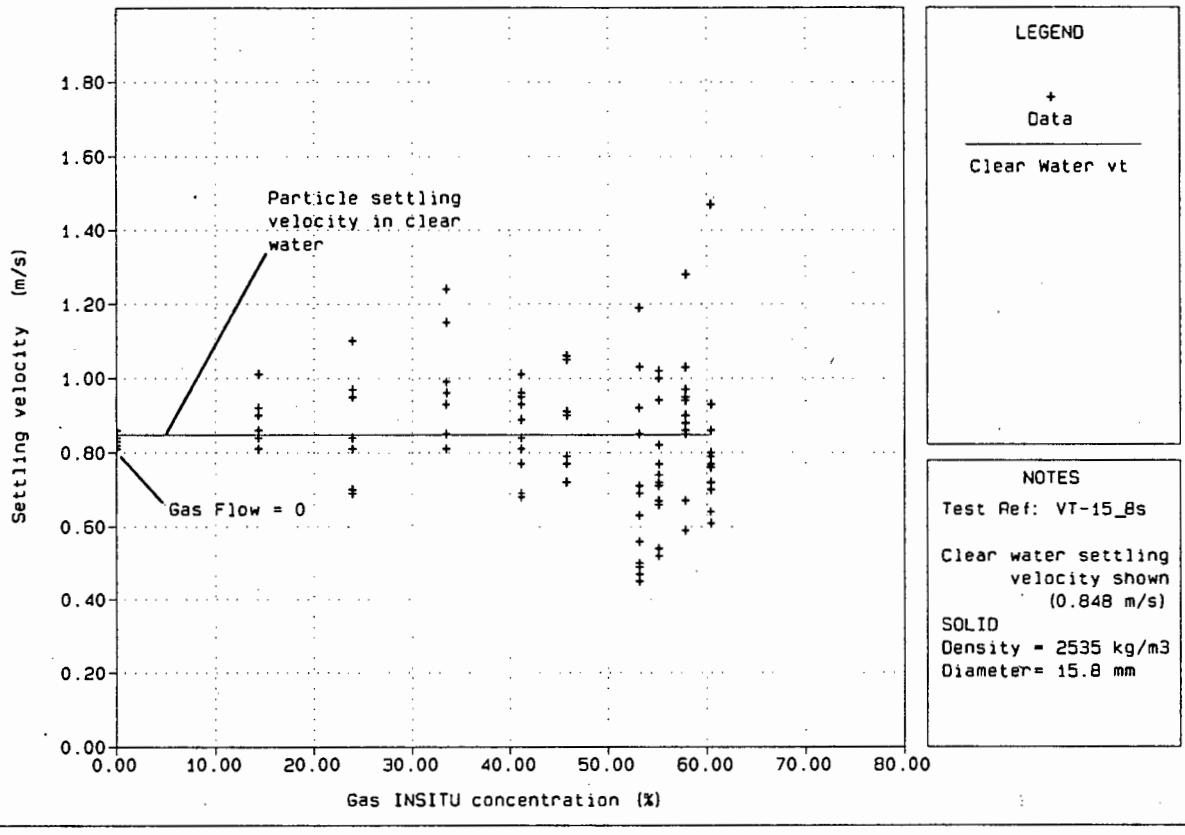

Figure : 8.23
Description : Liquid/Gas Settling Velocities

Airlift Pump Investigation

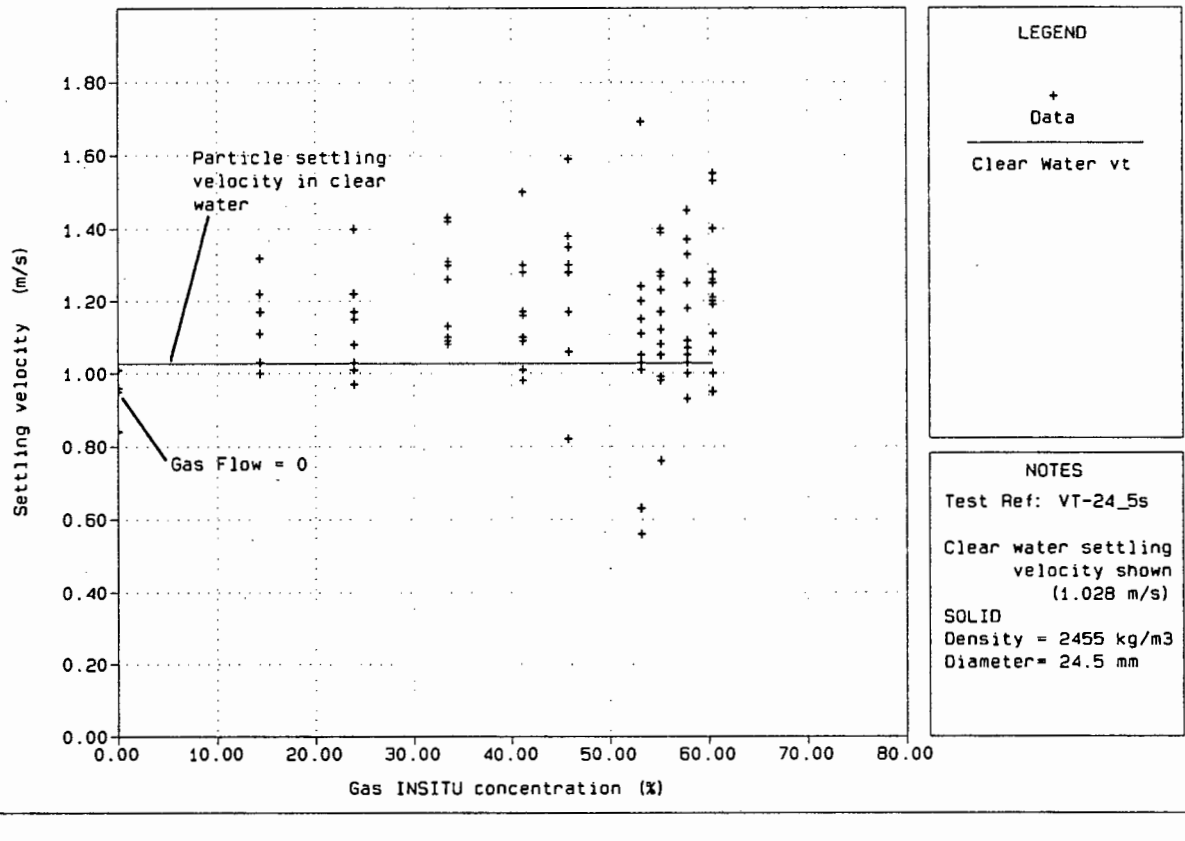

Figure : 8.24
Description : HINDERED SETTLING OBSERVATIONS

Airlift Pump Investigation

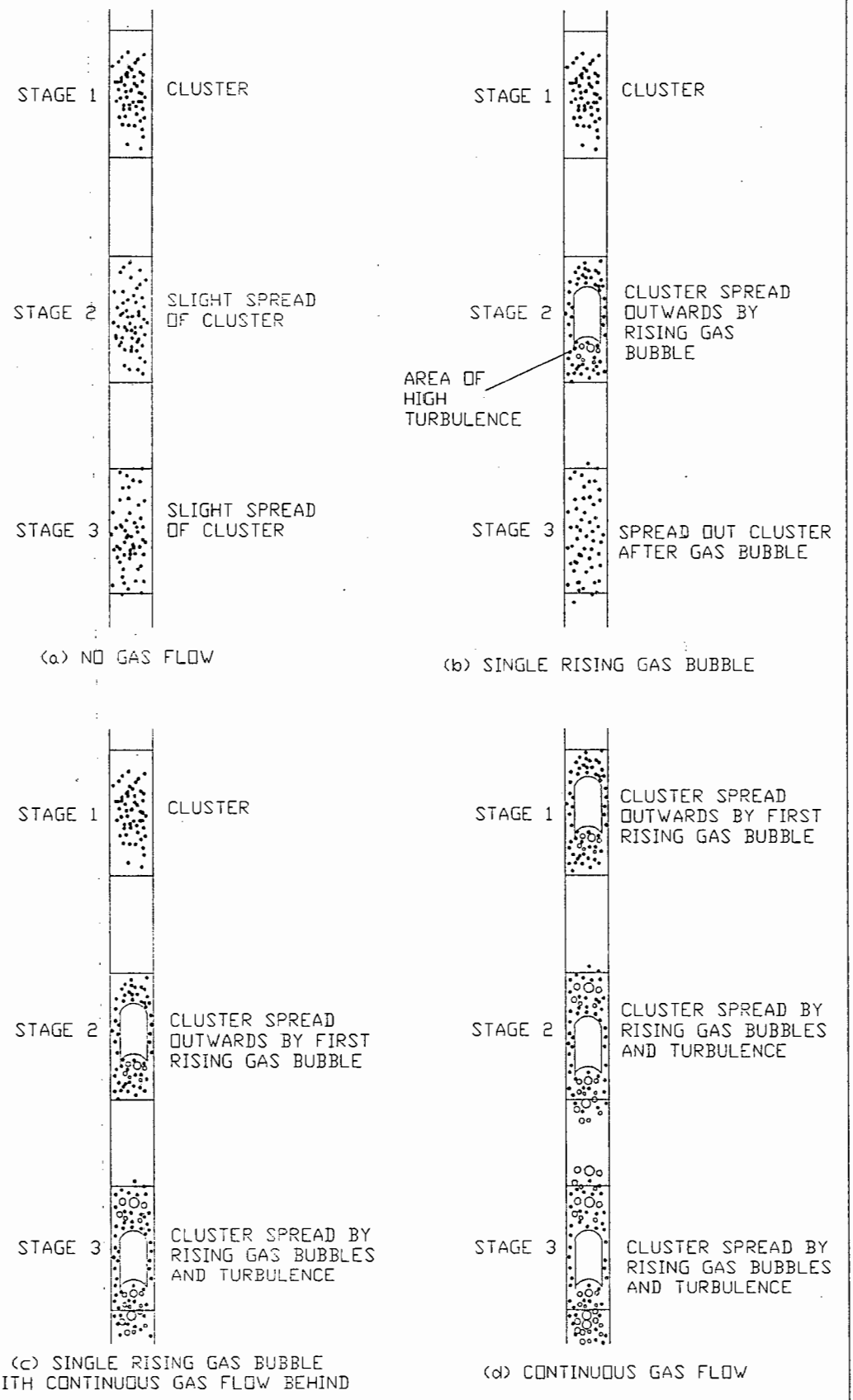

Figure : 8.25 Airlift Pump
Description : Liquid/Gas Settling Velocities Investigation

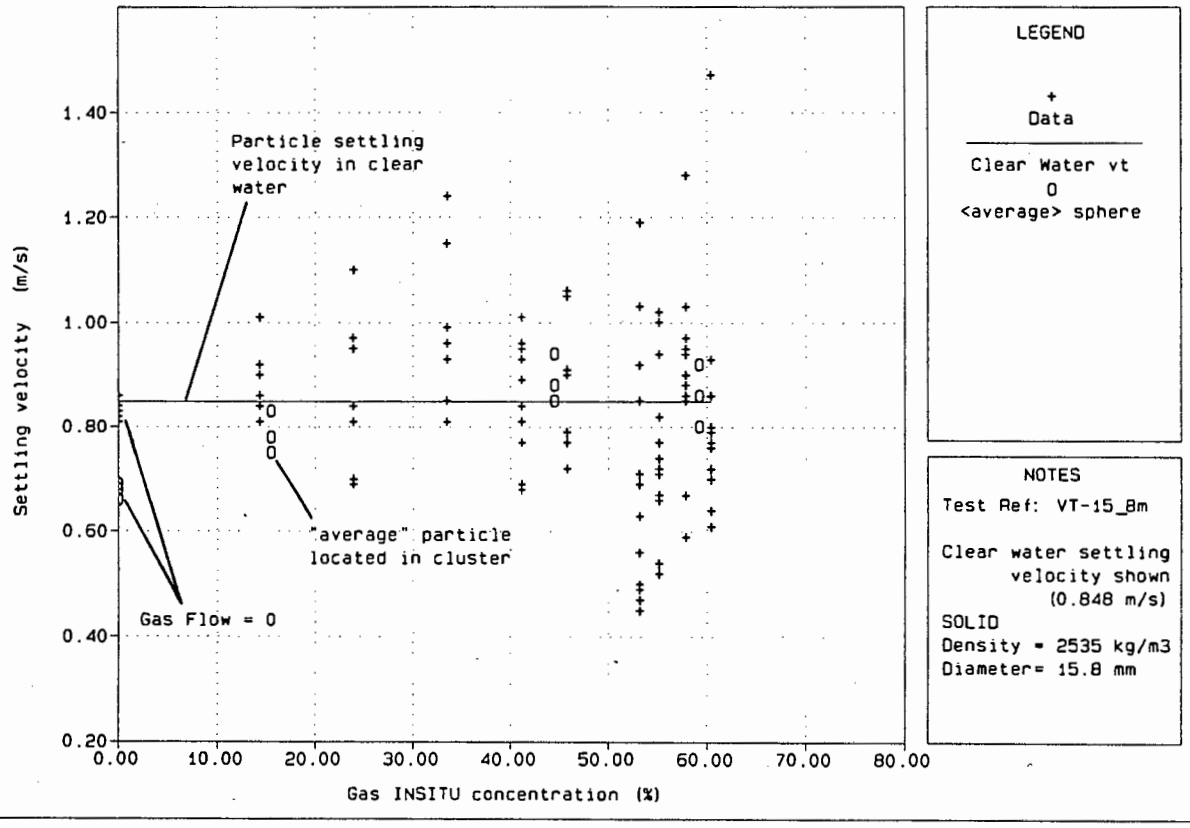

8.5 VERTICAL THREE PHASE *IN SITU* VOLUMETRIC CONCENTRATION TESTS

Purpose :

Measure solid and gas in situ volumetric concentrations in vertically moving three phase solid-liquid-gas mixtures.

MOST MEASUREMENTS DURING THE VERTICAL THREE PHASE *IN SITU* CONCENTRATION TESTS ARE PERFORMED IN THE DELIVERY PIPE INCREMENT BETWEEN THE TWO KNIFE GATE VALVES (REFER FIGURES 5.5 & 5.6). THUS, THE EVALUATION OF THE THREE PHASE *IN SITU* CONCENTRATIONS, SHEAR STRESS, WEIGHT AND PRESSURE LOSS PREDICTIONS ARE PERFORMED WITH PARTICULAR REFERENCE TO THIS DELIVERY PIPE INCREMENT.

8.5.1 Vertical three phase solid and gas *in situ* volumetric concentrations ($C_{vt}^{s/g}$ & $\epsilon_g^{s/g}$)

Table 8.5 lists three phase solid and gas *in situ* volumetric concentration theories evaluated.

Author/Theory	$C_{vt}^{s/g}$ Equation	$\epsilon_g^{s/g}$ Equation	$C_{vt}^{s/}$ Equation	$\epsilon_g^{/g}$ Equation
Proposed	4.40	4.42	-	-
Weber (1976)	iteration using		3.5	3.13
Dedegil and Weber (1982)	iteration using		3.7	3.27
Kato	-	3.29	-	-
Giot	3.31	3.33	-	-

TABLE 8.5 : Three phase *in situ* concentration theories evaluated

In order to evaluate the validity of Weber's (1976) equation, for calculating the gas *in situ* volumetric concentration in a liquid-gas mixture, the static dilation ($\epsilon_{go}^{/g}$) of the water column in the pipe is

required. Extensive tests have been conducted in three pipe sizes and the static dilation has been measured and compared to available literature sources. These results are presented in a previous dissertation (Berg 1988).

Figures 8.26 a & b show the results of tests conducted in the 90 mm airlift pump delivery pipe at a 4% solid delivered volumetric concentration. Shown in the figures are a comparison of theoretical gas and solid *in situ* volumetric concentration predictions respectively, compared to the measured data. This comparison is in the form of deviation graphs of measured versus calculated phase *in situ* volumetric concentration.

Referring to Figure 8.26 a, the Proposed theory gives the closest approximation of the gas *in situ* volumetric concentration by plotting closest to the 100% agreement line. These predictions are largely within 5% of the measured data. Kato, Weber (1982) and Dedegil's theories over-predict the measured data slightly, however, they approximate the measured data to an accuracy of 10%. Giot's theory is shown to over-predict by more than 10% while Weber's earlier theory under-predicts by more than 10%.

Referring to Figure 8.26 b, the Proposed theory agrees closely with Giot's theory. Although approximations of the solid *in situ* volumetric concentrations are less accurate than the gas *in situ* volumetric concentrations, both these theories give more favourable approximation of the measured solid *in situ* volumetric concentration than the other theories evaluated. Both of Weber's theories (1976 and 1982) as well as Dedegil's theory are shown to severely over- predict the solid *in situ* volumetric concentration.

Figures 8.27 a and b show the results of tests conducted at 6% delivered volumetric concentration in the 90 mm airlift pump. Referring to Figure 8.27 a and the prediction of gas *in situ* volumetric concentration, the best approximation is again obtained with the Proposed theory. This is shown to calculate the gas *in situ* concentration to well within 5% accuracy when compared with the measured data. Kato, Weber (1982) and Dedegil's predictions again over-predict, however, the comparison is still within 10% accuracy. As before, Giot over-predicts the gas *in situ* volumetric concentration severely, while the earlier theory of Weber under-predicts. The theories by both these authors differ from the measured data in excess of 15%.

Referring to Figure 8.27 b, the solid *in situ* volumetric concentration is again predicted less accurately than the gas *in situ* volumetric concentration. The Proposed theory agrees favourably with Giot's theory and both give a much closer approximation of the measured data than the other theories evaluated. Weber's 1976 and 1982 theories, as well as Dedegil's theories, over-predict the solid *in situ* volumetric concentrations severely.

At 8% delivered volumetric concentrations (Figure 8.28 a), the closest prediction of the gas *in situ* volumetric concentration is again achieved with the Proposed theory. Predictions are within 5% of the measured data. As with the other tests, Weber's later and Dedegil's theories over-predict the data. At these higher delivered volumetric concentrations, Kato's calculation approach is shown to over-predict more severely than before and his predictions along with Giot's predictions fall outside a 15% accuracy. Weber's 1976 theory is shown to under-predict the gas *in situ* volumetric concentrations by more than 15%.

Referring to Figure 8.28 b and the solid *in situ* volumetric concentrations, the Proposed theory agrees closely with Giot's theory, and both are now shown to under-predict the solid *in situ* volumetric concentrations. The approximations are, however, closer still to the measured data than the other theories. Weber's (1982) and Dedegil's theories are shown to over-predict while Weber's 1976 theory is shown to over-predict severely.

Figure 8.29 a shows the results of tests conducted in the 40 mm airlift pump at approximately 4% delivered volumetric concentration using 0,62 mm particle sizes. Referring to Figure 8.29 a and the prediction of gas *in situ* volumetric concentration, all theories exhibit an unexplainable trend of under-prediction at lower gas *in situ* volumetric concentrations and over-prediction at higher gas *in situ* volumetric concentrations. The predictions with the Proposed theory, however, fall mostly within 10% of the measured data, especially at concentrations above 50%.

Kato, Giot and Dedegil are shown to result in slightly higher predictions of gas *in situ* volumetric concentrations compared with the Proposed theory and over-predict by 15% to 20% at concentrations above 50%. Weber's earlier theory (1976) under-predicts in excess of 15% to 20% throughout.

Referring to Figure 8.29 b and the solid *in situ* volumetric concentrations, difficulty in concentration measurement allowed only 2 data points for theoretical comparisons. As with the 90 mm airlift pump, theoretical predictions of the solid *in situ* volumetric concentration is less accurate than the gas *in situ* concentration.

Predictions fall well outside a 10% accuracy compared with the measured data. However, as with the 90 mm airlift pump, the Proposed theory agrees closely to Giot's approach and gives a better approximations of the solid *in situ* volumetric concentration than the other theories evaluated.

For the tests conducted in the 40 mm airlift pump with larger 2,46 mm particle sizes (Figures 8.30 a & b), similar trends as for the smaller 0,62 mm particle size tests are observed. Referring to Figure 8.30 a, the Proposed theory predicts the gas *in situ* volumetric concentration to a higher accuracy compared with other authors and predictions are well within 10%. The same unexplainable trend of under-prediction in the gas *in situ* volumetric concentrations at low concentrations and over-predictions at high concentrations is observed. Kato over-predicts by 10 - 20% while Weber's earlier theory (1976) under-predicts by more than 20% throughout.

Referring to Figure 8.30 b and the solid *in situ* volumetric concentrations, again only 3 data points are extracted from the tests for theoretical comparisons. All theoretical models over-predict the measured solid *in situ* volumetric concentration data, however, Giot and the Proposed theory result in more favourable predictions than both Weber's (1976 and 1982) and Dedegil's theories.

For all tests conducted, the three phase gas in situ volumetric concentration is best calculated with the Proposed theory. Predictions within 5 to 10% of the measured data are obtained. Although prediction of the three phase solid in situ volumetric concentration is not as accurate, a closer approximation of the data is obtained using the

Proposed or Giot's theory, when compared with other theories. As discussed in Section 8.2.2, the advantage of predicting three phase solid in situ concentrations with the Proposed theory is the ability to accommodate a wide range of particle sizes, particle size distributions and particle shapes. This is achieved by considering each particle size, fraction and characteristic during the evaluation of the solid in situ volumetric concentration.

8.5.2 Vertical three phase solid-liquid-gas weight (W_m^{slg})

Having evaluated both the gas and solid *in situ* volumetric concentrations, the three phase solid-liquid-gas weight pressure can be calculated using Equations 4.36 and 4.37.

Figures 8.31 to 8.35 show the three phase weight pressure calculated with the theoretical gas and solid *in situ* volumetric concentrations compared with the three phase weight pressure calculated with measured gas and solid *in situ* volumetric concentrations. This comparison is in the form of deviation graphs giving "measured" versus "calculated" weight pressures.

Figures 8.31 to 8.33 show that the Proposed theory gives the best approximation (compared with the other theories) of the three phase weight pressure in the 90 mm airlift pump for a range of delivered volumetric concentration. The predictions agree to an accuracy of 5% with the weight pressure calculated using measured gas and solid *in situ* volumetric concentrations. For all delivered volumetric concentrations tested, Giot, Kato, Weber (1982) and Dedegil are shown to under-predict the three phase weight pressure. This effect is the result of the over-prediction of the gas *in situ* volumetric concentration by these authors (refer Section 8.5.1). Similarly,

Weber's (1976) theory over-predicts the three phase weight as a result of the under-prediction of the gas *in situ* volumetric concentration (refer Figures 8.26 a & 8.28 a). An under-prediction in the amount of lower density gas phase results in a large amount of higher density liquid and solid phases. This consequently leads to a higher overall three phase weight.

On the 40 mm airlift pump (Figures 8.34 to 8.35), the Proposed theory predicts the three phase weight to a 10% accuracy. Favourable agreement is also obtained by Giot, Dedegil and Weber (1982). As before, Weber's earlier theory (1976) severely over-predicts the three phase weight. On the 40 mm airlift pump, the trend of under-prediction at lower three phase weights changing to over-prediction at higher three phase weights is caused by the same trend noticed in the gas *in situ* volumetric concentration (refer to Section 8.5.1).

8.5.3 Vertical three phase solid-liquid-gas shear stress (τ_{om}^{slg})

Analogous to Section 8.2.1 the three phase "measured" shear stress is evaluated from the measured absolute pressures at the beginning and end of the delivery pipe increment (between the two knife gate valves), the measured solid and gas *in situ* volumetric concentrations (C_{vt}^{slg} & ϵ_g^{slg}) and the calculated momentum change over the measurement section.

From Equation 4.33 and Figure 4.1 the shear stress is expressed as :

$$\tau_{om}^{slg}\ \pi\ D\ l\ =\ -\ W_m^{sl}\ -\ [\ (p + \rho_m^{slg}\ (v_m^{slg})^2)\ A\ ]^{TOP} + [\ (p + \rho_m^{slg}\ (v_m^{slg})^2)\ A\ ]^{BOTTOM} \qquad (8.7)$$

where TOP and BOTTOM refer to the measurement section between the two knife gate valves in the delivery pipe (refer to Figures 5.5 & 5.6).

The weight term (W_m^{sl}) in Equation 8.7 is furthermore expanded using Equations 4.36 and 4.37 and calculated using measured solid and gas *in situ* volumetric concentrations. The change in momentum in Equation 8.7 is negligible compared to the shear stress and weight components, because measurements are taken over a small delivery pipe increment.

Figure 8.36 shows the contribution of the three phase momentum change to the total three phase pressure loss over the measurement section. For the purpose of establishing the three phase shear stress loss, this term is evaluated using Equation 3.50 and the measured solid and gas *in situ* volumetric concentrations.

Having evaluated the weight and momentum contributions as discussed, division of Equation 8.7 by the pipe area (A), allows calculation of shear stress in terms of primarily measured quantities. Therefore the "measured" shear stress is obtained.

Comparison of theoretical three phase shear stresses with "measured" three phase shear stresses in this section is performed by comparing three phase friction pressures. This facilitates a further comparison of the relative magnitude (in Pa) of the various components (weight, friction and momentum) of the total pressure loss. The three phase friction pressure is defined as :

$$\text{friction pressure} = \tau_{om}^{slg} \pi D l/A$$

Table 8.6 lists the three phase shear stress theories evaluated.

Author/Theory	Shear Stress Equation	Friction Factor Equation
Proposed Theory	4.49	4.28
Weber	3.41	3.40
Dedegil	3.45	3.40
Giot	3.41	3.40
Kato	3.46	3.49

TABLE 8.6 : Three phase shear stress theories evaluated

Figures 8.37 to 8.40 show the theoretically calculated friction pressures compared with the "measured" friction pressure. The comparison is in the form of deviation graphs giving "measured" friction pressure versus theoretically calculated friction pressure.

Figure 8.37 shows comparisons at 4% delivered volumetric concentration in the 90 mm airlift pump. All theories, except the Proposed theory, are shown to severely under-predict the three phase friction pressure. Weber's separated flow model (also used by Giot), gives the lowest and worst predictions, while Dedegil's theory appears to give better approximation than Kato. The friction pressure calculated with the Proposed theory scatter favourably about the 100% agreement line, with 4 out of 7 data points predicting to a 10% accuracy.

At an 8% delivered volumetric concentration in the 90 mm airlift pump (Figure 8.38), the Proposed theory is less accurate, however, predictions of the three phase friction pressure are still closer when compared with theories by other authors. As before, Weber and Giot under-predict severely while Kato's approximation is slightly better. Dedegil's predictions plot between the predictions of Kato and the Proposed theory.

In the 40 mm airlift pump (Figures 8.39 & 8.40), the most favourable predictions of the three phase friction pressure are again obtained with the Proposed theory. All other authors under-predict severely, with Dedegil's approximation slightly better than Giot, Weber and Kato.

Dedegil (1982) mentions that evaluation of the three phase pressure loss caused by friction is difficult. This sentiment is echoed throughout the literature. From the above discussion, the Proposed method of calculating three phase friction pressure is shown to be more accurate than other methods presented in the literature. Even though this method under-predicts at higher delivered volumetric concentrations, this under-prediction is not as severe as those of Kato, Giot, Weber and, to a lesser extent, Dedegil.

8.5.4 Vertical three phase solid-liquid-gas total pressure loss (Δp_3)

Having evaluated both the three phase solid and gas *in situ* volumetric concentrations and friction pressure, the total vertical pressure loss across the delivery pipe increment can be calculated and compared to the measured total pressure loss.

In the calculations, the theories listed in Table 8.7 are evaluated :

Author	Shear Stress Equation	Friction Factor Equation	Phase *in situ* Concentration Theory		
			$C_{vt}^{s/g}$	$\epsilon_g^{s/g}$	Other
Proposed Theory	4.49	4.28	4.40	4.42	
Weber	3.41	3.40	iteration using 3.5 & 3.13		
Dedegil	3.45	3.40	iteration using 3.7 & 3.27		
Giot	3.41	3.40	3.31	3.33	
Kato	3.46	3.49	-	3.29	

TABLE 8.7 : Three phase pressure theories evaluated

Figures 8.41 a & b and 8.44 a & b show comparisons of the three phase total pressure loss theories with measured total pressure loss data. The comparisons are both on a graph of total pressure loss versus input gas flow rate, and on deviation graphs of measured total pressure loss versus calculated total pressure loss.

Figures 8.41 a & b and 8.42 a & b show comparisons in the 90 mm airlift pump at ± 4% and ± 8% delivered volumetric concentrations respectively. The Proposed theory results in the most favourable approximation of the total three phase pressure loss when compared to the other theories. Approximations are found to be within 10% of the measured data for delivered volumetric concentrations of 4% and 8%.

Weber's (1976) approximation is shown to over-predict the pressure loss, which is a result of the under-prediction in the gas *in situ* volumetric concentration and consequently an over-prediction in the

three phase weight and total pressure loss (refer Section 8.5.1 & 8.5.2). This, combined with the under-prediction in three phase friction (refer to Section 8.5.3), results in a cancelling effect, causing the total pressure prediction to fall within 20% accuracy as shown in Figure 8.41. *Thus, evaluation of the total pressure loss has to be treated with circumspection if either the weight or shear stress components are not correctly predicted to within reasonable accuracy.* Because of Weber's (1976) adverse under-prediction in gas *in situ* volumetric concentration, this theory is not considered in the comparisons of predicted versus measured operating curves (refer to Section 8.6).

Dedegil, Giot and Kato all under-predict the three phase pressure loss. This being a result of an over-prediction in gas *in situ* volumetric concentrations and consequent under-prediction in three phase weight. This, combined with an under-prediction in the three phase shear stress, results in an overall under-prediction in the three phase pressure loss in the delivery pipe increment.

On the 40 mm airlift pump (Figures 8.43 and 8.44), the Proposed theory again shows the most favourable approximations of the measured three phase total pressure loss. Weber's theory results in higher three phase pressure losses, but, as explained previously, these approximations are a result of a predicted three phase weight cancelled by an under-predicted three phase shear stress. As with the 90 mm airlift pump, Giot and Kato result in an under-approximated three phase pressure loss when compared with the Proposed theory. Dedegil's favourable comparison at higher pressure losses is the result of an over-prediction in the three phase weight being cancelled by an under-prediction in the three phase shear stress.

Figure 8.45 shows a summary of all three phase total pressure loss predictions in the form of a mass deviation graph, while Table 8.8 gives the log standard error. From the figure, three phase pressure loss predictions calculated with the Proposed theory are shown to be scattered mostly within the 10% deviation lines. Weber (1976) generally over-predicts in excess of 10% while Giot and Kato under-predict in excess of 20%. Dedegil tends to under-predict between 10% and 25% throughout. These trends are confirmed in Table 8.8, where the Proposed theory results in the highest and most favourable log standard error. This next favourable approximation is obtained by Dedegil, followed by the other authors.

Author	Log Standard Error
Proposed Theory	0,99046
Weber	0,98376
Dedegil	0,97871
Giot	0,94281
Kato	0,95381

TABLE 8.8 : Log standard error

The three phase pressure loss is most favourably predicted with the Proposed theory. Accuracies generally within 10% of the measured data are obtained and the log standard error indicates a good correlation.

Figure : 8.26a
Description : Solid/Liquid/Gas Eg Theories

Airlift Pump Investigation

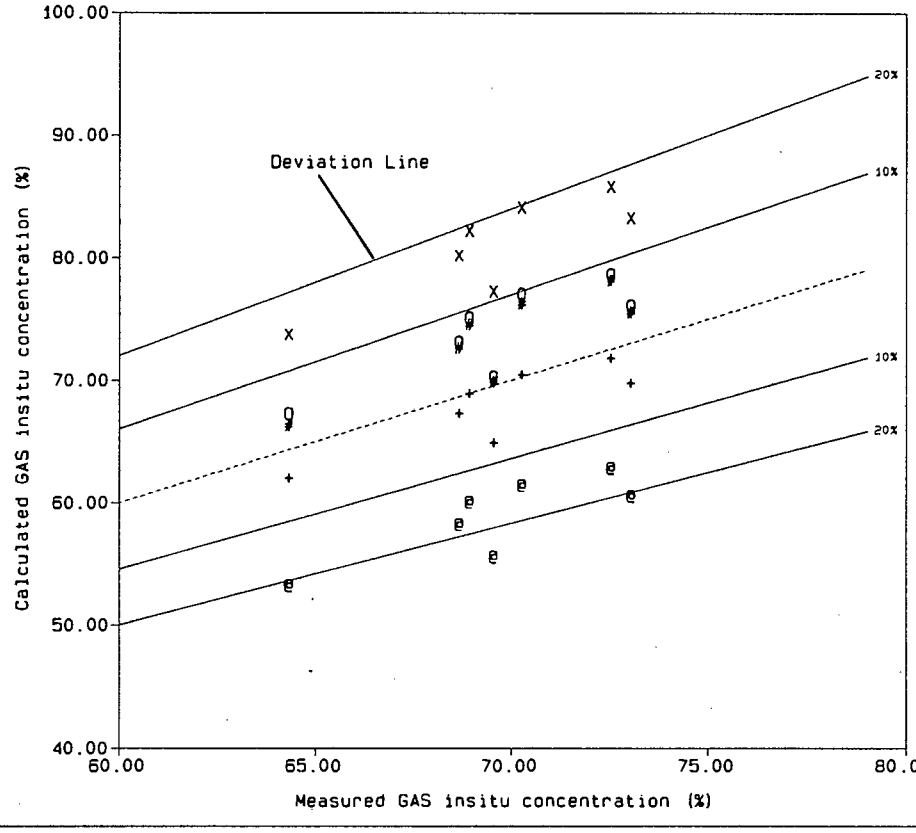

LEGEND

+ Proposed Theory
@ Weber (1976)
0 Weber (1982) &Dedegil
X Giot
Kato

100% Agreement Line

NOTES

Test Ref: DB042203

Apparatus: Airlift
Pipe Diam: 90mm NB
Material : Mar.Grav
Inj.Depth: 5.212m
Suc.Lngth: 1.320m
Lift Hght: 4.315m
apprx Cvd: 4 %

Figure : 8.26b
Description : Solid/Liquid/Gas Cvt Theories

Airlift Pump Investigation

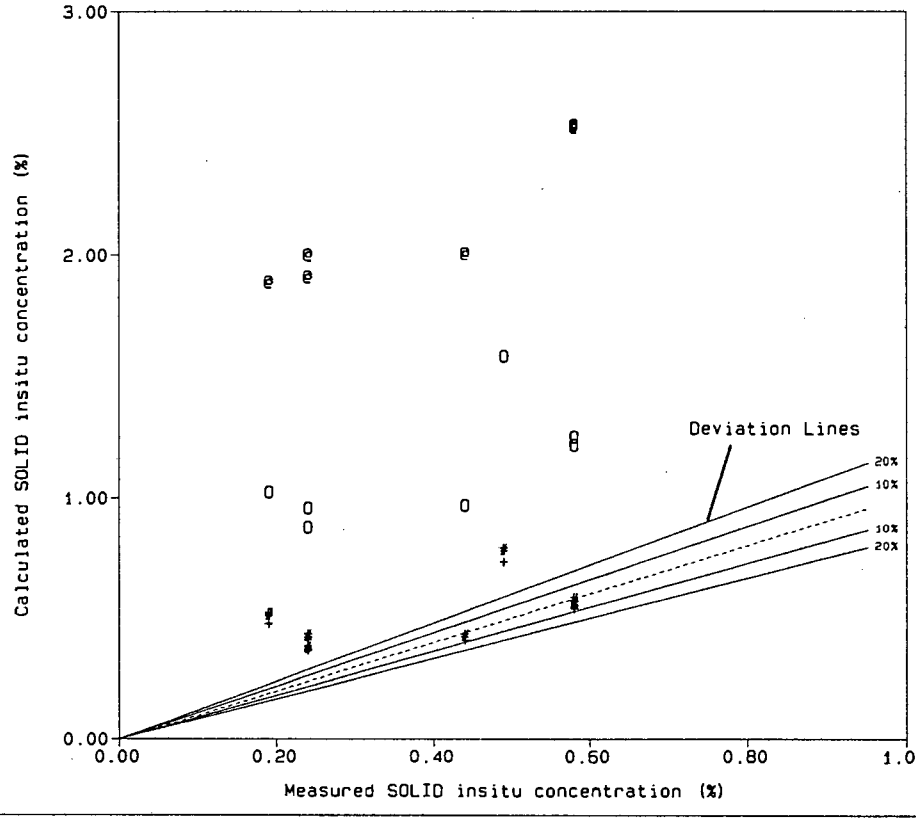

LEGEND

+ Proposed Theory
@ Weber (1976)
0 Weber (1982) &Dedegil
Giot

100% Agreement Line

NOTES

Test Ref: DB042203

Apparatus: Airlift
Pipe Diam: 90mm NB
Material : Mar.Grav
Inj.Depth: 5.212m
Suc.Lngth: 1.320m
Lift Hght: 4.315m
apprx Cvd: 4 %

Figure : 8.27a
Description : Solid/Liquid/Gas Eg Theories

Airlift Pump Investigation

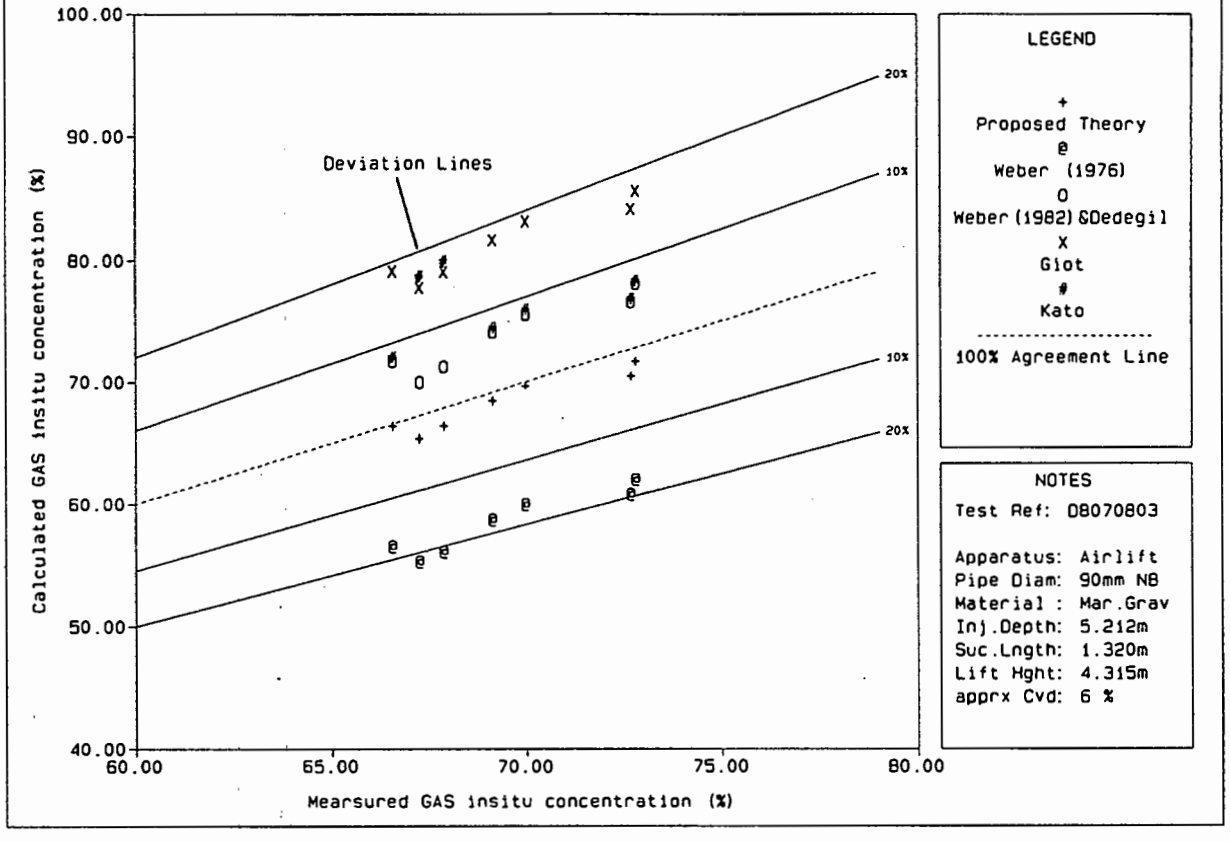

Figure : 8.27b
Description : Solid/Liquid/Gas Cvt Theories

Airlift Pump Investigation

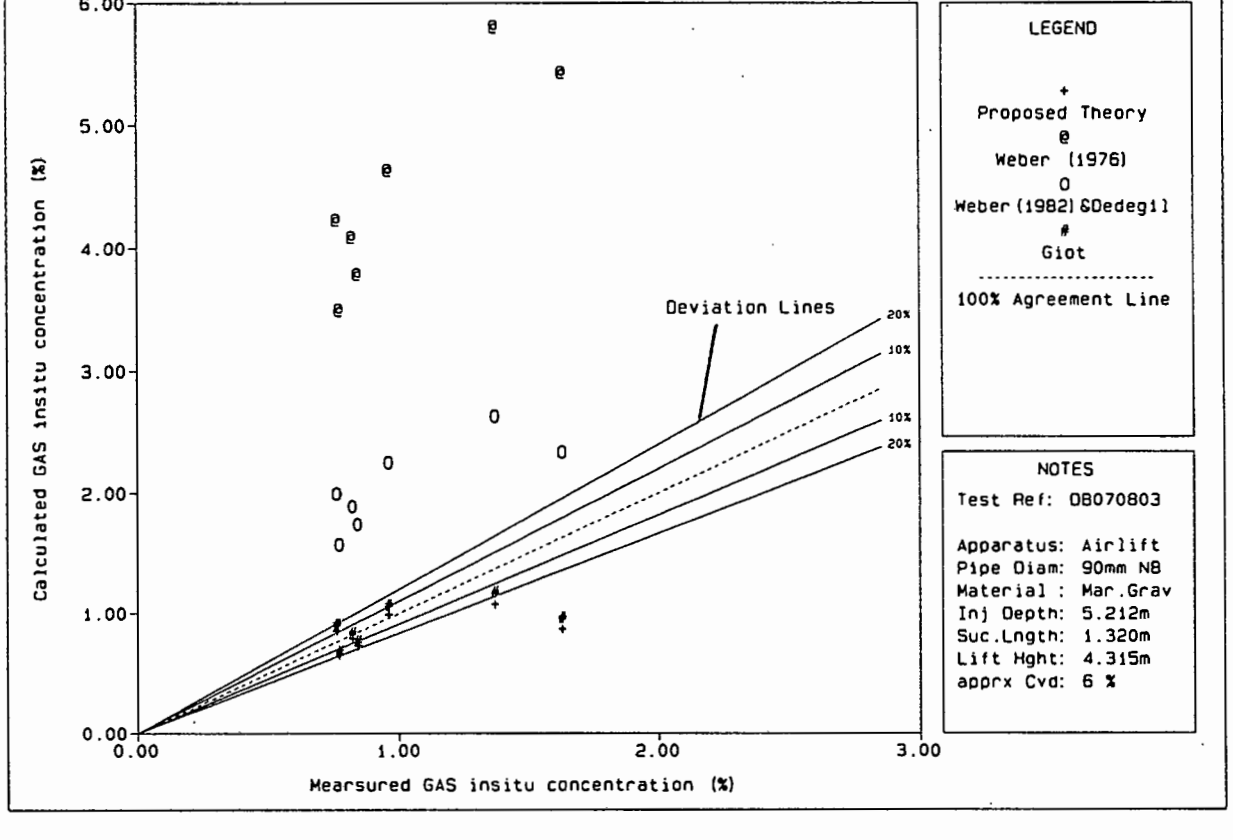

Figure : 8.28a
Description : Solid/Liquid/Gas Eg Theories

Airlift Pump Investigation

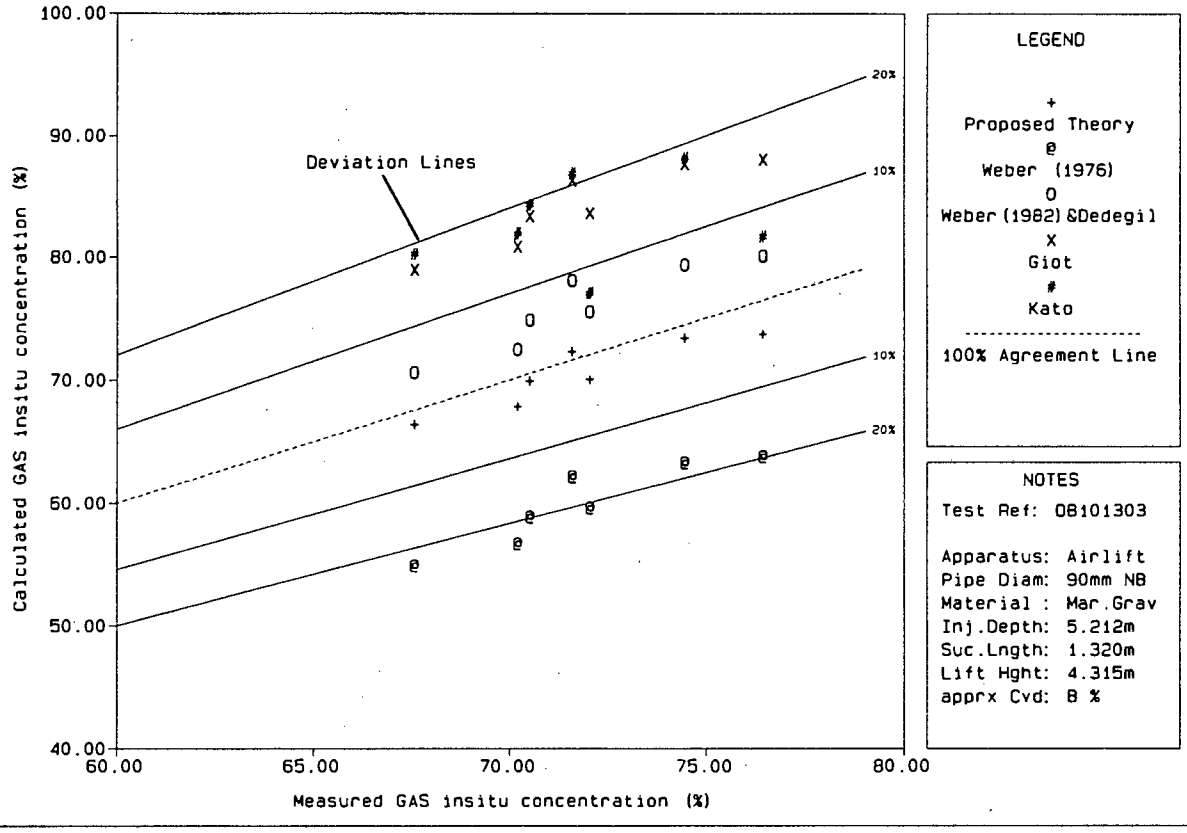

Figure : 8.28b
Description : Solid/Liquid/Gas Cvt Theories

Airlift Pump Investigation

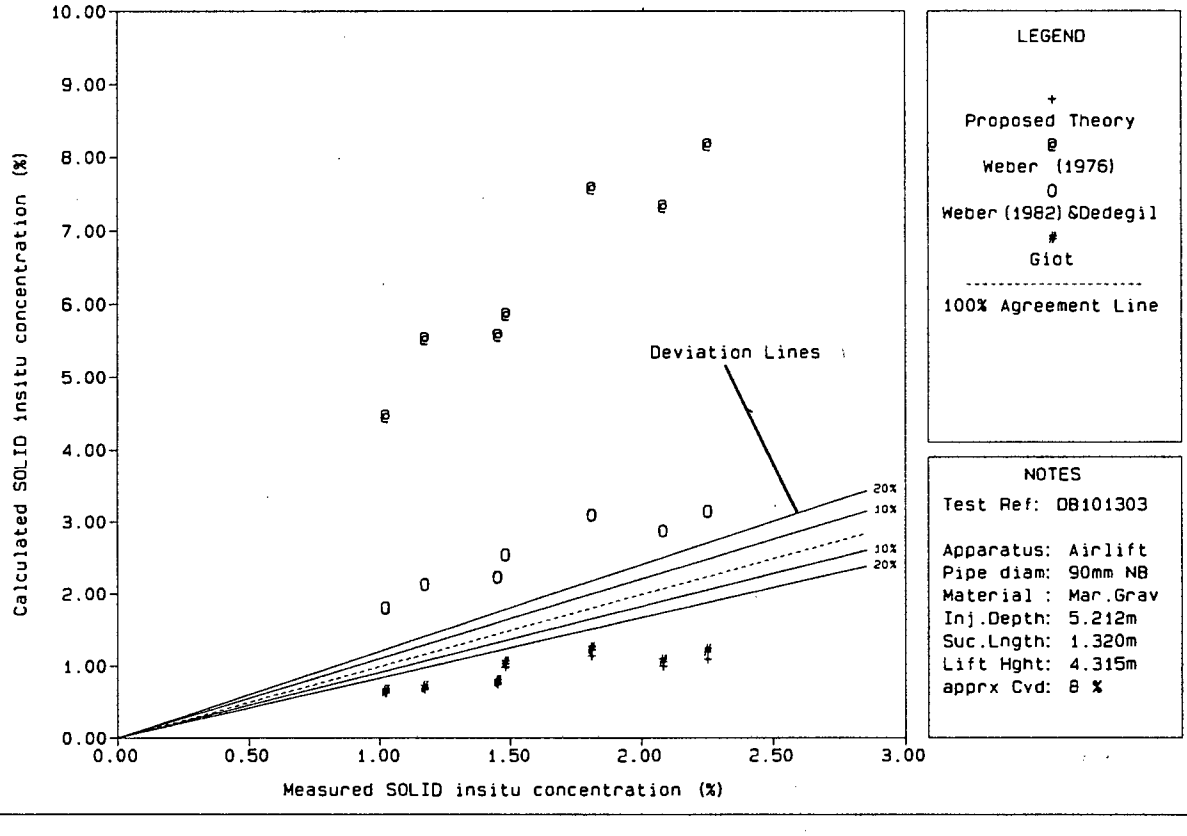

Figure : 8.29a
Description : Solid/Liquid/Gas Eg Theories

Airlift Pump Investigation

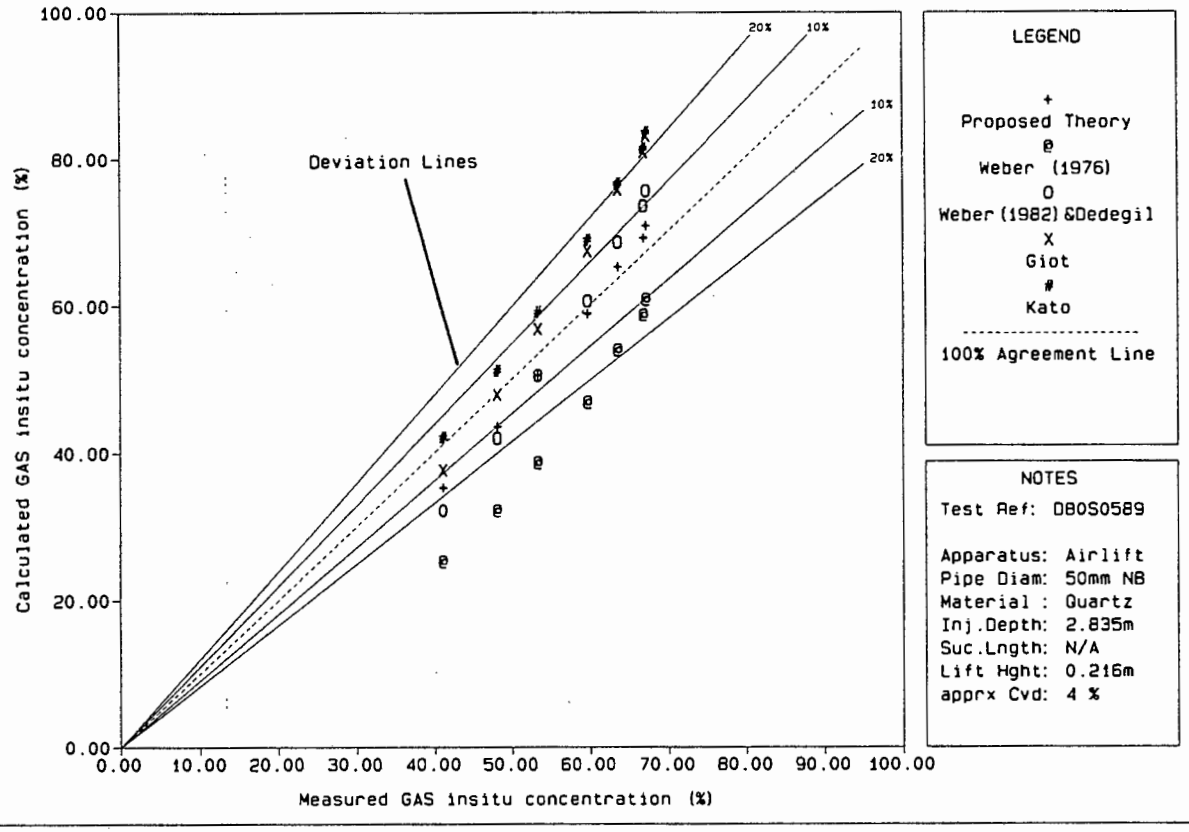

Figure : 8.29b
Description : Solid/Liquid/Gas Cvt Theories

Airlift Pump Investigation

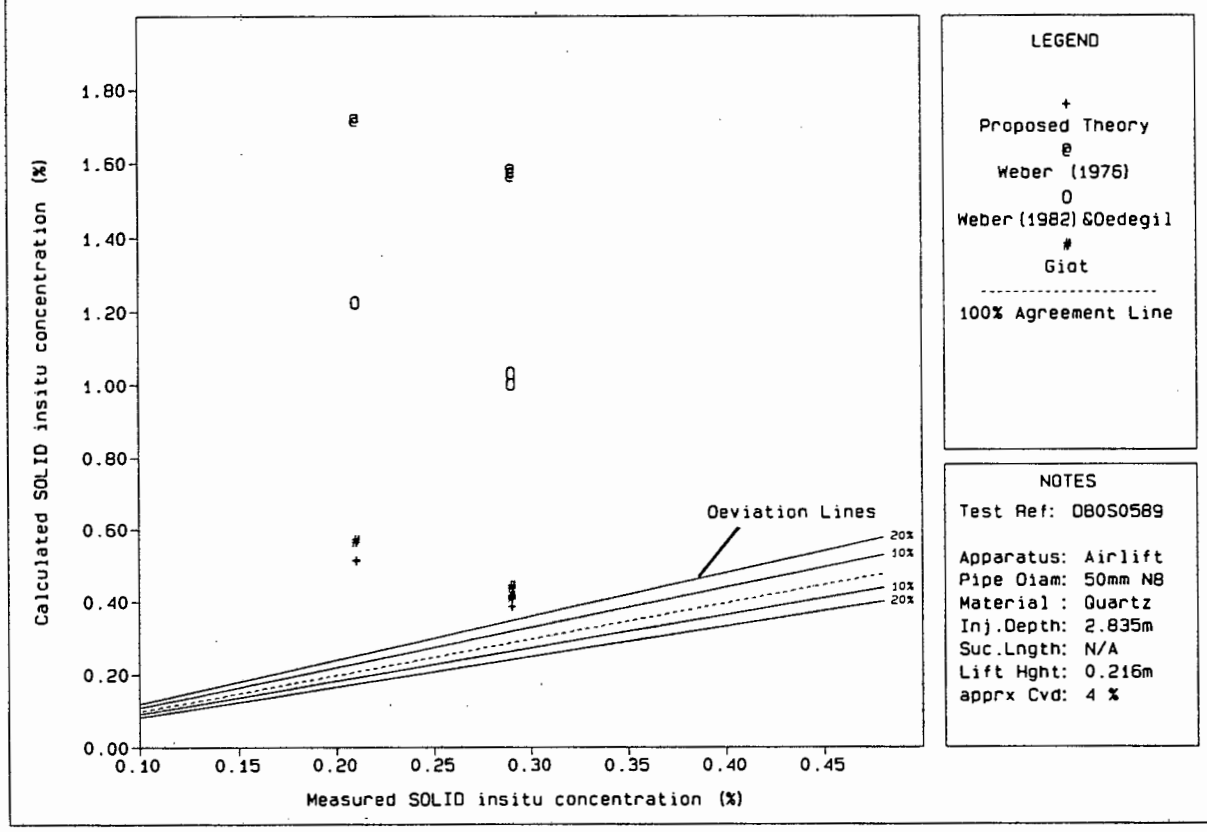

Figure : 8.30a
Description : Solid/Liquid/Gas Eg Theories

Airlift Pump Investigation

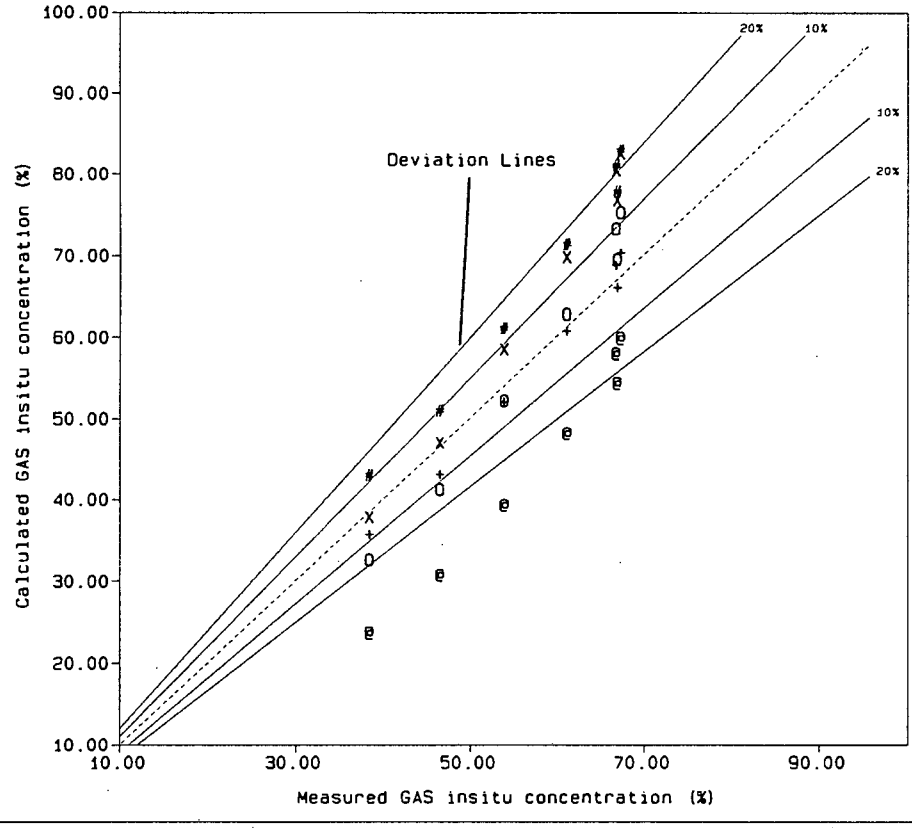

LEGEND

+ Proposed Theory
@ Weber (1976)
O Weber (1982) &Dedegil
X Giot
Kato

100% Agreement Line

NOTES

Test Ref: OB0L0589

Apparatus: Airlift
Pipe Diam: 50mm NB
Material : Quartz
Inj.Depth: 2.835m
Suc.Lngth: N/A
Lift Hght: 0.216m
apprx Cvd: 4 %

Figure : 8.30b
Description : Solid/Liquid/Gas Cvt Theories

Airlift Pump Investigation

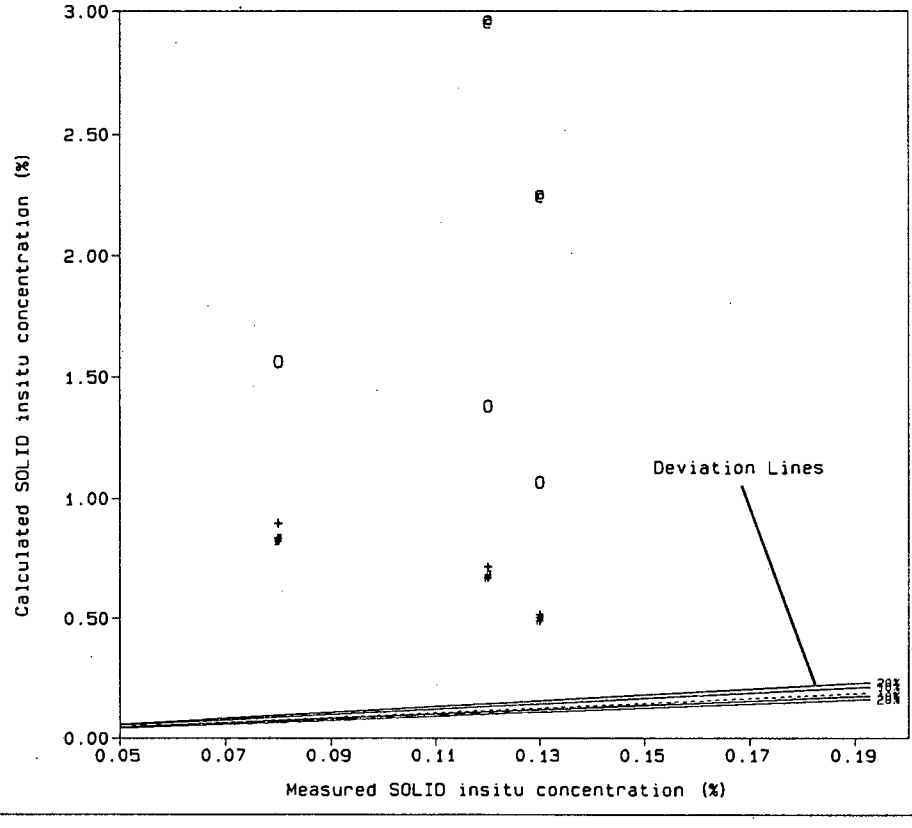

LEGEND

+ Proposed Theory
@ Weber (1976)
O Weber (1982) &Dedegil
Giot

100% Agreement Line

NOTES

Test Ref: OB0L0589

Apparatus: Airlift
Pipe Diam: 50mm NB
Material : Quartz
Inj.Depth: 2.835m
Suc.Lngth: N/A
Lift Hght: 0.216m
apprx Cvd: 4 %

Figure : 8.31 Airlift Pump
Description : Solid/Liquid/Gas Weight Pressure Theories Investigation

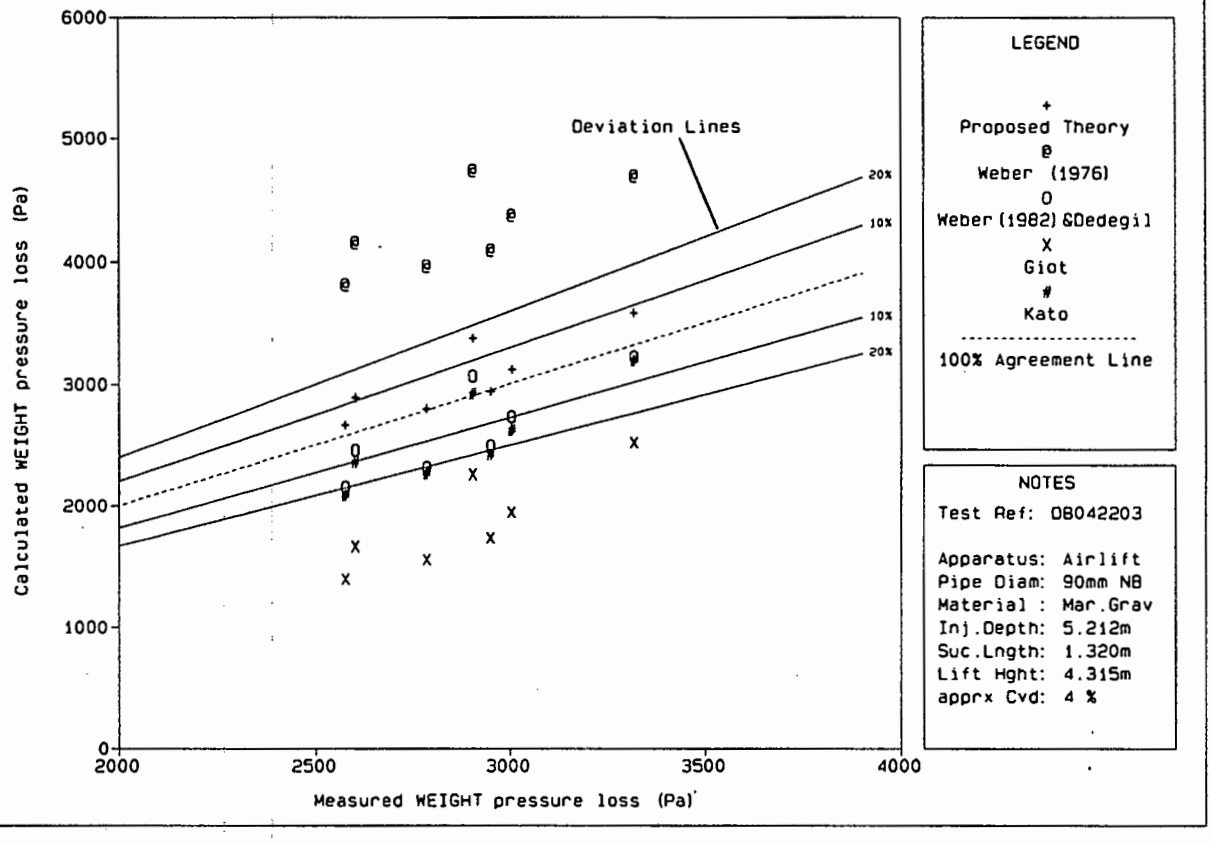

Figure : 8.32 Airlift Pump
Description : Solid/Liquid/Gas Weight Pressure Theories Investigation

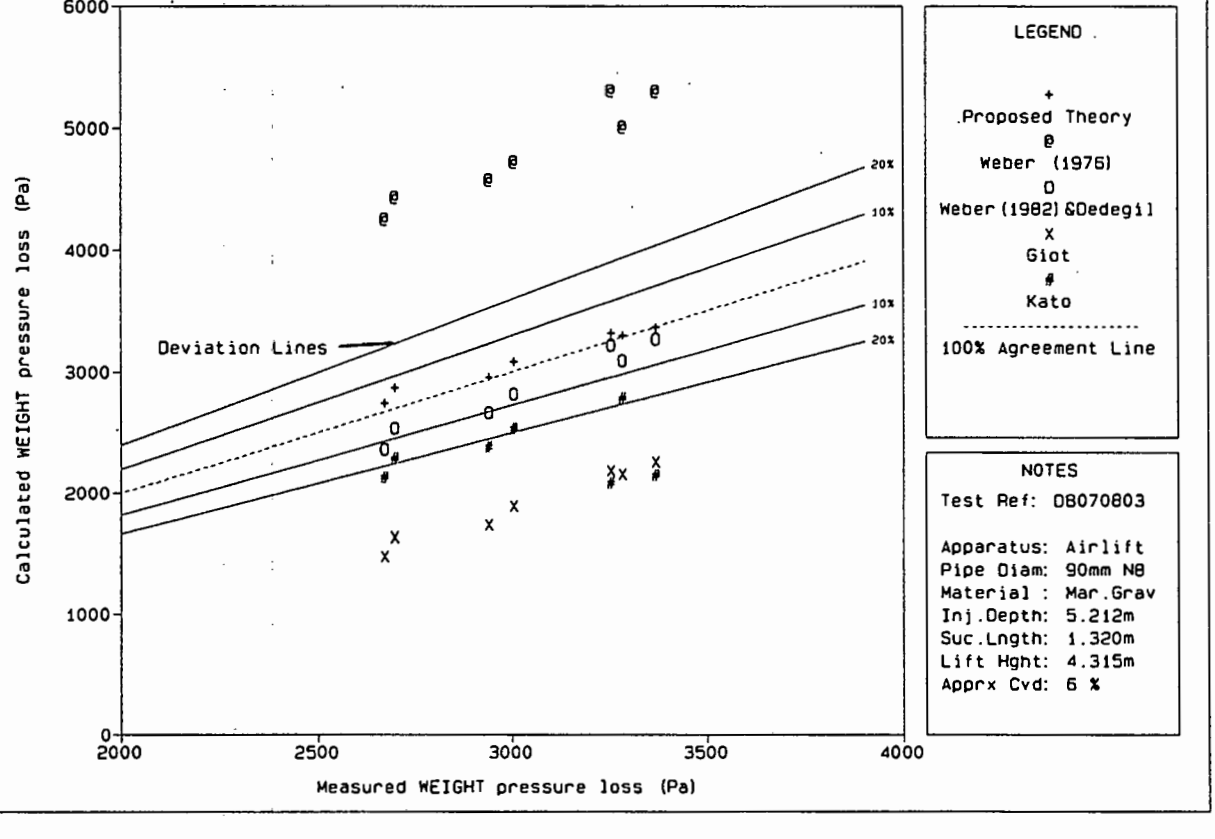

Figure : 8.33 Airlift Pump
Description : Solid/Liquid/Gas Weight Pressure Theories Investigation

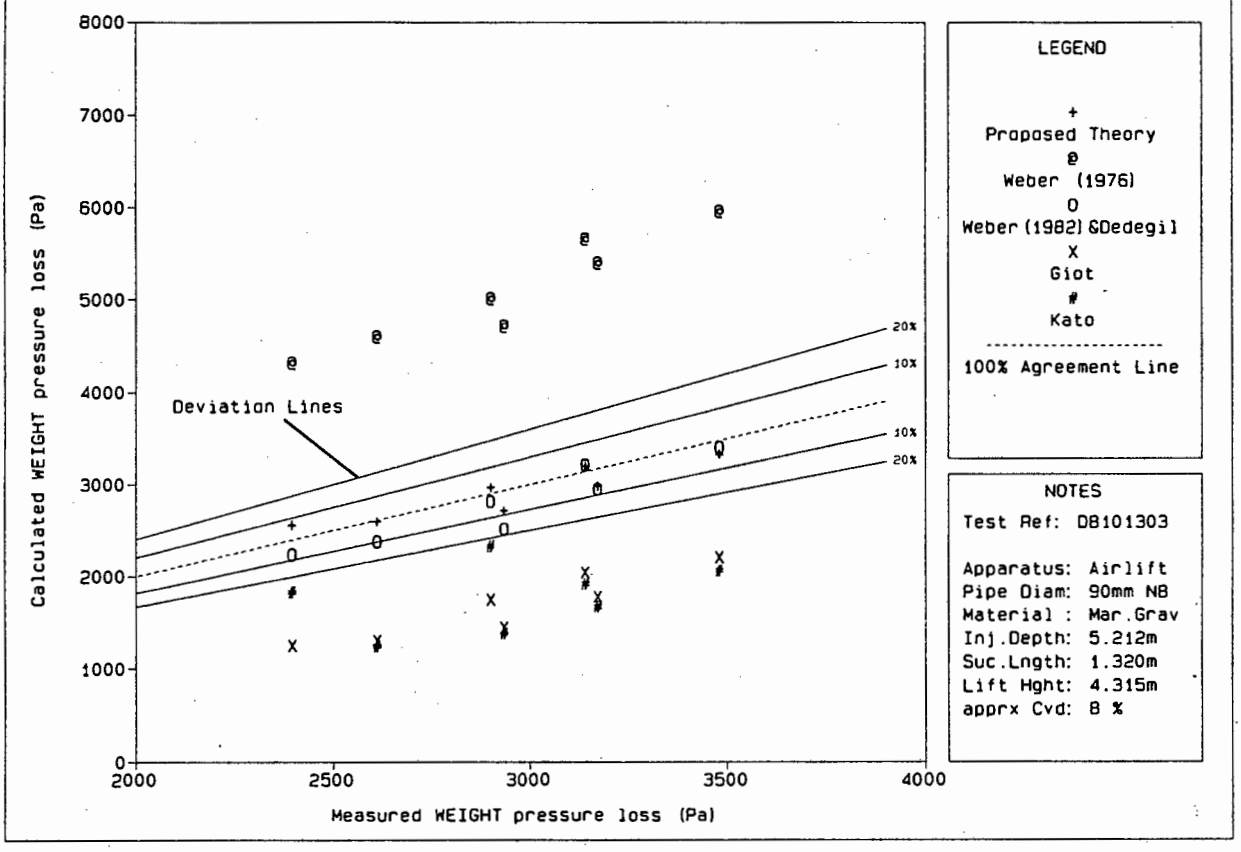

Figure : 8.34 Airlift Pump
Description : Solid/Liquid/Gas Weight Pressure Theories Investigation

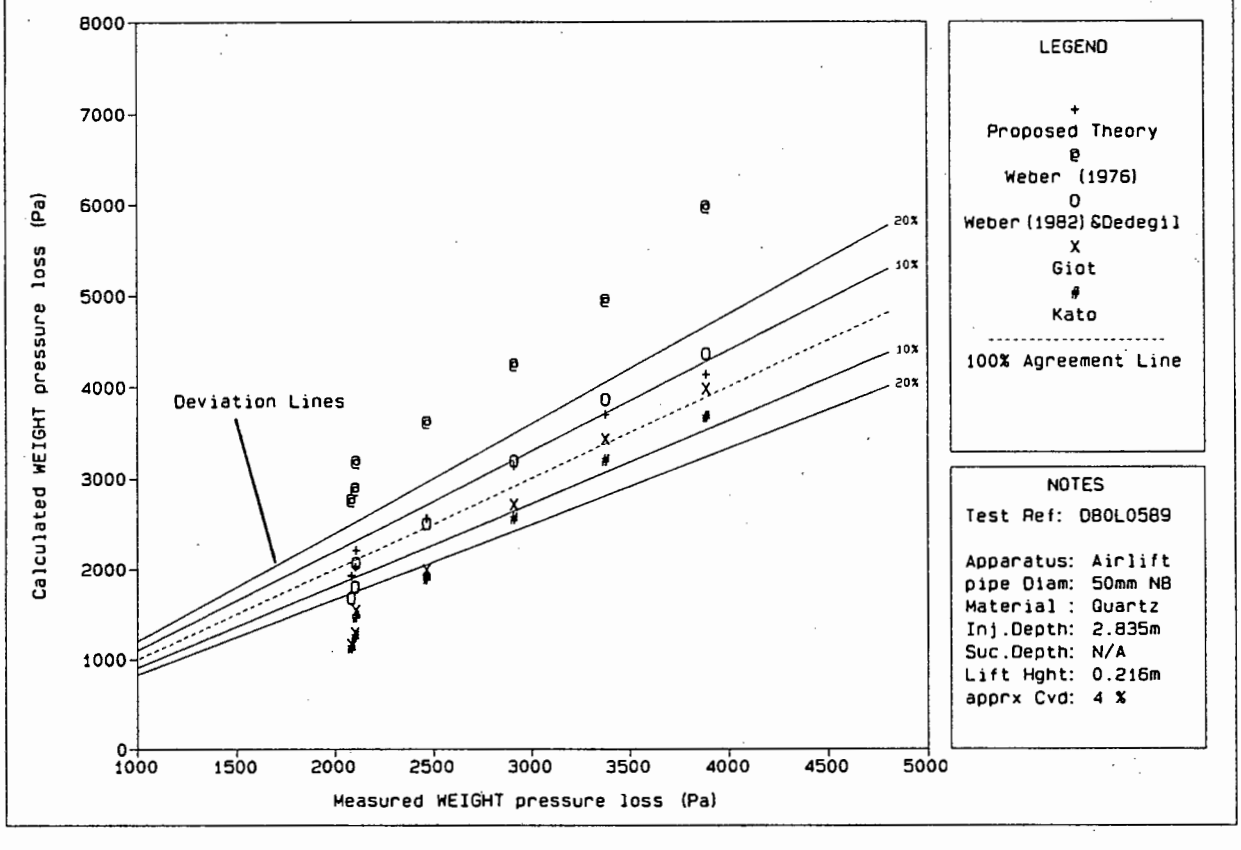

Figure : 8.35 Airlift Pump
Description : Solid/Liquid/Gas Weight Pressure Theories Investigation

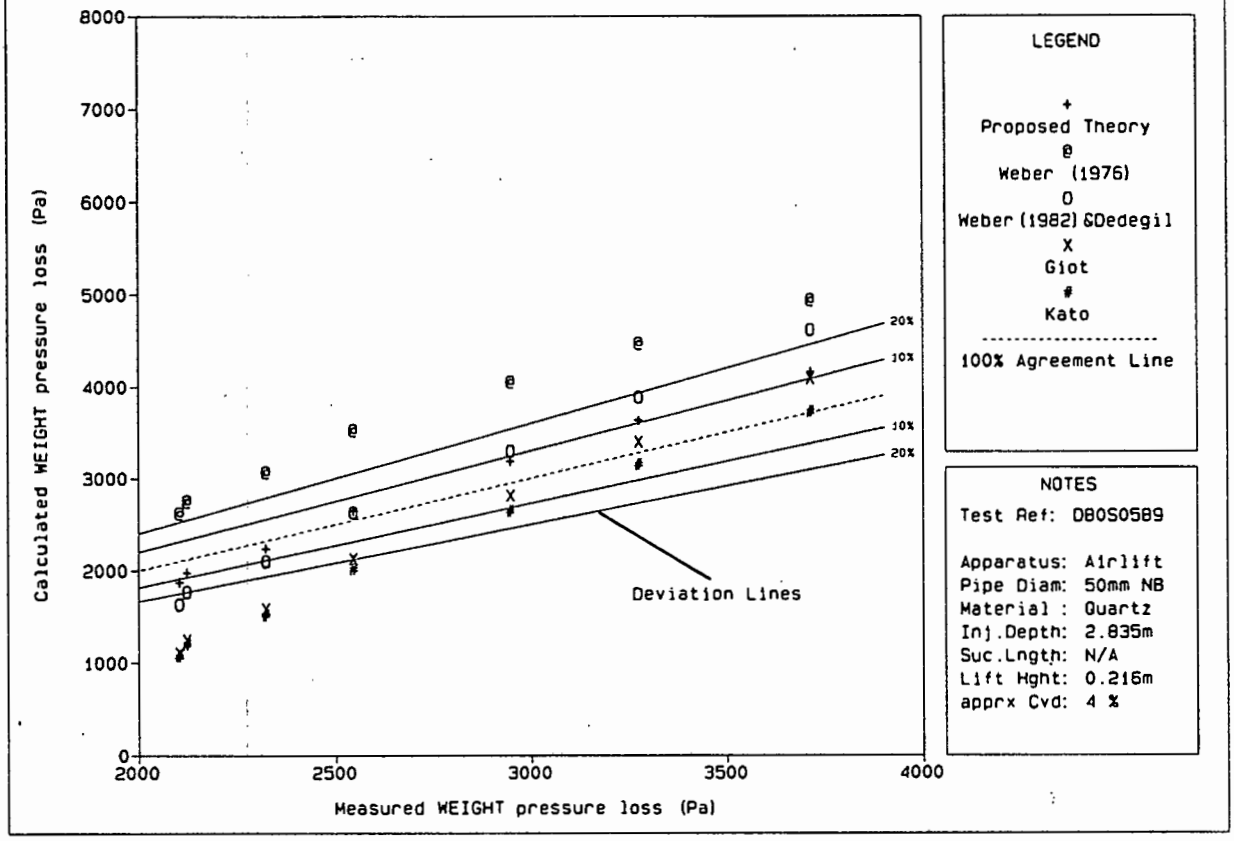

Figure : 8.36 Airlift Pump
Description : Weight, Friction & Momentum Contribution Investigation

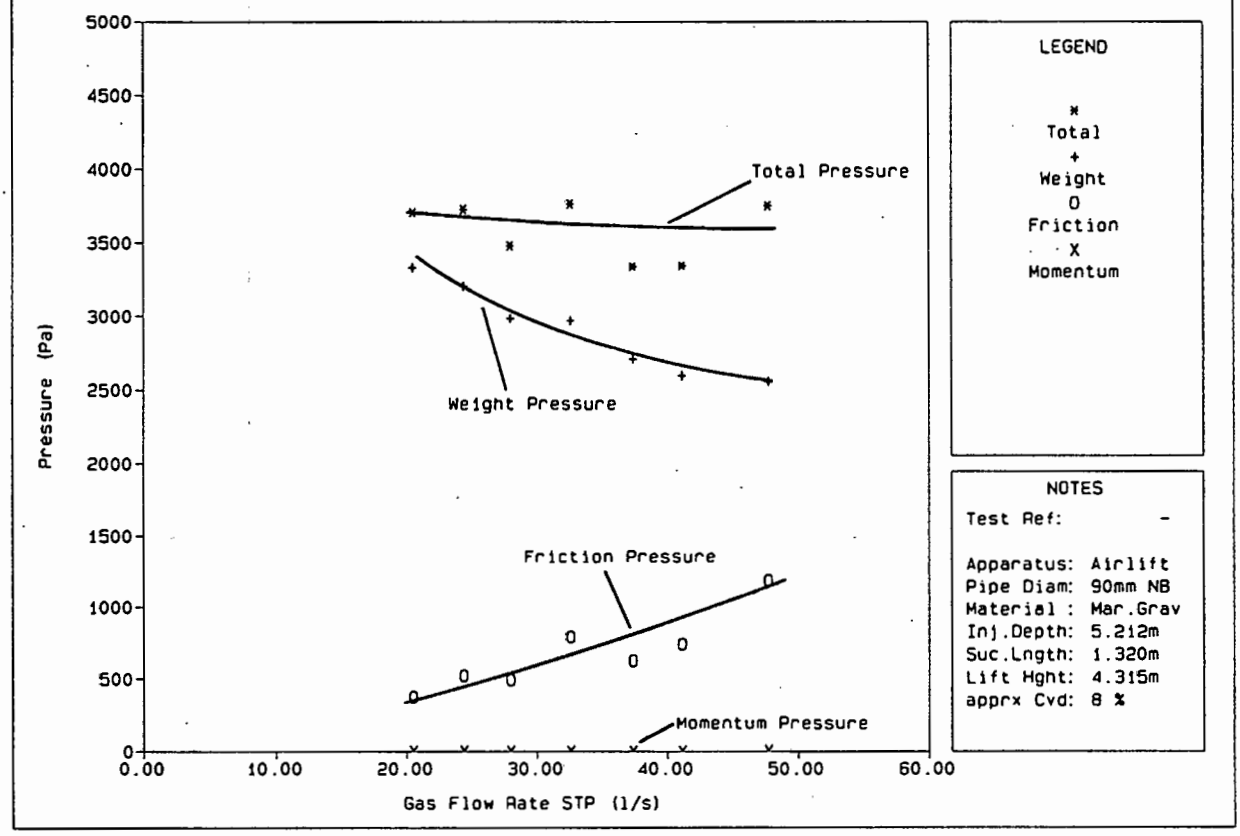

Figure : 8.37 Airlift Pump
Description : Solid/Liquid/Gas Friction Pressure Theories Investigation

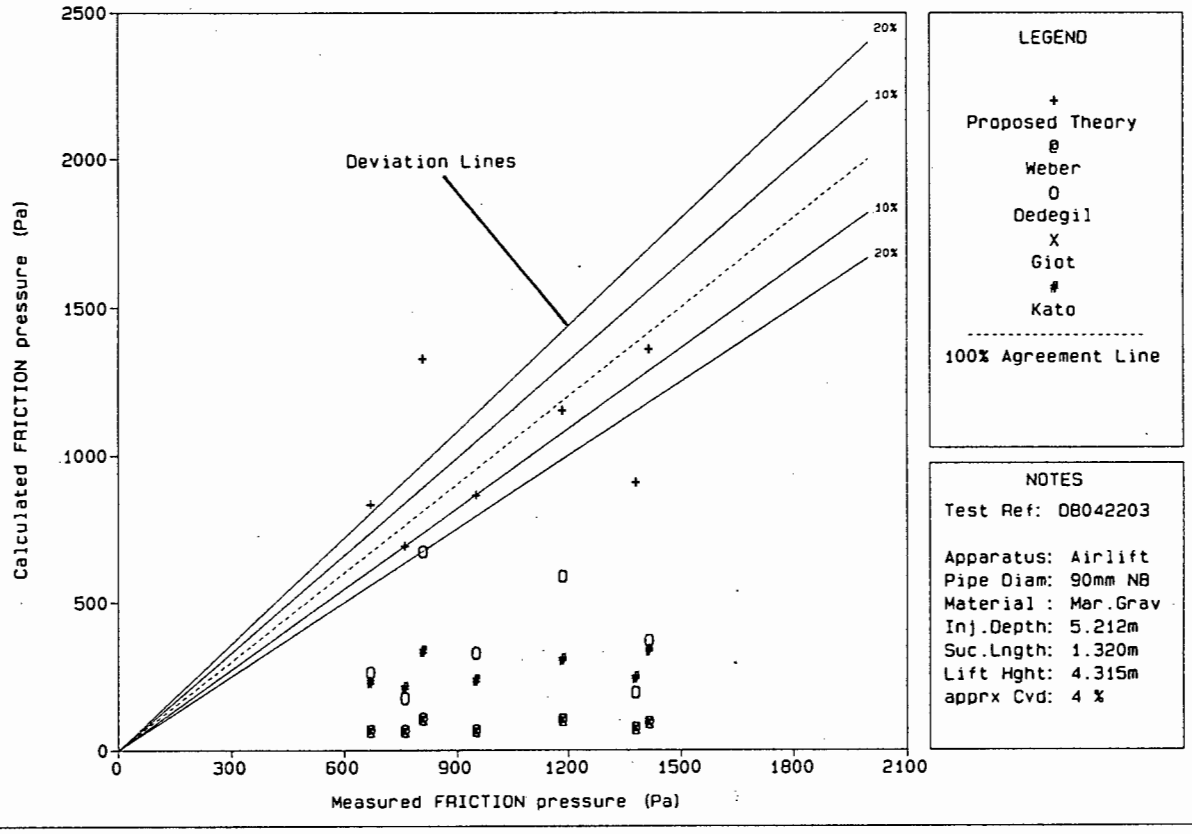

Figure : 8.38 Airlift Pump
Description : Solid/Liquid/Gas Friction Pressure Theories Investigation

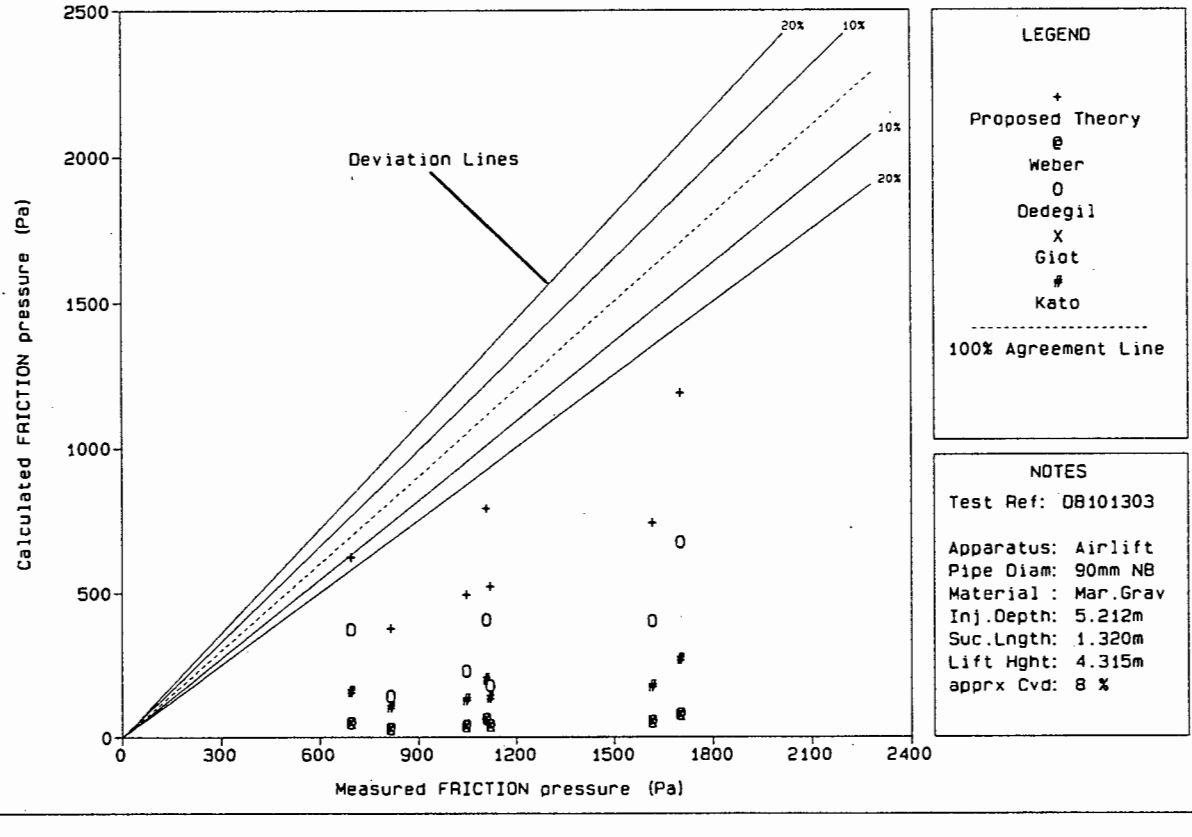

Figure : 8.39 Airlift Pump
Description : Solid/Liquid/Gas Friction Pressure Theories Investigation

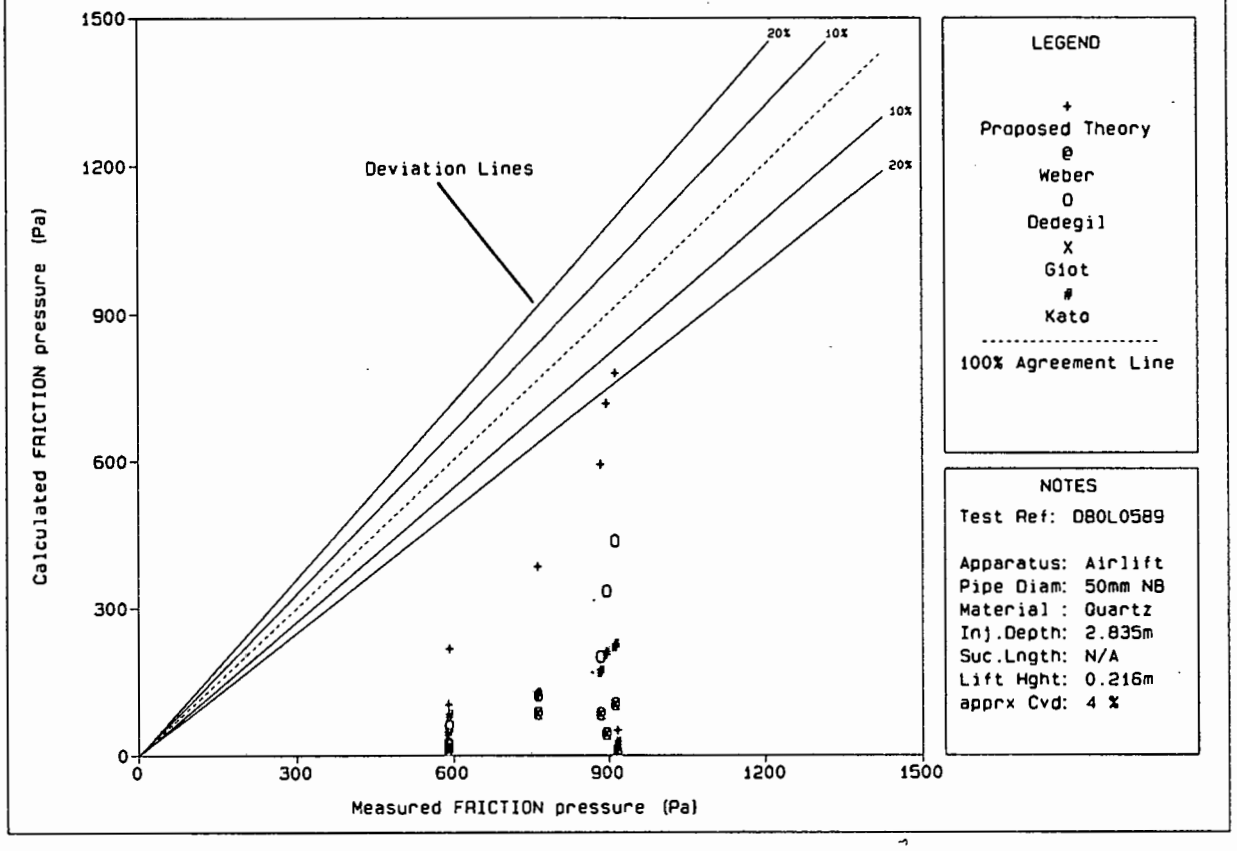

Figure : 8.40 Airlift Pump
Description : Solid/Liquid/Gas Friction Pressure Theories Investigation

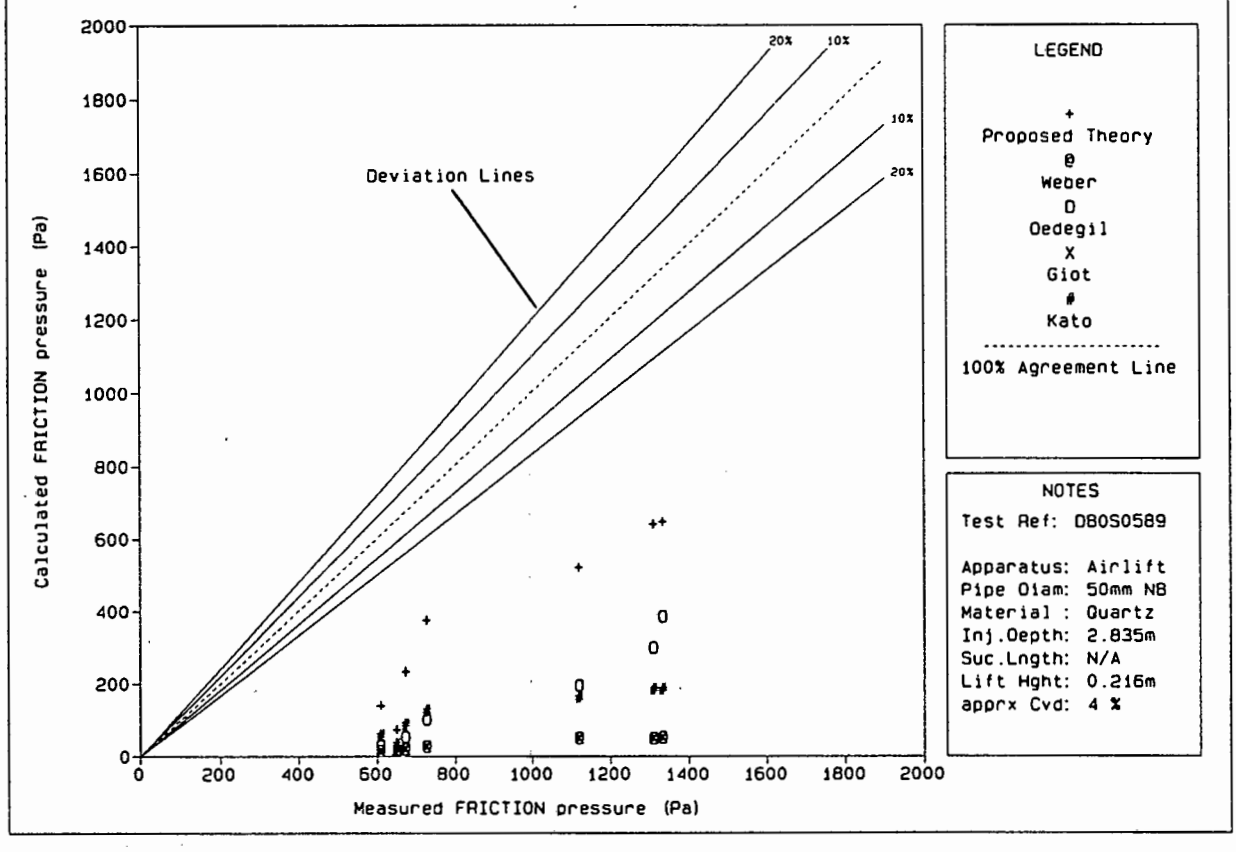

Figure : 8.41 Airlift Pump
Description : Solid/Liquid/Gas Total Pressure Theories Investigation

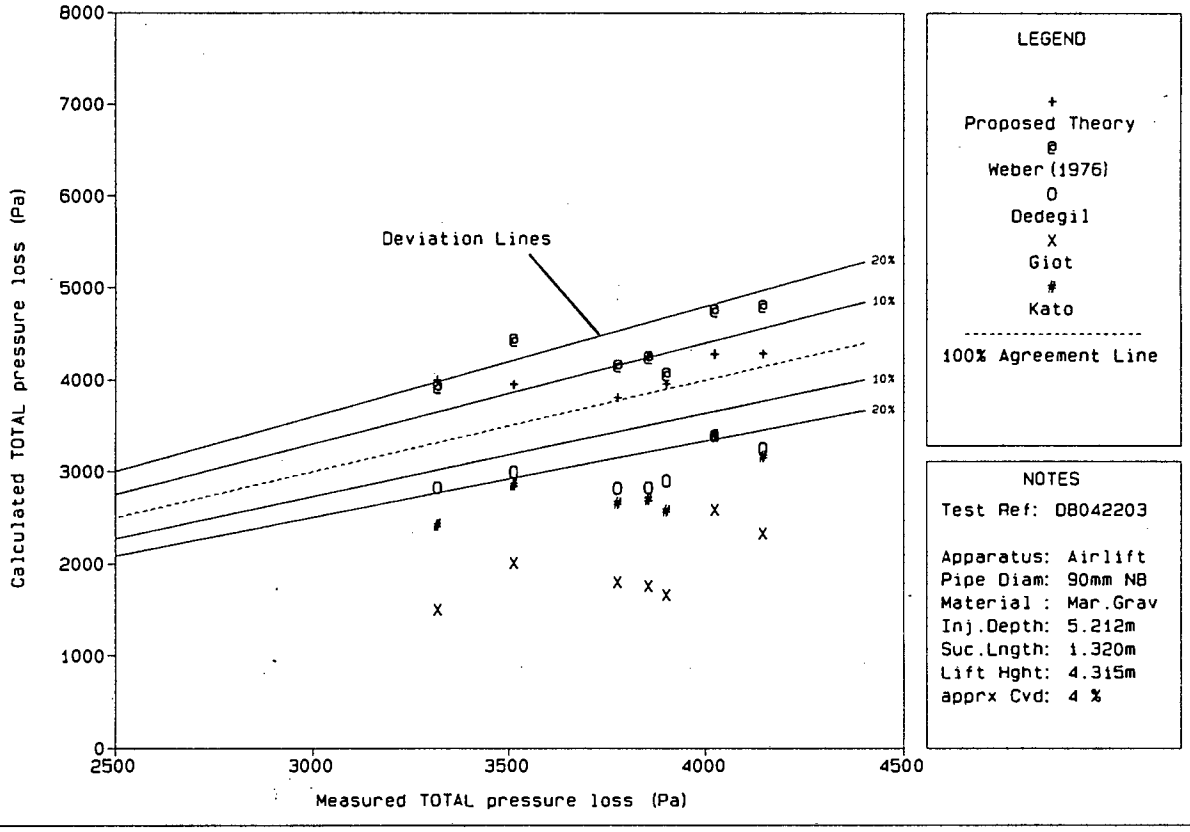

Figure : 8.42 Airlift Pump
Description : Solid/Liquid/Gas Total Pressure Theories Investigation

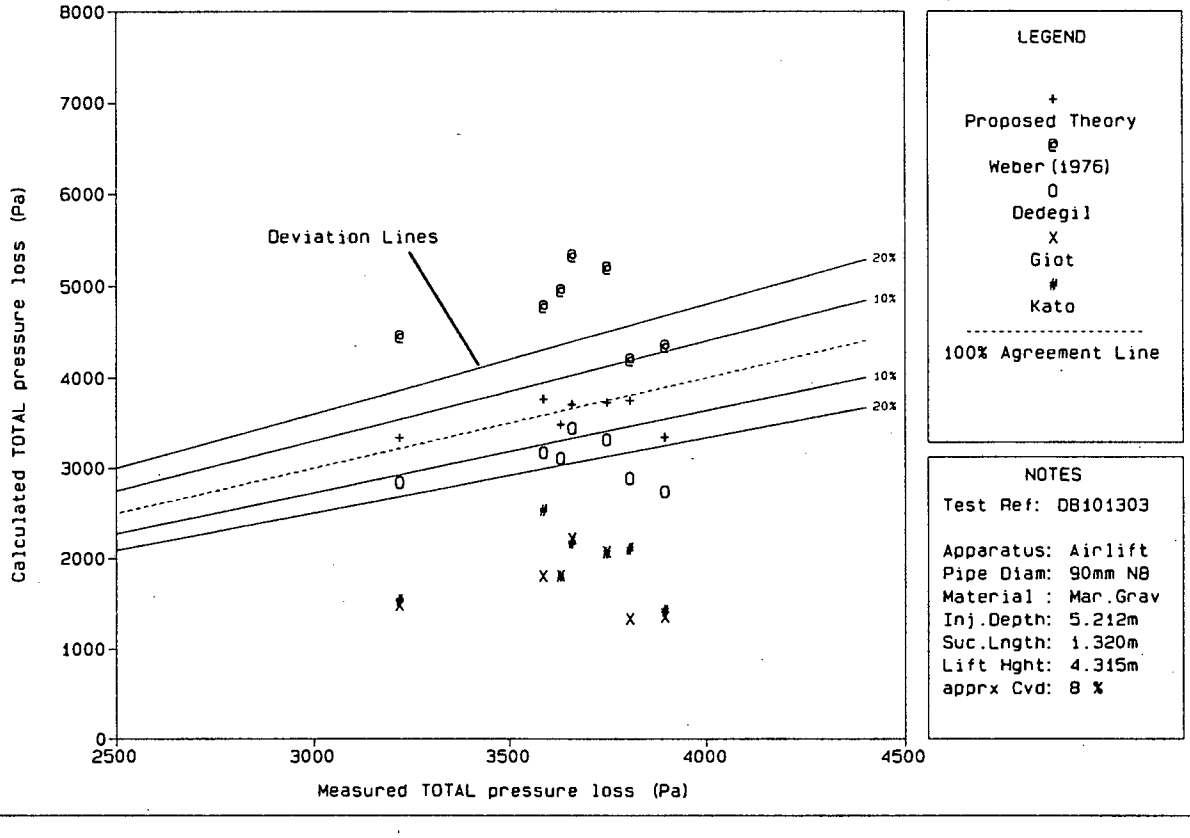

Figure : 8.43
Description : Solid/Liquid/Gas Total Pressure Theories

Airlift Pump Investigation

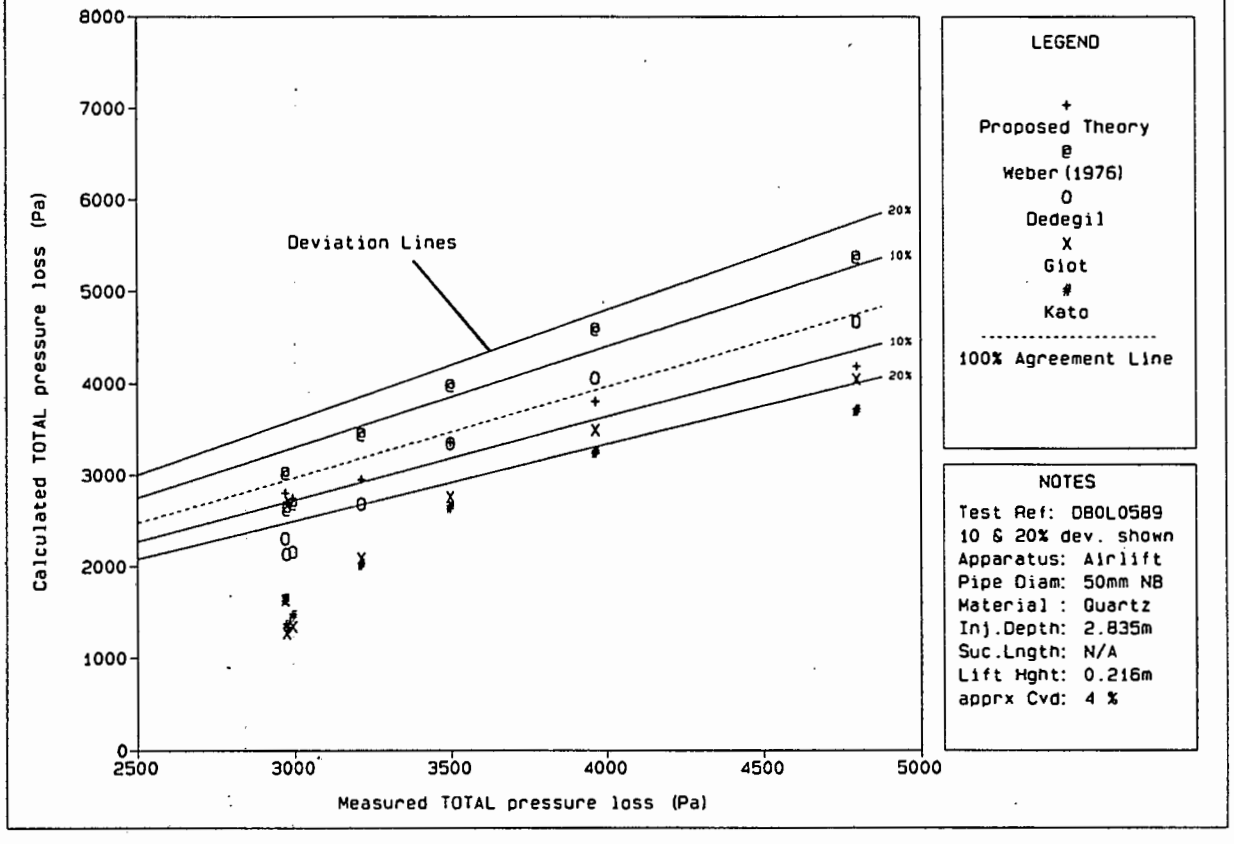

Figure : 8.44
Description : Solid/Liquid/Gas Total Pressure Theories

Airlift Pump Investigation

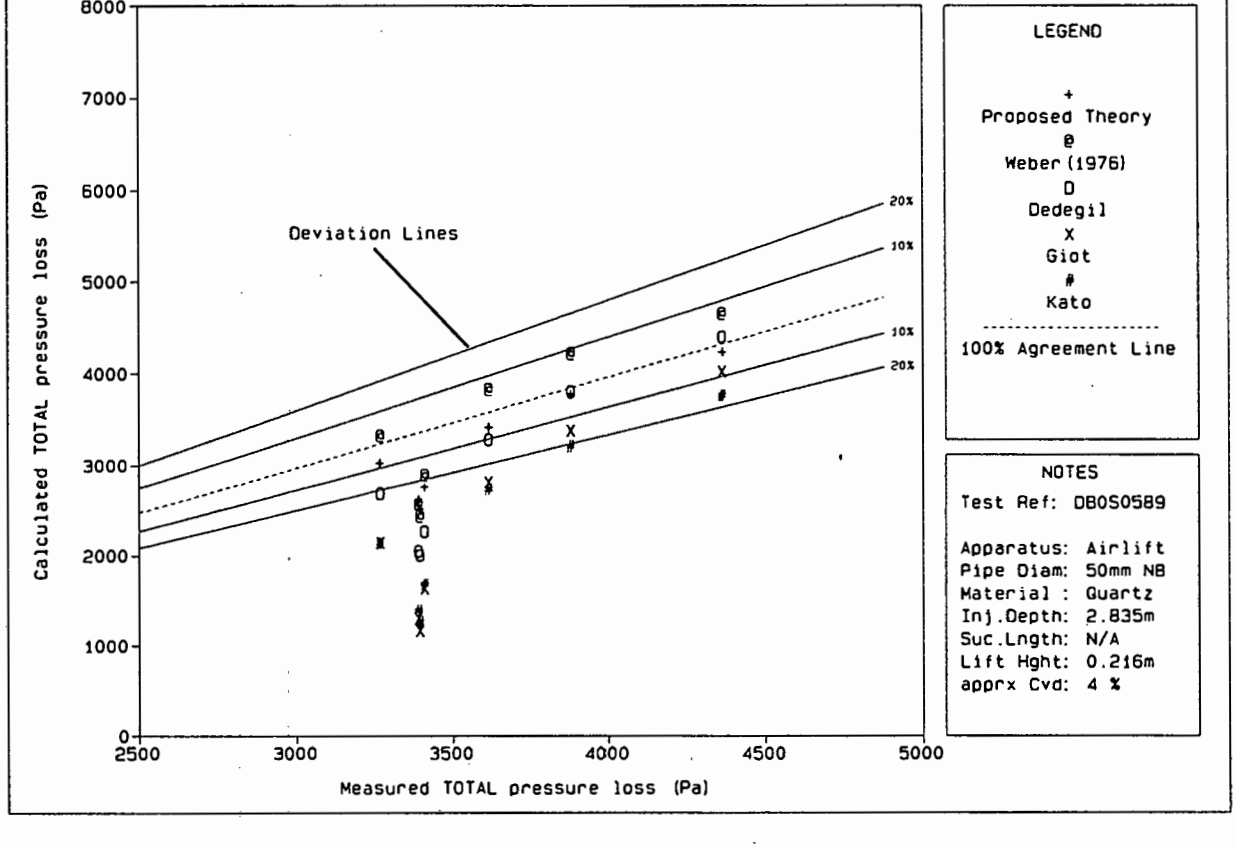

Figure : 8.45 Airlift Pump
Description : Solid/Liquid/Gas Total Pressure Theories Investigation

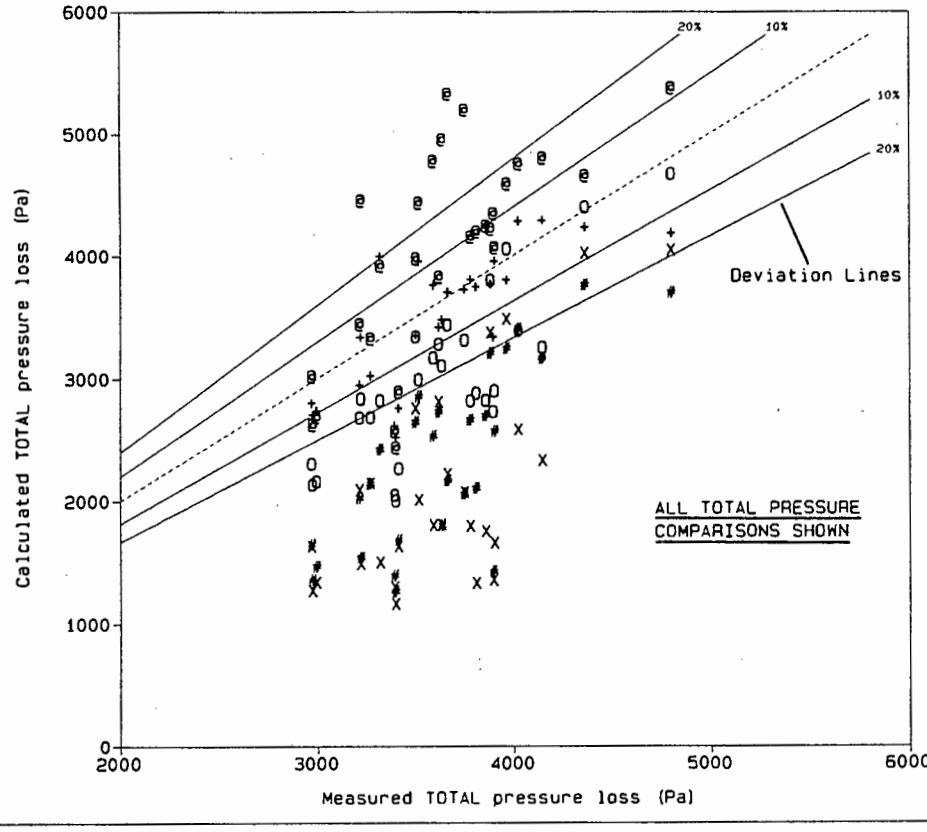

LEGEND

+ Proposed Theory
@ Weber (1976)
O Dedegil
X Giot
Kato

100% Agreement Line

NOTES

Test Ref: ALL DATA

Apparatus: Airlift
Pipe Diam: 50 & 90mm

all data shown

8.6 AIRLIFT PUMP OPERATING TESTS - PREDICTION OF OUTPUT LIQUID AND SOLID FLOW RATES

As mentioned in Chapter 7, a series of operating tests have been performed to observe and measure the behaviour of airlift pumps under a range of conditions. In this section, these operating tests are simulated using each of the previously discussed theories, and the accuracy of the theoretically predicted output liquid and solid flow rates are evaluated.

In each of the simulations, the calculation procedure described in Appendix C is used to evaluate output flow rates for a range of input gas flow rates.

Unfortunately, the 90 mm airlift pump has an elaborate delivery outlet consisting of a series of bends and a flow diverter (Figure 5.6), while the 40 mm airlift pump has an elaborate inlet configuration forming part of the recirculating system (Figure 5.3). Thus in the 90 mm airlift pump simulation, the iteration (refer Appendic C) ends when the calculated outlet pressure is equal to the absolute static pressure at the last pressure tapping before the elaborate delivery pipe outlet. *Because of fluctuations in these measured static pressures for a range of gas flow rates, the typical smooth airlift pump operating curve as shown in Figure 2.2 is not obtained. For this purpose, comparisons of predicted and measured output flow rates is best achieved with deviation graphs, showing measured liquid and solid output versus theoretically calculated liquid and solid output.*

Similarly on the 40 mm airlift pump, the iteration starts with the absolute static pressure just below the gas injectors.

Again fluctuations in these measurements prevent the recording of smooth airlift pump operating curves. Thus comparisons of predicted and measured output flow rates is again best achieved with deviation graphs.

The two phase pressure loss in the suction pipe (Δp_2) is small compared with the other pressure losses and is evaluated with the Proposed theory (Equations 4.5 to 4.28). Also, because of Weber's (1976) adverse under-prediction of the gas and solid *in situ* volumetric concentration in the airlift pump delivery pipe, only Weber's later (1982) theory is evaluated.

Table 8.9 below summarizes all theories evaluated.

Author	3 Phase Shear Stress Equation	Friction Factor Equation	Phase *in situ* Concentration Theory	
			$C_{vt}^{s/g}$	$\epsilon_g^{s/g}$
Proposed Theory	4.49	4.28	4.40	4.42
Dedegil	3.45	3.40	iteration using 3.7 & 3.27	
Giot	3.41	3.40	iteration using 3.31 & 3.33	
Kato	3.46	3.49	[4.40]	3.29
Weber	3.41	3.40	iteration using 3.7 & 3.27	

TABLE 8.9 : Operating curve theories evaluated

Figures 8.46 to 8.59 a & b show comparison of predicted and measured liquid and solid output flow rates for a range of delivered volumetric concentrations, gas flow rates, particle sizes, particle densities and pipe sizes. In all the figures, the Proposed theory results in the most favourable simulation of the liquid and solid output flow rates, by plotting closest to the 100% agreement line. The simulated liquid and solid flow rates are found to agree largely within 10% of the measured data and only a few predictions deviating by 15-20%.

All other theories (Dedegil, Giot, Kato, Weber) mostly over-predict the measured output flow rates by more than 15-20%. This over-prediction is a result in the under-estimation of the three phase pressure losses discussed in Section 8.5.4. [Note: In Section 8.5.4, the three phase pressure losses were shown to be under-estimated in <u>one</u> delivery pipe increment between the two knife gate valves. For the simulation of the operating curves, a <u>series</u> of delivery pipe increments are evaluated and the under-estimation of each three phase pressure loss results in a compounding effect when integrating over the total delivery pipe length]. The calculated three phase pressure losses due to the conveyed mixture are therefore much lower than the actual three phase pressure losses and consequently the calculation assumes that more mixture can be conveyed.

The calculated log standard error of all the simulated liquid and solid output flow rates shown in Figures 8.46 to 8.59 a & b are listed in Table 8.10. Referring to this table, the Proposed theory gives the highest and most favourable log standard error, compared with other authors, indicating the best agreement with the measured data.

The Proposed theory successfully simulates the operation of airlift pumps in three phase flow for a range of gas flow rates, delivered concentrations, pipe sizes and particle characteristics. Furthermore, the predictions are more accurate when compared with various theoretical approaches cited in the literature.

Author	Log Standard Error
Proposed Theory	0,97035
Dedegil	0,91735
Giot	0,89390
Kato	0,93670
Weber	0,90581

TABLE 8.10 : Log standard error (output flow rates)

Figure : 8.46a
Description : Solid/Liquid/Gas Operating Curves

Airlift Pump Investigation

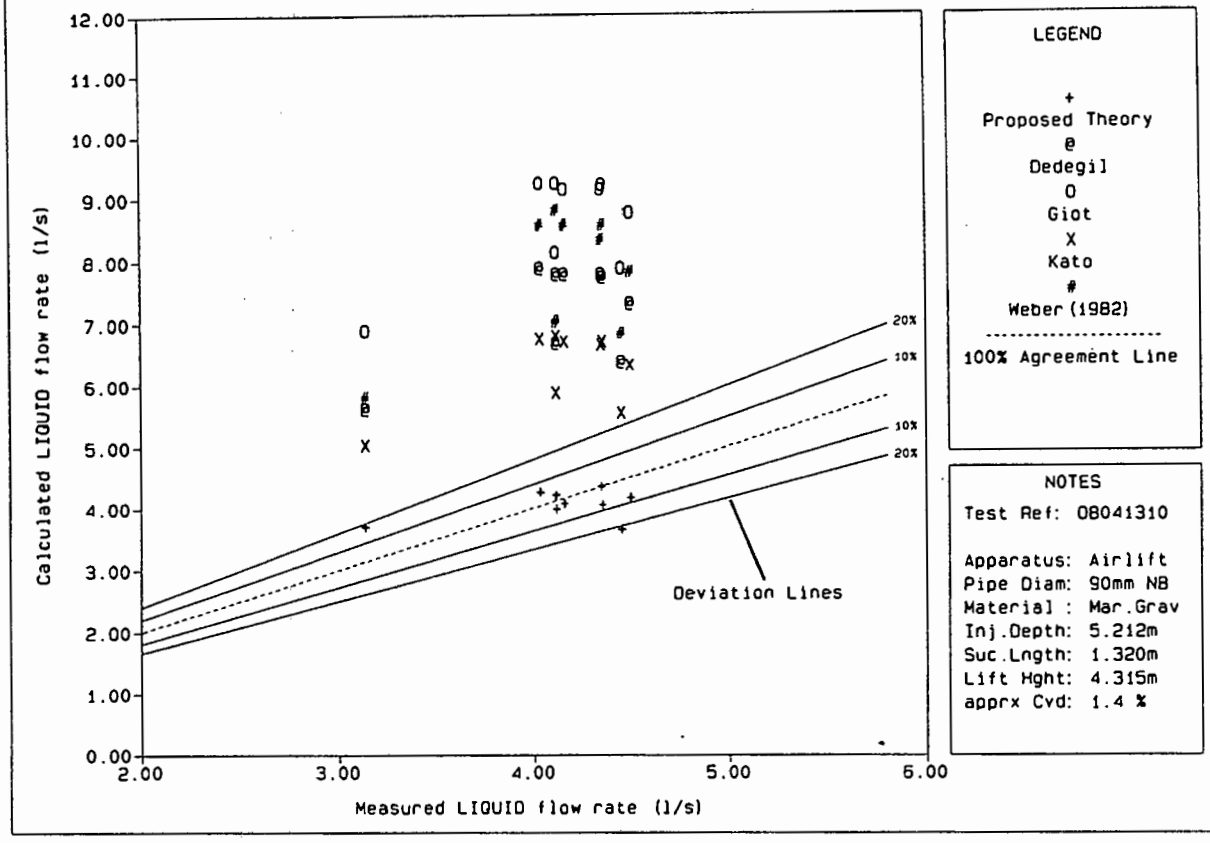

Figure : 8.46b
Description : Solid/Liquid/Gas Operating Curves

Airlift Pump Investigation

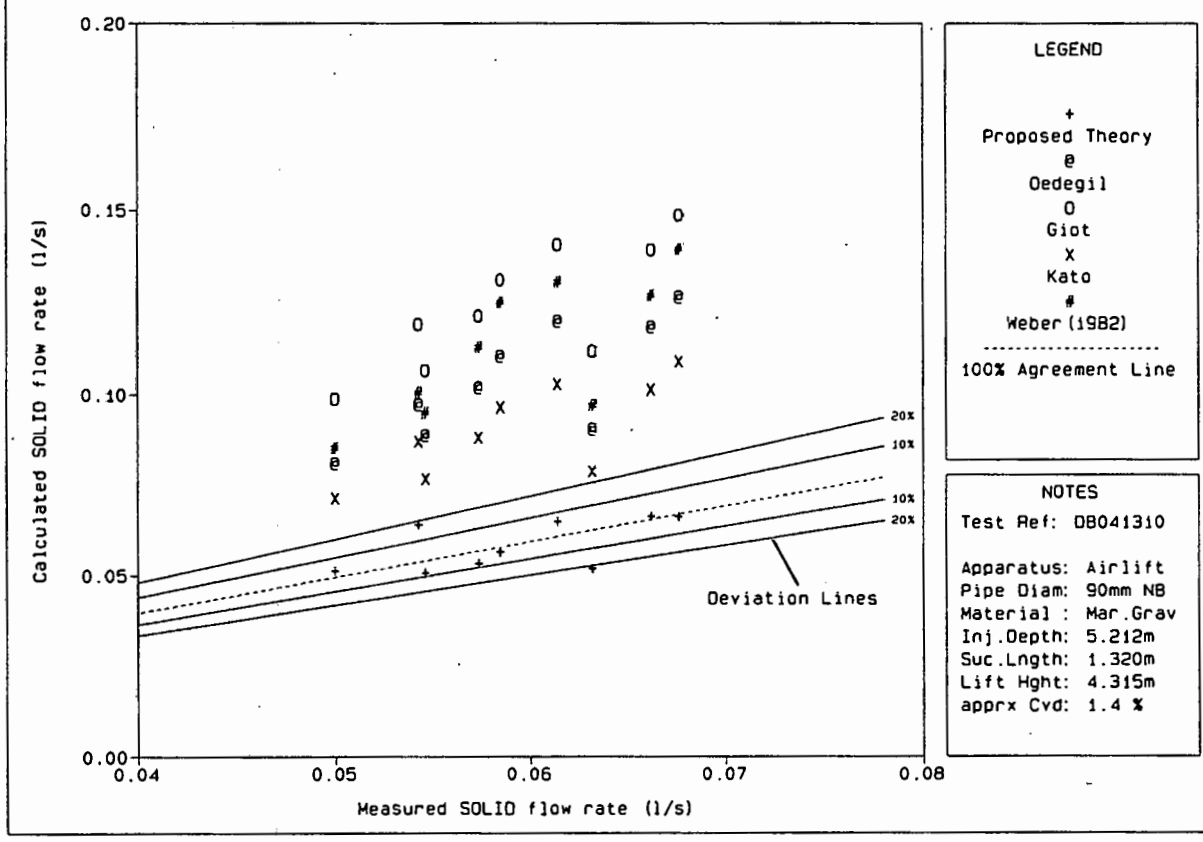

Figure : 8.47a
Description : Solid/Liquid/Gas Operating Curves

Airlift Pump Investigation

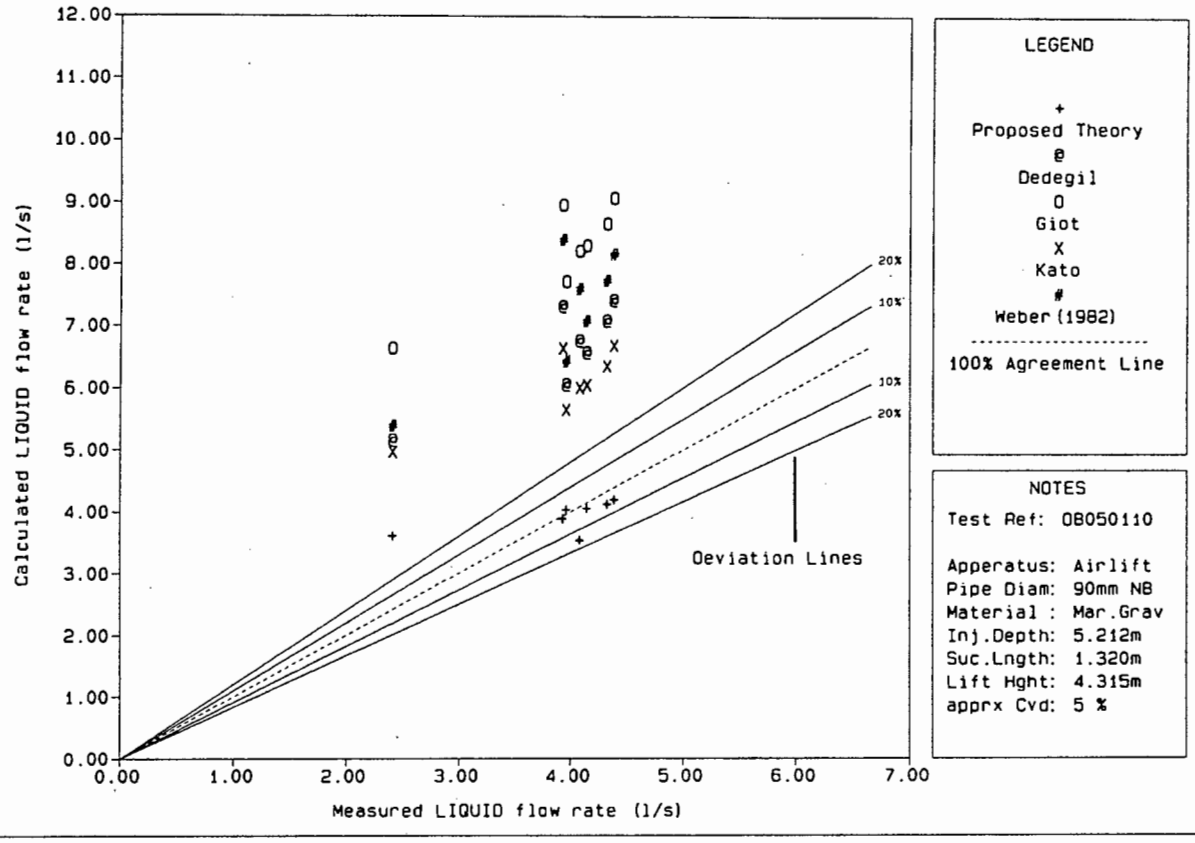

Figure : 8.47b
Description : Solid/Liquid/Gas Operating Curves

Airlift Pump Investigation

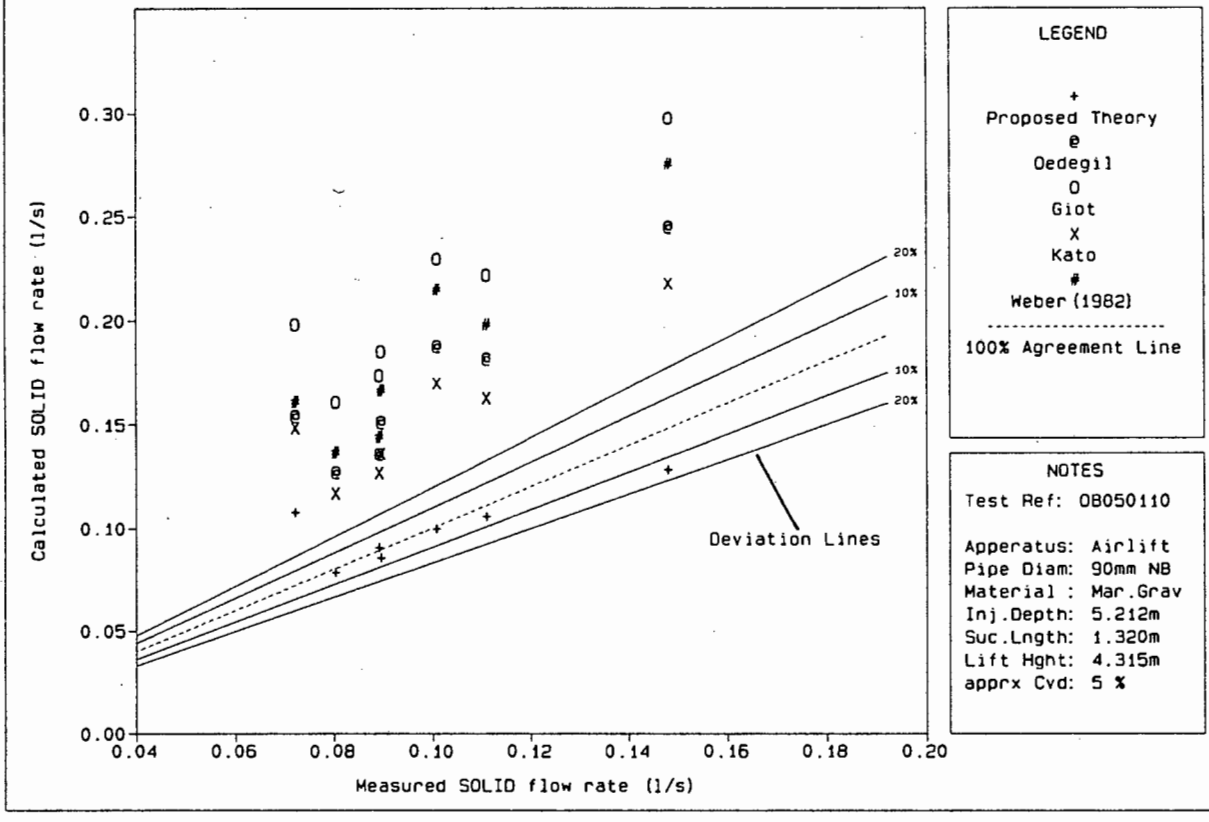

Figure : 8.48a
Description : Solid/Liquid/Gas Operating Curves

Airlift Pump Investigation

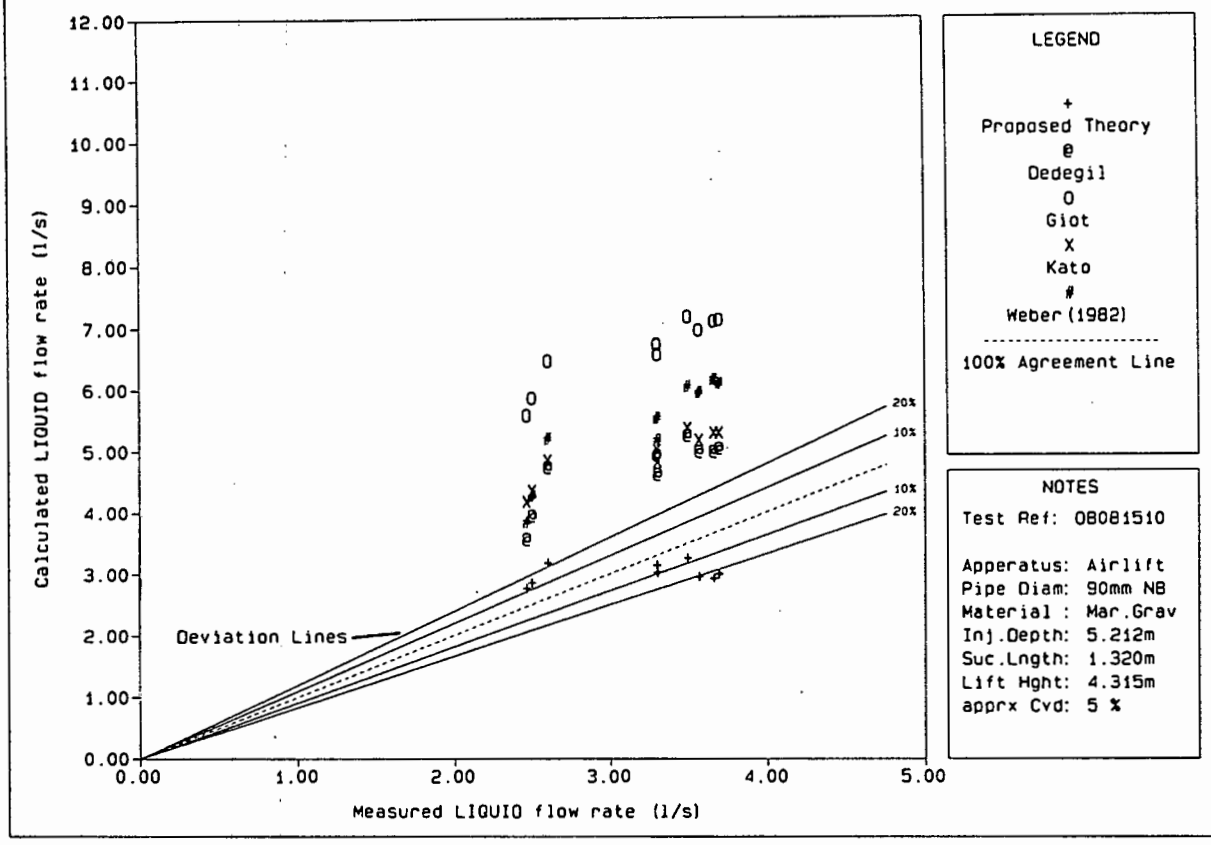

Figure : 8.48b
Description : Solid/Liquid/Gas Operating Curves

Airlift Pump Investigation

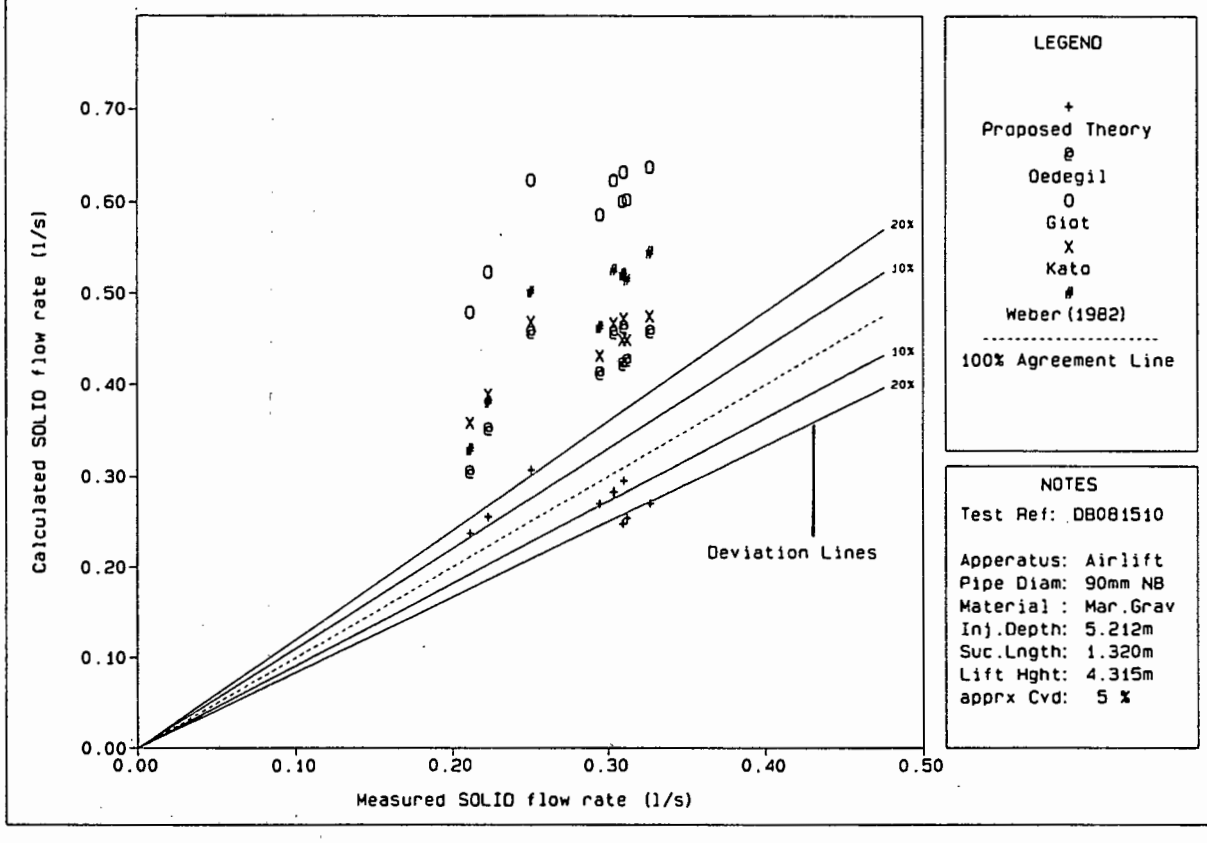

Figure : 8.49a
Description : Solid/Liquid/Gas Operating Curves

Airlift Pump Investigation

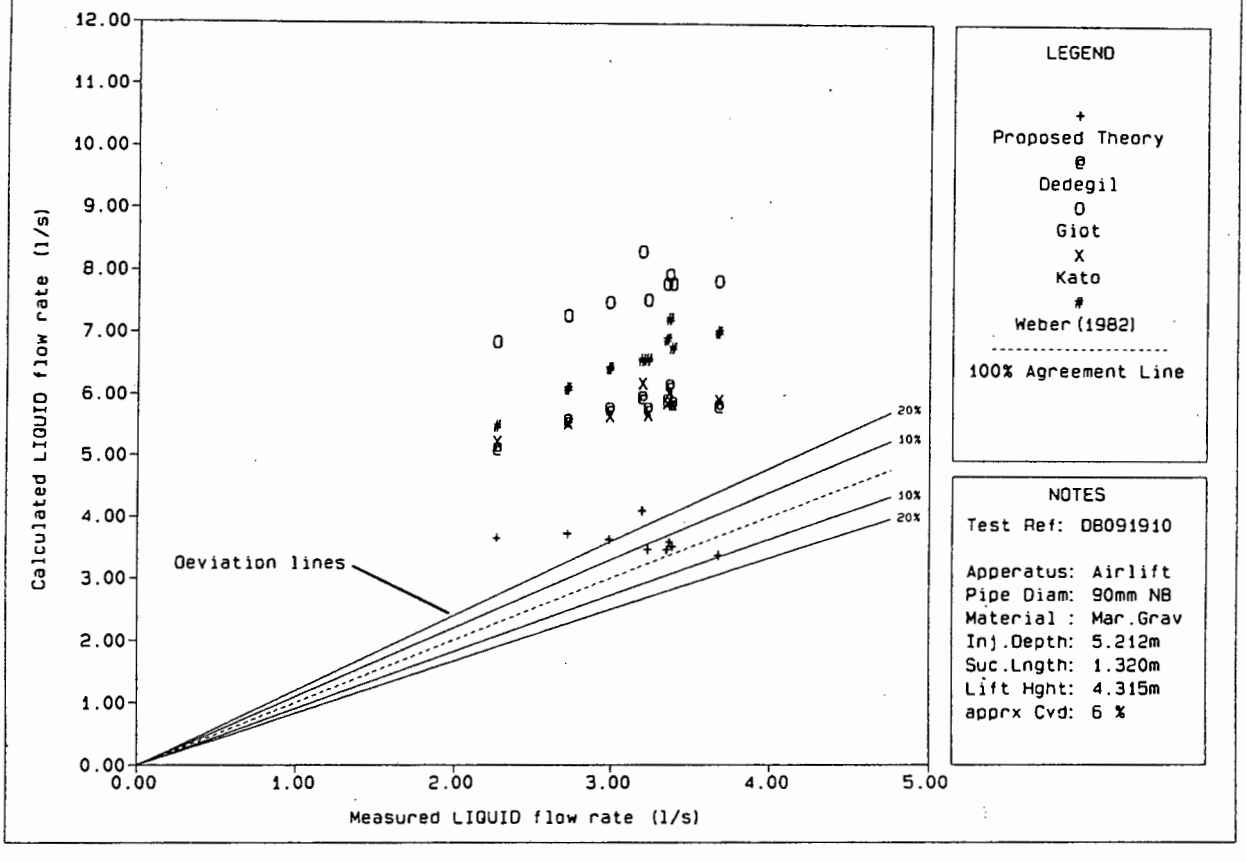

Figure : 8.49b
Description : Solid/Liquid/Gas Operating Curves

Airlift Pump Investigation

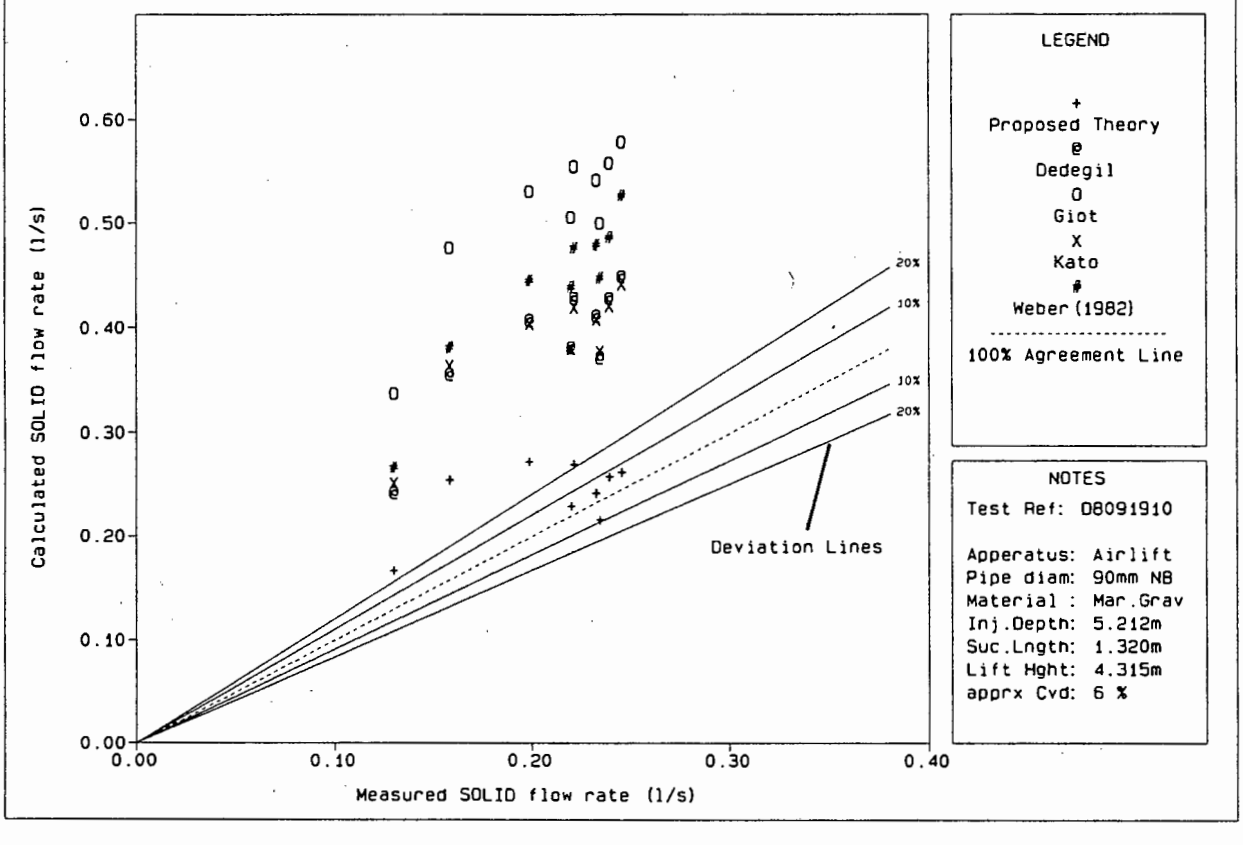

Figure : 8.50a
Description : Solid/Liquid/Gas Operating Curves

Airlift Pump Investigation

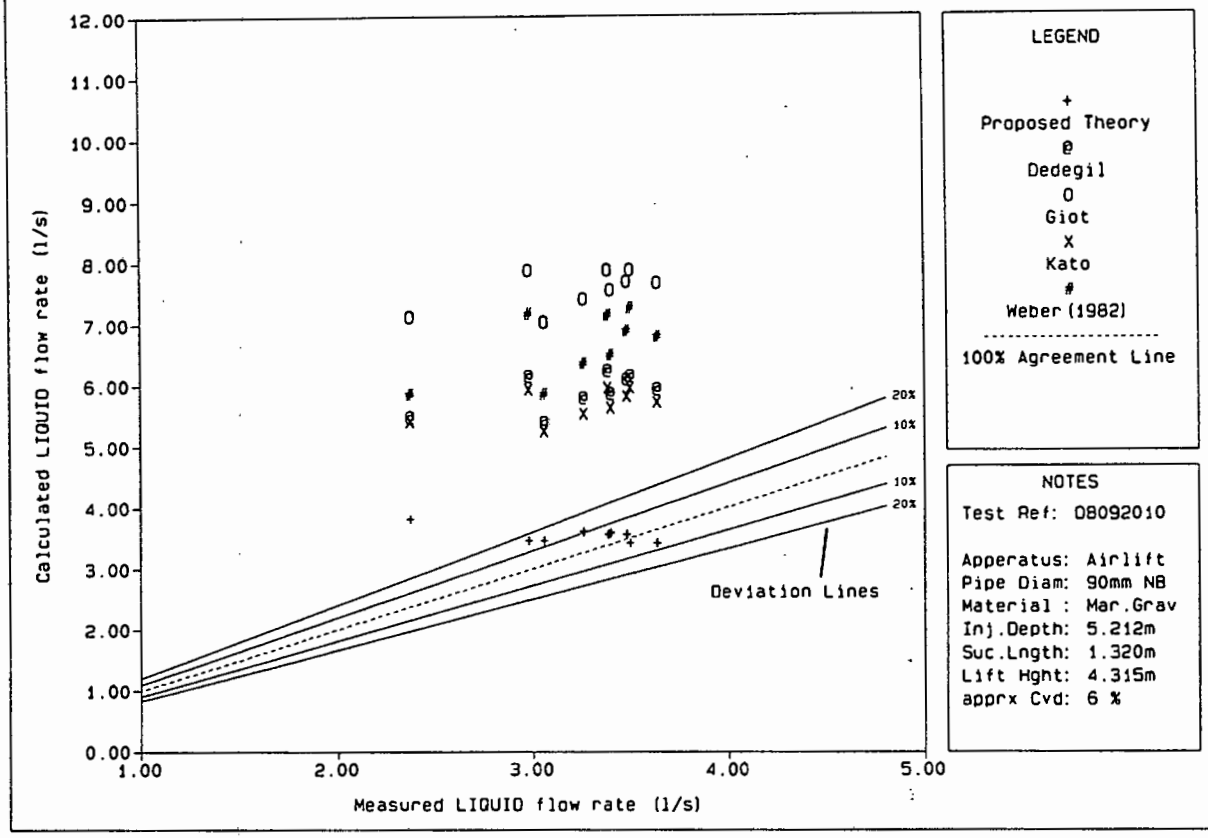

Figure : 8.50b
Description : Solid/Liquid/Gas Operating Curves

Airlift Pump Investigation

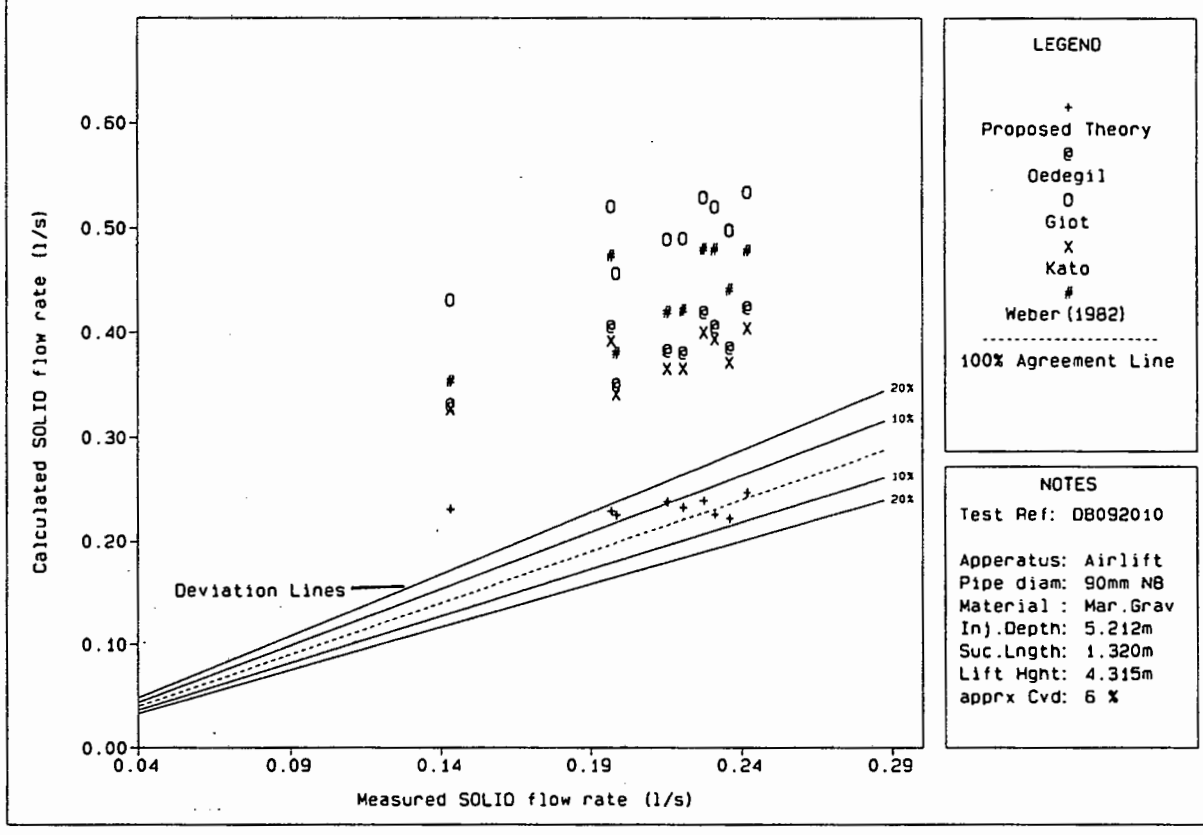

Figure : 8.51a
Description : Solid/Liquid/Gas Operating Curves

Airlift Pump Investigation

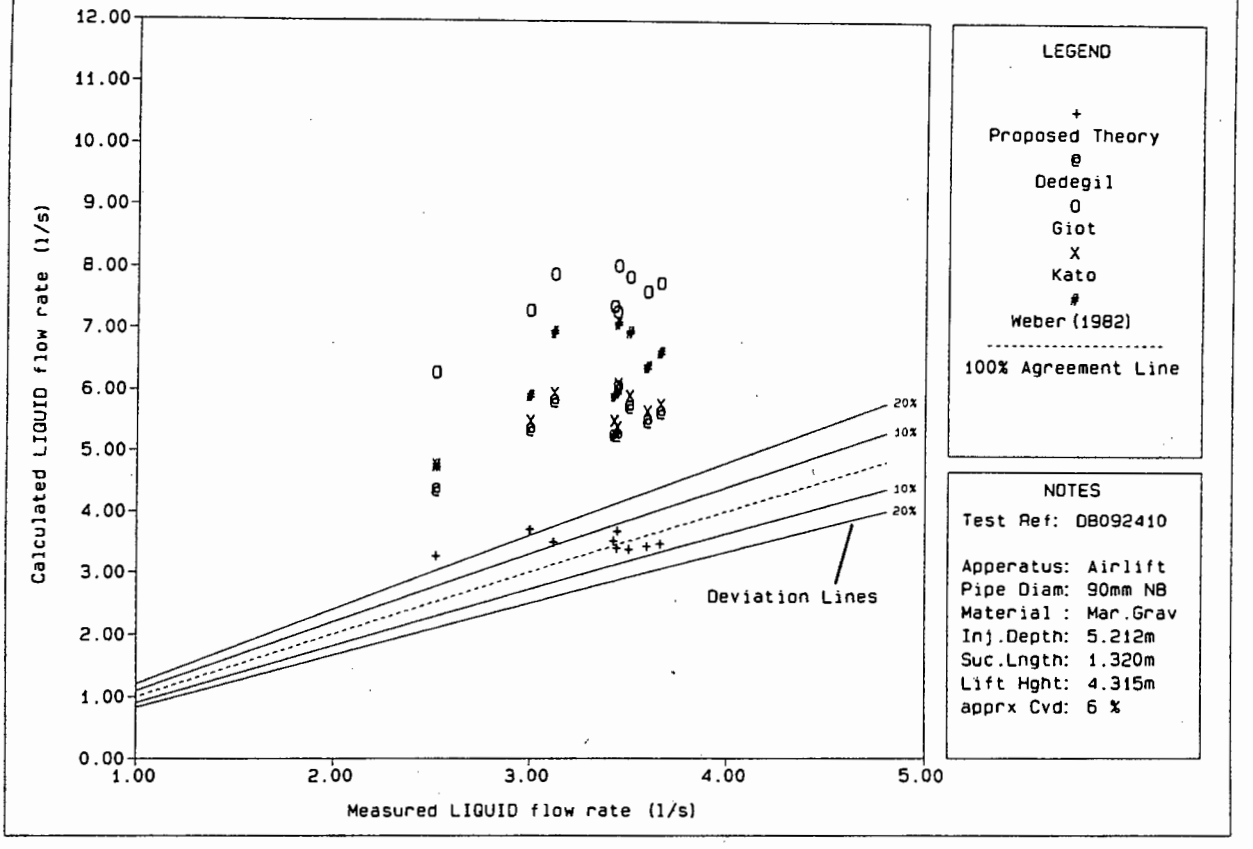

Figure : 8.51b
Description : Solid/Liquid/Gas Operating Curves

Airlift Pump Investigation

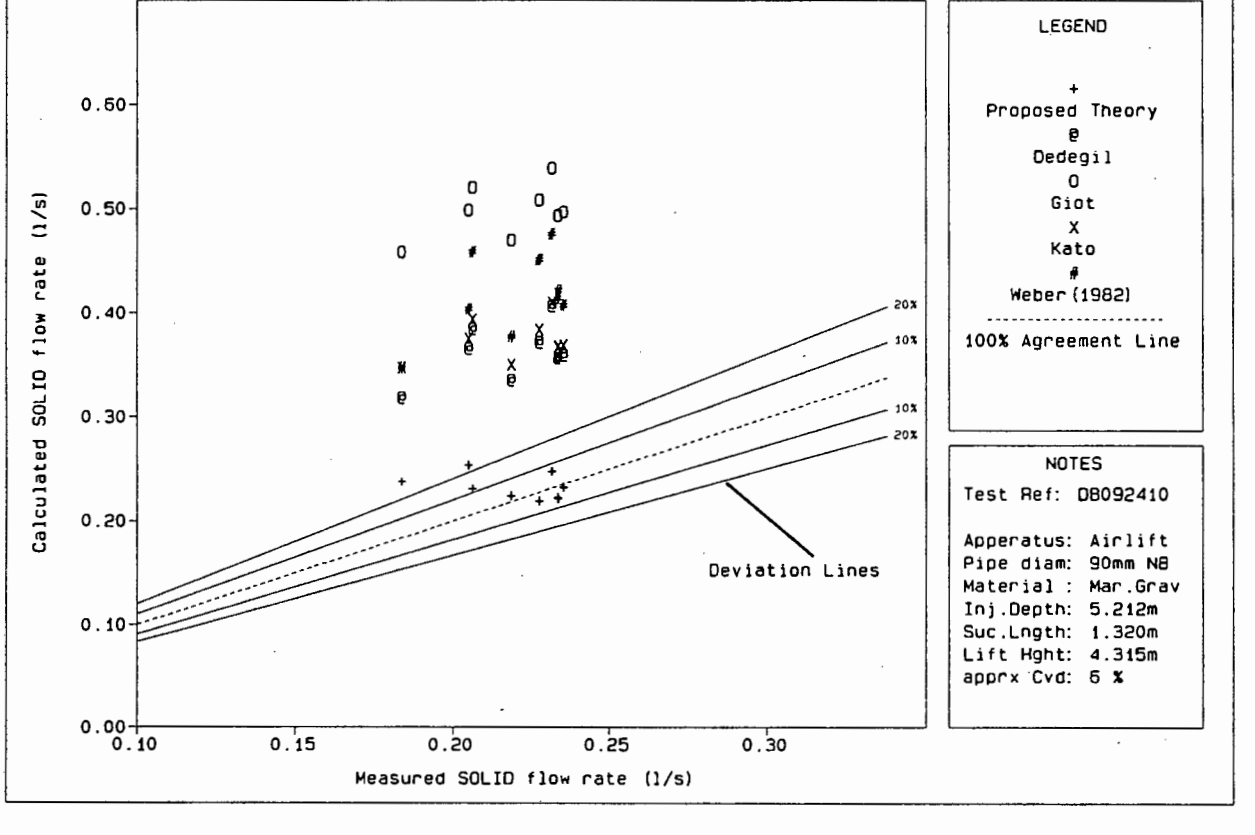

Figure : 8.52a
Description : Solid/Liquid/Gas Operating Curves

Airlift Pump Investigation

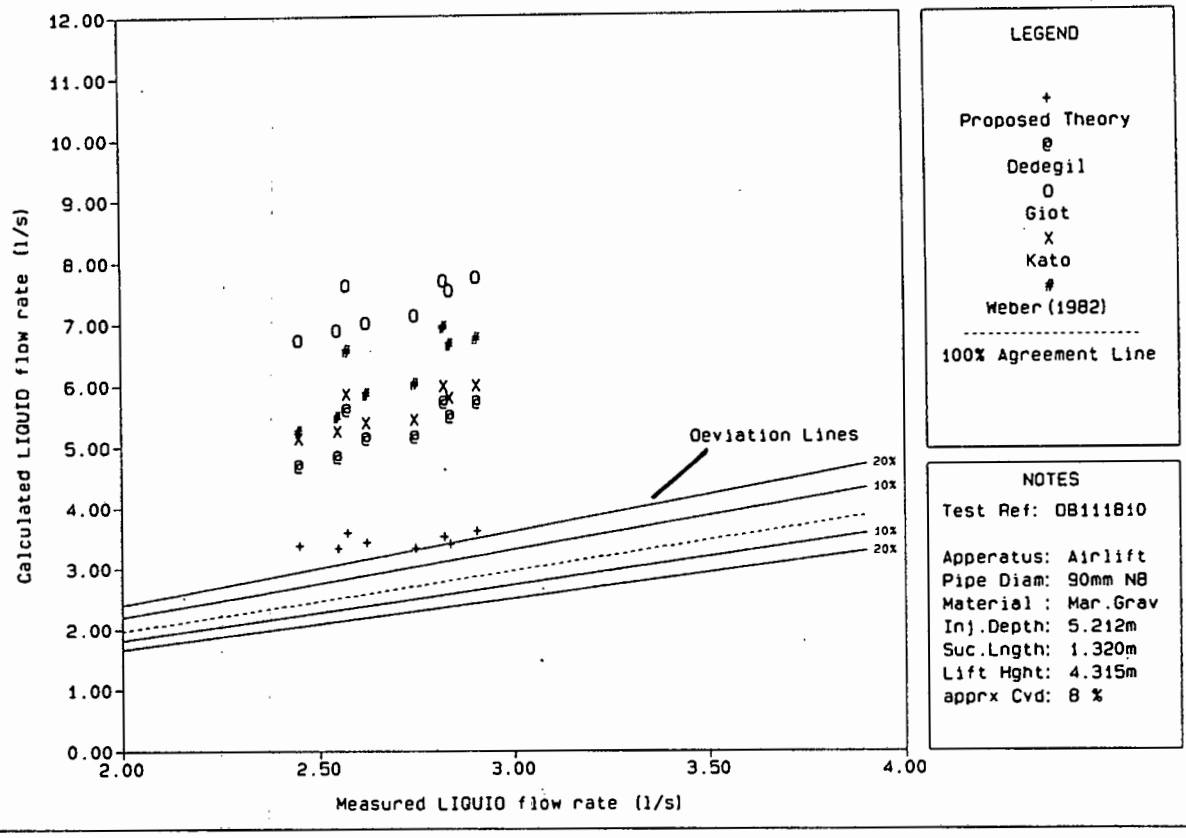

Figure : 8.52b
Description : Solid/Liquid/Gas Operating Curves

Airlift Pump Investigation

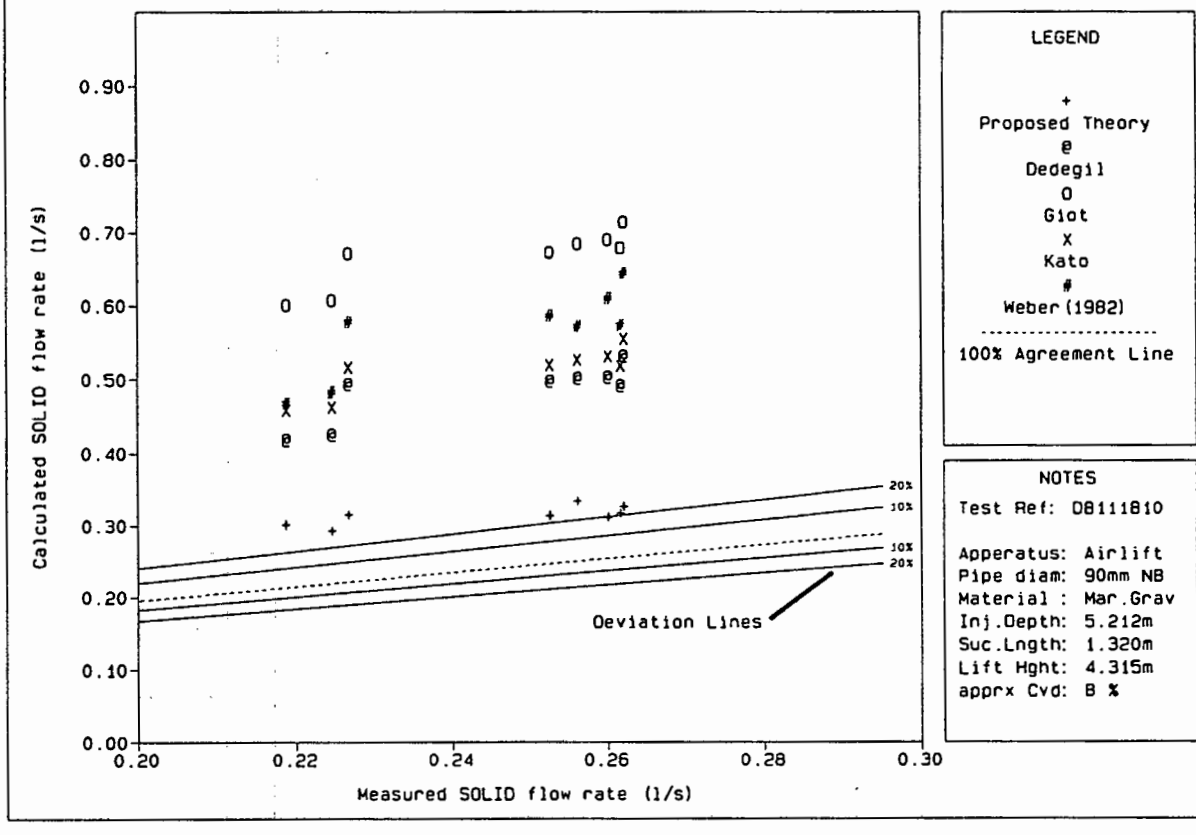

Figure : 8.53a
Description : Solid/Liquid/Gas Operating Curves

Airlift Pump Investigation

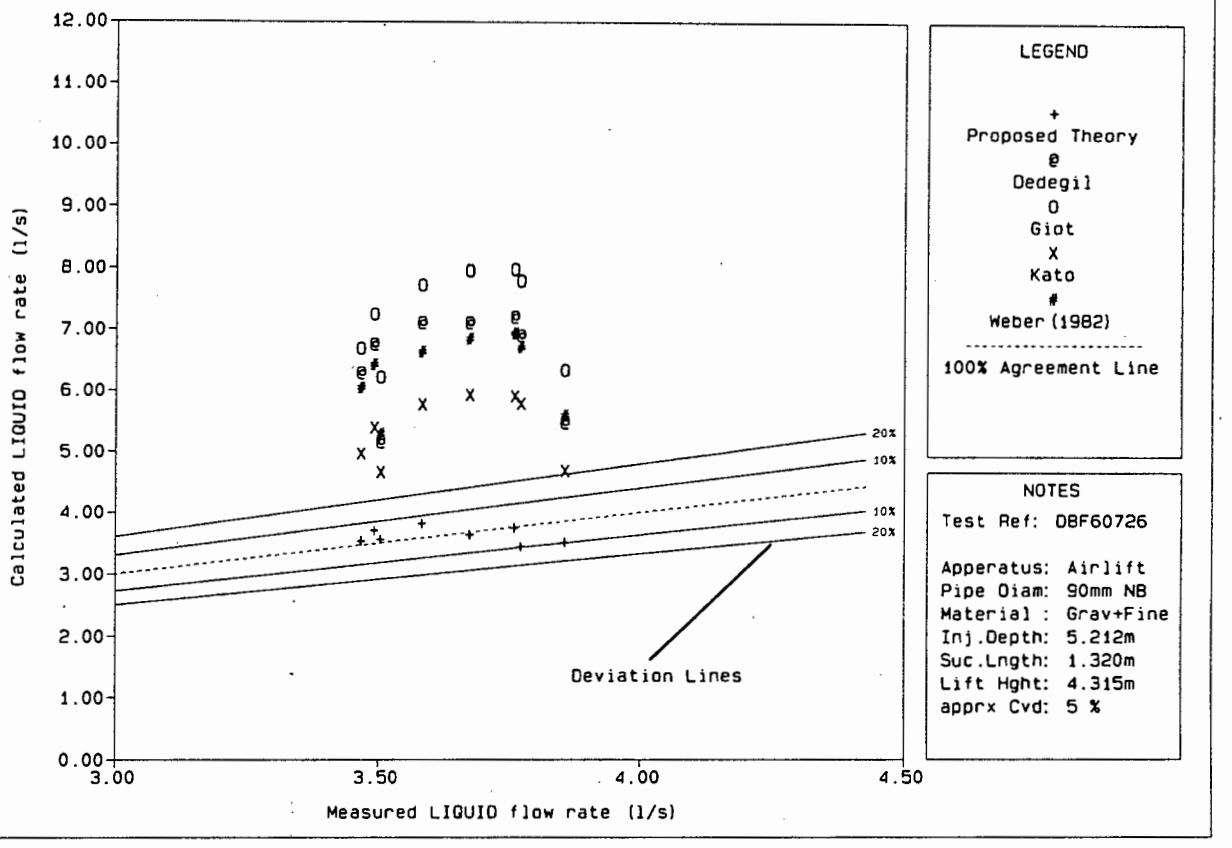

Figure : 8.53b
Description : Solid/Liquid/Gas Operating Curves

Airlift Pump Investigation

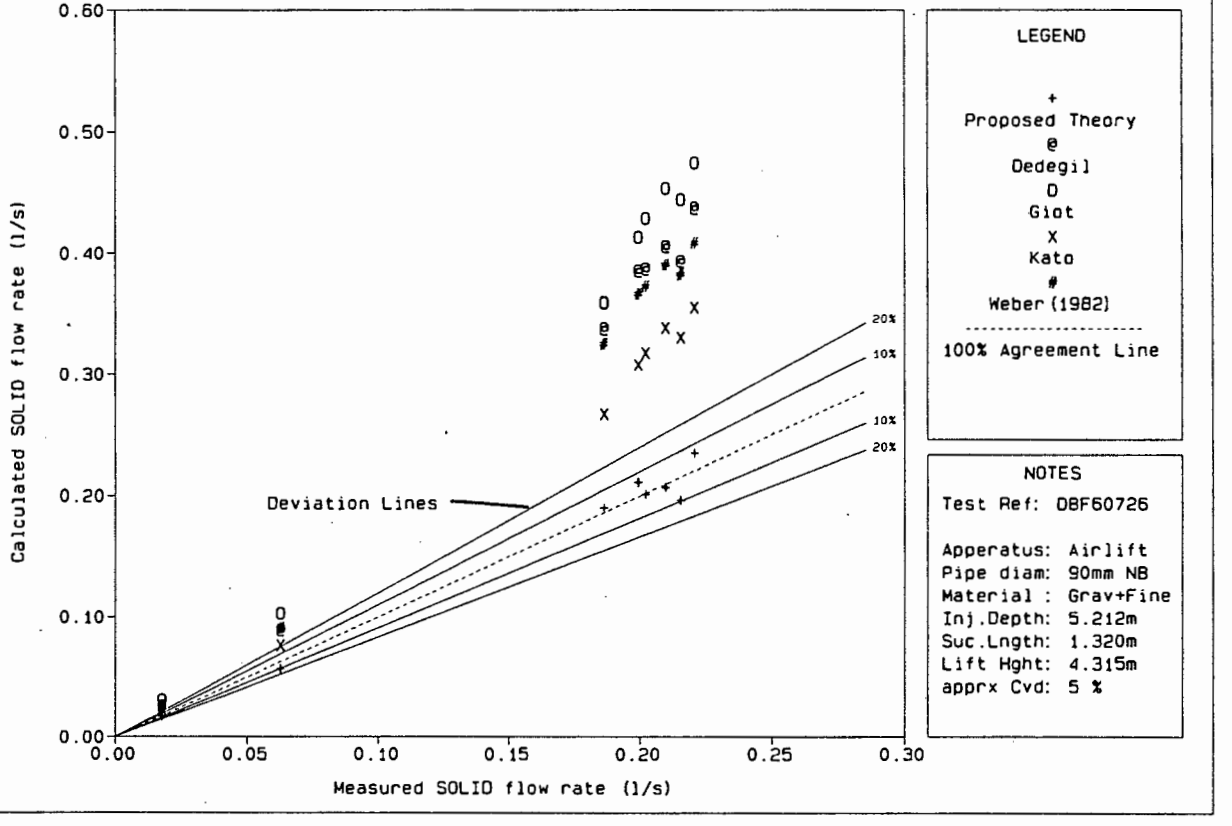

Figure : 8.54a
Description : Solid/Liquid/Gas Operating Curves

Airlift Pump Investigation

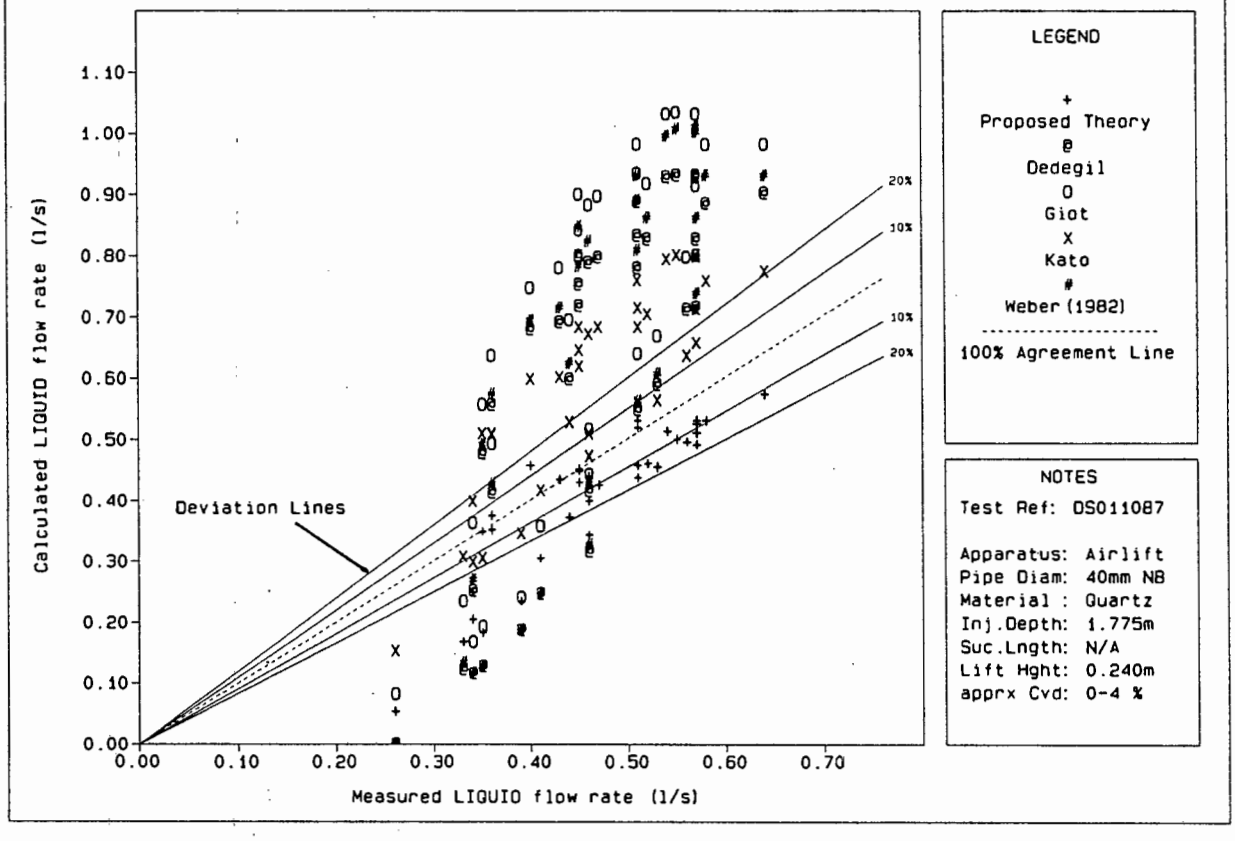

Figure : 8.54b
Description : Solid/Liquid/Gas Operating Curves

Airlift Pump Investigation

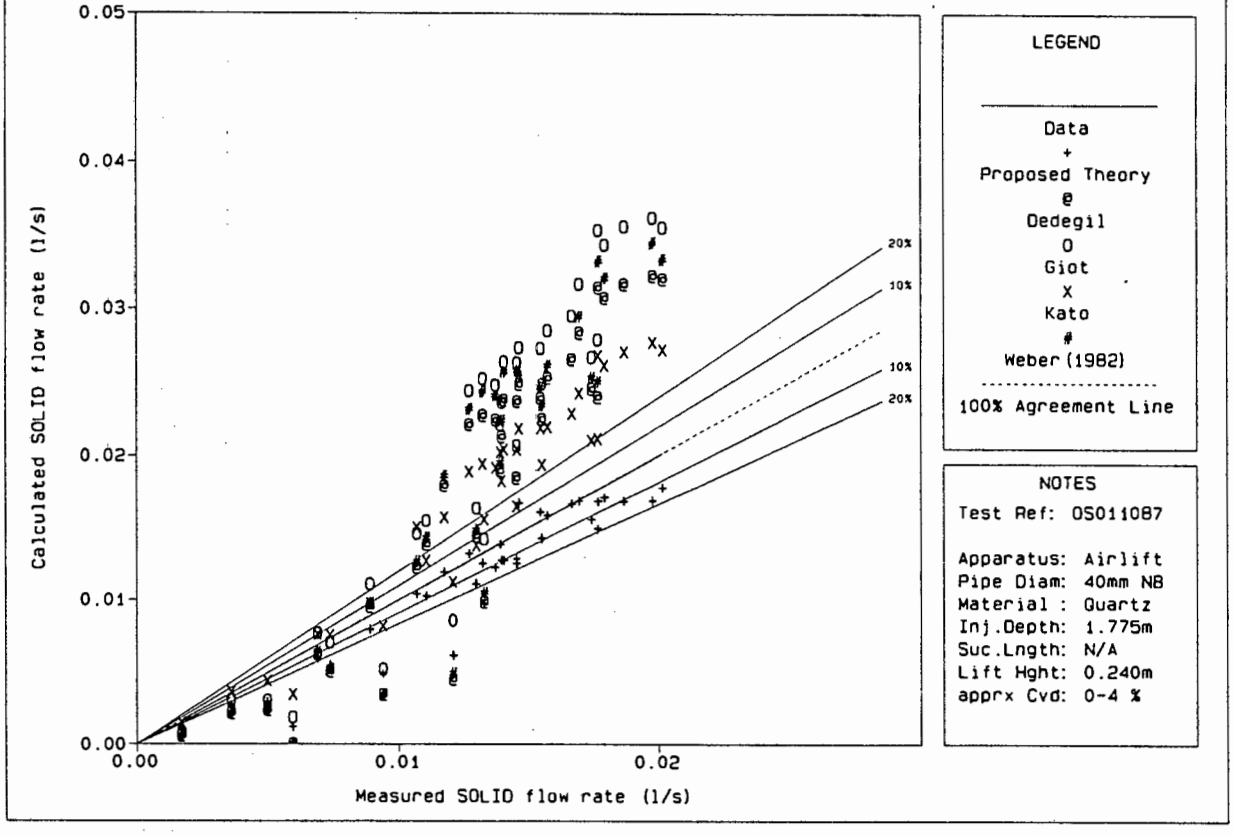

Figure : 8.55a
Description : Solid/Liquid/Gas Operating Curves

Airlift Pump Investigation

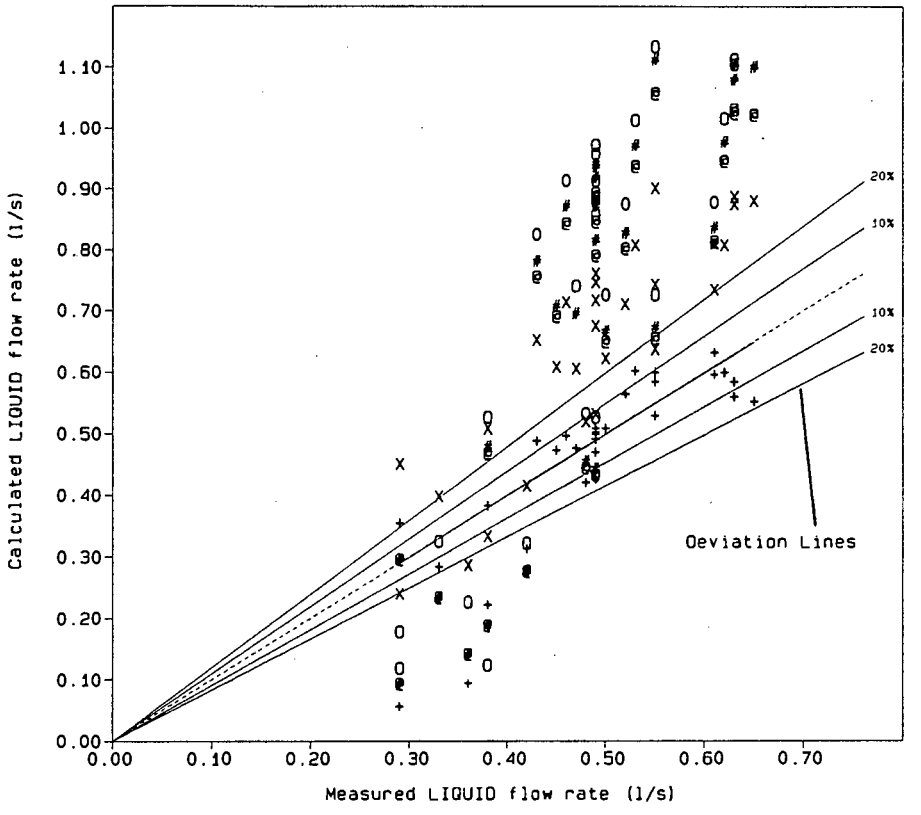

Figure : 8.55b
Description : Solid/Liquid/Gas Operating Curves

Airlift Pump Investigation

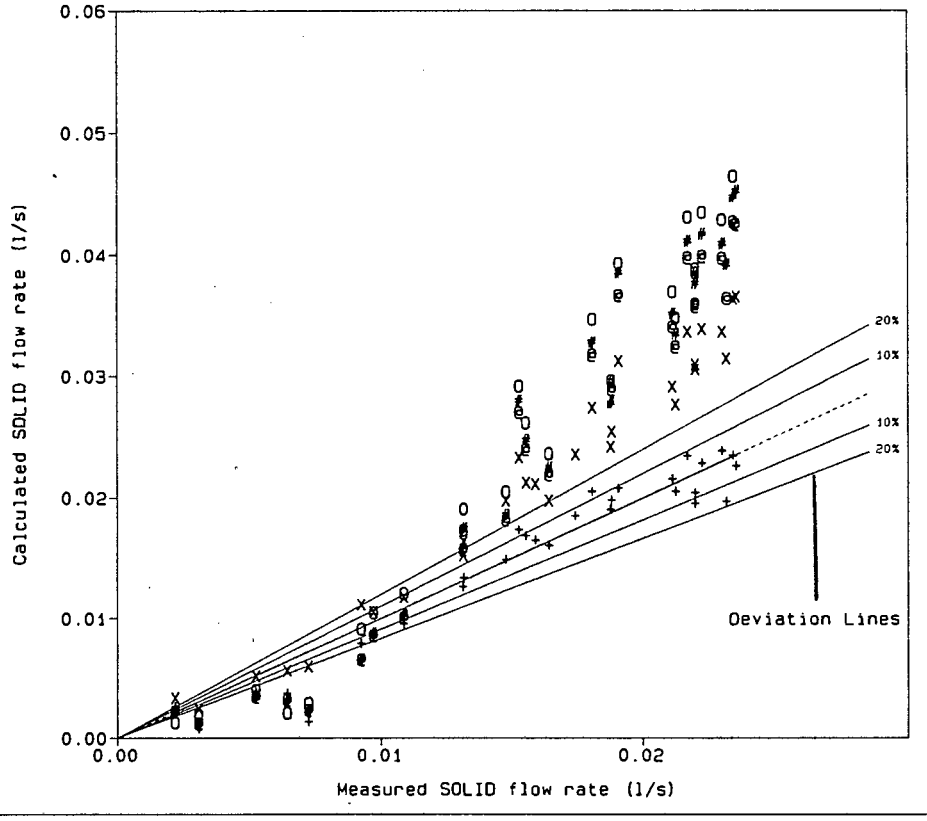

Figure : 8.56a
Description : Solid/Liquid/Gas Operating Curves

Airlift Pump Investigation

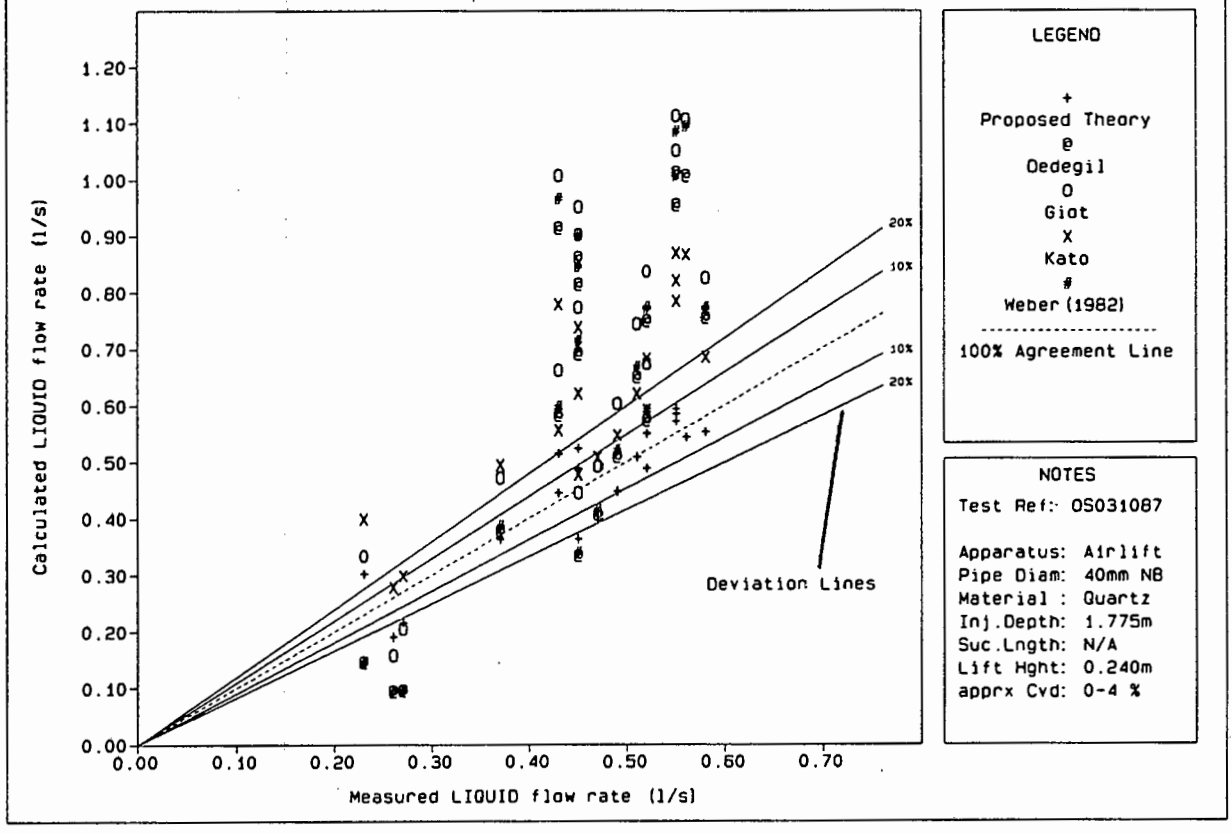

Figure : 8.56b
Description : Solid/Liquid/Gas Operating Curves

Airlift Pump Investigation

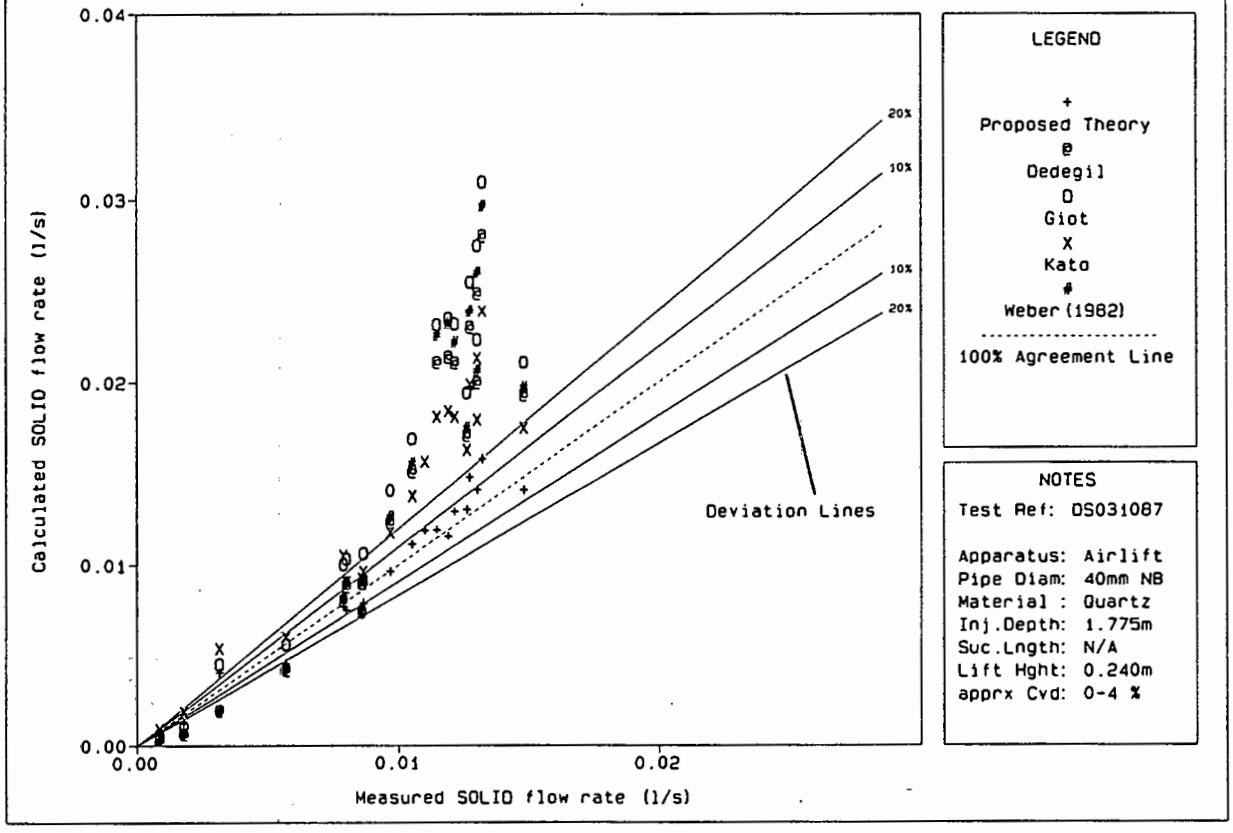

Figure : 8.57a
Description : Solid/Liquid/Gas Operating Curves

Airlift Pump Investigation

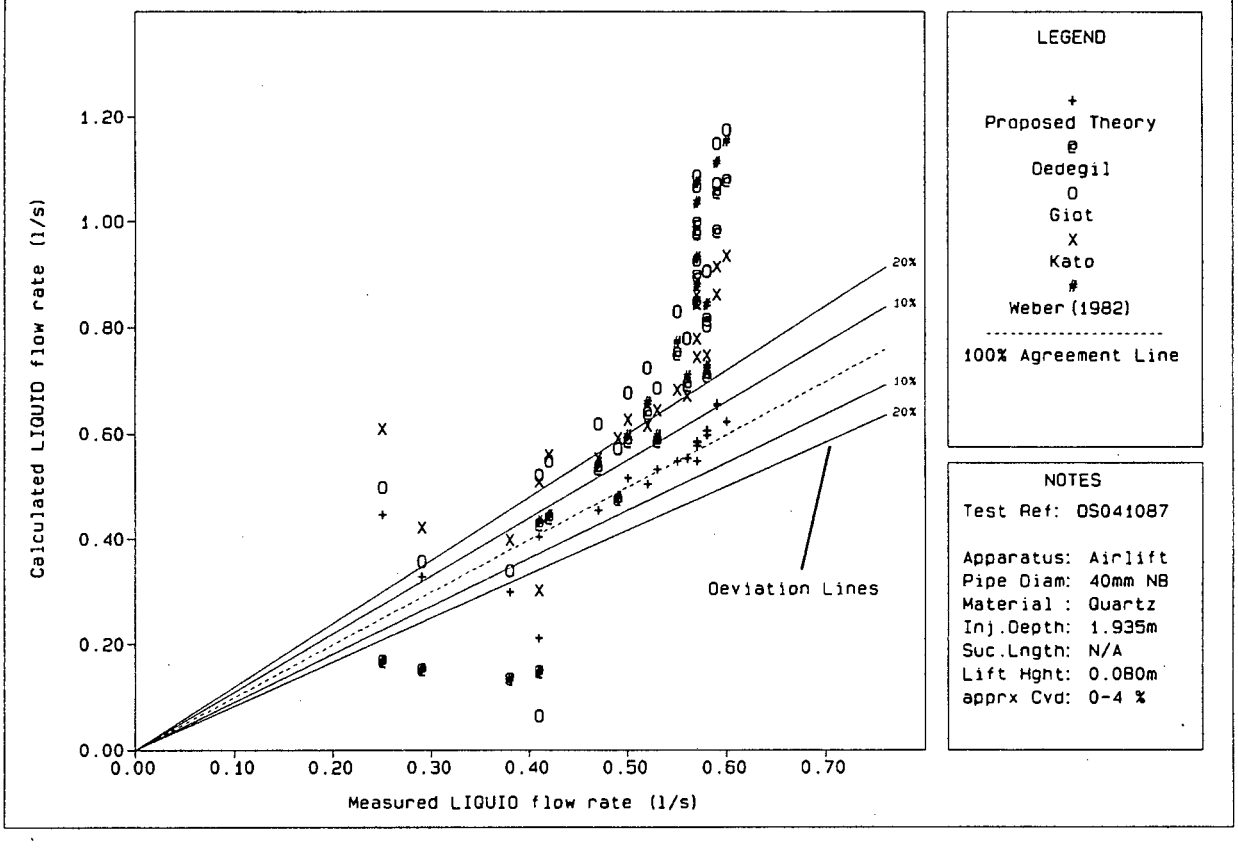

Figure : 8.57b
Description : Solid/Liquid/Gas Operating Curves

Airlift Pump Investigation

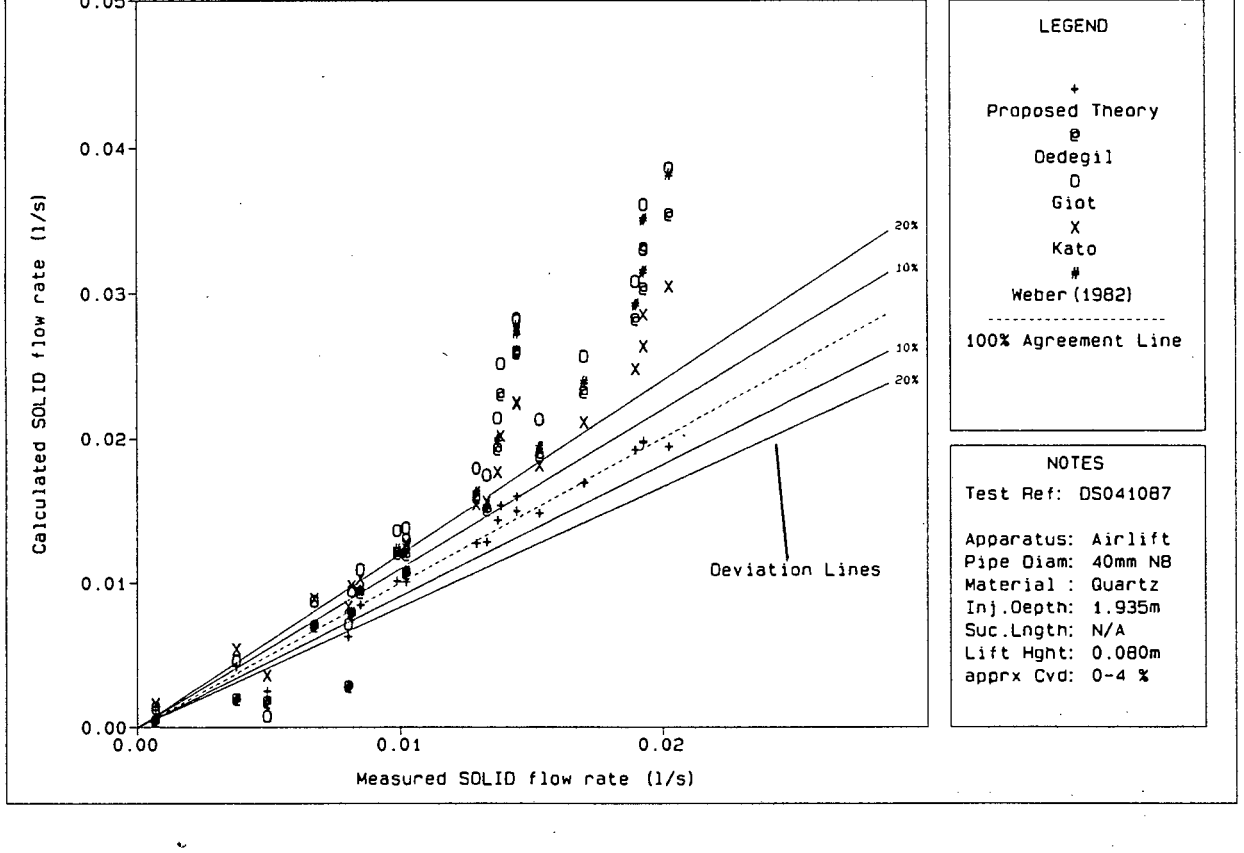

Figure : 8.58a
Description : Solid/Liquid/Gas Operating Curves

Airlift Pump Investigation

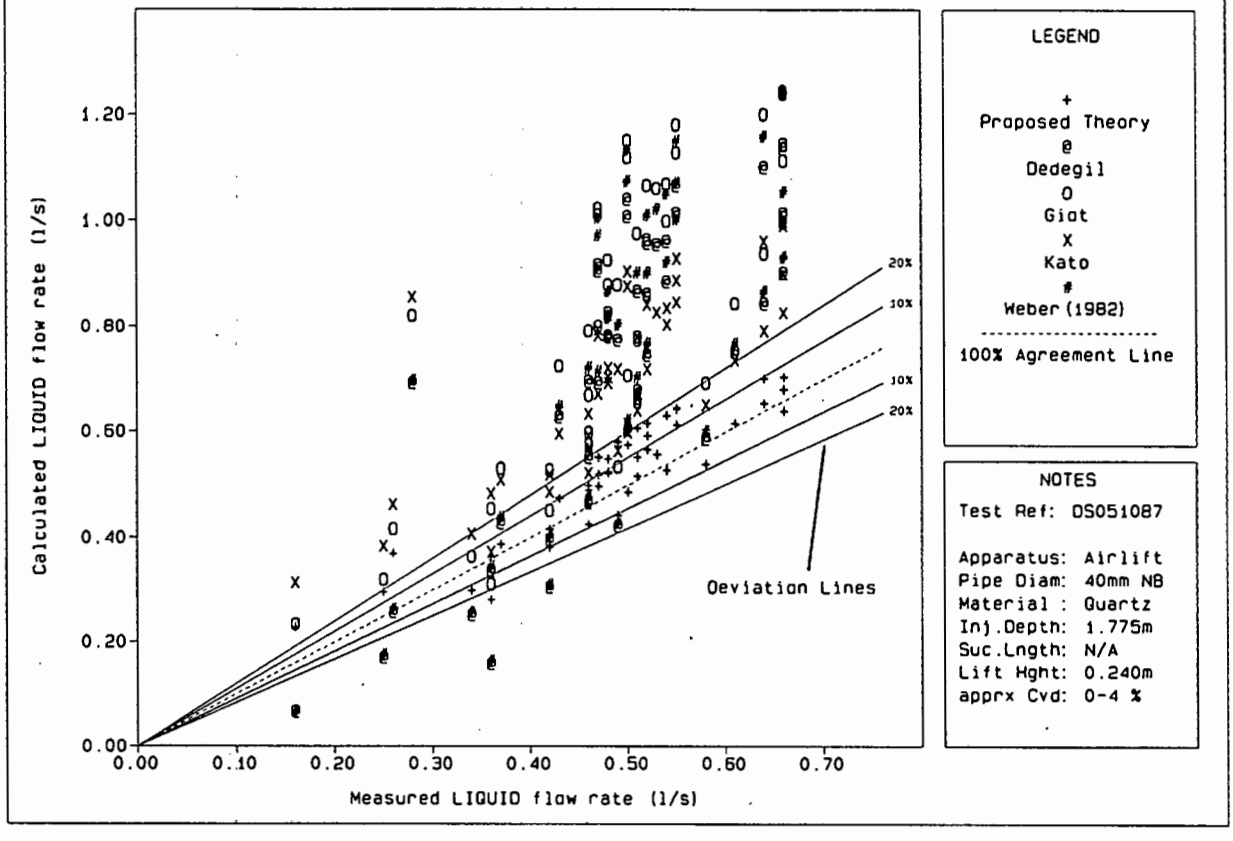

Figure : 8.58b
Description : Solid/Liquid/Gas Operating Curves

Airlift Pump Investigation

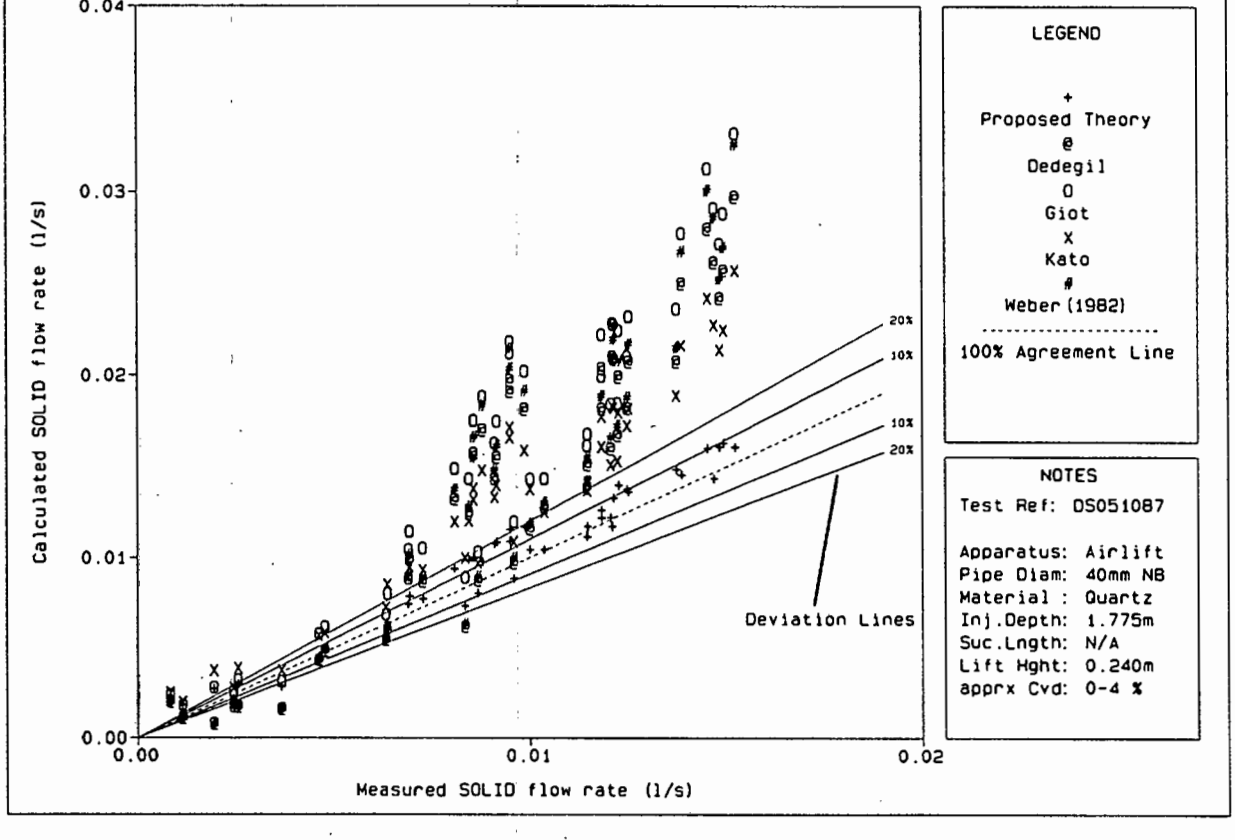

Figure : 8.59a
Description : Solid/Liquid/Gas Operating Curves

Airlift Pump Investigation

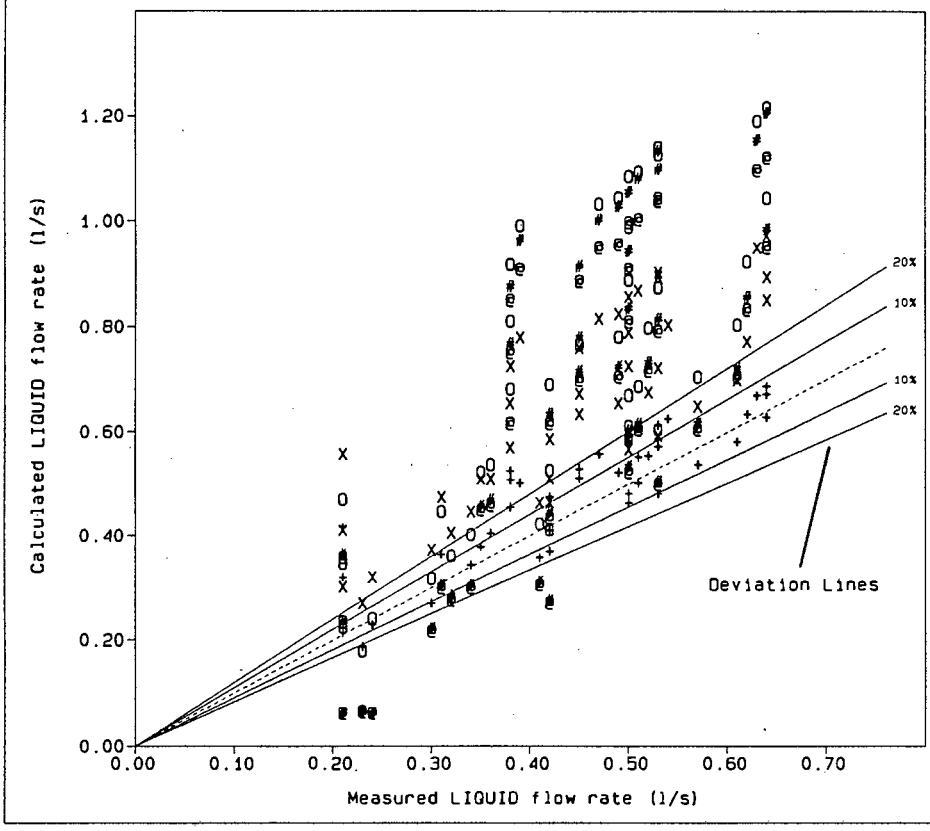

Figure : 8.59b
Description : Solid/Liquid/Gas Operating Curves

Airlift Pump Investigation

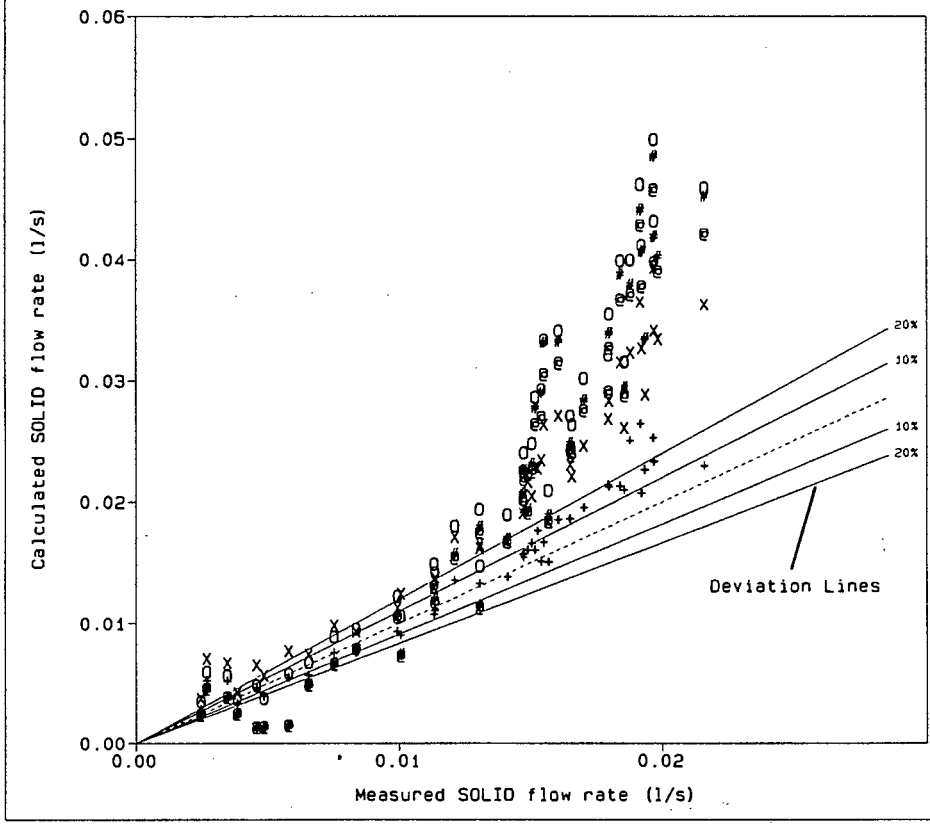

8.7 AIRLIFT PUMP OPERATING TESTS - OBSERVATIONS AND FINDINGS

Purpose :

Measure, observe and report on the effect of a range of variables on airlift pump delivered output and performance and to gather test data for evaluation of theories discussed in Chapters 3 and 4.

8.7.1 Particle size tests (40 mm airlift pump)

Referring to Chapter 5, the 40 mm airlift pump research apparatus is constructed as a recirculating system making it difficult to maintain a constant solid-liquid delivered volumetric concentration. Thus, for each gas flow rate, a different delivered concentration is recorded. In order to evaluate the influence of particle sizes, experimental results at constant solid-liquid delivered volumetric concentrations are required. Therefore all test data is plotted and results are obtained by visually interpolating contours of constant delivered volumetric concentrations.

Figures 8.60 to 8.62 show plots of solid-liquid mixture and solid mass flow rates for a range of gas flows at the interpolated constant delivered volumetric concentrations.

Figures 8.60 a & b represent results for tests conducted at an 88% submergence ratio (refer to 7.6.2) and solid-liquid delivered volumetric concentrations of 2% to 2,5%. From the figures, the smaller particle sizes result in higher solid-liquid mixture flow rates at both delivered concentrations. The effect of particle size is, however, less significant on the solid mass flow rate and it appears that the particle size has little effect on the solid mass output.

Figures 8.61 a & b represents results for tests conducted at submergence ratios of 96% and solid-liquid delivered volumetric concentrations of 2,5% to 3%. From the figures, at delivered concentrations of 2,5% the smaller particles again result in slightly higher mixture and solid mass flow rates, while at 3% delivered concentration the reverse is observed.

Figures 8.62 a & b show results for tests conducted at submergence ratios of 96% and delivered volumetric concentrations of 3,5% to 4% with a larger, 2,46 mm particle size. The figures show the opposite effect to that observed in Figures 8.60 to 8.61. Here the large particle sizes result in higher mixture flow rates at both delivered concentrations. This trend is also shown in the solid mass flow rate, where the larger particles resulted in higher output than the smaller particles.

From the above variations in experimental results no conclusive trend showing the effect of particle size on mixture and solid output flow rates was established.

8.7.2 Submergence ratio tests (40 mm airlift pump)

As discussed in Section 8.7.1, all data is plotted and the presented curves are obtained by visually interpolating constant solid-liquid delivered volumetric concentrations.

Figures 8.63 to 8.65 show plots of solid-liquid mixture and solid mass flow rates for a range of gas flow rates.

Figures 8.63 a & b show results for tests conducted with 2,46 mm particles at submergence ratios of 88% and 96% and solid-liquid delivered volumetric concentrations of 3,5%. The figures show that a small 8% increase in the submergence ratio results in a ± 25% increase in the mixture, and a ± 17% increase in solid mass flow rates.

Figures 8.64 a & b show results for tests conducted with 1,42 mm particles at 88% and 96% submergence ratios and solid-liquid delivered volumetric concentrations of 2,5%. Again, a small (8%) increase in the submergence ratio results in a ± 25% increase in the mixture and solid mass output flow rates. In these results, however, the increase in solid mass flow rate is of a similar order of magnitude as the solid-liquid mixture flow rate.

Figures 8.65 a & b show results for tests conducted with 0,62 mm particles at 88% and 96% submergence ratios and solid-liquid delivered concentrations of 2,5%. Similar to the above results, the figures show that a small (8%) increase in submergence ratio has a significant effect on the solid-liquid mixture and solid mass flow rates.

Thus a small increase in the submergence rate has a significant effect on the output flow rates of an airlift pump. For the particle sizes tested in the 40 mm airlift pump, an increase of 8% in the submergence ratio resulted in a ± 25% increase in the mixture and 17-20% increase in solid mass flow rate.

8.7.3 Solid delivered volumetric concentration tests (90 mm airlift pump)

Figure 8.66 a shows the output solid mass and solid-liquid mixture flow rates for a range of delivered volumetric concentrations and gas flow rates. An increased delivered volumetric concentration results in a decrease in the mixture and an increase in the solid mass output flow rates. With increasing delivered volumetric concentrations, a higher gas flow rate is required to attain the maximum mixture flow rate. Furthermore, the gas flow rate at which the maximum mixture flow rate is attained, coincides with the maximum solid mass flow rate at each concentration. A further observation is that the increase in solid mass flow rate becomes less with increasing delivered volumetric concentration.

Figure 8.66 b shows a plot of the absolute pressures recorded at various levels in the airlift pump suction and delivery pipes. Shown also are the air injection level, the external liquid level and static liquid pressure. From the figure, it is observed that the pressure inside the airlift pump pipe is less than the external liquid static pressure for the lower 3,0 m. Above 3,0 m, the pressure inside the airlift pump is greater than the external pressure and decreases until eventually the pressure at the delivery outlet becomes atmospheric. The reason why the pressure has not reached atmospheric pressure at the 9 m level is that the last pressure measurement occurs before the flow diverter at the top of the 90 mm airlift pump (refer to Figure 5.6). Considerable pressure is dissipated over this last portion of the pipe.

Figure 8.66 b shows that a decrease in delivered volumetric concentration results in a lower absolute pressure for the bottom 4 m of the airlift pump. This is explained by the increased mixture flow rate, velocity ($v_m^{s\ell}$) and consequently shear stress with decreasing delivered volumetric concentration. Above the lower 4 m, the pressures inside the airlift pump pipe appear to be less affected by an increase in the delivered concentration.

Also shown on the figure is the non-linear change in pressure in the airlift pump pipe, with a higher pressure drop below air injection due to the absence of gas in the mixture and consequently higher mixture weight.

8.7.4 Annular air injector tests (90 mm airlift pump)

Figure 8.67 a shows a plot of solid mass and mixture flow rates for a range of gas flow rates. Referring to the figure, the annular aperture area has no dramatic effect on solid-liquid mixture or the solid mass throughput.

Figure 8.67 b shows a plot of the absolute pressures recorded at various points in the airlift pump suction and delivery pipes. Shown also are the air injection level, the external liquid level and the static liquid pressure.

The figure confirms that the annular aperture area has no visible effect on the pressure profiles.

Thus the annular aperture area is found to have no significant effect on the output flow rates of the airlift pump.

8.7.5 Fines tests (90 mm airlift pump)

Figures 8.68 to 8.69 show results of tests using finer material compared to tests with coarser material at similar solid-liquid delivered volumetric concentrations.

Referring to Figure 8.68 a, the tests using coarser material result in lower solid-liquid mixture flow rates than the finer material. These lower output flow rates appear more significant at low gas flow rates than at high gas flow rates. This effect can be explained by a higher solid *in situ* concentration with the coarser material at lower gas flow rates, leading to higher solid-liquid-gas mixture weights in the airlift pump delivery pipe and consequently the lower solid-liquid mixture flow rates are reduced. This higher solid *in situ* concentration is the result of the higher settling velocities of the particles in coarser material.

Referring to Figure 8.68 b, larger solid volume and mass flow rates are obtained with the finer material than the coarser material.

Also shown on Figure 8.68 a, are the solid-liquid delivered volumetric concentrations which remain constant at ± 5% throughout the tests.

Figure 8.69 a and b show the results of the tests using finer material mixed with a large percentage of building lime compared with coarser material test results. Shown are solid-liquid mixture and solid mass flow rates for tests conducted at ± 3,5% delivered volumetric concentration. The figure confirms that the fines plus the building lime resulted in higher solid-liquid mixture, solid mass and solid volume flow rates for the range of gas flow rates tested. However, in

these tests the high concentration of building lime caused the mixture flow rates to be larger for all gas flow rates. The delivered volumetric concentrations are shown to be constant at ± 3,5%, in Figure 8.69 b.

The addition of a large percentage of fines and fines plus building lime leads to higher solid-liquid mixture, solid mass and solid volume output flow rates than the coarser material.

Figure : 8.60a
Description : Particle Size Tests

Airlift Pump Investigation

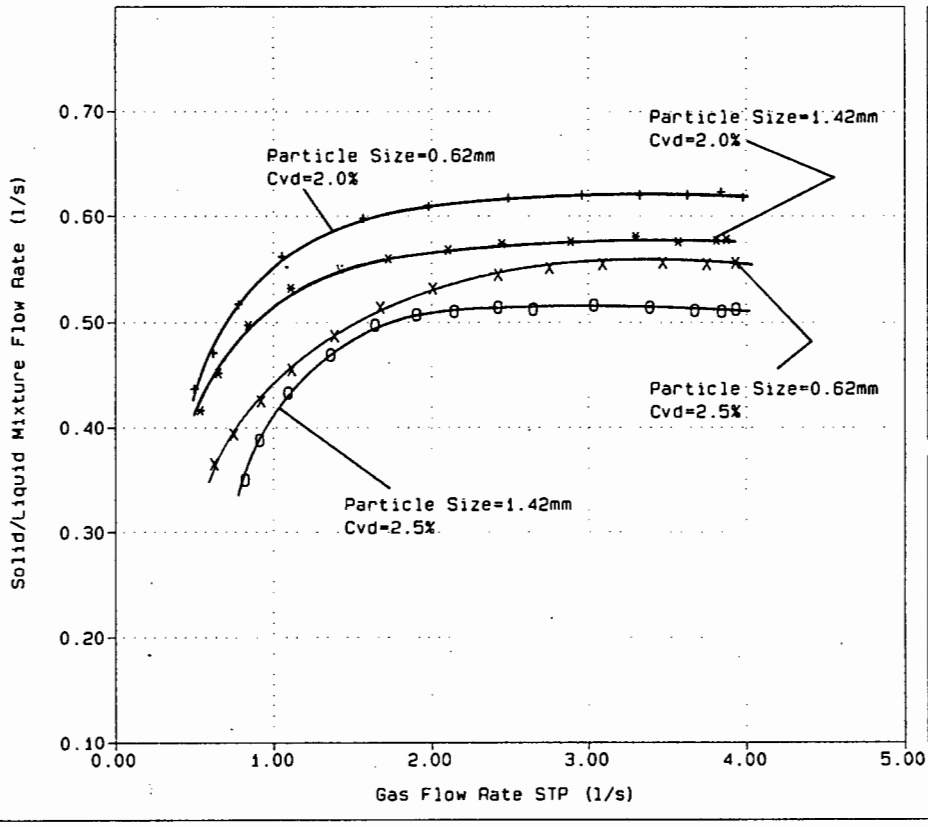

LEGEND

+
ds 0.62mm Cvd 2.0%
*
ds 1.42mm Cvd 2.0%
X
ds 0.62mm Cvd 2.5%
O
ds 1.42mm Cvd 2.5%

NOTES

Test Ref: Extract1
Apparatus: Airlift
Pipe Diam: 40mm NB
Material : Quartz
Inj.Depth: 1.775m
Suc.Lngth: N/A
Lift Hght: 0.240m
apprx Cvd: 2-2.5 %

Figure : 8.60b
Description : Particle Size Tests

Airlift Pump Investigation

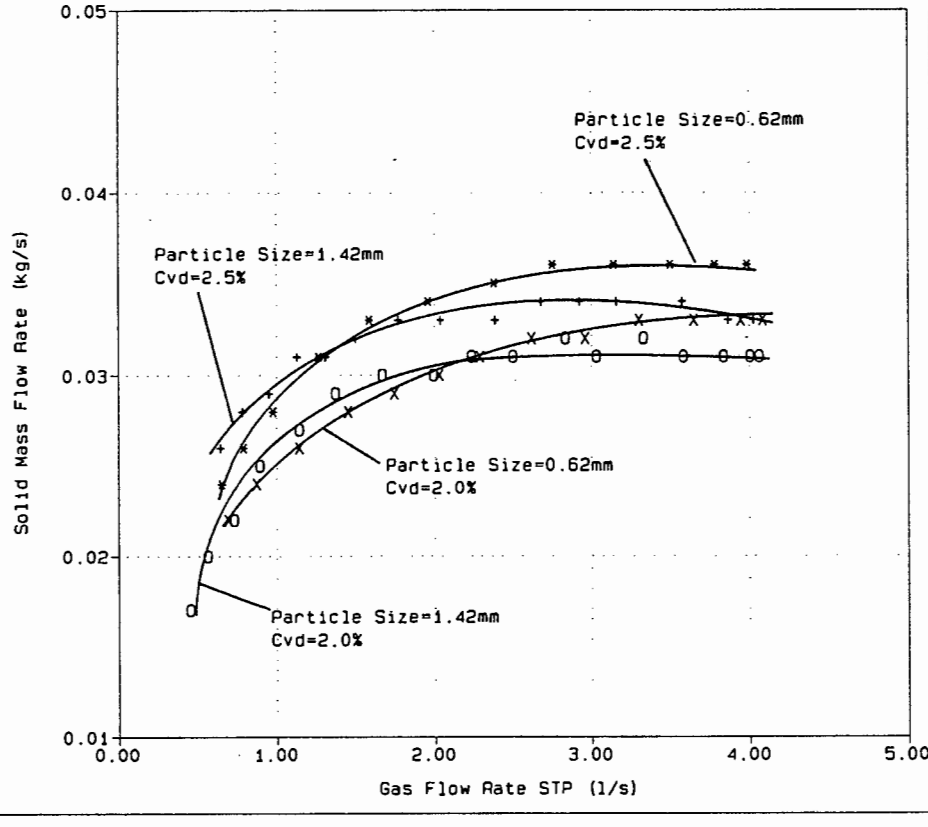

LEGEND

+
ds 1.42mm Cvd 2.5%
*
ds 0.62mm Cvd 2.5%
X
ds 0.62mm Cvd 2.0%
O
ds 1.42mm Cvd 2.0%

NOTES

Test Ref: Extract2
Apparatus: Airlift
Pipe Diam: 40mm NB
Material : Quartz
Inj.Depth: 1.775m
Suc.Lngth: N/A
Lift Hght: 0.240m
apprx Cvd: 2-2.5%

Figure : 8.61a
Description : Particle Size Tests

Airlift Pump Investigation

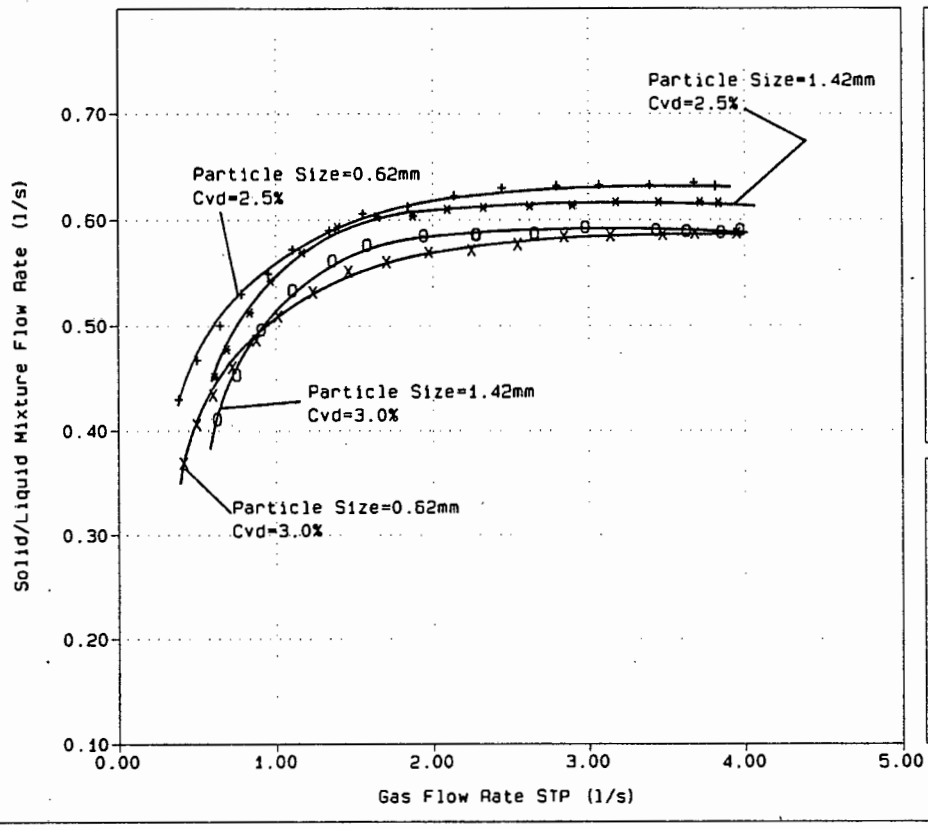

LEGEND

+ ds 0.62mm Cvd 2.5%
* ds 1.42mm Cvd 2.5%
X ds 0.62mm Cvd 3.0%
O ds 1.42mm Cvd 3.0%

NOTES

Test Ref: Extract3
Apparatus: Airlift
Pipe Diam: 40mm NB
Material : Quartz
Inj.Depth: 1.935m
Suc.Lngth: N/A
Lift Hght: 0.080m
apprx Cvd: 2.5-3 %

Figure : 8.61b
Description : Particle Size Tests

Airlift Pump Investigation

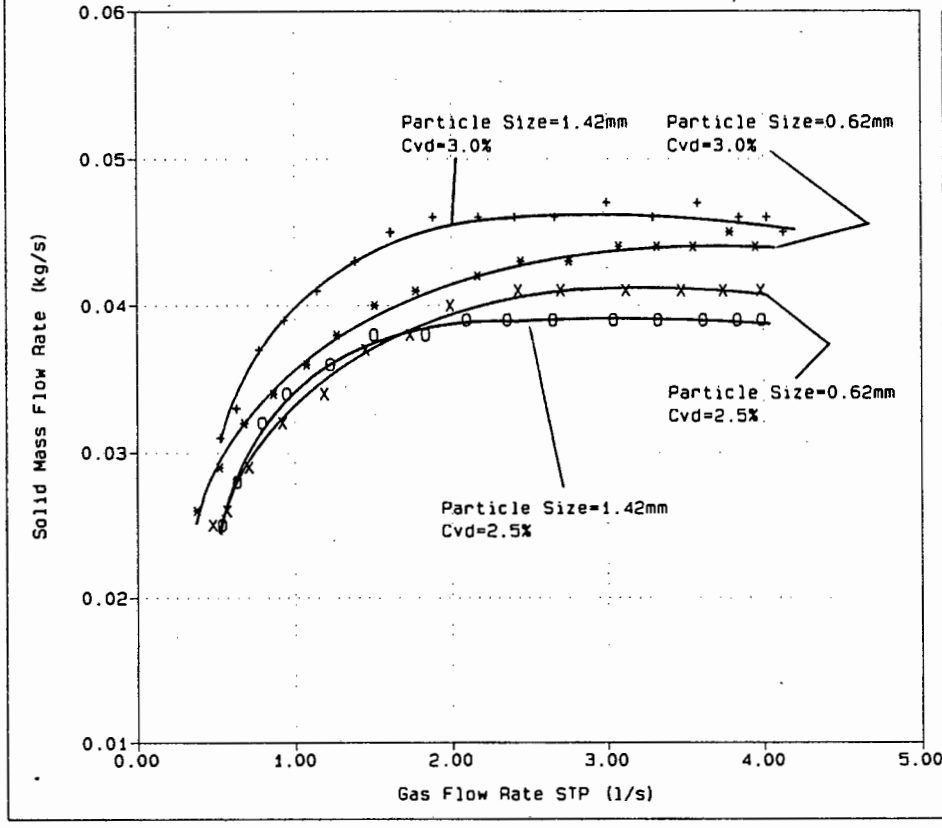

LEGEND

+ ds 1.42mm Cvd 3.0%
* ds 0.62mm Cvd 3.0%
X ds 0.62mm Cvd 2.5%
O ds 1.42mm Cvd 2.5%

NOTES

Test Ref: Extract4
Apparatus: Airlift
Pipe Diam: 40mm NB
Material : Quartz
Inj.Depth: 1.935m
Suc.Lngth: N/A
Lift Hght: 0.080m
apprx Cvd: 2.5-3 %

Figure : 8.62a
Description : Particle Size Tests

Airlift Pump Investigation

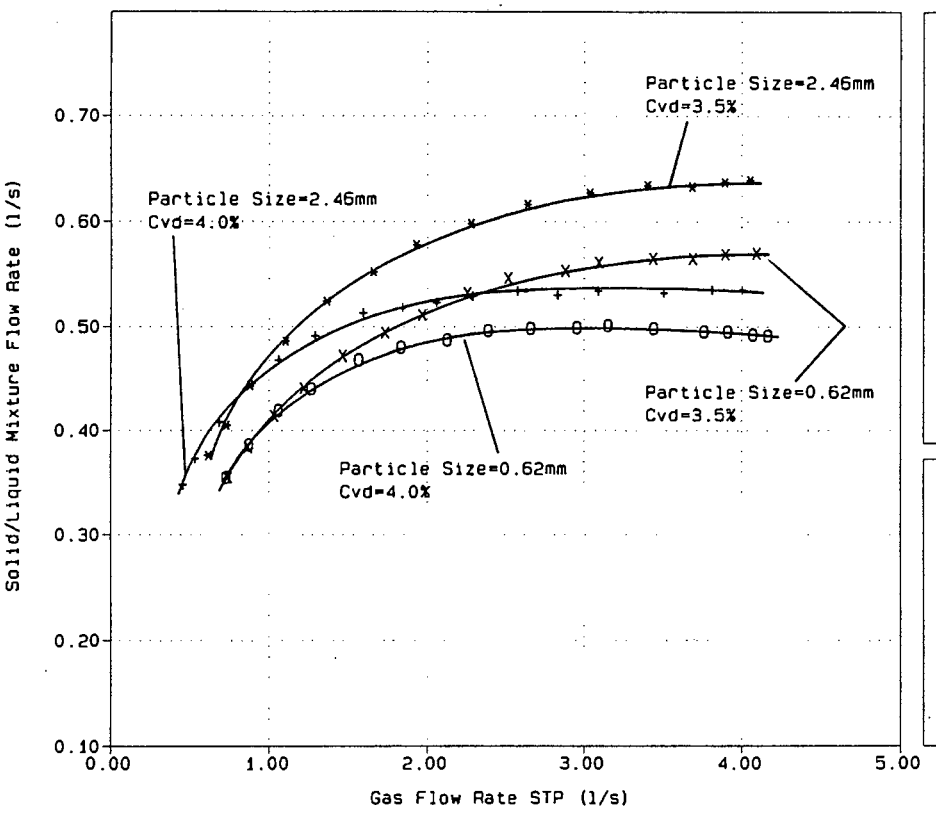

LEGEND

+ ds 2.46mm Cvd 4%
* ds 2.46mm Cvd 3.5%
X ds 0.62mm Cvd 3.5%
O ds 0.62mm Cvd 4%

NOTES

Test Ref: Extract5
Apparatus: Airlift
Pipe Diam: 40mm N8
Material : Quartz
Inj.Depth: 1.935m
Suc.Lngth: N/A
Lift Hght: 0.080m
apprx Cvd: 3.5-4 %

Figure : 8.62b
Description : Particle Size Tests

Airlift Pump Investigation

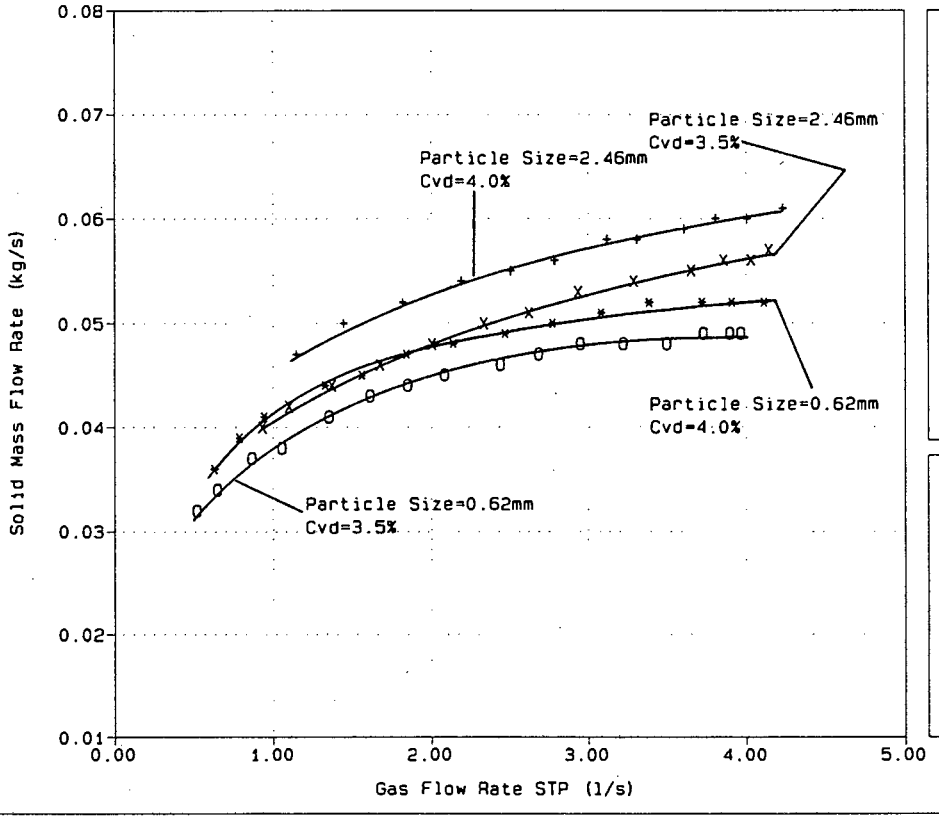

LEGEND

+ ds 2.46mm Cvd 4%
* ds 0.62mm Cvd 4%
X ds 2.46mm Cvd 3.5%
O ds 0.62mm Cvd 3.5%

NOTES

Test Ref: Extract6
Apparatus: Airlift
Pipe Diam: 40mm N8
Material : Quartz
Inj.Depth: 1.935m
Suc.Lngth: N/A
Lift Hght: 0.080m
apprx Cvd: 3.5-4 %

Figure : 8.63a
Description : Submergance Ratio Tests

Airlift Pump Investigation

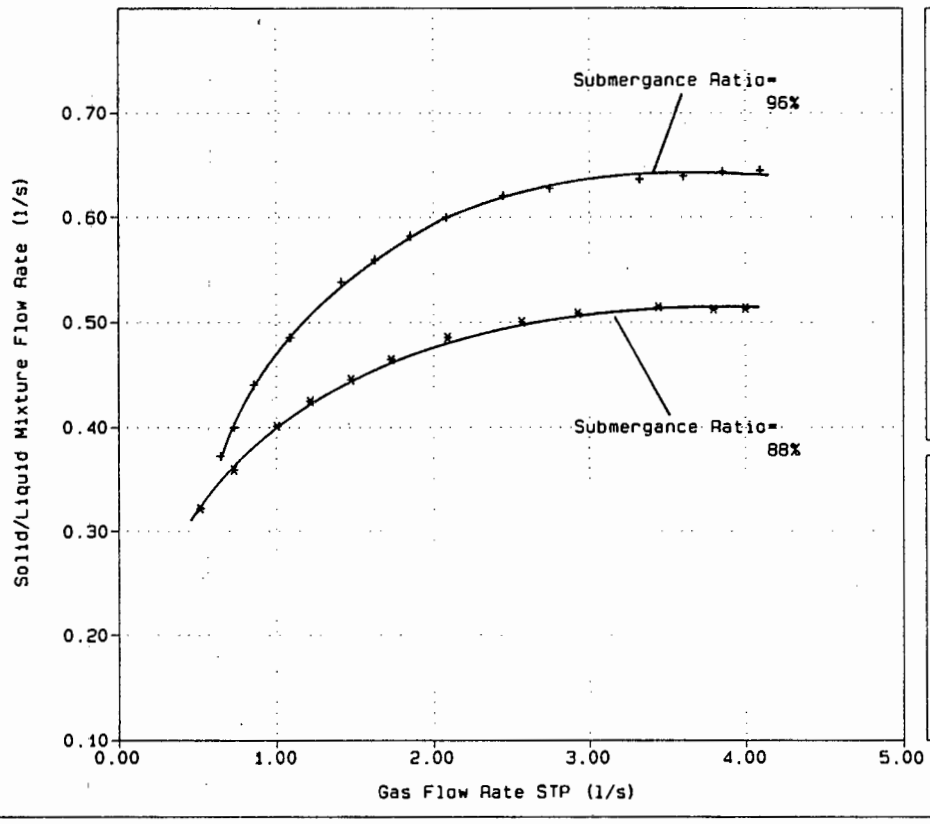

Figure : 8.63b
Description : Submergance Ratio Tests

Airlift Pump Investigation

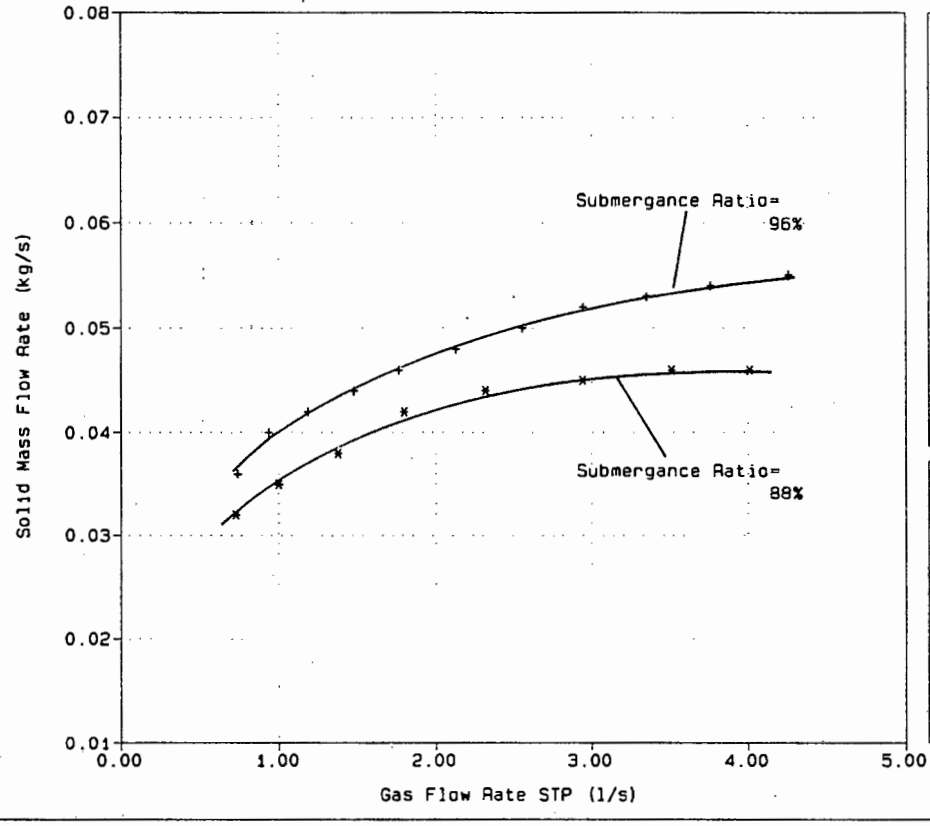

Figure : 8.64a
Description : Submergance Ratio Tests

Airlift Pump Investigation

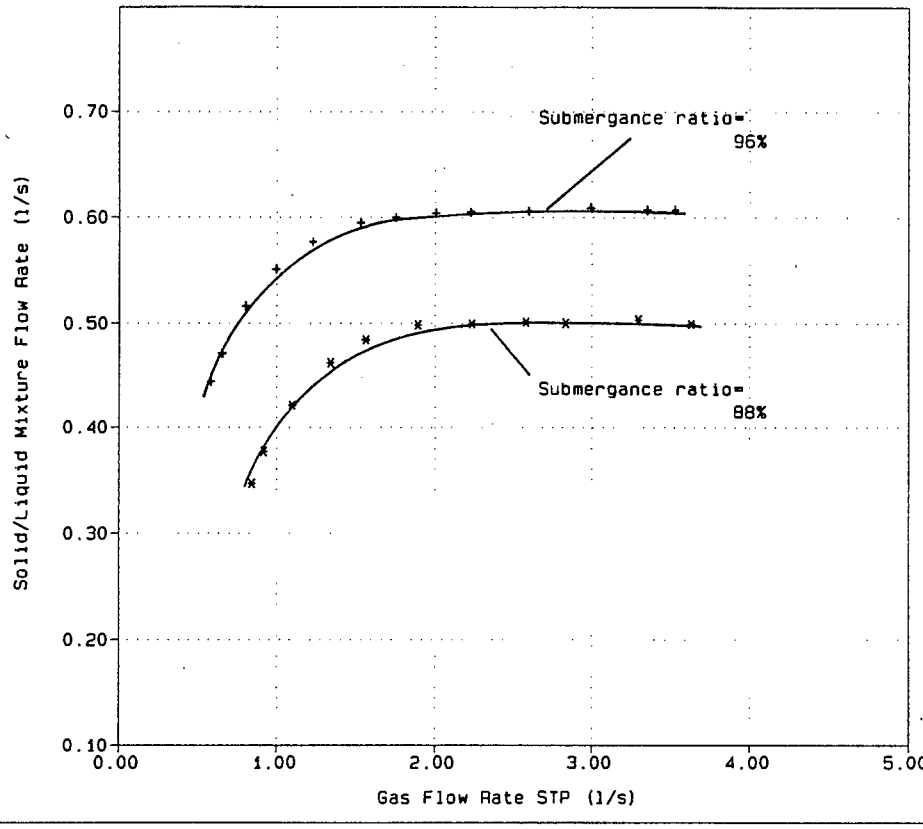

Figure : 8.64b
Description : Submergance Ratio Tests

Airlift Pump Investigation

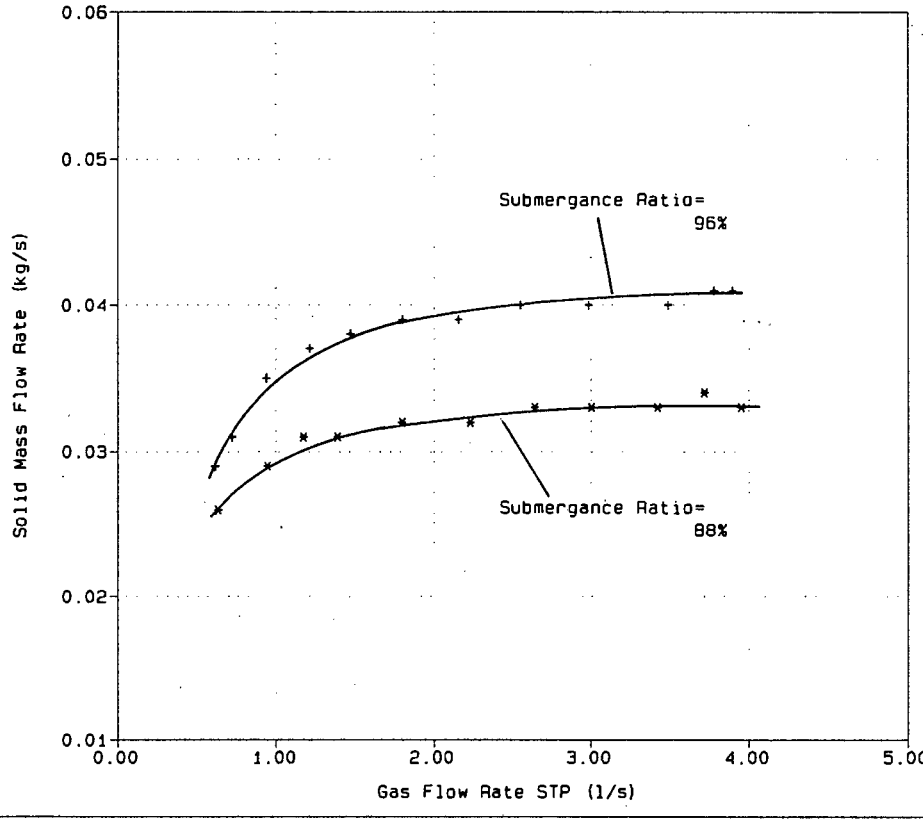

Figure : 8.65a
Description : Submergance Ratio Tests

Airlift Pump Investigation

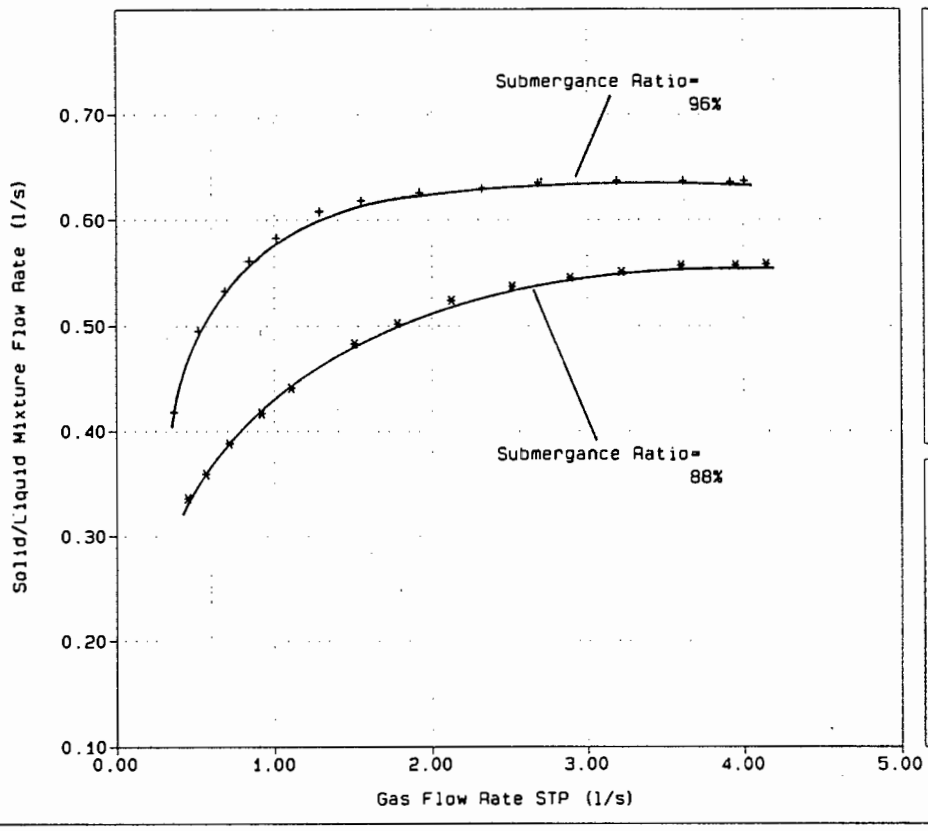

LEGEND

\+
SR 96%
*
SR 88%

NOTES

Test Ref: Extract5
Apparatus: Airlift
Pipe Diam: 40mm N8
Material : Quartz
Inj.Dep : variable
Suc.Lngth: N/A
Lift Hght: variable
apprx Cvd: 2.5 %
Delivery Pipe Length = 2.015m

Figure : 8.65b
Description : Submergance Ratio Tests

Airlift Pump Investigation

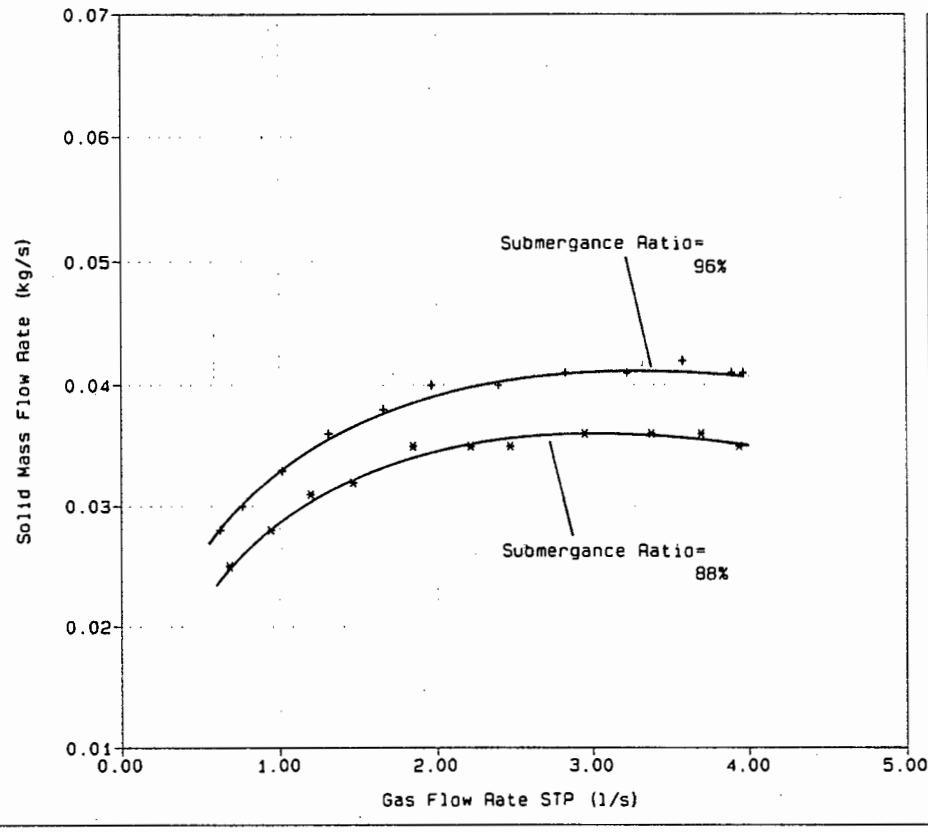

LEGEND

\+
SR 96%
*
SR 88%

NOTES

Test Ref: Extract6
Apparatus: Airlift
Pipe Diam: 40mm N8
Material : Quartz
Inj.Depth: variable
Suc.Lngth: N/A
Lift Hght: variable
apprx Cvd: 2.5 %
Delivery Pipe Length = 2.015m

Figure : 8.66a
Description : Solid Delivered Concentration Tests

Airlift Pump Investigation

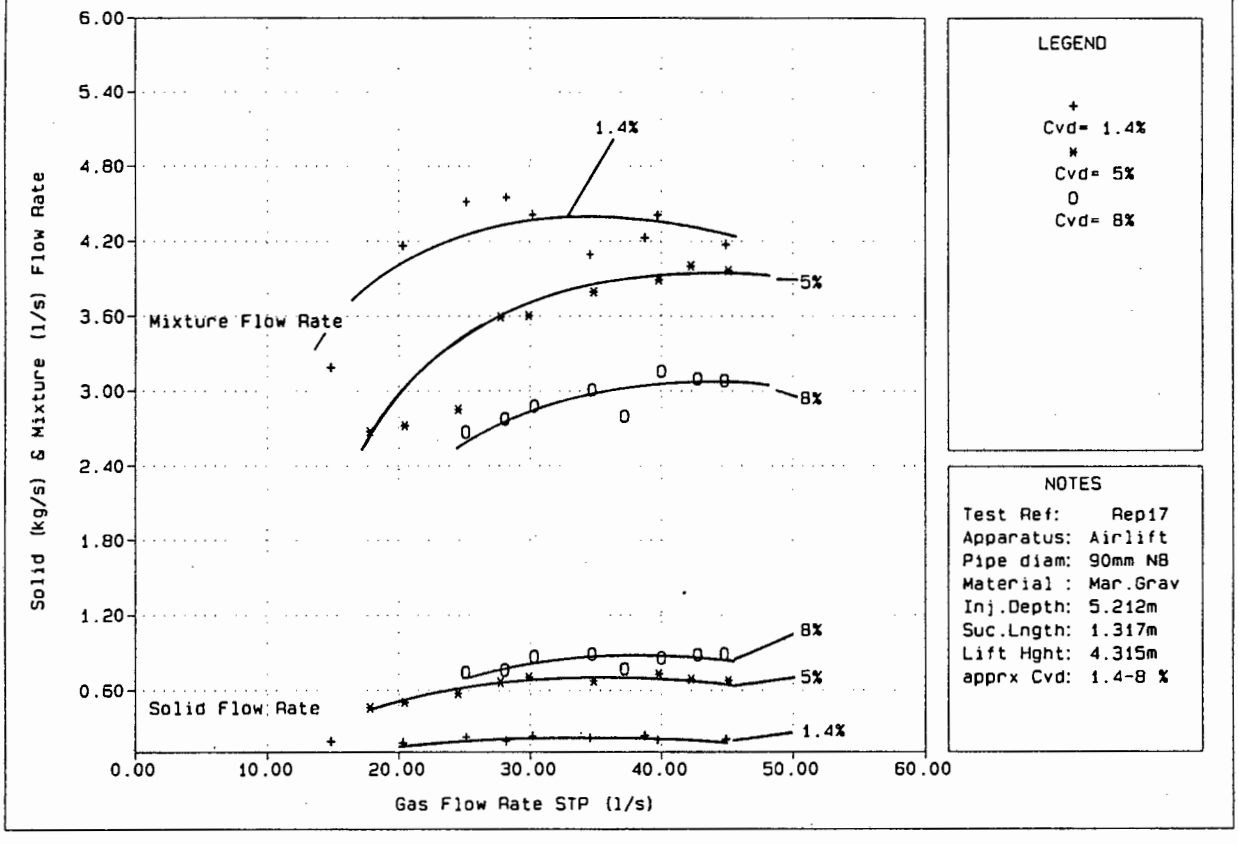

Figure : 8.66b
Description : Solid Delivered Concentration Tests

Airlift Pump Investigation

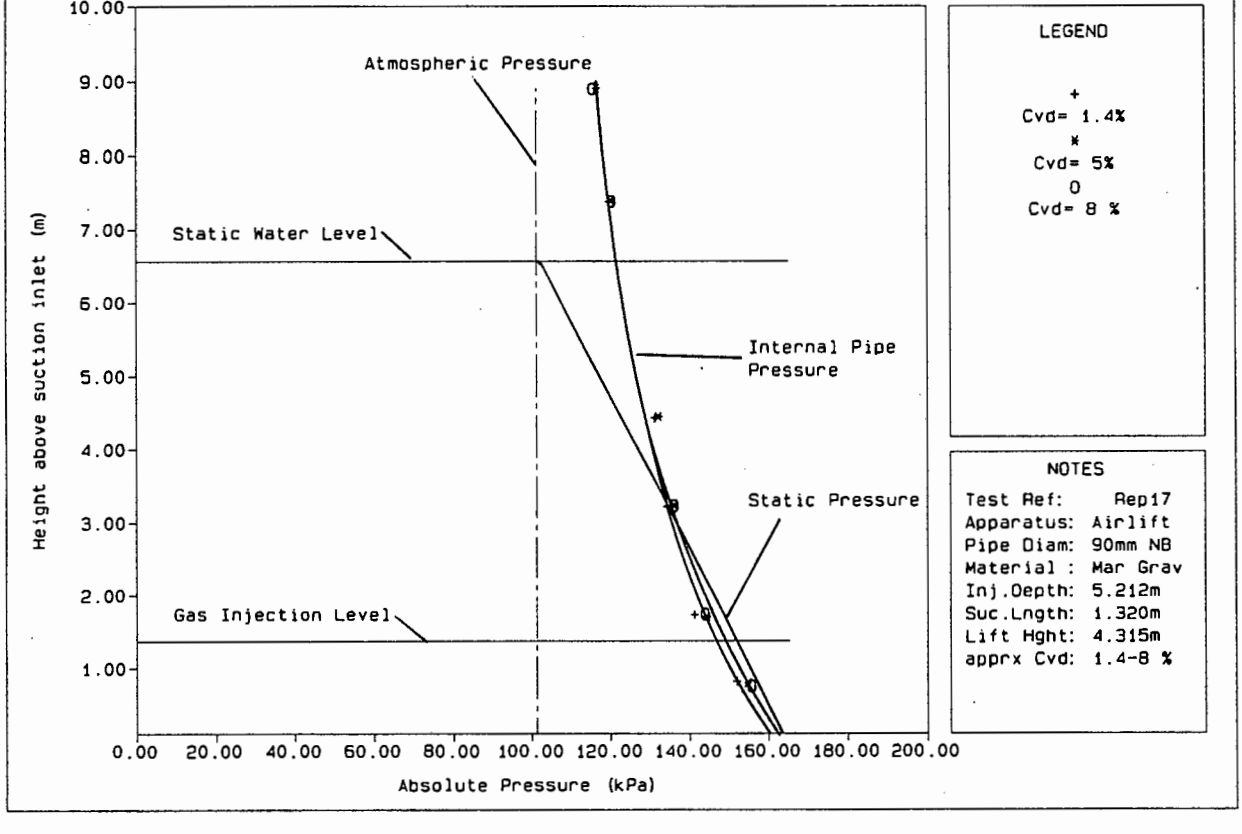

Figure : 8.67a
Description : Annular Gas Injector Tests

Airlift Pump Investigation

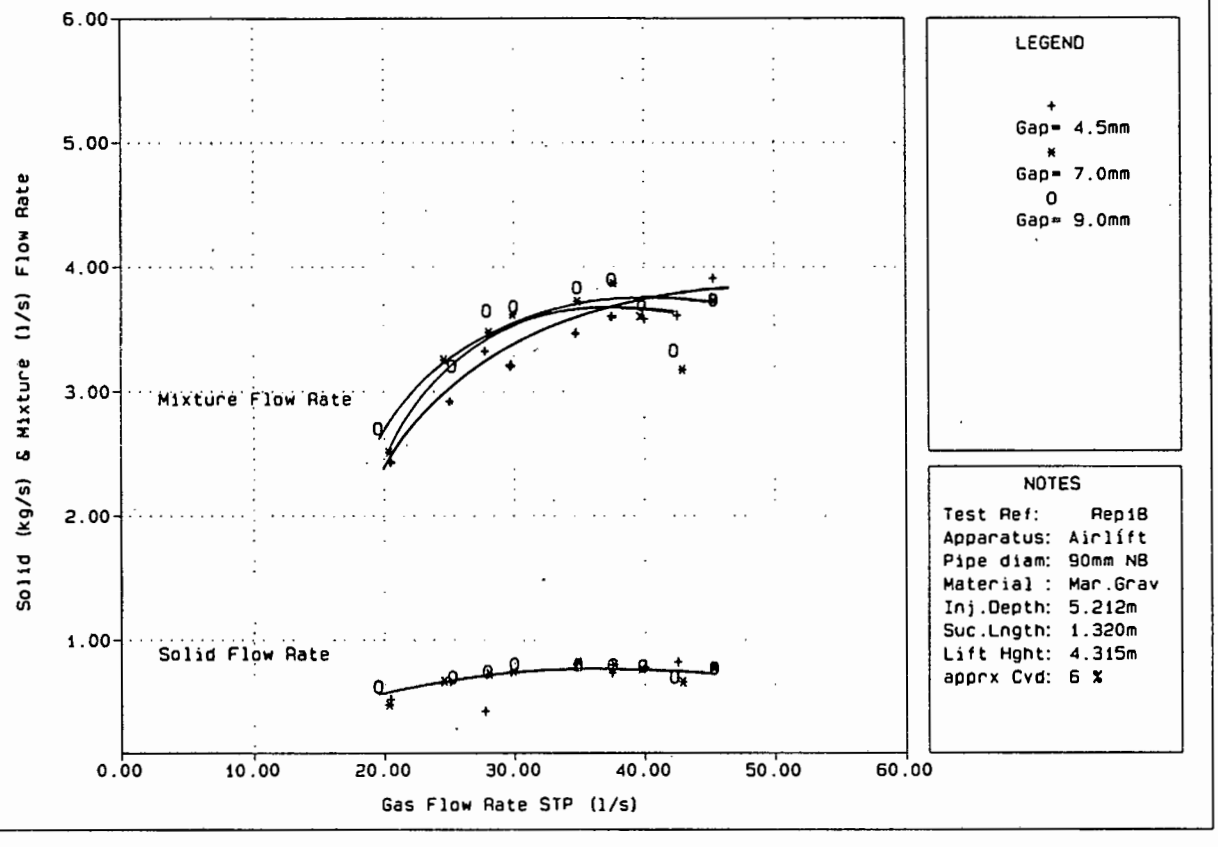

Figure : 8.67b
Description : Annular Gas Injector Tests

Airlift Pump Investigation

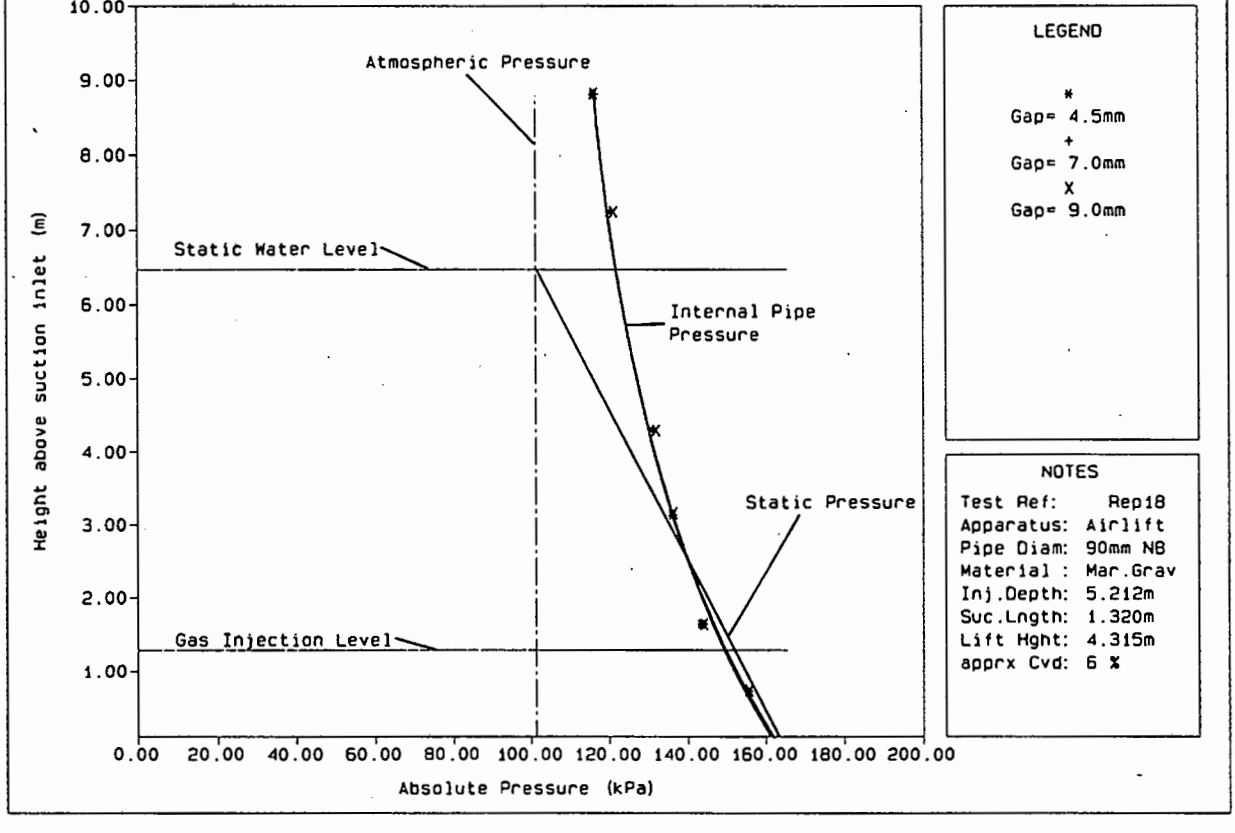

Figure : 8.68a
Description : Fines Tests (Fines)

Airlift Pump Investigation

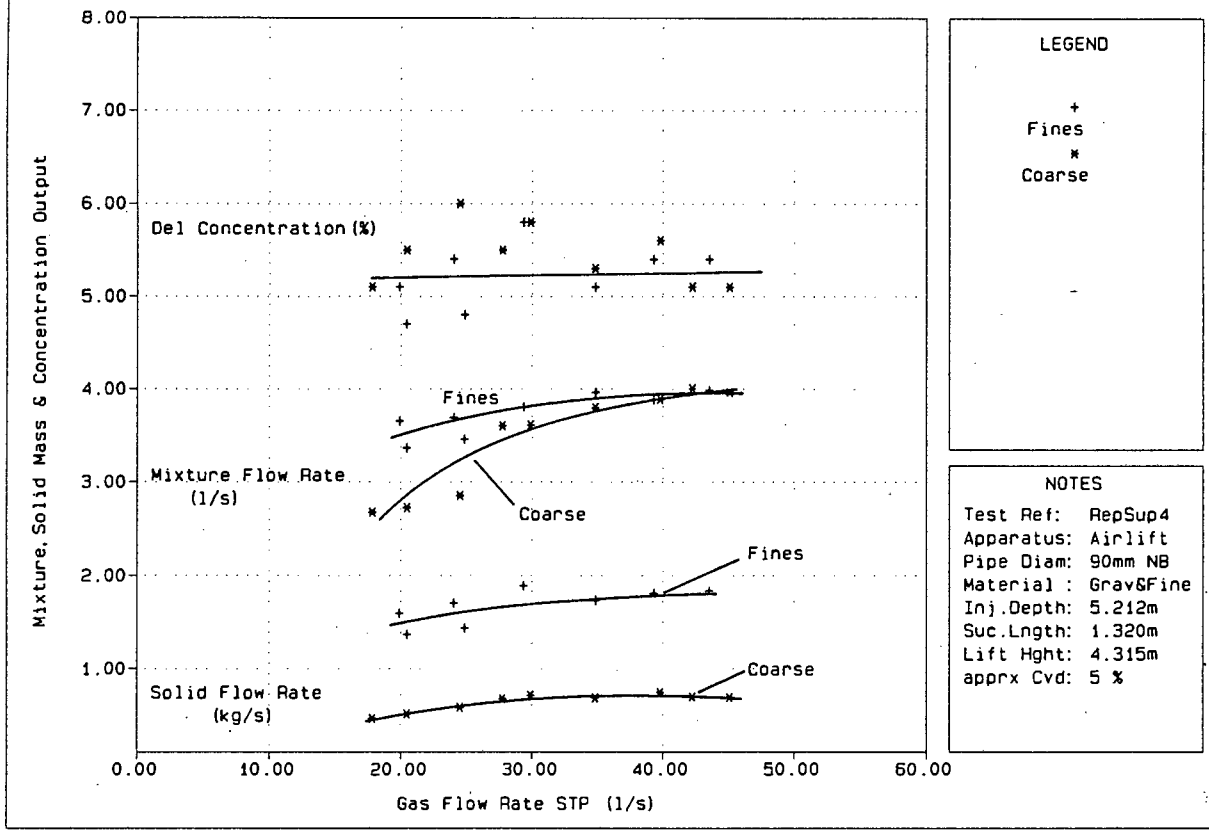

Figure : 8.68b
Description : Fines Tests (Fines)

Airlift Pump Investigation

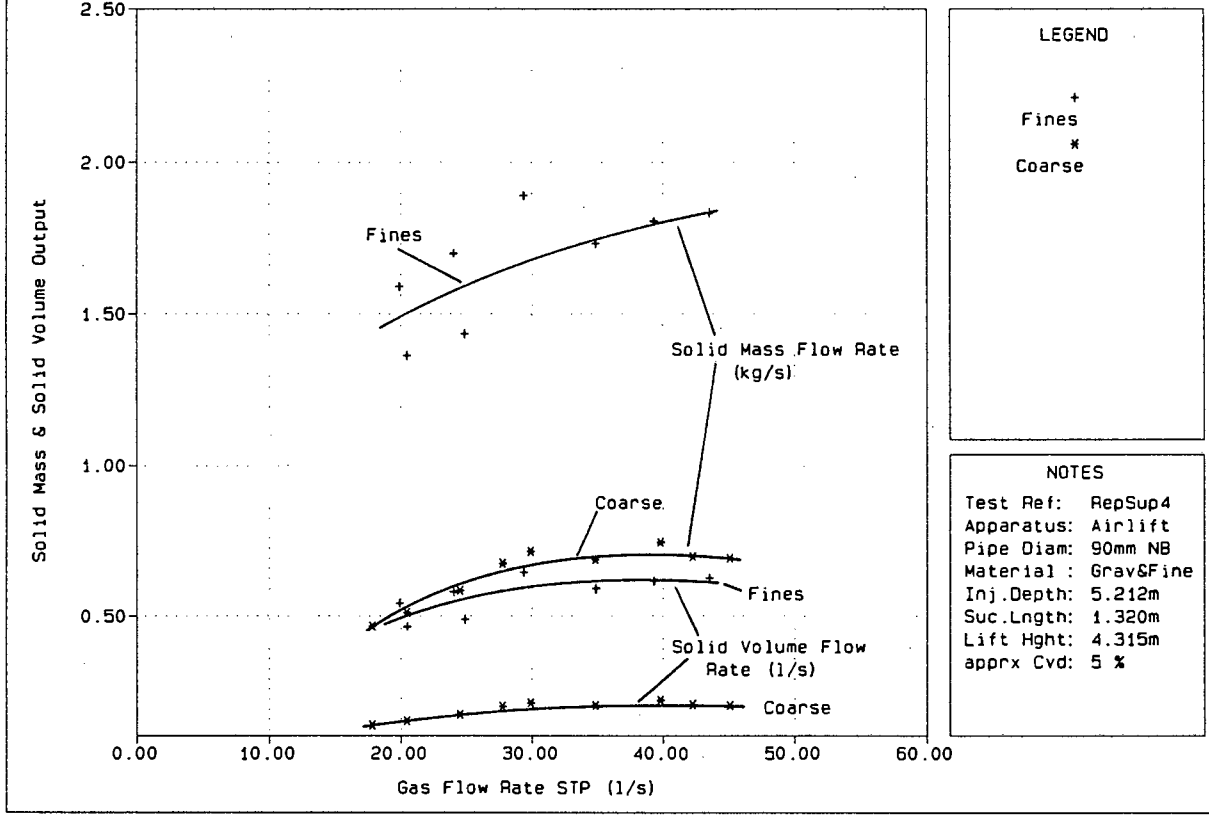

Figure : 8.69a
Description : Fines Tests (Fines + Lime)

Airlift Pump Investigation

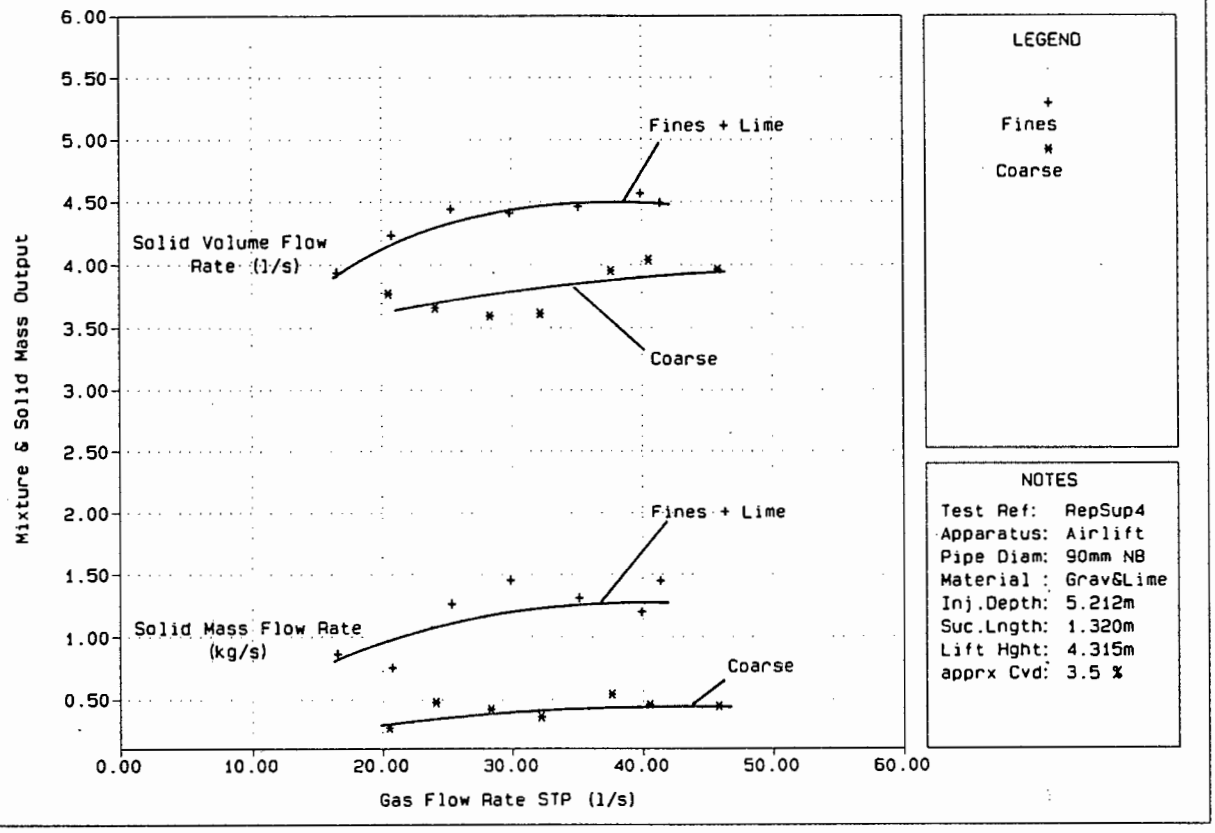

Figure : 8.69b
Description : Fines Tests (Fines + Lime)

Airlift Pump Investigation

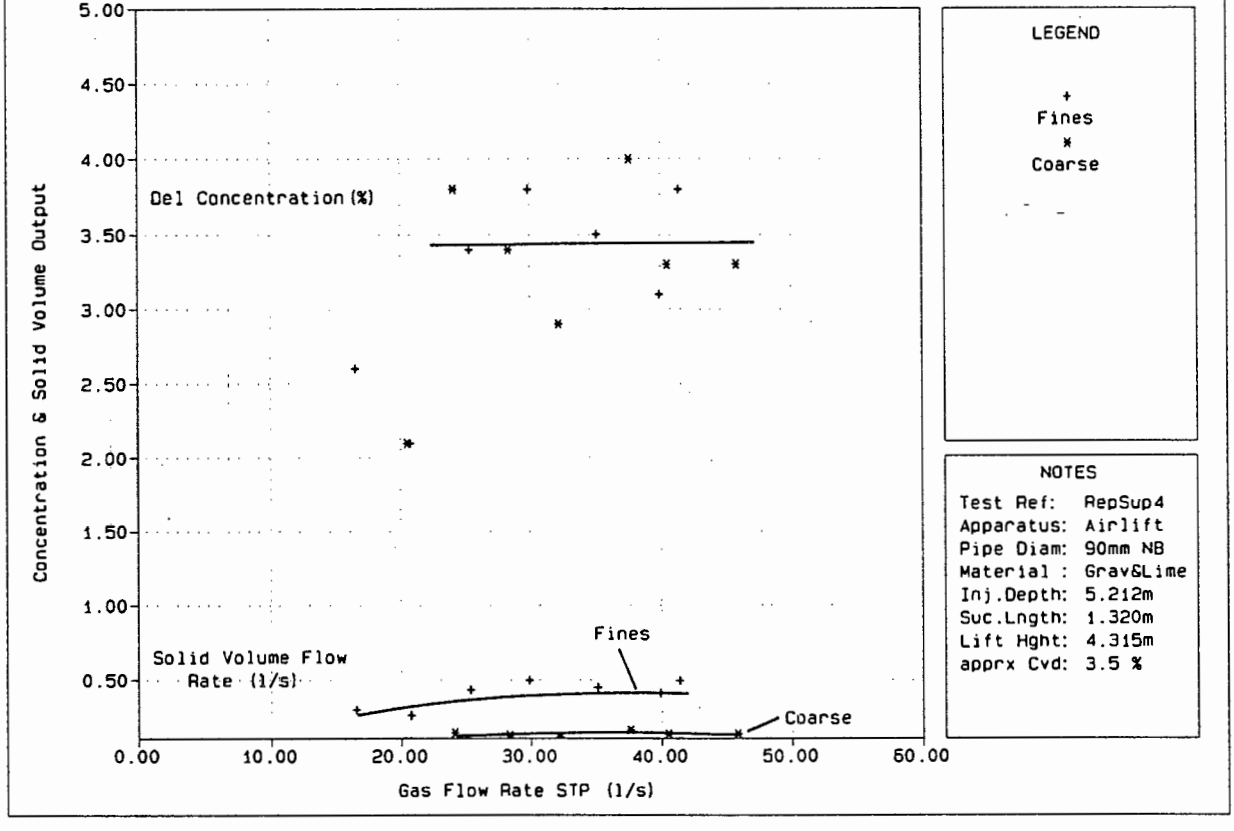

CHAPTER 9

CONCLUSIONS

9.1 INTRODUCTION

This chapter lists the conclusions made throughout this dissertation. These primarily relate to the results and discussion in Chapter 8.

9.2 TWO PHASE SOLID-LIQUID PIPELINE TESTS

9.2.1 Vertical two phase solid-liquid shear stress (τ_{om}^{sl})

9.2.1.A The shear stress contributes a small portion (3-13%) of the overall pressure loss in the suction pipe for velocities up to 6 m/s and delivered volumetric concentration up to 15%.

9.2.1.B Clear water shear stresses are adequately predicted using Churchill's friction factor Equation 4.28 (Chisholm 1983).

9.2.1.C At delivered volumetric concentrations of ± 5%, the Homogeneous, Weber and Giot's theories result in slightly larger, over-predicted shear stresses in both pipe sizes.

9.2.1.D At delivered volumetric concentrations of 10% and 15% in the 160 mm NB pipeline, the Proposed theory compares more favourably with the "measured" data than the other authors. However, slight inaccuracies in *in situ* concentration measurement result in slightly inaccurate "measured" shear stresses.

9.2.1.E *In general, the Proposed theory results in a slightly lower approximation of the two phase shear stress than the other theories evaluated and consequently predicts the "measured" shear stresses more accurately.*

9.2.2 Vertical two phase solid-liquid *in situ* volumetric concentration (C_{vt}^{sl})

9.2.2.A Solid-liquid *in situ* volumetric concentrations (C_{vt}^{sl}) are a function of the delivered concentration (C_{vd}^{sl}), which is an input variable for the airlift pump analysis.

9.2.2.B Theories based on the delivered volumetric concentrations result in favourable approximation of the solid *in situ* volumetric concentration for smaller particle sizes (3-15 mm) at higher velocities (above ± 2 m/s).

9.2.2.C All theories considered, generally predict solid *in situ* volumetric concentration to within 10% of the measured data.

9.2.2.D *The Proposed theory agrees favourably with measured data and other theories. The advantages of the proposed theory are the ability to accommodate variables such as a range of particle sizes, particle size distributions, particle shapes and the hindered settling effect. This makes the Proposed theory more desirable for evaluating solid in situ volumetric concentration for marine gravels.*

9.2.3 Vertical two phase solid-liquid total pressure loss (Δp_2)

9.2.3.A Vertical two phase solid-liquid pressure losses calculated by the theories evaluated, agree to within 5% of the measured data for the range of velocities and concentrations tested.

9.2.3.B *The Proposed theory results in slightly lower and better approximations than the other theories evaluated.*

9.3 SINGLE PARTICLE SETTLING VELOCITY TESTS (AIR-WATER MIXTURES)

9.3.A At low gas flow rates and low gas *in situ* volumetric concentrations (less than ± 40%), the settling velocities of the small diameter spheres (15,8 mm) is increased by 5% compared with the theoretical clear water settling velocity.

9.3.B At higher gas flow rates and gas *in situ* volumetric concentrations the small diameter sphere fall behaviour becomes erratic with large scatter about the theoretical clear water settling velocity.

9.3.C The erratic settling velocity of a single spherical solid in a gas-liquid mixture increases with increased gas flow rate and gas *in situ* volumetric concentrations.

9.3.D The settling velocity for the large spheres (24,5 mm) is increased by 5% at all gas *in situ* concentrations and flow rates compared with the theoretical clear water settling velocity.

9.3.E The erratic fall behaviour of the larger diameter spheres is less than with the smaller diameter particles.

9.3.F Because of the erratic fall behaviour of both diameter spheres, no terminal settling velocity is defined.

9.3.G The settling velocity of spheres in gas-water mixtures does not deviate significantly from the *clear water* terminal settling velocity calculated from Equation 4.20.

9.3.H *The theoretical clear water spherical settling velocity Equation (4.20) can be used in the gas-liquid mixture environment.*

9.4 MULTIPLE PARTICLES SETTLING VELOCITY TESTS (AIR WATER MIXTURES)

9.4.A Under conditions of no gas flow, the hindered settling velocities of multiple particles is less than single particles due to particle interaction.

9.4.B A cluster of particles falling through gas-liquid mixtures tend to be spread out by rising gas bubbles and by turbulence behind the gas bubbles. Thus no particle interaction or hindered effect is observed or measured.

9.4.C *There appears to be no such phenomenon as hindered settling in gas liquid mixtures as compared with hindered settling in liquids.*

9.5 THREE PHASE *IN SITU* VOLUMETRIC CONCENTRATION TESTS

9.5.1 Vertical three phase solid and gas *in situ* concentrations (C_{vt}^{slg} & ϵ_{g}^{slg})

9.5.1.A Gas *in situ* volumetric concentrations are best predicted with the Proposed theory. Predictions agree to within 5% compared with the measured data in the 90 mm diameter pipe and to within 10% in the 50 mm diameter pipe for a range of delivered volumetric concentrations and particle sizes.

9.5.1.B Giot, Kato, Weber (1982) and Dedegil over-predict while Weber (1976) under-predicts the gas *in situ* volumetric concentration at all delivered concentrations tested.

9.5.1.C The closest approximation of the measured solid *in situ* volumetric concentration data is obtained with either the Proposed or Giot's theories.

9.5.1.D *Although Giot and the Proposed solid in situ concentration theories agree favourably, the advantage of the Proposed theory is the ability to accommodate variables such as particle sizes, distribution and shape factors.*

9.5.2 Vertical three phase solid-liquid-gas weight (W_m^{slg})

9.5.2.A The three phase solid-liquid-gas weight is best predicted using the Proposed theory. On the 90 mm airlift pump, predictions agree to within 5% compared with the weight calculated from measured gas and solid *in situ* concentrations. On the 40 mm airlift pump agreement is to within 10%.

9.5.2.B Giot, Kato, Weber (1982) and Dedegil under-predict the three phase weight in the 90 mm airlift pump while Weber's earlier theory severely over-predicts the three phase weight throughout. This is a result of an over-prediction or under-prediction in the lower density gas phase respectively (refer 9.5.1.B).

9.5.3 Vertical three phase solid-liquid-gas shear stress (τ_{om}^{slg})

9.5.3.A All theoretical three phase shear stress approximations presented in the literature severely under-predict the "measured" shear stress data.

9.5.3.B Kato and Dedegil's theories are slightly better than those obtained using Weber and Giot's models. However, under-predictions are in the excess of 50%.

9.5.3.C The Proposed theory results in much better approximations than the other theories evaluated. At 4% delivered volumetric concentrations in the 90 mm airlift pump, the three phase friction pressures agree favourably with the measured data. At higher concentrations, in the 40 mm airlift pump, the predictions are less favourable. However, they are significantly better than the others predictions.

9.5.4 Vertical three phase solid-liquid-gas total pressure loss

9.5.4.A The Proposed theory results in the most favourable approximations of the three phase pressure loss in the delivery pipe increment.

9.5.4.B Generally, predictions with the Proposed theory are within 10% of the measured data. This was confirmed at delivered concentrations of 4% and 8%, in two pipe sizes and for various particle sizes.

9.5.4.C Weber's (1976) theory tends to over-predict while Dedegil, Giot and Kato under-predict the three phase pressure losses. Comparing the accuracy of their predictions, however, has to be performed with circumspection, due to an over-prepredicted weight cancelling with an under-predicted shear stress in some cases.

9.6 AIRLIFT PUMP OPERATING CURVES - PREDICTION OF OUTPUT LIQUID AND SOLID FLOW RATES

9.6.A The Proposed theory simulates output liquid and solid flow rates to generally within a 10% accuracy of the measured data, with some predictions deviating by 15 - 20%.

9.6.B All other theories evaluated (Dedegil, Giot, Kato and Weber) over-predict output liquid and solid flow rates by an excess of 15-20%.

9.6.C *The Proposed theory successfully simulates the operation of airlift pumps in three phase flow to a higher accuracy than other theories cited in the literature for a range of flow rates, delivered concentrations, pipe sizes and particle characteristics.*

9.7 AIRLIFT PUMP OPERATING TESTS

9.7.1 Particle size tests

9.7.1.A Smaller particles resulted in higher mixture output flow rates than larger particles at 2% and 2,5% delivered volumetric concentrations and submergence ratio of 88%.

9.7.1.B The effect of particle size on the solid mass output flow rate appears less significant than on the solid-liquid mixture flow rate.

9.7.1.C At a 99% submergence ratio, smaller particles result in higher mixture output flow rates at 2,5% delivered concentration while the reverse occurs at 3% delivered concentration.

9.7.1.D At 3,5% to 4% delivered volumetric concentration, smaller particles resulted in lower mixture and solid mass output flow rates which is the opposite effect to items 9.7.1.A and C.

From the large variations in the experimental results it is difficult to establish a definite trend showing the effect of the particle size on the mixture and solid output flow rates.

9.7.2 Submergence ratio tests

9.7.2.A An 8% increase in submergence ratio resulted in approximately 25% increase in mixture flow rate.

9.7.2.B An 8% increase in the submergence ratio resulted in a 15-20% increase in the solid mass flow rate.

9.7.2.C *A small change in the submergence ratio has a significant effect on the solid-liquid mixture and solid mass output flow rates.*

9.7.3 Solid delivered volumetric concentration tests

9.7.3.A An increased delivered volumetric concentration results in a decrease in mixture flow rates and an increase in solid mass flow rate. With increasing delivered concentration the maximum mixture and solid mass flow rates are attained at a higher gas flow rates.

9.7.3.B Maximum solid-liquid mixture flow rates coincide with maximum solid mass flow rates.

9.7.3.C With increasing solid-liquid delivered volumetric concentrations, the increase in solid mass flow rate becomes less.

9.7.3.D Pressures inside the airlift pump are less than the external static pressure for the lower 3 m. Above 3 m, the pressure inside the airlift pump becomes larger than the external pressures.

9.7.3.E A decrease in solid-liquid delivered volumetric concentrations results in lower absolute pressures for the bottom 4 m of the airlift pump as a result of increased shear stresses caused by increased mixture flow rates.

9.7.3.F Pressure changes inside the airlift pump pipe are non-linear with a larger pressure drop below gas injection level.

9.7.4 Annular air injector tests

9.7.4.A A change in the annular aperture area has little effect on the solids throughput.

9.7.4.B At low gas flow rates and low aperture area, a slight increase in mixture flow rate is observed (± 5%) for increasing aperture areas. This increase in mixture flow rate diminishes at higher gas flow rates.

9.7.4.C The pressure changes inside the airlift pump are nonlinear, with a larger pressure drop below gas injection.

9.7.4.D Annular aperture areas have no visible effect on the pressure profiles inside the airlift pump delivery pipe.

9.7.5 Fine tests

9.7.5.A The addition of finer material results in higher solid-liquid mixture and solid mass output flow rates.

9.7.5.B At lower gas flow rates, these higher output flow rates appear more significant than at higher gas flow rates.

9.7.5.C Addition of a high percentage of building lime to the finer material resulted in higher solid-liquid mixture flow rates. The trend of more significant output flow rates at lower gas flow rates was not observed.

CHAPTER 10

SENSITIVITY OF THEORETICAL VARIABLES

10.1 INTRODUCTION

A range of input variables are required for calculation of airlift pump operating curves with the proposed model discussed in Chapter 4.

This chapter presents the results of a sensitivity analysis performed on all input variables, with the purpose of determining their relative influence on airlift pump operation and the output flow rates.

The sensitivity analysis is performed with the developed user friendly software - AIRLIFT (refer Appendix A).

10.2 IDENTIFICATION OF VARIABLES USED IN THE THEORETICAL MODEL

Referring to Chapter 4, the following pressure components require calculation :

1. the static pressure gain ($\Delta p1$)
2. pressure drop in the suction pipe ($\Delta p2$)
3. pressure drop across the gas injector ($\Delta p3$)
4. pressure drop on the delivery pipe ($\Delta p4$)

Table 4.2 summarizes the equations used to evaluate each of the above pressure components.

From these equations, Table 10.1 below identifies all the components as input variables, constants or calculated values.

SYMBOL	NAME	UNITS	IDENTIFICATION
$\Delta p1$	static pressure gain	N/m^2	calculated
$\Delta p2$	pressure drop in the suction pipe	N/m^2	calculated
$\Delta p3$	pressure drop across the gas injector	N/m^2	calculated
$\Delta p4$	pressure drop in the delivery pipe	N/m^2	calculated
ℓ_1	injection depth	m	variable
ℓ_2	suction pipe length	m	variable
ℓ_3	delivery pipe length (see lift height and injection depth)	m	N/A
$(\ell_3-\ell_1)$	lift height	m	variable
ρ_ℓ	liquid density	kg/m^3	variable
ρ_s	solid density	kg/m^3	variable
ρ_g	gas density	kg/m^3	variable
g	gravitational constant = 9,81	m/s^2	constant
D_{suct}	suction pipe diameter	m	variable
D_{del}	delivery pipe diameter	m	variable
A_{suct}	suction pipe area	m^2	calculated
A_{del}	delivery pipe area	m^2	calculated
$W_m^{s\ell}$	weight of the solid-liquid mixture (2 phase)	N	calculated
$W_m^{s\ell g}$	weight of the solid-liquid-gas mixture (3 phase)	N	calculated
$C_{vt}^{s\ell}$	solid insitu concentration (2 phase)	-	calculated
$C_{vd}^{s\ell}$	solid delivered concentration (2 phase)	-	calculated
$C_{vt}^{s\ell g}$	solid insitu concentration (3 phase)	-	calculated
$C_{vd}^{s\ell g}$	solid delivered concentration (3 phase)	-	calculated
$\epsilon_g^{s\ell g}$	gas insitu concentration (3 phase)	-	calculated
$v_m^{s\ell}$	mixture velocity (2 phase)	m/s	calculated
v_{tsph}	spherical settling velocity	m/s	calculated
v_ℓ	liquid velocity	m/s	calculated
v_s	solid velocity	m/s	calculated
v_g	gas velocity	m/s	calculated
$v_m^{s\ell g}$	mixture velocity (3 phase)	m/s	calculated
$v_B^{s\ell}$	bubble rise velocity (3 phase)	m/s	calculated
S_f	particle shape factor	-	variable
R_n	percentage retained - sieve analysis	%	variable
τ_o	mixture shear stress	N/m^2	calculated
f	friction factor	-	calculated
k_{suct}	suction pipe roughness	mE-6	variable
k_{del}	delivery pipe roughness	mE-6	variable
Q_{gSTP}	gas flow rate	m^3/s	variable
$Q_m^{s\ell}$	solid-liquid mixture flow rate	m^3/s	variable
Q_s	solid volume flow rate	m^3/s	variable

TABLE 10.1 : Theoretical model variables, constants, calculated values

Note : 2 phase - refers to solid-liquid flow in the airlift pump suction pipe.

3 phase - refers to solid-liquid-gas flow in the airlift pump delivery pipe.

From Table 10.1 the components listed in Table 10.2 are identified as variables :

NUMBER	INPUT VARIABLE	NAME
1	ℓ_1	injection depth
2	ℓ_2	suction length
3	$(\ell_3 - \ell_1)$	lift height
4	ρ_1	liquid density
5	ρ_s	solid density
6	ρ_g	gas density
7	D_{suct}	suction pipe diameter
8	D_{del}	delivery pipe diameter
9	k_{suct}	suction pipe roughness
10	k_{del}	delivery pipe roughness
11	$C_{vd}^{s\ell}$	solid-liquid delivered concentration (2 phase)
12	S_f	shape factor
13	R_n	percentage retained - sieve analysis
14	Q_{gSTP}	gas flow rate
15	$Q_m^{s\ell}$	solid-liquid mixture flow rate
16	Q_s	solid volume flow rate

TABLE 10.2 : Theoretical model input variable

Referring to Table 10.2, the analysis in this chapter shows the effect of each component (1) to (13) on the solid-liquid mixture flow rate (15) and solid volume flow rate (16) for a range of gas flow rates (14).

The effect of the percentage retained (R_n) on each sieve is examined by considering samples of differing particle size distributions.

10.3 PROCEDURE

For the purpose of performing a sensitivity analysis on the abovementioned variables, a standard airlift pump layout has been chosen. This standard layout depicts typical prototype conditions and the variables in this layout are summarized in Table 10.3. Also given are the changes that are imposed on each variable for sensitivity examination. With these changes, the operating curves, and output solid and liquid flow rates are re-calculated. These are compared to the operating curves calculated with the standard layout.

For the purpose of determining the sensitivity of particle size, the particle size distributions in Figures 10.1 and 10.2 are used. The standard particle size distribution is given in Figure 10.1.

ITEM	UNITS	STANDARD	VARIATION 1	VARIATION 2
injection depth	m	120	100	140
suction length	m	3	2	4
lift height	m	10	8	12
liquid density	kg/m^3	1 000	900	1 020
solid density	kg/m^3	2 600	2 400	2 800
gas density	kg/m^3	1,204	1,000	1,400
suction pipe diameter	m	0,200	0,180	0,220
delivery pipe diameter	m	0,200	0,180	0,220
suction pipe roughness	mE-6	50	100	150
delivery pipe roughness	mE-6	50	100	150
solid delivery concentration (by volume)	%	5	3	7
shape factor	-	0,8	0,6	0,7

TABLE 10.3 : Sensitivity variables

10.4 RESULTS

10.4.1 Variable injection depth

Figures 10.3 and 10.4 show the effect of injection depth on the solid-liquid mixture and solid volume flow rates respectively. An increase in the injection depth results in an increase in both the mixture and solid flow rates at higher gas flow rates. At low gas flow rates, a change in the injection depth does not influence the operating curves.

From the figures, a ± 16% increase in the injector depth results in a ± 3% increase in both the mixture and solid flow rates.

The reason for the increased output at the higher input gas flow rates only, is explained by an increased static pressure at the gas injector. Because the outlet pressures remain the same (atmospheric) a higher change in pressure has to be dissipated across a longer pipe length. At lower gas flow rates where the weight pressure loss of the three phase mixture is the predominant factor (compared to the friction pressure loss), this higher change in pressure is counteracted primarily by the longer pipe length and consequently increased three phase mixture weight. The weight is not a function of the mixture flow rates and consequently the mixture flow rates are not significantly influenced.

At higher gas flow rates, however, the friction plays a greater role in the overall three phase pressure drop. The higher pressure is now counteracted by the weight to a lesser extent than the friction, which is a function of the mixture flow rates. Consequently the increased pressure drop (due to increased injection depth) is dissipated by increased friction pressure losses caused by an increased mixture flow rate.

10.4.2 Variable lift height

Figures 10.5 and 10.6 show the effect of lift height on solid-liquid mixture and solid volume flow rates respectively. A 25% increase in the lift height results in a 3% decrease in both the mixture and solid flow rates for all gas flow rates.

The effect of increasing the lift height is the same as increasing the delivery pipe length. The pressures at the gas injector and the delivery outlets remain the same, however, at higher lift heights, the pressure drop between the gas injector and the delivery outlet occurs across a longer pipe length. Thus the pressure drop per unit length is lower and, consequently, lower mixture and solid flow rates are obtained.

10.4.3 Variable suction pipe length

Figures 10.7 and 10.8 show the effect of increased suction length on the airlift pump operating curves.

In prototype airlift pumps, injection depths are normally close to the suction inlet, rendering short suction pipes with respect to other airlift pump dimensions. Thus, variable suction pipe lengths in the order of 30% have little effect on the airlift pump operating curve.

10.4.4 Variable delivery pipe diameter

Figures 10.9 and 10.10 show the effect of a 1% change in the delivery pipe diameter on the airlift pump operating curves.

From the figures, a 3% increase in both mixture and solid flow rates is observed at higher gas flow rates only. From Equation 4.34 (Table 4.2), it can be shown that the shear stress is directly proportional to the delivery pipe diameter. As discussed in Section 10.4.1, the friction pressure loss component, which is a function of the mixture flow rate, is more dominant at higher gas flow rates when compared to the weight and momentum pressure

loss components. Thus increasing the delivery pipe diameters will have a greater flow effect on the output mixture flow rates at high gas flow rates.

Figures 10.11 and 10.12 show the sensitivity of a 10% change in the delivery pipe diameter. From the figure, the mixture and solid flow rates are observed to change by 27%.

By substituting Equation 4.49 into Equation 4.34 and applying continuity, it can be shown that mixture flow rate is proportional to the delivery pipe diameter raised to the power 5/2. Therefore, a small increase in the delivery pipe diameter results in a proportionally greater increase in mixture output flow rate.

10.4.5 Variable delivery pipe roughness

The effect of delivery pipe roughness on the airlift operating curves is shown in Figures 10.13 and 10.14. Only the friction component is affected by the roughness and thus, as before, the effect on the operating curves is more predominant of higher gas flow rates. A 100% increased roughness results in higher pressure losses and consequently a 6% decrease in mixture and solid flow rates.

10.4.6 Variable suction pipe diameter

The pressure loss across the suction pipe length is small with respect to the total pressure loss. Therefore, a 10% change in the suction pipe diameter results in the negligible effect on the airlift operating curves shown in Figures 10.15 and 10.16.

10.4.7 Variable suction pipe roughness

Analogous to the delivery pipe roughness, only the friction component is a function of the suction pipe roughness. Furthermore, this component is small when compared with the total suction pipe pressure drop and the other pressure drops encountered in the airlift pump. Therefore, the change in suction pipe roughness is shown to be negligible in Figures 10.17 and 10.18.

10.4.8 Variable liquid density and temperature

Figures 10.19 and 10.20 show the effect of three liquid densities on the airlift pump operating curves. A 10% change in liquid density from 1 000 kg/m^3 to 900 kg/m^3 shows to have a 2% effect on the airlift pump operating curves.

A variation of 10% on the liquid temperature is shown to have a negligible effect on the mixture and solid flow rates (refer Figures 10.21 and 10.22).

10.4.9 Variable solid density

Figures 10.23 and 10.24 show operating curves for three solid densities. Increasing the solid density by 15% results in a 3% decrease in the mixture and solid flow rates at high gas flow rates and a 10% decrease in mixture and solid flow rates at low gas flow rates. This variation occurs because the weight component is a function of the solid density. Analogous to 10.4.1, this variable is predominant at lower gas flow rates than higher gas flow rates, thus the effect is predominant here.

10.4.10 Variable gas density

The gas density is small compared to the densities of the other phases. Therefore, the operating curves are not very sensitive to a ± 40% change in this variable. This is confirmed in Figures 10.25 and 10.26.

10.4.11 Variable gas outlet pressure

In the analysis, the gas outlet pressure refers to the pressure at the delivery outlet and mean sea level. These two pressures are always equal, and therefore are not influenced in any way. This is confirmed on Figures 10.27 and 10.28.

10.4.12 Variable solid-liquid delivered concentration

Referring to Figure 10.29, a change in the solid-liquid delivered concentration has a larger effect on the mixture flow rate at low gas flows. The mixture weight is a function of the solid-liquid concentration, which is predominant at lower gas flow rates. The mixture flow rate decreases with increasing concentration because of larger weight and consequently larger pressure losses.

Referring to Figure 10.30, the solid volume flow rate increases with an increase in the delivered concentration for all flow rates. Furthermore, the output solid volume flow rates are observed to be very sensitive to small variations on the solid-liquid delivered concentration. This is therefore an important variable.

10.4.13 Variable particle size distribution

Shown in Figure 10.31 and 10.32 are the output operating curves for the analysis using the two particle size distributions shown in Figures 10.1 and 10.2. An increased particle diameter results in a higher settling velocity in gas flow ranges where the weight pressure drop is predominant. Thus at the same input gas flow rate, less large particles will be hoisted than small particles. At higher gas flow rates, a friction pressure loss is predominant and the above effect becomes negligible.

10.4.14 Variable particle shape factor

Figures 10.33 and 10.34 show the output flow rates for operating curves calculated using particles with shape factors of 0,6, 0,7 and 0,8. From the figures, it is observed that the operating curves are not very sensitive for variations in the shape factor.

10.5 CONCLUSIONS

10.5.A An increase in injection depth results in a larger increase in the output flow rates at higher gas flows. At lower gas flows, effect on the operating curves appear to be negligible.

10.5.B Increasing lift heights result in decreasing mixture and solid flow rates for all gas flows.

10.5.C Because the suction pipe pressure drop and length is small with respect to the rest of the airlift pump, small variations (± 10%) in suction pipe lengths, diameters and roughness have negligible effect on output operating curves.

10.5.D The output operating curves are very sensitive to changes in the delivery pipe diameter. An increased diameter results in increased output mixture and solid flow rates.

10.5.E The delivery pipe roughness is important at higher gas flow rates where friction pressure drop components are predominant. Here higher roughnesses resulted in lower output flow rates.

10.5.F 10% variations in the liquid, density and temperature have little effect on the airlift operating curves.

10.5.G A variation in the solid density of ± 15% has a larger effect at lower gas flow rates than at higher gas flow rates. This effect was attributed to the mixture weight being predominant at lower gas flow rates.

10.5.H Output mixture and solid volume flow rates are not very sensitive to changes in the gas density and gas output pressures.

10.5.I Output solid volume flow rates are highly sensitive to changes in the solid-liquid delivered concentrations. The solid volume flow rate increases with increasing solid-liquid delivered concentrations. The mixture flow rates are more sensitive at lower gas flow rates than at higher gas flow rates. Mixture flow rates decrease with increasing concentrations.

10.5.J At very low gas flow rates, the larger particle size distribution results in higher settling velocities. Thus less output flow

rates will be obtained for the same input gas flow rate. This effect is negligible at higher gas flow rates where the operating curves are shown to be less sensitive.

10.5.K The operating curves are not very sensitive to changes in the particle shape factors ranging from 0,6 to 0,8.

10.5.L Operating curves are most sensitive to the following variables :

- delivery pipe diameter
- injection depth
- lift height
- delivery pipe roughness
- solid density
- solid-liquid delivery concentration
- particle size distribution

10.5.M Operating curves are least sensitive to the following variables :

- gas outlet pressure
- liquid temperature
- suction pipe diameter
- suction pipe roughness
- suction pipe length
- liquid density
- gas density
- shape factor.

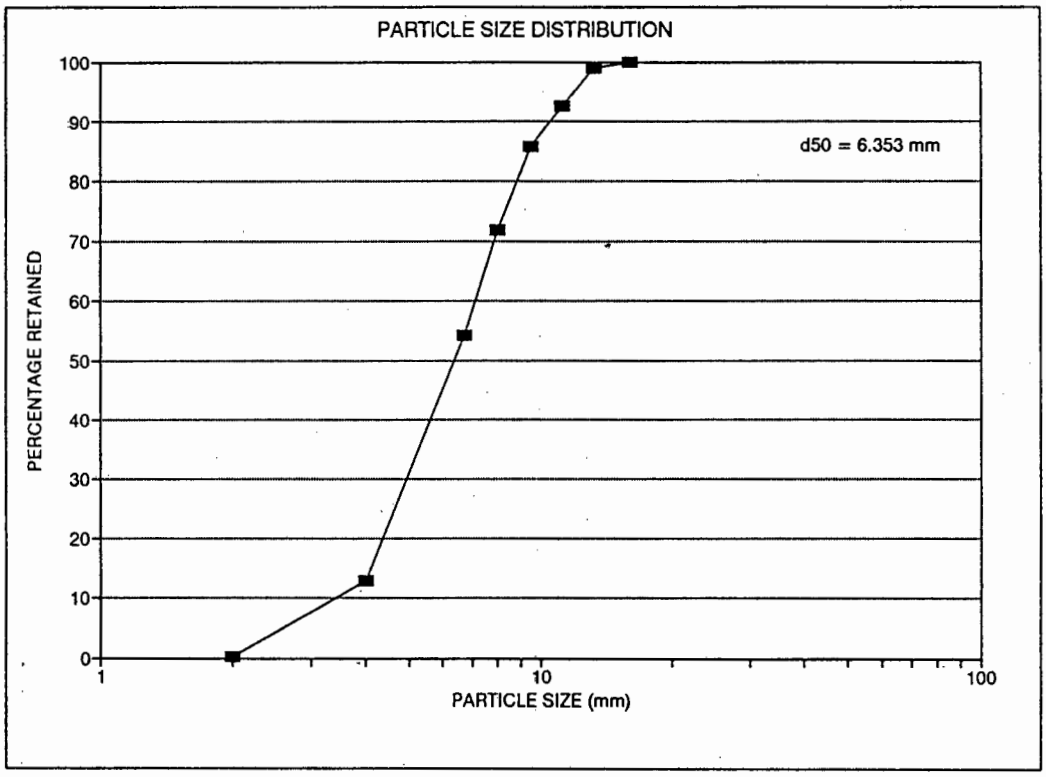

Figure 10.1 : Particle size distribution 1 (standard distribution)

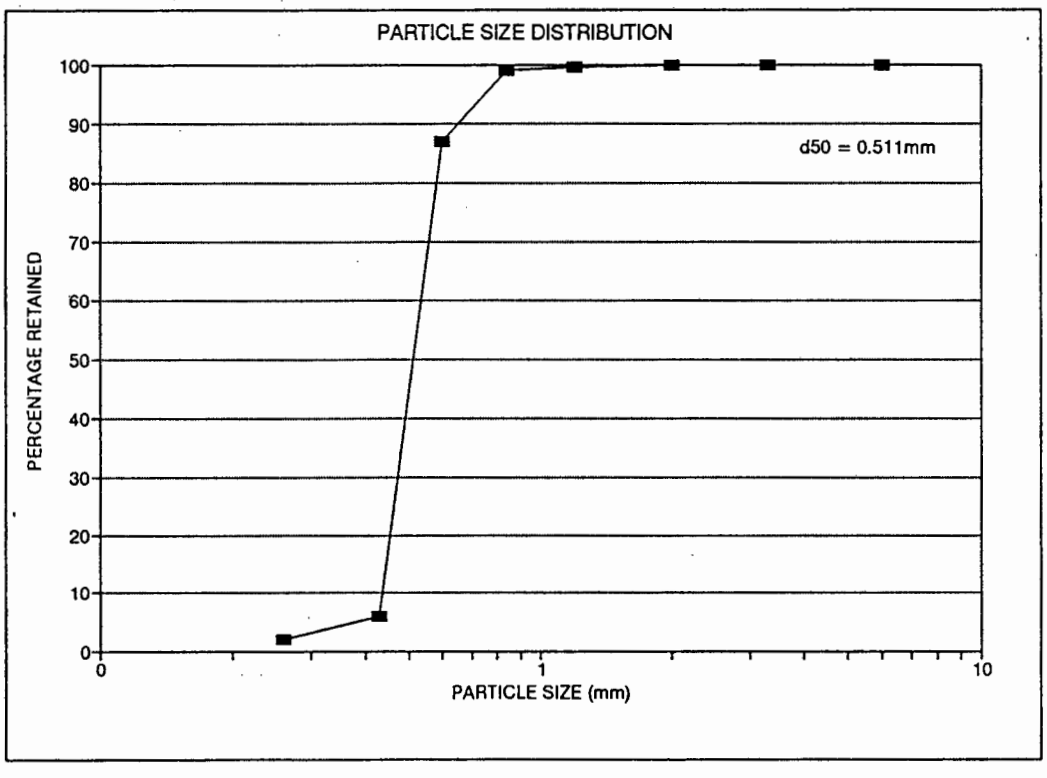

Figure 10.2 : Particle size distribution 2 (variation distribution)

Figure : 10.3
Description : Sensitivity: Injection Depth

Airlift Pump Investigation

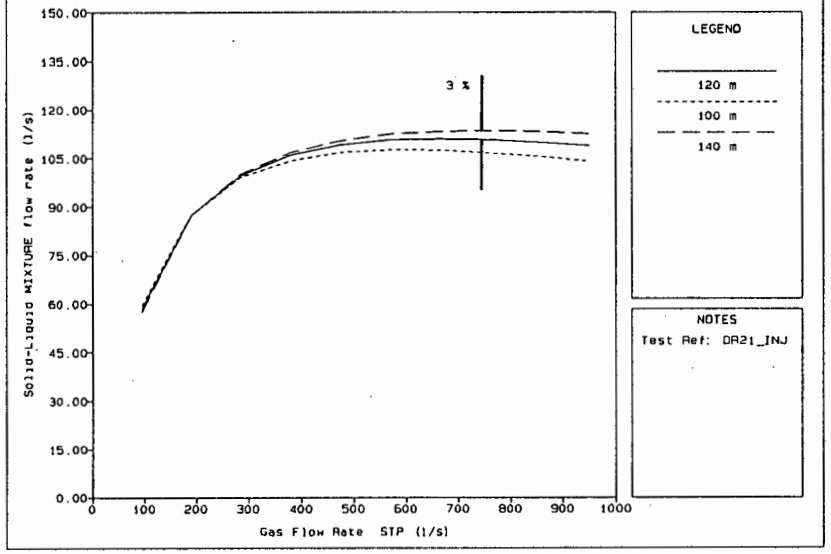

Figure : 10.4
Description : Sensitivity: Injection Depth

Airlift Pump Investigation

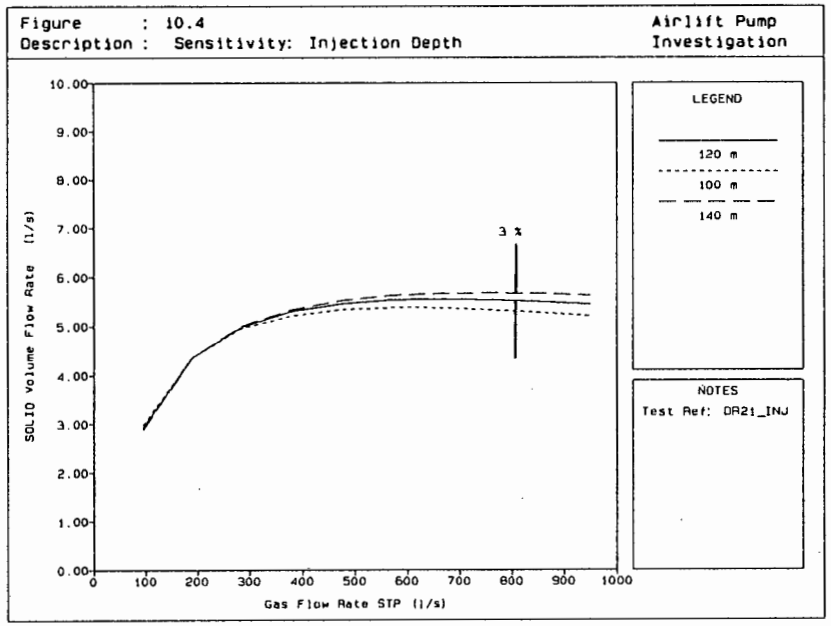

Figure : 10.5
Description : Sensitivity: Lift Height

Airlift Pump Investigation

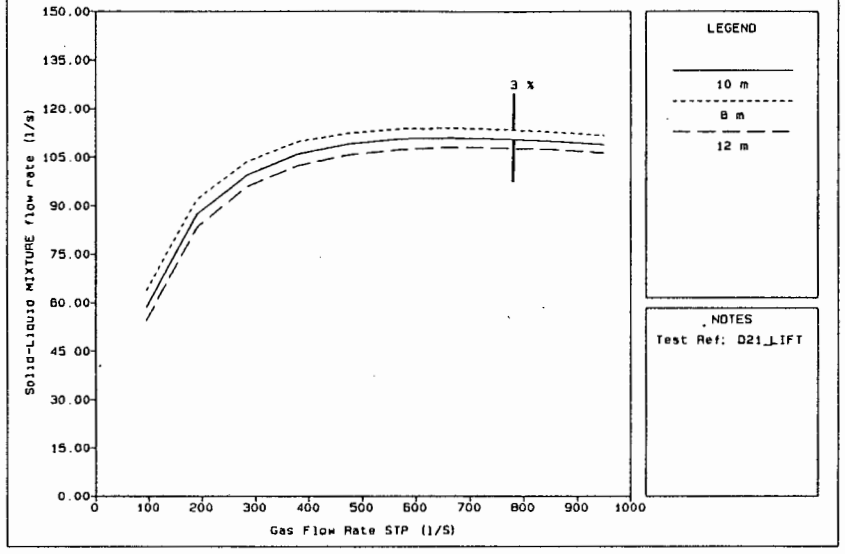

Figure : 10.6
Description : Sensitivity: Lift Height

Airlift Pump Investigation

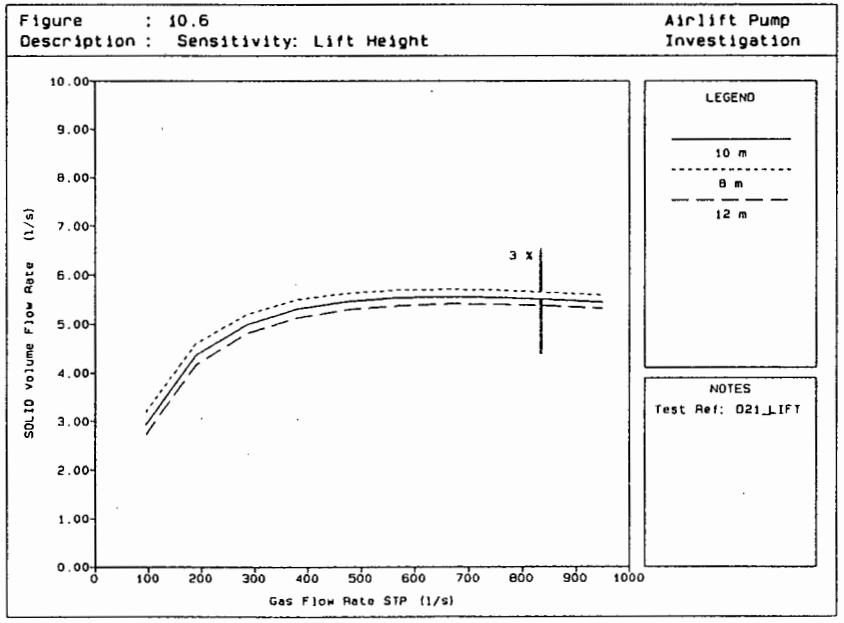

Figure : 10.7
Description : Sensitivity: Suction Pipe Length

Airlift Pump Investigation

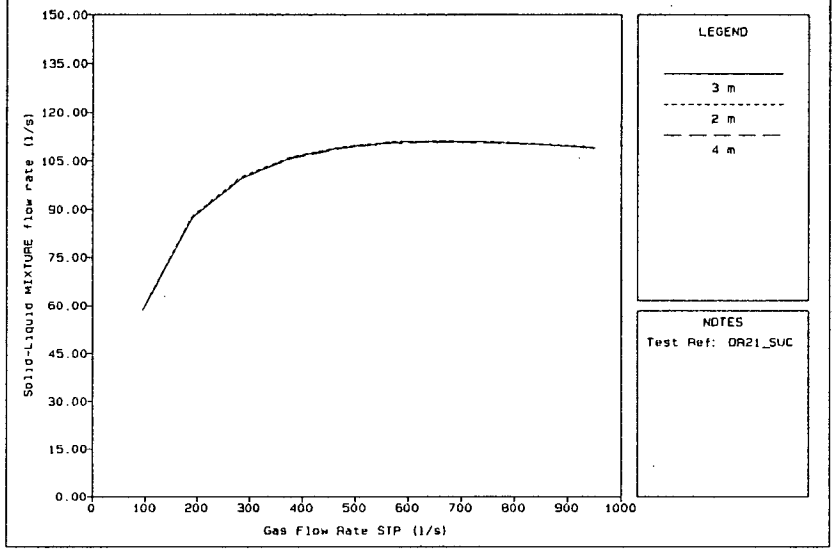

Figure : 10.8
Description : Sensitivity: Suction Pipe Length

Airlift Pump Investigation

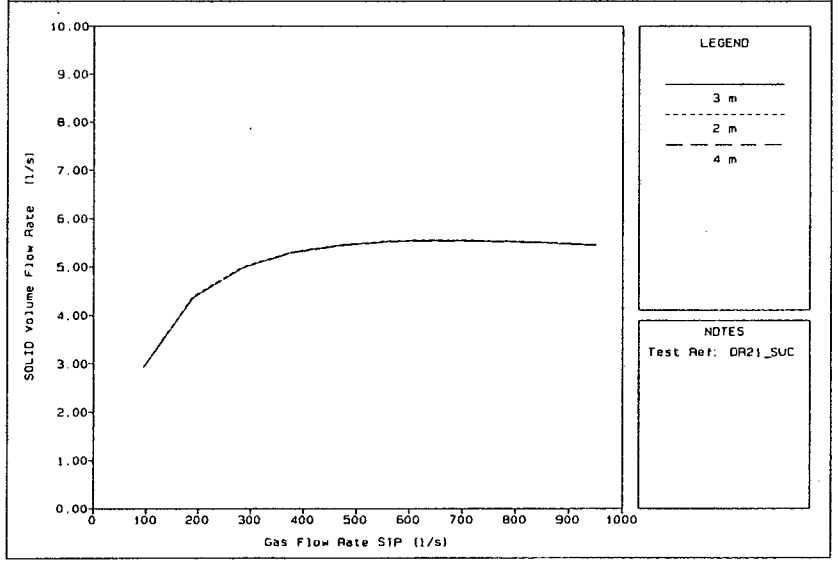

Figure : 10.9
Description : Sensitivity: Delivery Pipe Diameter

Airlift Pump Investigation

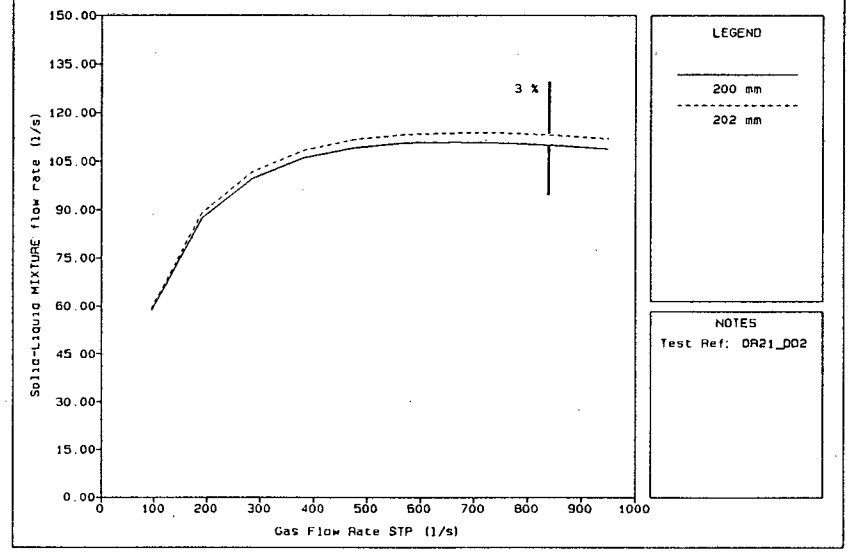

Figure : 10.10
Description : Sensitivity: Delivery Pipe Diameter

Airlift Pump Investigation

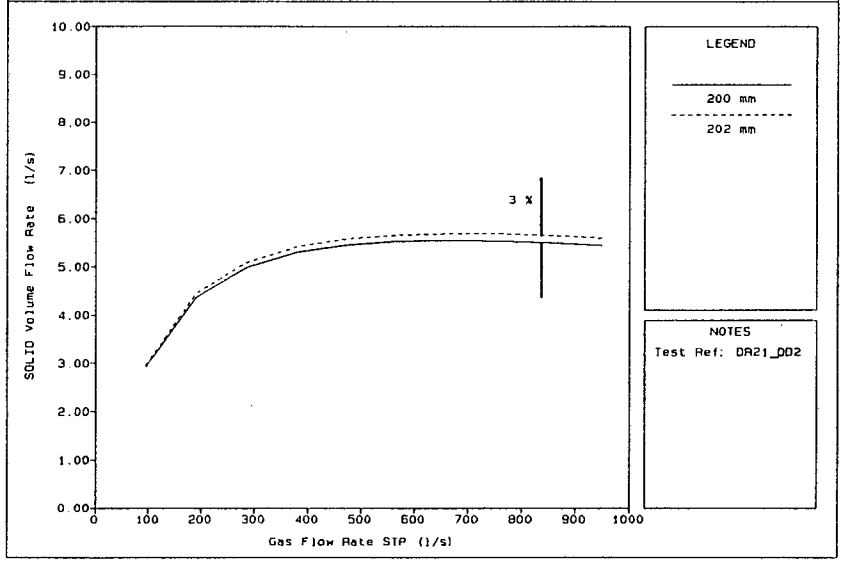

Figure : 10.11
Description : Sensitivity: Delivery Pipe Diameter

Airlift Pump Investigation

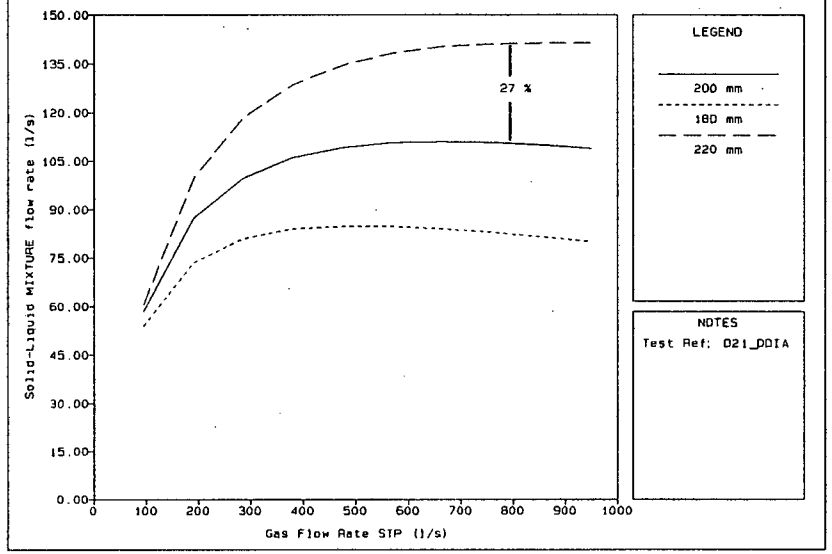

Figure : 10.12
Description : Sensitivity: Delivery Pipe Diameter

Airlift Pump Investigation

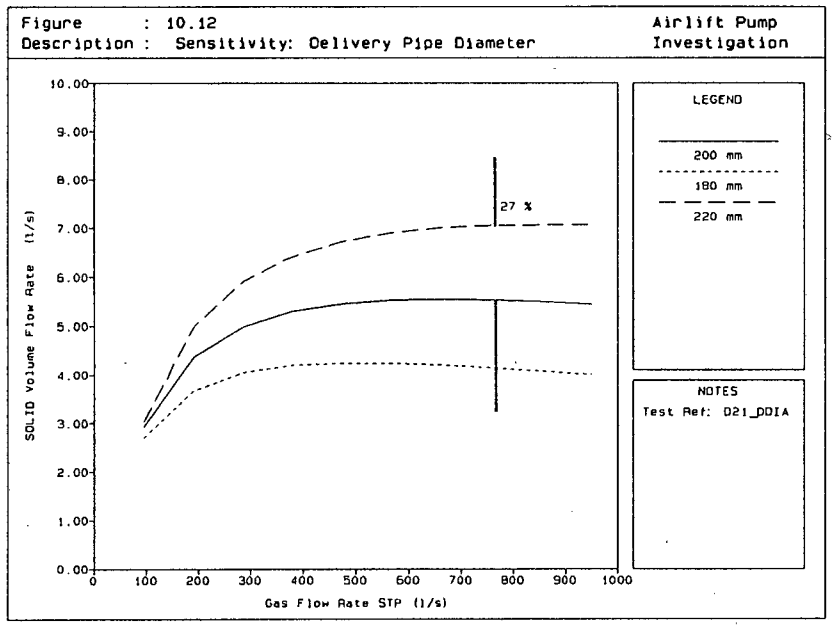

Figure : 10.13
Description : Sensitivity: Delivery Pipe Roughness

Airlift Pump Investigation

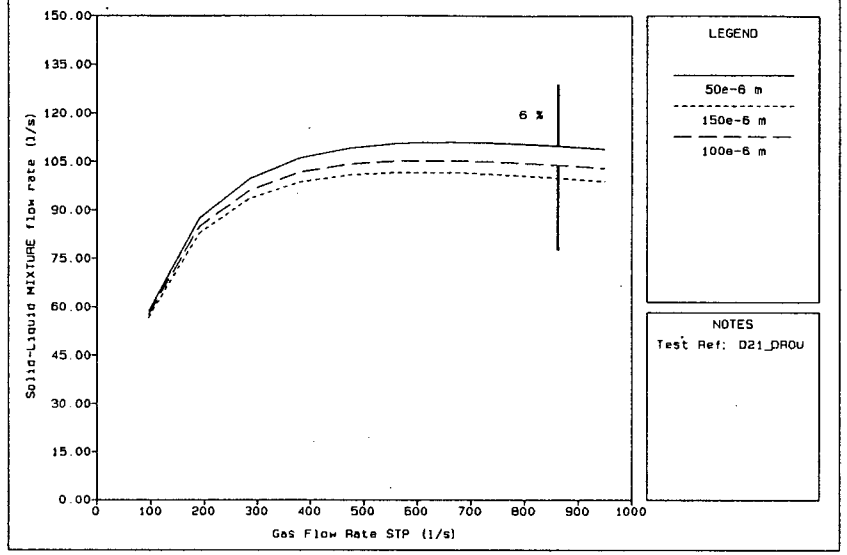

Figure : 10.14
Description : Sensitivity: Delivery Pipe Roughness

Airlift Pump Investigation

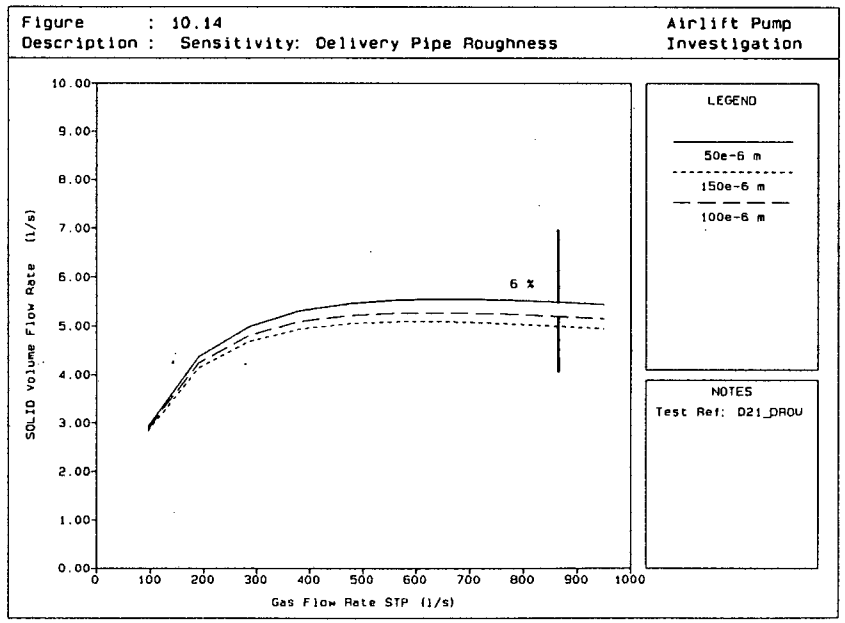

Figure : 10.15 Airlift Pump
Description : Sensitivity: Suction Pipe Diameter Investigation

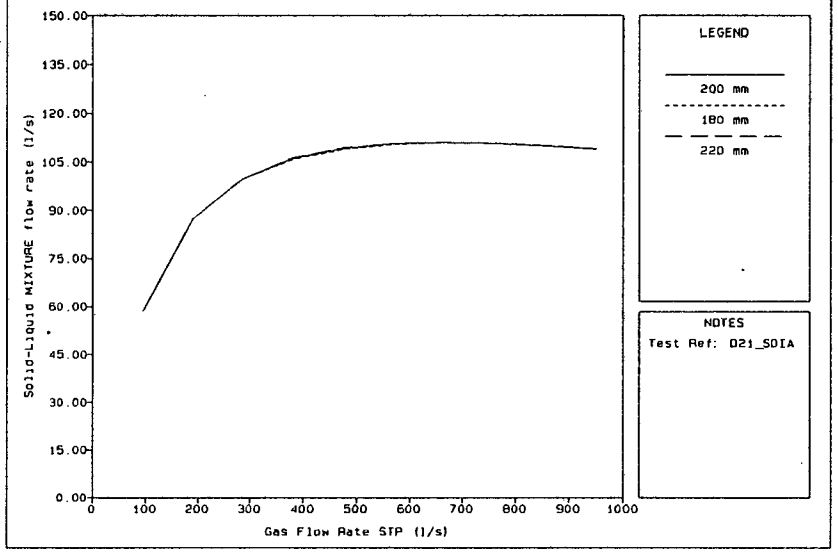

Figure : 10.16 Airlift Pump
Description : Sensitivity: Suction Pipe Diameter Investigation

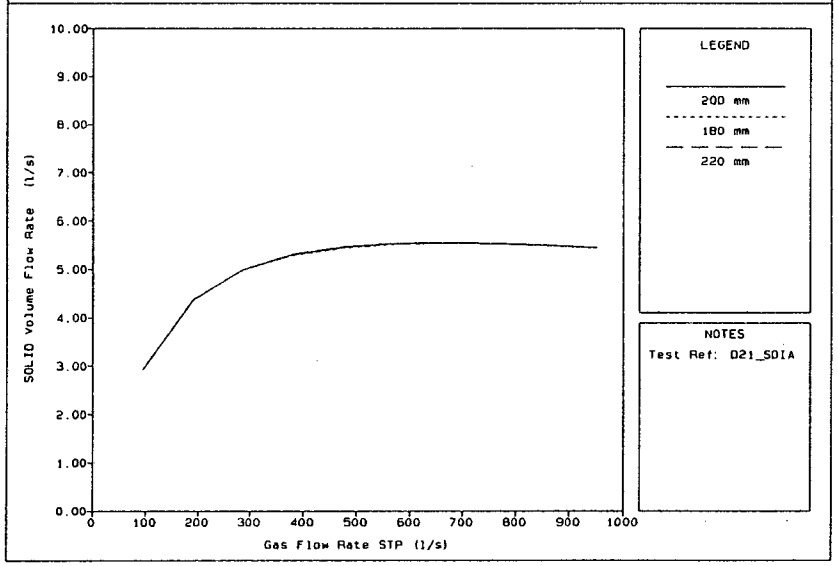

Figure : 10.17 Airlift Pump
Description : Sensitivity: Suction Pipe Roughness Investigation

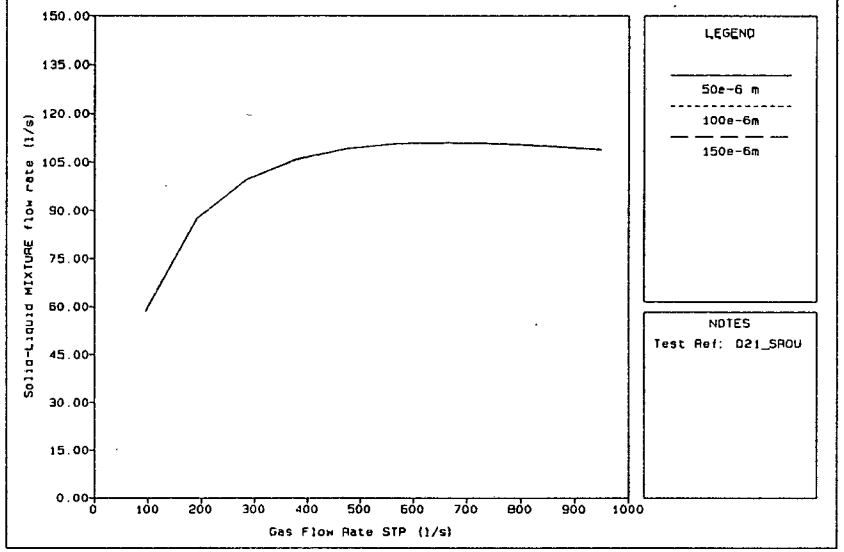

Figure : 10.18 Airlift Pump
Description : Sensitivity: Suction Pipe Roughness Investigation

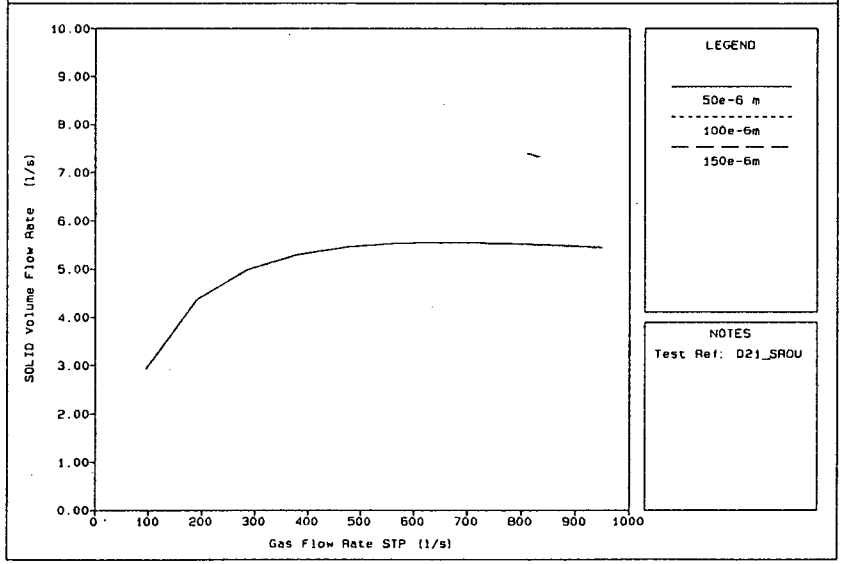

Figure : 10.19 Airlift Pump
Description : Sensitivity: Liquid Density Investigation

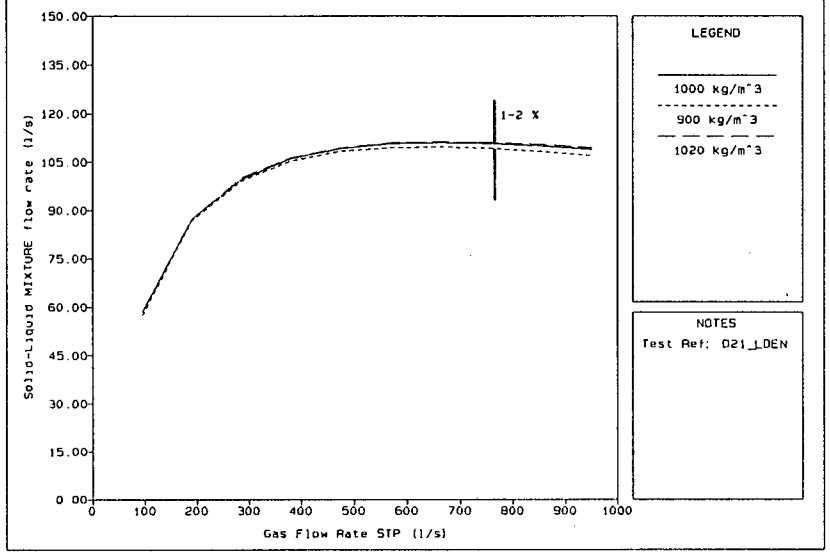

Figure : 10.20 Airlift Pump
Description : Sensitivity: Liquid Density Investigation

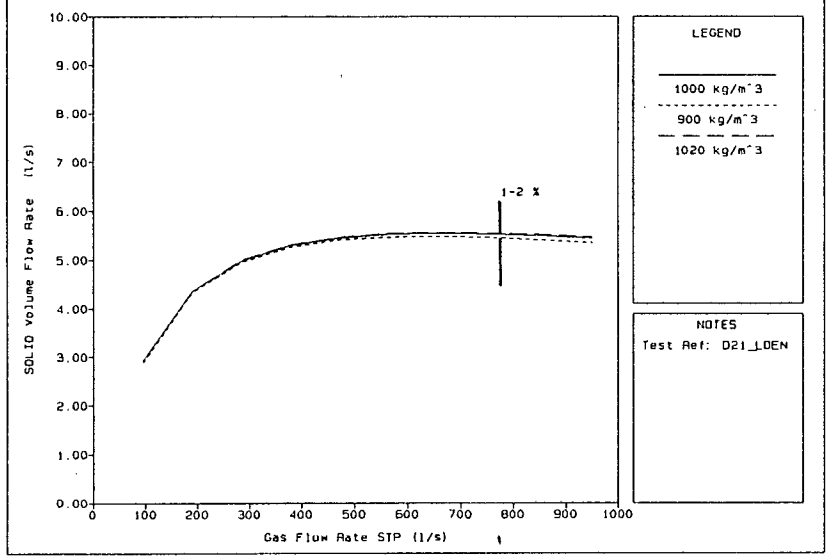

Figure : 10.21 Airlift Pump
Description : Sensitivity: Liquid Temperature Investigation

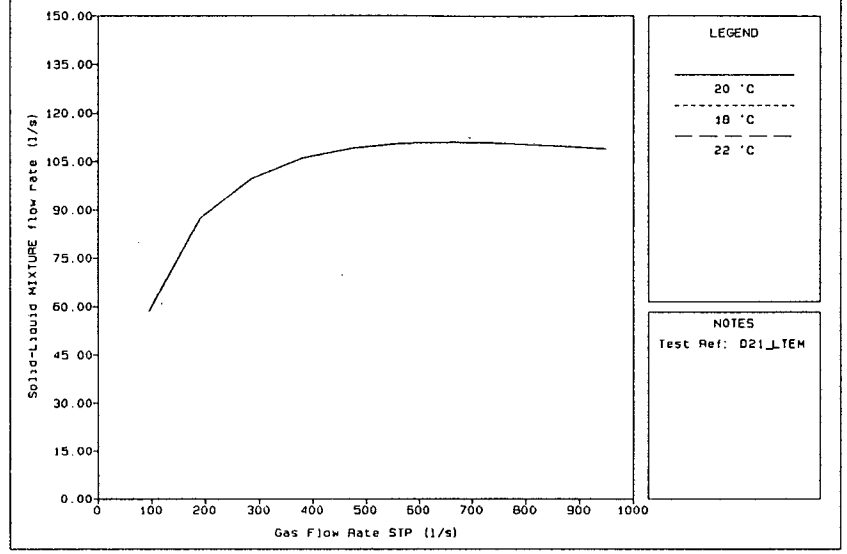

Figure : 10.22 Airlift Pump
Description : Sensitivity: Liquid Temperature Investigation

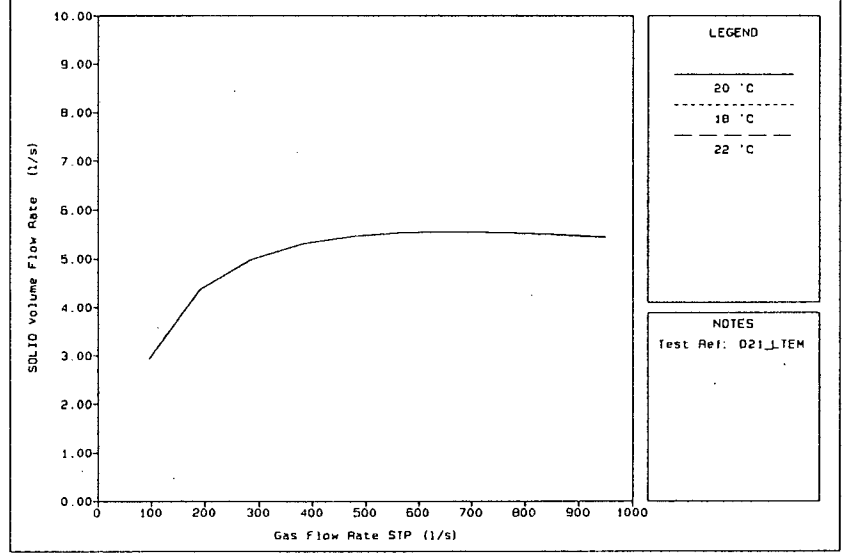

Figure : 10.23
Description : Sensitivity: Solid Density

Airlift Pump Investigation

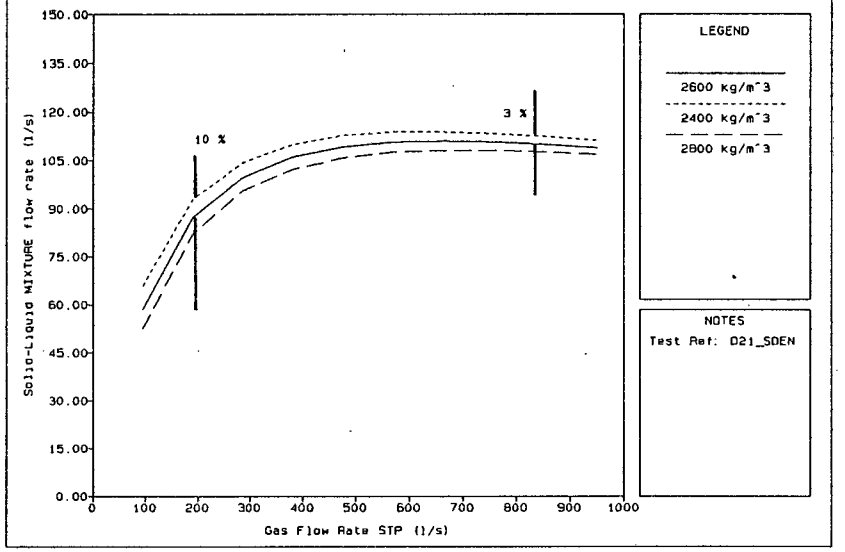

Figure : 10.24
Description : Sensitivity: Solid Density

Airlift Pump Investigation

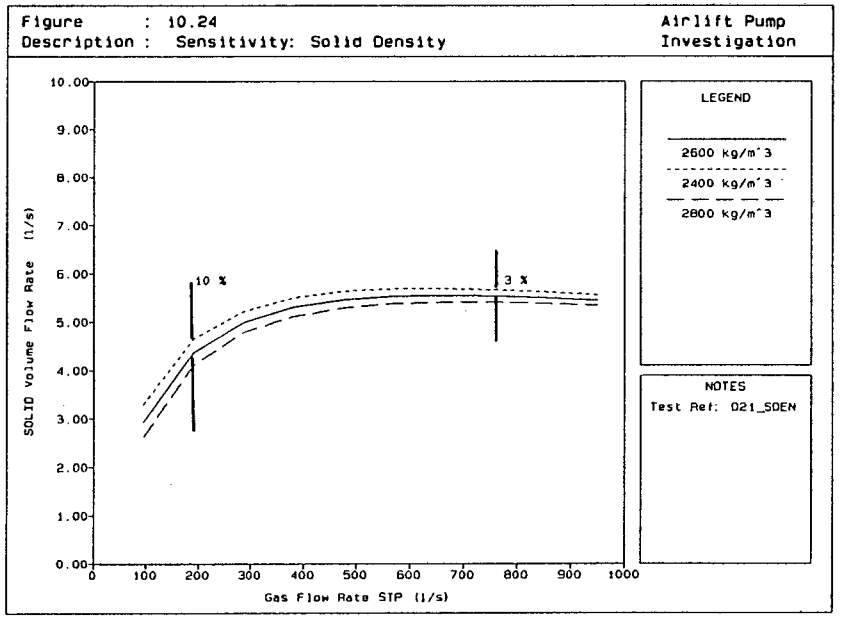

Figure : 10.25
Description : Sensitivity: Gas Density

Airlift Pump Investigation

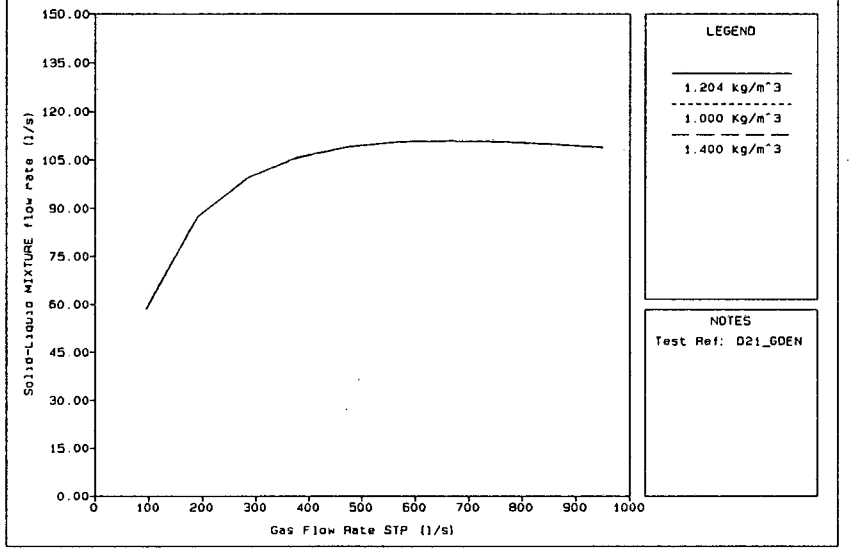

Figure : 10.26
Description : Sensitivity: Gas Density

Airlift Pump Investigation

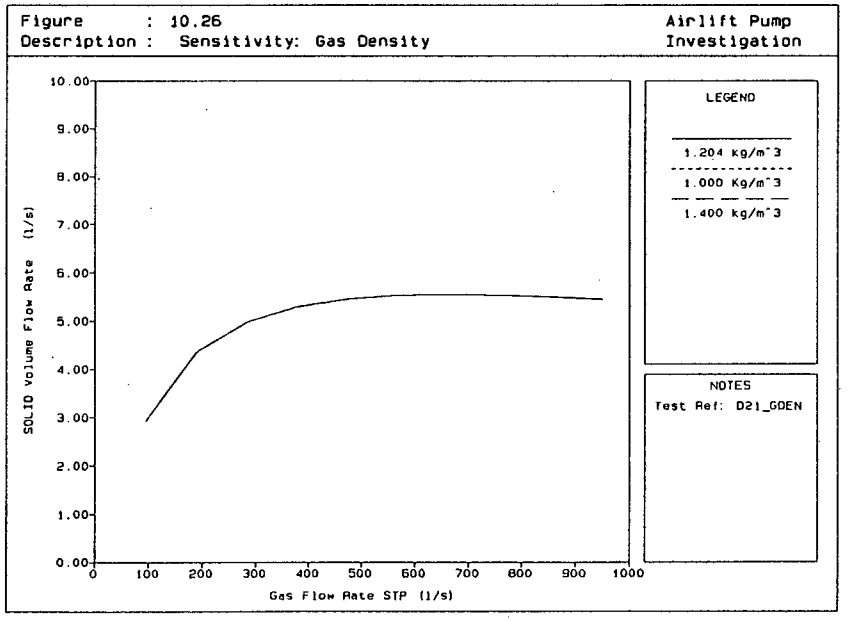

Figure : 10.27 Airlift Pump
Description : Sensitivity: Gas Outlet Pressure Investigation

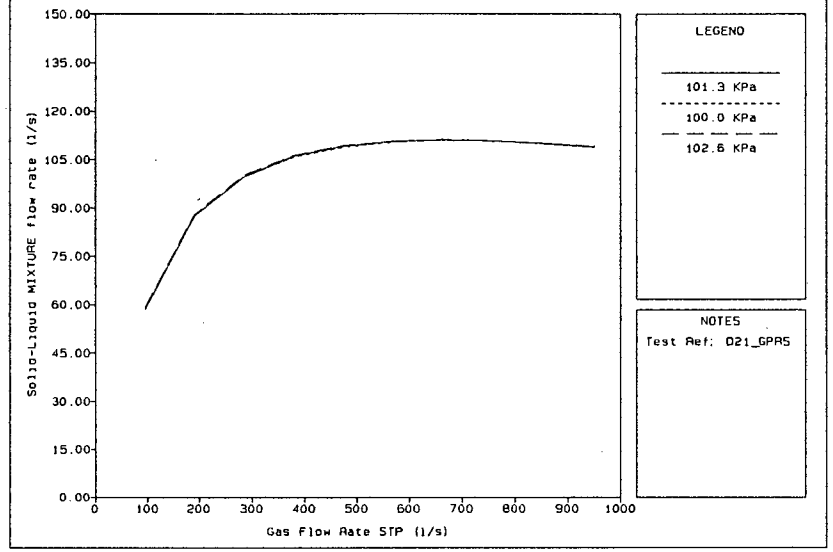

Figure : 10.28 Airlift Pump
Description : Sensitivity: Gas Outlet Pressure Investigation

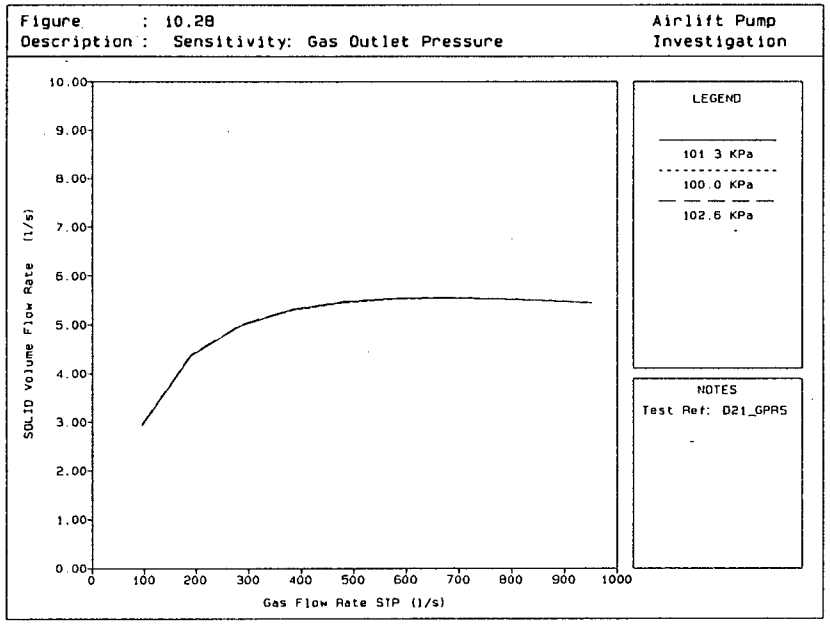

Figure : 10.29 Airlift Pump
Description : Sensitivity: Delivered Vol. Concentration Investigation

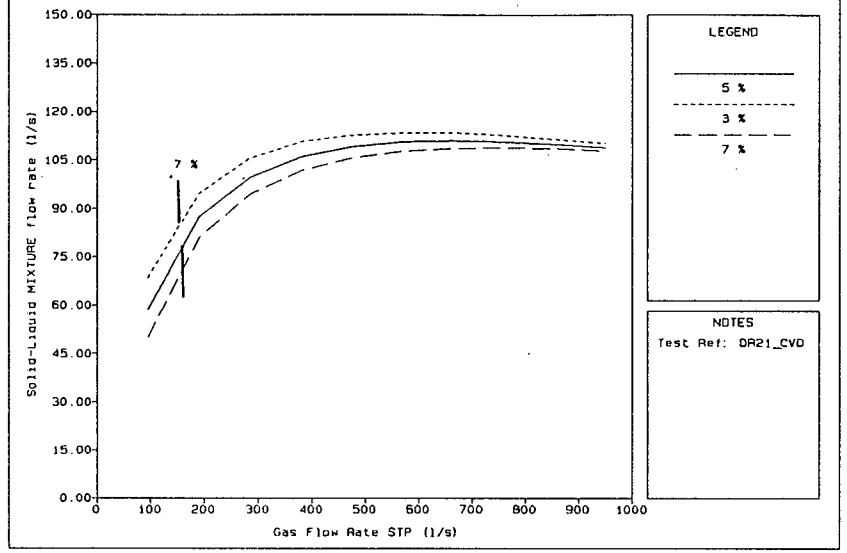

Figure : 10.30 Airlift Pump
Description : Sensitivity: Delivered Vol. Concentration Investigation

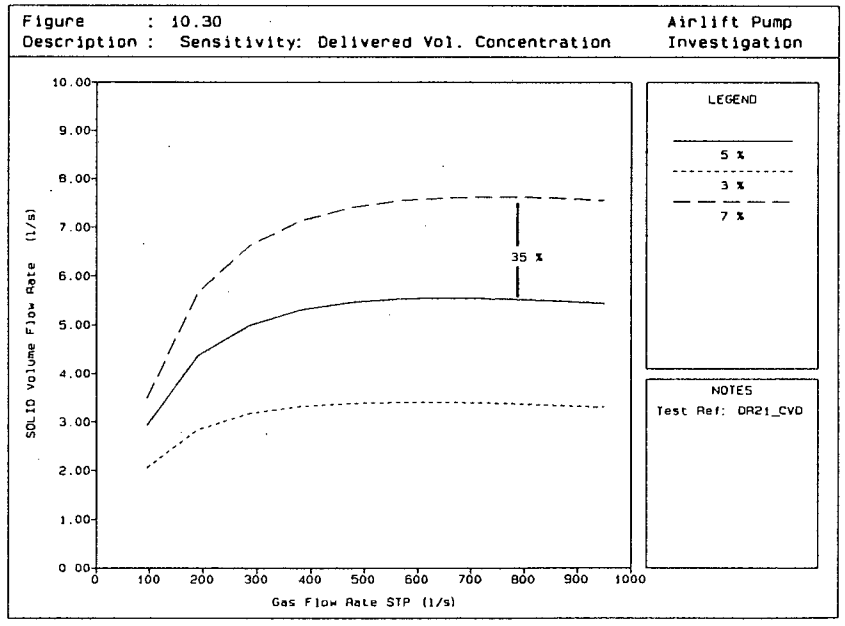

Figure : 10.31
Description : Sensitivity: Particle Size Distribution

Airlift Pump Investigation

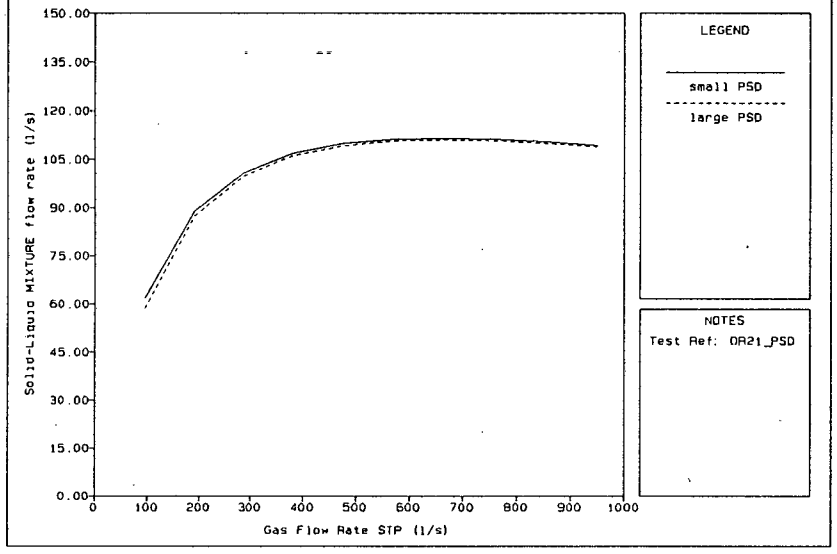

Figure : 10.32
Description : Sensitivity: Particle Size Distribution

Airlift Pump Investigation

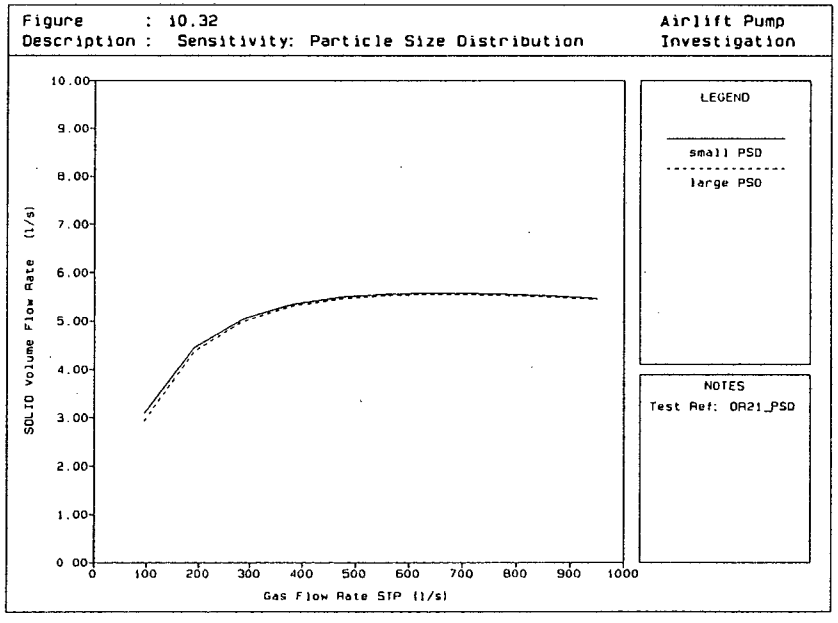

Figure : 10.33
Description : Sensitivity: Particle Shape Factor

Airlift Pump Investigation

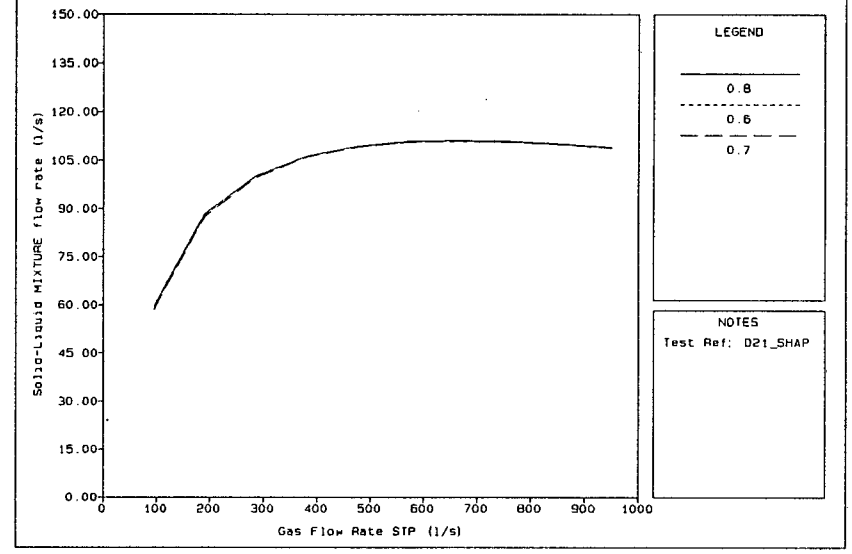

Figure : 10.34
Description : Sensitivity: Particle Shape Factor

Airlift Pump Investigation

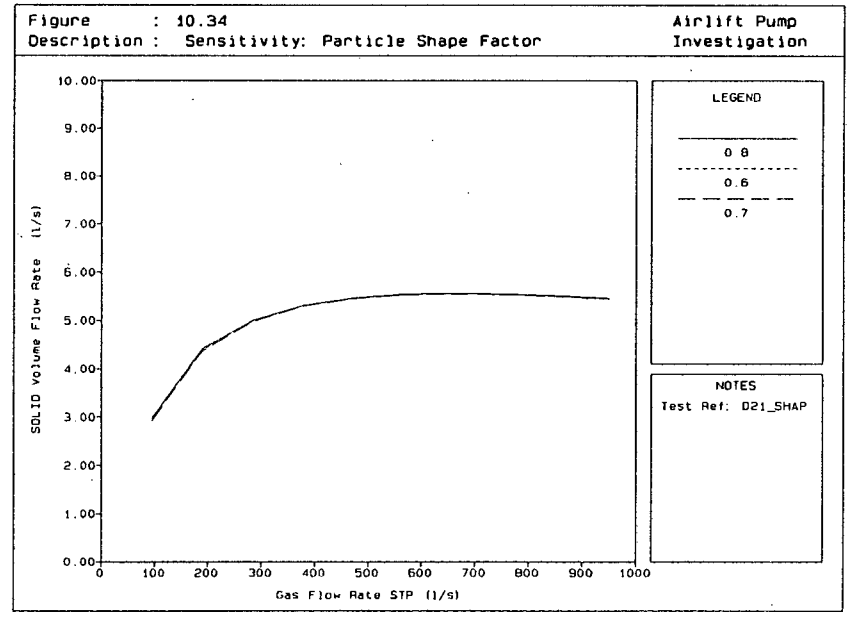

CHAPTER 11

AIRLIFT PUMP EFFICIENCY

Giot (1982) defines the efficiency of an airlift pump as

$$\eta = \frac{\text{power required for lifting solids}}{\text{power input by compressor}} \tag{11.1}$$

Referring to figure 4.1, Giot (1982) expresses equation (11.1) as

$$\eta = \frac{Q_s\, g\, [(l_1 + l_2)(\rho_s - \rho_l) + (l_3 - l_1)\, \rho_s]}{Q_g \text{STP}\, P_{atm}\, ln \frac{P_{atm} + l_1 g \rho_l}{P_{atm}}} \tag{11.2}$$

Throughout the literature (Weber 1976, Giot 1982) airlift pump efficiencies have been shown to be low. Furthermore the point of maximum efficiency corresponds to air flow rates that are lower than required to achieve maximum mixture output flow rates. Figure 11.1, 11.2 and 11.3 respectively show the effect on airlift pump efficiency of varying lift height, injection/sea depth and delivery pipe diameter. The graphs have been shown for the standard airlift pump layout discussed in Chapter 10, with changes in the lift height, injection/sea depth and delivery pipe diameter variables listed in Table 10.3.

Referring to figure 11.1, with increased lift height, there is a decrease in the airlift pump efficiency and solid volume flow rate. The decrease in efficiency is in the order of ± 3% at lower gas flow rates. The figure also shows the trend of maximum efficiency at lower gas flow rates than required for maximum output. The maximum efficiency for this particular airlift pump configuration is approximately 25-30% at gas flow rate of 120 l/s.

Figure 11.2 shows the effect of injection depth on the airlift pump efficiency. The figure shows that an increase in the injection/sea depth results in an increase in the airlift pump efficiency.

Similar to the injection/sea depth, referring to figure 11.3, an increase in the delivery pipe diameter also results in an increase in the airlift pump efficiency. In both these instances the airlift pump efficiency is low and maximum efficiencies occur at lower gas flow rates than required for maximum output flow rates.

From the above, it can be seen that increases in the injection/sea depth, and delivery pipe diameters result in increased efficiencies while an increase in the lift height results in a decreased efficiency. Generally, the maximum efficiency occurs at gas flow rates much lower than required for maximum output flow rates and overall, airlift pump efficiencies are generally low.

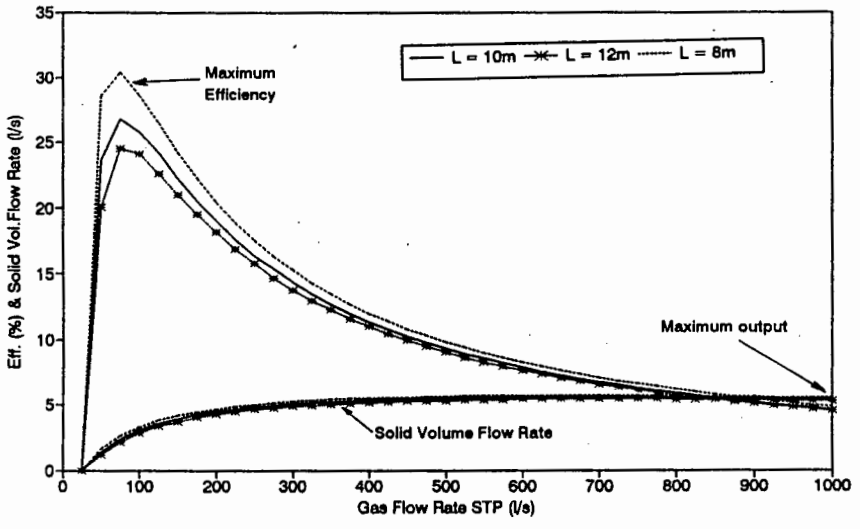

FIGURE 11.1 : Airlift pump efficiency : effect of lift height

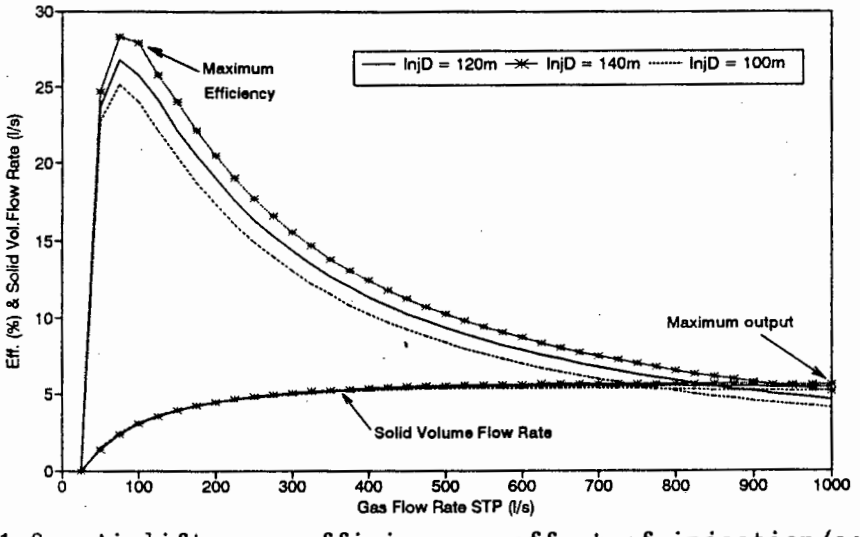

FIGURE 11.2 : Airlift pump efficiency : effect of injection/sea depth

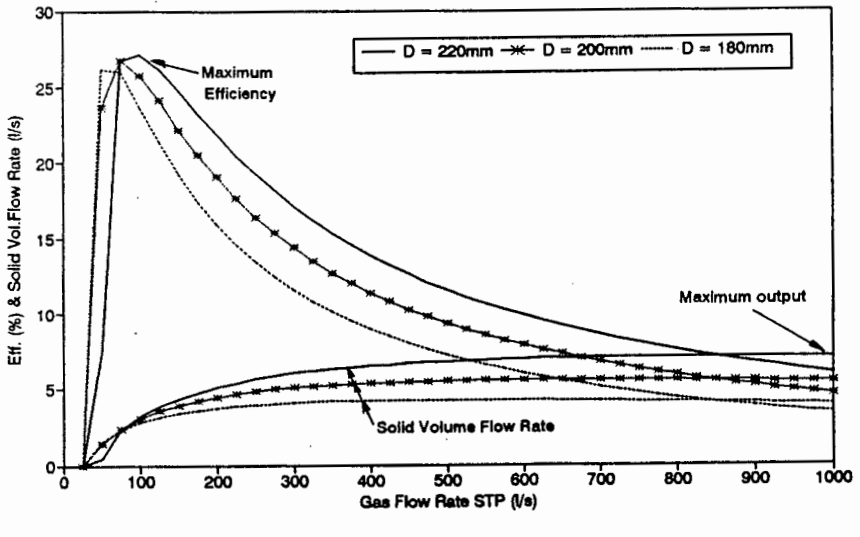

FIGURE 11.3 : Airlift pump efficiency : effect of delivery pipe diameter

CHAPTER 12

SUGGESTIONS FOR FUTURE STUDIES

The scope of this airlift pump study and the data collected was limited to laboratory test facilities of two pipe diameters. Future studies should be conducted on test facilities of differing pipe diameters to obtain more data for the three phase flow model verification. Future studies should also include a higher degree of prototype test data in the model verification.

Prototype airlift pump installations normally discharge the hoisted marine gravel slurry through bends, elbows or pipe wheels on board the vessel. Future studies should be directed at investigating pressure losses associated with these changes in flow direction and ascertain their influence on overall airlift pump performance.

A further suggestion for future study is to investigate the effect of non-vertical airlift pump suction and delivery pipes on delivered output.

It must be stressed, that future studies should include the measurement of all the basic components of three phase flow (such as friction losses and *in situ* concentration) to obtain a firm three phase flow data base for further analytical model verification.

REFERENCES

BERG. R. (1988a): "Hydro-pneumatic conveying of liquid by means of an airlift pump". *MSc dissertation*, University of Cape Town.

BRINKWORTH, B.J. (1968): "An introduction to experimentation", *English University Press*, London.

CHISHOLM, D. (1983): "Two-phase flow in pipelines and heat exchangers", *Pitman Press Ltd.*

CLARK, N.N., MELOY, T.P., FLEMMER, R.L.C. (1985): "Predicting the lift of airlift pumps in the bubble flow regime", *Chem. S.A.*, Vol. 22, pp. 14-17.

CLARK, N.N., DABOLT, R.J. (1986): "A general design equation for airlift pumps operating in slug flow", *Aiche Journal*, Vol. 32, No. 1, pp. 56-63.

COOKE, R. (1991): "The dense phase hydraulic transport of high concentration cyclone classified tailings in pipelines", *PhD Dissertation*, University of Cape Town.

DEDEGIL, M.Y. (1974): "Feststoff Förderung nach dem Lufthebe Verhahren", *Fördern und Heben*, Vol. 24, No. 14.

DEDEGIL, M.Y. (1982 a): "Increase of the suction head by means of the "airlift" method", *Bulk solids handling*, Vol. 2, No. 2, pp. 267-269.

DEDEGIL, M.Y. (1982 b): "Principles of airlift techniques", Chapter 12 in unknown source, *Institute für Fördertechnik, Abteilung Strömmings - fördertechnik*, University of Karlsruhe.

EINSTEIN, H.A. GRAF, W.H. (1966): "Loop system for measuring sand water mixtures", *Journal of Hyd. Div.*, ASCE, Vol. 92, No HY1.

GIBSON, L.A. (1925): "The airlift pump", *Hydraulics and its applications*, 3rd edition, Constable and Company Limited.

GIOT, M., BERLEUR (1986): "Application of the airlift principal to solve maintenance problems", *Hydrotransport 10*, Paper D2.

GOVIER, G.W., AZIZ, K. (1972): "The flow of complex mixture in pipes", *Van Nostrand Reinhold Company.*

GIOT, M. (1982): "Three phase flow", *Handbook of Multiphase systems - G Hetsroni*, Ch. 7.2, Hemisphere Publishing Corp.

HALDE, R., SVENSSON, M. (1981): "Design of airlift pumps for continuous sand filters", *Chemical Engineering Journal*, (21); pp. 223-227.

HETSRONI, G. (1982) "Handbook of Multiphase Systems", Hemisphere Publishing Corp.

KYTOMAA, H.K., BRENEN, C.E. (1986): "Some observations of flow patterns and statistical properties of three component flows", *International Symposium on Slurry flow, ASME*, pp. 95-101.

KATO, H., MIYAZAWA, T., TIMAYA, S., IWASAKI, T. (1975): "A study of an airlift pump for solid particles", *Bul. of the JSME*, Vol. 18, No. 117, pp. 286-294.

LAZARUS, J.H. (1982): "Pump and pipeline instrumentation", *Short Course preceding Hydrotransport 8*, Paper 1 and Paper 14.

LAZARUS, J.H., NEILSON, I.D. (1978): "A generalised correlation for friction head losses of settling mixtures in horizontal smooth pipelines", *5th Int. Conf. on the Hydraulic Transport of Solids in Pipes*, Paper B1, p.B1-1 to B1-33.

RICHARDSON, J.F., ZAKI, W.N. (1954 a): "The sedimentation of a suspension of uniform spheres under conditions of viscous flow", *Chemical Engineering Science*, Vol. 3, pp. 65-73.

RICHARDSON, J.F., ZAKI, W.N. (1954 b): "Sedimentation and Fluidisation: Part 1", Traus, Just, Chem. Eng. Vol. 32, pp. 35-53.

STENNING, A.H., MARTIN C.B. (1968): "An analytical experimental study of airlift pump performance", *Journal of Eng. for Power*, Transactions of ASME, pp. 106-110.

SHEBATIN, V.G., SOKOLOV, V.N., DOMANSKII, I.V., DAVYDOV, I.V. (1977): "Airlift conveying of liquids and suspensions", *Journal of Applied Chemistry of the USSR*, Vol. 50(4), pp. 823-826.

SIVE, A.W. (1988): "An analytical and experimental investigation of the hydraulic transport of high concentration mixed regime slurries", *PhD dissertation*, University of Cape Town.

WEBER, M., DEDEGIL, M.Y. (1976 a): "Transport of solids according to the airlift principle", *Hydrotransport 4, BHRA Fluid Engineering*, Paper H1 pp. H1-1 to H1-14.

WEBER, M. (1976 b): "Das airlift verfahren und seine Einsetzbarkeit zur Förderung von Mineralien aus der Tiefsee", *Meerestechnique 7*, 1976, pp. 189-199.

WEBER, M., DEDEGIL, Y., FELDLE, G. (1978): "New experimental results regarding extreme operating conditions in airlifting and vertical hydraulic transport of solids according to the jet lift principle and its applicability to deep-sea mining", *Hydrotransport 5, BHRA Fluid Engineering*, Paper F7, pp. F7-109 to F7-132.

WEBER, M. (1982): "Vertical hydraulic conveying of solids by airlift", *Journal of Pipelines 3*, No. 2, pp. 137-152.

WEBBER, N.B. (1971): *Fluid Mechanics for Civil Engineers*, Chapman and Hall Ltd.

ZUBER, N., FINDLAY, J.A. (1965): "Average volumetric concentration in two-phase flow systems", *Journal of Heat Transfer*, Trans of the ASME, Vol. 87, pp. 453-468.

BIBLIOGRAPHY

APAZIDES, N., (1985) : "Influence of bubble expansion and relative velocity on the performance and stability of an airlift pump", *International Journal of Multiphase Flow*, Vol. 11(4), pp. 459-479.

ALVES, G.E. (1954) : "Two phase flow in pipes", *Fluid and Particle Mechanics*, Ch. 6.

BAIN, A.G., BONNINGTON, S.T. (1970) : "Flow in vertical pipes", *Hydraulic Transport of Solids by Pipeline*, Vol. 5, Ch. 2, pp. 33-35.

BERG, R.R., LAZARUS, J.H. (1987 a) : "Airlift pumps for ocean mining application", *Research Report 1 for De Beers Marine*, HTR, University of Cape Town.

BERG, R.R., LAZARUS, J.H. (1987 b) : "Airlift pumps for ocean mining application", *Research Report 2 for De Beers Marine*, HTR, University of Cape Town.

BERG, R.R., LAZARUS, J.H. (1987 c) : "Airlift pumps for ocean mining application", *Preliminary to Research Report 3 for De Beers Marine*, HTR, University of Cape Town.

BERG, R.R., LAZARUS, J.H. (1987 d) : "Airlift pump investigation: static dilation tests", *Research Report 3 for De Beers Marine*, HTR, University of Cape Town.

BERG, R.R., LAZARUS, J.H. (1987 e) : "Airlift pump investigation: dynamic void ratios", *Research Report 4 for De Beers Marine*, HTR, University of Cape Town.

BERG, R.R. (1985) : "Settling velocities", *BSc dissertation*, University of Cape Town.

BERG, R.R., LAZARUS, J.H. (1988 b) : "Airlift pump investigation: requirements for 3 phase flow analysis", *Research Report 6 for De Beers Marine*, HTR, University of Cape Town.

BERG, R.R., LAZARUS, J.H. (1988 c) : "Airlift pump investigation: 3 phase flow analysis", *Research Report 7 for De Beers Marine*, HTR, University of Cape Town.

BERG, R.R., LAZARUS, J.H. (1988 d) : "Airlift pump investigation: 2 phase solid-liquid vertical pipeline tests", *Research Report 8 for De Beers Marine*, HTR, University of Cape Town.

BERG, R.R., LAZARUS, J.H. (1988 e) : "Airlift pump investigation: development of equations to model solid-liquid hoisting in the suction pipe of an airlift pump", *Research Report 9 for De Beers Marine*, HTR, University of Cape Town.

BERG, R.R., LAZARUS, J.H. (1988 f) : "Airlift pump investigation: sensitivity analysis on variables in the model used to predict solid-liquid hoisting in the suction pipe of an airlift pump", *Research Report 10 for De Beers Marine*, HTR, University of Cape Town.

BERG, R.R., LAZARUS, J.H. (1988 g) : "Airlift pump investigation: single particle settling velocities in air-water mixtures", *Research Report 11 for De Beers Marine*, HTR, University of Cape Town.

BERG, R.R., LAZARUS, J.H. (1988 h) : "Airlift pump investigation: hindered settling velocity of particles in air-water mixtures", *Research Report 12 for De Beers Marine*, HTR, University of Cape Town.

BERG, R.R., LAZARUS, J.H. (1989 a) : "Airlift pump investigation: 3 phase *in situ* concentration tests - 50 mm airlift pump", *Research Report 13 for De Beers Marine*, HTR, University of Cape Town.

BERG, R.R., LAZARUS, J.H. (1989 b) : "Airlift pump investigation: 3 phase *in situ* concentration tests - 90 mm airlift pump", *Research Report 14 for De Beers Marine*, HTR, University of Cape Town.

BERG, R.R., LAZARUS, J.H. (1988 i) : "Airlift pump investigation: 3 phase experimental 40 mm airlift pump particle size tests", *Research Report 15 for De Beers marine*, HTR, University of Cape Town.

BERG, R.R., LAZARUS, J.H. (1989 c) : "Airlift pump investigation: 3 phase experimental 40 mm airlift pump submergence ratio tests", *Research Report 16 for De Beers Marine*, HTR, University of Cape Town.

BERG, R.R., LAZARUS, J.H. (1988 j) : "Airlift pump investigation: 3 phase experimental 90 mm airlift pump concentration tests", *Research Report 17 for De Beers Marine*, HTR, University of Cape Town.

BERG, R.R., LAZARUS, J.H. (1988 k) : "Airlift pump investigation: 3 phase experimental 90 mm airlift pump annular gas injector tests", *Research Report 18 for De Beers Marine*, HTR, University of Cape Town.

BERG, R.R., LAZARUS, J.H. (1989 d) : "Airlift pump investigation: verification of 3 phase analysis technique", *Research Report 19 for De Beers Marine*, HTR, University of Cape Town.

BERG, R.R., LAZARUS, J.H. (1989 e) : "Airlift pump investigation: sensitivity on variables in the model used to predict operating curves for prototype airlift pumps", *Research Report 21 for De Beers Marine*, HTR, University of Cape Town.

BERG, R.R., LAZARUS, J.H. (1989 f) : "Airlift pump investigation: software for the design of airlift pumps - user manual", *Research Report 20 for De Beers marine*, HTR, University of Cape Town.

BERG, R.R., LAZARUS, J.H. (1989 g): "Airlift pump investigation: fines investigation", *Research Report Sup. 4 for De Beers Marine*, HTR, University of Cape Town.

BERGEAUD, F. (April 1973): "How to calculate airlifts for marine dredging and mining", *Ocean Industry*, pp. 169-172.

BERNARD, J., FITREMANN, J-M. (1987): "Gas-liquid-solid transient vertical flow - the gas lifting of polymetallic nodules", *3rd Int. Conf. on Multi-Phase Flow, BHRA Fluid Eng.*, Paper K3, pp. 383-396.

BLEVIUS, R.D. (1984): "Applied fluid dynamics handbook", *Van Nostrand and Company Inc.*

BRAUER, H. (1971): "Grundlagen der Einphasen und Mehrphasenströmungen", Verlag Sauerländer Aarau und Frankfurt/Main.

CHISHOLM, D., SUTHERLAND, L.A. (1969): "Prediction of pressure gradients in pipeline systems during two-phase flow", *Institution of Mechanical Engineers*, Vol. 184, Part 3c, Paper 4.

CLAUSS, G. (1978 a): "Hydraulic lifting in deep-sea mining", *Marine Mining*, Vol. 1, No. 3, pp. 189-208.

CLAUSS, G. (b): "Theoretical and experimental investigations of deep ocean mining systems and their economic implications", Source unknown, *Institüt für Schiffstechnik, Technische Universität Berlin.*

DEDEGIL, M.Y. (1978): "Entwicklungsstand und Tendenzen beim Feststoffördern nach dem Lufthebe verfahren", *Maschinenmarkt, Würzenburg*, 34,39; pp. 765-769.

FELDE, G.: "Theoretische und Experimentelle Untersuchungen uber die Vertikale Hydraulische Feststöfförderung nach dem Strahlpumpverfahren", (dissertation), University of Karlsruhe.

FRITZ, H.R. (1969 a): "Theoretical and practical aspects of the airlift reverse circulation boring system", *Bohren, Sprengen, Räumen.*

FRITZ, H.R. (b): "Airlift drilling rigs serving for water supply, lowering of the ground water level and for pile foundation drillings", Offprint from: *Bohren Sprengen, Räumen.*

GIDDINGS, T. (1983): "The use of airlift pumps to develop wells", *Groundwater*, V.21(4), pp. 521-522.

GIEK, K. (1979): "A collection of technical formulae", 4th edition, Geick-verlag.

GOLAN, L.P., STENNING, A.M. (1969): "Two phase vertical flow maps", *Institution of Mechanical Engineers*, Vol. 184, Part 3c, Paper 14.

GRABOW, G. (1981): "Hydro-pneumatischer und hydraulischer Feststofftransport in Vertikalen Rohrleitungen", *Neue Bergbautechnik 11 Jg.*, Heft 8, pp. 447-451.

HILL, J.C.C. (1978): "Special dredging systems", *Reprint from Dredging and Port Construction.*

HEYWOOD, N.I., CHARLES, M.E. (1978): "The pumping of pseudo-homogeneous, shear-thinning suspensions using the airlift principle", *Hydrotransport 5, BHRA Fluid Eng.*, Paper F5, pp. F5-59 to F5-80.

JULIAN, F.M., DUKLER, A.E. (1965): "An eddy viscosity model for friction in gas-solid flow", *AICHE Journal*, Vol. 11, No. 5, pp. 853-858.

KOUREMENOUS, D.A., STAICOS, J. (1985): "Performance of a small airlift pump", *the International Journal of Heat and Flow*, vol. 6, No. 1, pp. 217-222.

KROHNE: "DH80 - Radiometric density meter", *Installation and Operating Instruction Handbook.*

LAZARUS, J.H., (1984): *CE302 - Hydraulic Engineering Laboratory Manual*, University of Cape Town.

LAZARUS, J.H. (1985 a): "Pumping of gravels from the ocean bed for diamond mining", *Research Report for ODM*, HTRU, University of Cape Town.

LAZARUS, J.H. (1985 b): "Ocean diamond mining", *Research Report for ODM*, HTRU, University of Cape Town.

LILLIE, E.S.B. (1987): "Thesis 42: 40 mm airlift pump", *BSc Dissertation*, University of Cape Town.

LOOMIS, A.W. (1980): "Compressed air and gas data", *Chapter 31: Airlift Pumping*, Ingersoll-Rand Company, Washington.

MARTIN, C.S. (1976): "Vertically downward two-phase slug flow", *Journal of fluids Eng.*, Trans of the ASME, pp. 715-722.

McINTOSCH, J. (1988): "Airlift pump investigation", *BSc Dissertation*, University of Cape Town.

STONE, J.H. (1987): "A program to calculate airlift pump performance", *Microsoftware for Engineers*, Vol. 3, No. 3.

STANISLAV, J.F., KOKAL, S., NICHOLSON, M.K. (1986): "Gas liquid flow in downward and upward inclined pipes", *The Canadian Journal of Chemical Engineering*, Vol. 64, pp. 881-886.

SHEBATIN, V.G., SOKOLOV, V.N., DOMANSKII, I.V., DAVYDOV, I.V. (1977): "Airlift conveying of liquids and suspensions", *Journal of Applied Chemistry of the USSR*, Vol. 50(4), pp. 823-826.

TONG, L.S. (1965): "Boiling heat transfer and two phase flow", *John Wiley & Sons, Inc.*

TEIFKE, J., BOHNET, M. (1980): "Dreiphasenströmung im Senkrechten Rohr", *Verfahrenstechnik 14*, No. 4, pp. 227-231.

UNKNOWN: "A versatile Italian dredge pump system", Reprint from "*World Dredging & Marine Construction Magazine*".

WEBER, M., SCHAUKI, N. (1967): "Pneumatische und Hydraulische Förderung", *Auf-bereitungs technik*; *Jahrgang 8*, N10, pp. 594-558.

APPENDIX A

USERS MANUAL FOR AIRLIFT PUMP SOFTWARE

(AIRLIFT)

APPENDIX A

USERS MANUAL FOR AIRLIFT PUMP SOFTWARE

(AIRLIFT)

A.1 INTRODUCTION

This appendix serves as a user manual for the program "AIRLIFT" which incorporates the proposed theory discussed in this dissertation.

The program predicts operating curves for the following range of input variables :

1. Injection depth
2. Lift height
3. Suction pipe length
4. Delivery pipe
   - diameter
   - roughness
5. Suction pipe
   - diameter
   - roughness
6. Liquid
   - density
   - temperature
7. Solid density
8. Gas
   - density
   - pressure at outlet
9. Particle
   - dimension
   - size percentages
   - shape factors
10. Solid-liquid delivered volumetric concentration.

In an added feature, the above variables can be altered to perform a sensitivity analysis and check the relative effect on the operating curves.

The program is extremely user friendly and numerous help screens aid the operator through the input and simulation routines. Furthermore, the program is menu driven with a range of topics for each choice.

All input is in tabular format allowing changes to be made and updated with ease.

The output operating curves can be plotted as :

1. Solid-liquid mixture flow rates at the delivery outlet
2. Liquid flow rates at the delivery outlet
3. Solid volume flow rates at the delivery outlet
4. Solid mass flow rates at the delivery outlet
5. Solid-liquid mixture velocity in the suction pipe.

Calculation of these output operating curves is achieved with the procedure outlined in Appendix C.

After installation the program maintains the following directory structure :

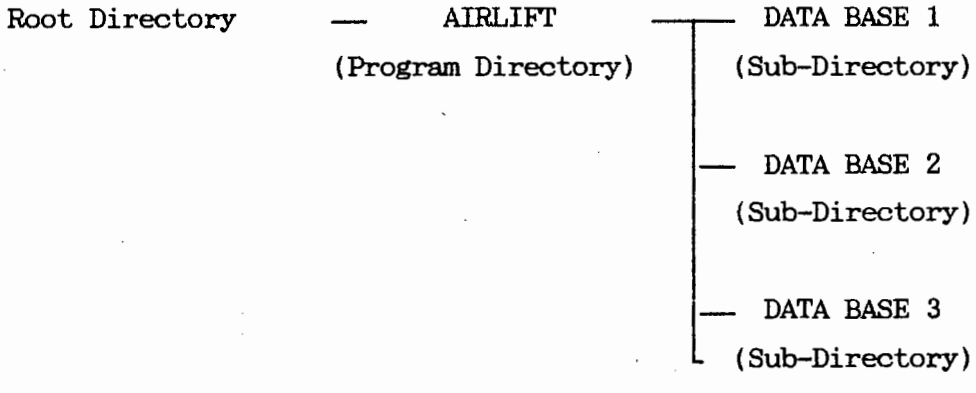

All data files are saved in these sub-directories and have the extension .HTR for recognition, e.g. DBO71324.HTR

To run the program, change directory to the main program directory, then type "AIRLIFT.EXE" and press Return at the DOS prompt.

Note :

Throughout the program the left, right, up and down cursor keys are used to move around the screen. The current position is always highlighted by reverse video mode.

A.2 MAIN MENU

The main menu of the "AIRLIFT" program is shown in Figure A.1.

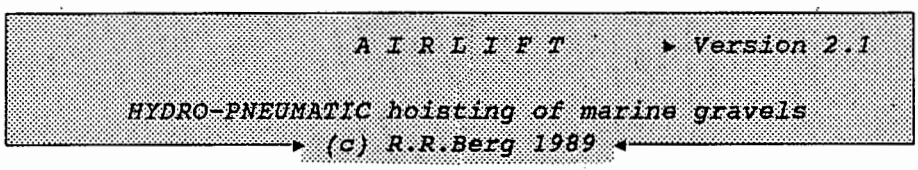

Main Menu	Topic Menu
1 Exit Program	1 Returns to DOS
2 File Management	
3 Edit input data	
4 Analysis Output Options	
5 Utilities	

CURRENT DATA FILE : No Files in use

Use ↑ ↓ → and ◂┘ to select Topic Menu

Figure A.1

To activate one of the above choices, press either the number preceding the option, or highlight the option using the cursor keys. Then press the "ENTER" key to select the required option.

On highlighting each option in the Main Menu column, the available sub-topics are shown in the "Topic Menu" column on the righthand side.

A.3 EXIT PROGRAM

To exit the program, press "1" or highlight "Exit Program" and press "ENTER".

A.3.1 Return to DOS

To exit to DOS, press return when "Return to DOS" is highlighted. To return to the program, press "ESCAPE" or use the arrow keys to move back to the Main Menu column on the lefthand side.

A.4 FILE MANAGEMENT

Figure A.2 shows the topics available under "File Management" in the Main Menu.

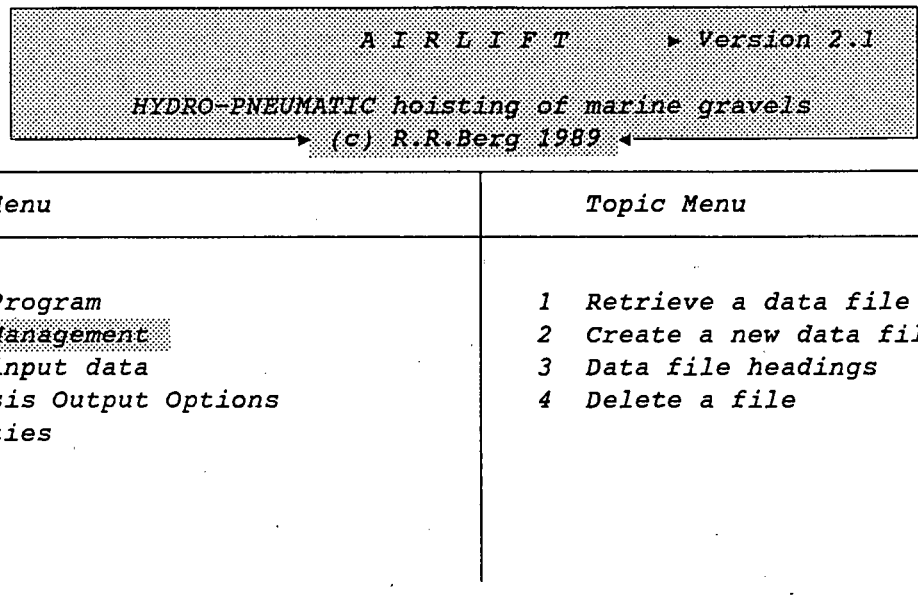

Figure A.2

To enter the topic menu, press "2" or use the cursor keys to highlight the desired topic.

A.4.1 Retrieve a data file

Figure A.3 shows the screen that appears on choosing the "Retrieve a data file" option.

RETRIEVE A DATA FILE *F1 = HELP*

SELECT THE DATABASE OR SUBDIRECTORY/DRIVE FROM WHICH TO RETRIEVE THE DATA FILE

1. *Data Base 1*
2. *Data Base 2*
3. *Data Base 3*
4. *User defined drive/directory*
5. *current directory*
6. *A: - Drive*

Enter choice 1 to 6..

Figure A.3

The user is prompted to select the sub-directory or drive where the data file is kept. The available choices are shown in Figure A.3. A choice is selected by using the numeric key indicated. For choice 4, the user is requested to indicate the drive, e.g. :

C:\AIRLIFT\USER

Incorrect specification results in an error warning.

A help option is activated by pressing the F1 key. Figure A.4 below shows the help screen that is superimposed on the existing screen.

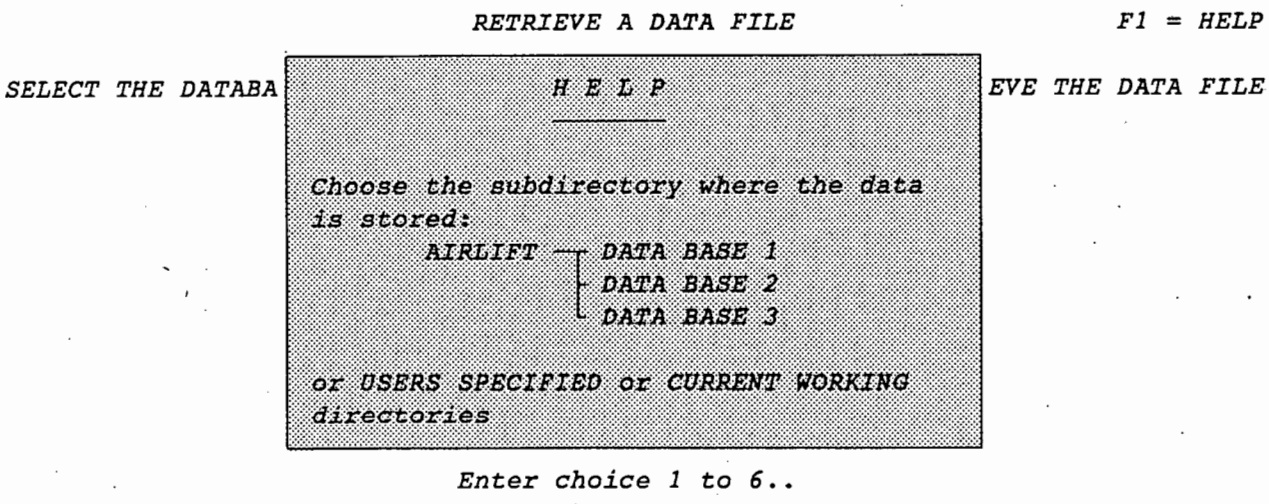

Figure A.4

After the drive or sub-directory in which the data file is kept has been specified, the "Select File Table" shown in Figure A.5 appears on the screen.

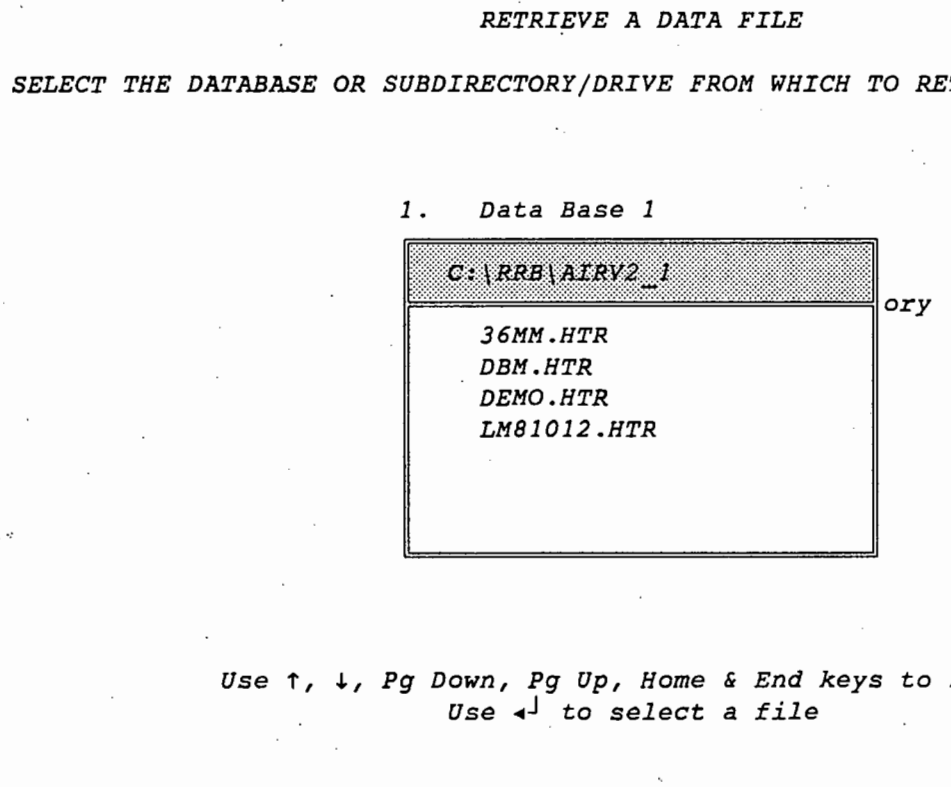

Figure A.5

This "Select File Table" appears whenever a file name is requested. Use the cursor keys to scroll up and down the list, highlighting the files. When the desired file is highlighted, press "ENTER". The main menu now appears and the data file name is displayed on the screen.

A.4.2 Create a new data file

This option creates a data file for use. Select the directory in which to store the data file as discussed in Section A.4.1 above. If the file exists, you will be prompted for a new file name.

Note :

The maximum length of a file name is 8 characters.

When the name has been accepted as valid, the file is created with zero values for all input parameters. These are edited by the user in Section A.5. ("Edit Input Data".)

In order to identify data files, a basic file header is saved along with the data. Therefore, the "Data File Headings" screen now appears for user input. This screen is discussed in A.4.3 below.

A.4.3 Data file headings

The screen to identify a data file is accessed while creating a file, but can also be accessed at any time by choosing the "Data File Headings" topic menu. Figure A.6 shows the screen that appears for items to be specified or changed.

E D I T F I L E D E T A I L S *F1 = HELP*

CURRENT FILE : LM81012.HTR

Material Description	*Malmsbury Shale*
Delivery pipe dia. (NB)	*6,8 & 12 "*
Solid-Liquid Conc. (%)	*2,5 & 7% by volume*
Block number	*n/a*
Sub block number	*n/a*
Test Date	*1991*
Operator	*RRBerg*
Additional comments	*Green Point Airlift*

Use ↑ ↓ to select cell [Type details and press RETURN (Max. 30 chars.)]
[Esc] to return to main menu

Figure A.6

A.4.4 Delete a file

The file to be deleted is again chosen using the "Select File Table". (Refer to A.4.1).

If the user selects the current file, a warning message appears on the screen. Pushing any key will not delete the file, however a prompt appears verifying the file to be deleted. To accept the command, press "ENTER" and the file is deleted. "ESCAPE" returns to the main menu without deleting the file.

A.5 EDIT INPUT DATA

Figure A.7 shows the topics available for "edit input data" in the main menu.

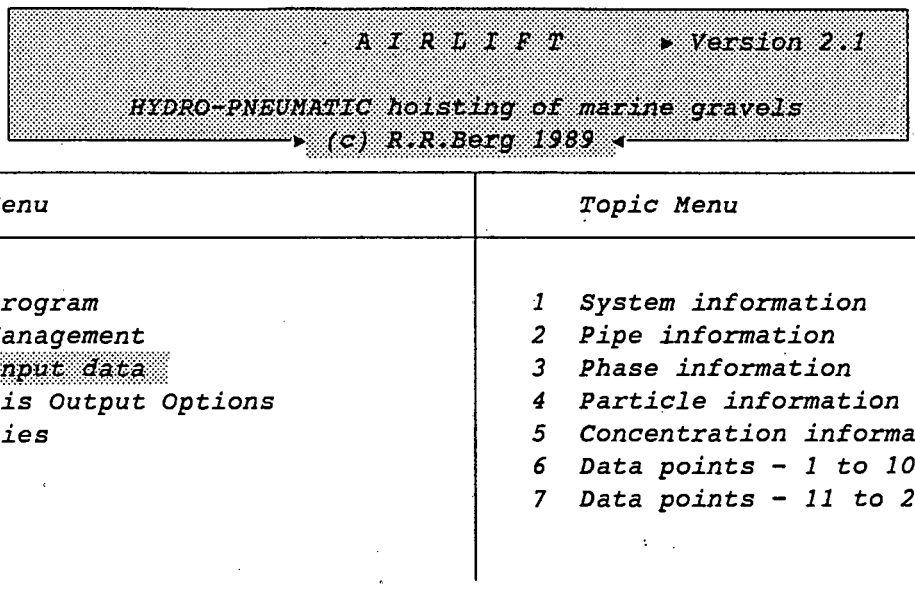

Figure A.7

In this section, the variables used for the analysis are entered into the various tables listed in the topic menu on the righthand side.

Note :

All changes made to any of the seven topic item tables are saved to the current file.

The following procedure is used for all tabular input :

1. The cursor keys are used to highlight the position for data entry.

2. The new value is entered. (At the bottom of the screen a prompt displays the data being entered).

3. Entered data is checked for validity. If the key is invalid, the program will "beep" and prevent the data from being entered.

   Furthermore, if the data entered is not within the range of the minimum and maximum entry permitted, the program indicates that the data is invalid.

4. Incorrect data entry may be deleted by using the backspace key.

5. On data entry completion, the "RETURN" key is pressed and the data will appear in the highlighted position in the table.

6. Once the data has been displayed in the highlighted position, the prompt at the bottom of the screen disappears until the next data entry.

7. If a complete column in a table requires repeated data, enter the data anywhere in the column and press the "R" key to repeat that data in the rest of the column.

8. To leave a table, press the "ESCAPE" key. This will automatically save the table on disk and return to the Main Menu.

On each table, except the "Particle Information" table, 10 layout options are given. Each layout option represents a different situation and allows comparisons of various operating conditions. Each layout option also results in a unique set of operating curves for those conditions, thus a sensitivity analysis can be performed.

Note :

The layout numbers in the first column of the tables correspond on each of the "Edit Input Data" topic screens, EXCEPT in the "Particle Information" and "Data Points" screens.

The first layout MUST always be completed in all the tables.

A.5.1 System information

The table for entering the system information is shown in Figure A.8.

I N P U T S Y S T E M T A B L E *F1 = HELP*

File in use : C:\RRB\AIRV2_1\DEMO.HTR

Layout number #	*Injection depth z1(m)*	*Lift height z2(m)*	*Suction length z3(m)*
1	*150.00*	*15.00*	*5.00*
2	*120.00*	*15.00*	*5.00*
3	*100.00*	*15.00*	*5.00*
4	*80.00*	*15.00*	*5.00*
5	*50.00*	*15.00*	*5.00*
6	*150.00*	*15.00*	*5.00*
7	*120.00*	*15.00*	*5.00*
8	*100.00*	*15.00*	*5.00*
9	*50.00*	*15.00*	*5.00*
10	*80.00*	*15.00*	*5.00*

Use ↑ ↓ → to select cell [Type new value and press RETURN]
R - to repeat column entry - [Esc] to return to main menu

Figure A.8

As stated before, the first layout MUST always be completed in all tables. The consequent layouts 2 to 10 are then used for comparisons in the sensitivity analysis.

Note :

In order to determine the number of operating conditions compared in the sensitivity analysis, the program checks the number of layouts completed in the "Injection Depth Column". To safeguard excessive calculation, each layout in this column has to be entered manually and a repeat operation is NOT permitted. On requesting a "repeat" in the Injection Depth Column, a warning message will appear.

A help screen is available by pressing the F1 key. This screen is shown in Figure A.9.

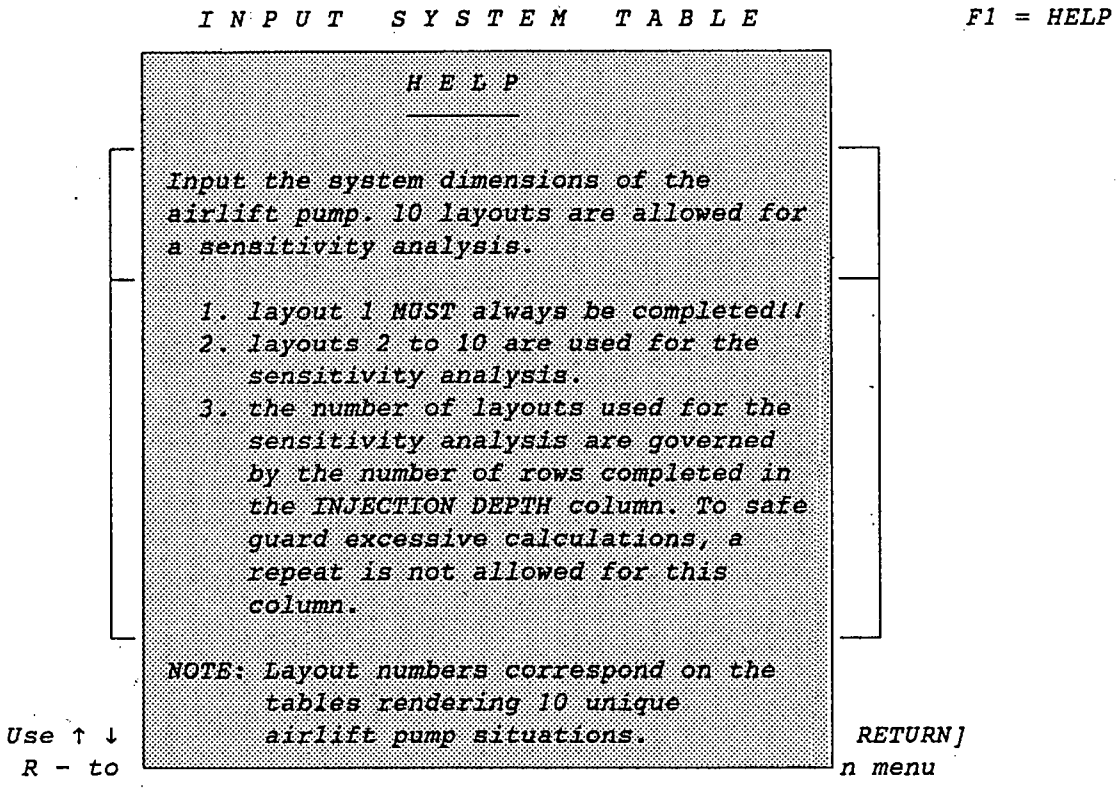

Figure A.9

In Figure A.8, the injection depth refers to the vertical distance from mean sea level to the depth where the gas is injected. The lift height is the vertical distance from mean sea level to the delivery pipe outlet, while the suction length is the vertical distance from the suction inlet to the gas injection point.

A.5.2 Pipe information

The pipe information is entered into the table shown in Figure A.10.

I N P U T P I P E T A B L E *F1 = HELP*

File in use : C:\RRB\AIRV2_1\DEMO.HTR

Layout number #	Delivery Pipe Diameter D(mm)	Delivery Pipe Roughness k(μm)	Suction Pipe Diameter D(mm)	Suction Pipe Roughness k(μm)
1	500.00	150.0	500.00	150.0
2	500.00	150.0	500.00	150.0
3	500.00	150.0	500.00	150.0
4	500.00	150.0	500.00	150.0
5	500.00	150.0	500.00	150.0
6	500.00	150.0	500.00	150.0
7	500.00	150.0	500.00	150.0
8	500.00	150.0	500.00	150.0
9	500.00	150.0	500.00	150.0
10	500.00	150.0	500.00	150.0

Use ↑ ↓ → to select cell [Type new value and press RETURN]
R - to repeat column entry - [Esc] to return to main menu

Figure A.10

Referring to the figure, the delivery pipe starts at the gas injection point and ends at the delivery outlet. The suction pipe starts at the suction inlet and ends at the gas injection point. Internal pipe diameters must be specified.

Figure A.11 shows the help screen that is available by pressing the F1 key.

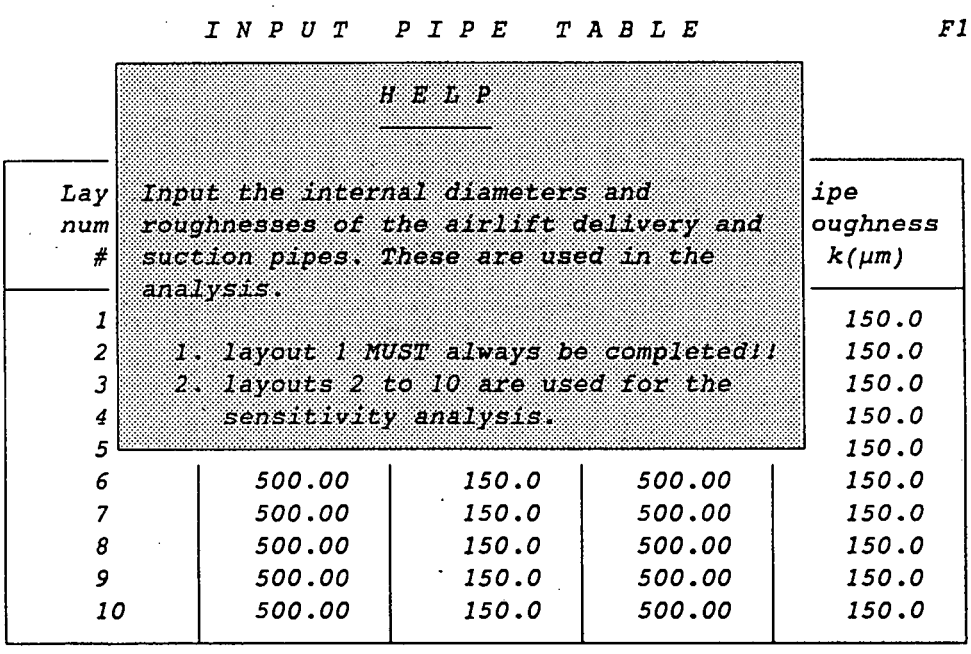

Figure A.11

A.5.3 Phase information

The phase information table (Figure A.12) is used to enter the properties of the solid, liquid and gas phases during operation.

I N P U T P H A S E T A B L E *F1 = HELP*

File in use : C:\RRB\AIRV2_1\DEMO.HTR

Layout number #	Liquid Density Sw	Liquid Temp. (°C)	Solid Density Ss	Gas Density kg/m^3	Gas Pressure STP (Pa)
1	1.025	20.0	2.600	1.204	101300.0
2	1.025	20.0	2.600	1.204	101300.0
3	1.025	20.0	2.600	1.204	101300.0
4	1.025	20.0	2.600	1.204	101300.0
5	1.025	20.0	2.600	1.204	101300.0
6	1.025	20.0	2.600	1.204	101300.0
7	1.025	20.0	2.600	1.204	101300.0
8	1.025	20.0	2.600	1.204	101300.0
9	1.025	20.0	2.600	1.204	101300.0
10	1.025	20.0	2.600	1.204	101300.0

Use ↑ ↓ → to select cell [Type new value and press RETURN]
R - to repeat column entry - [Esc] to return to main menu

Figure A.12

Referring to Figure A.12, the liquid and solid relative densities and the liquid temperature are entered in their respective columns.

Note :

The gas density is entered in kg/m³. The gas pressure refers to standard atmospheric pressure at mean sea level and at the delivery outlet.

The help screen for the phase table is shown in Figure A.13.

I N P U T P H A S E T A B L E *F1 = HELP*

H E L P

Input the properties of the 3 phases during operation. The gas pressure corresponds to the pressure at the delivery outlet. (usually atmospheric)

1. layout 1 MUST always be completed!!
2. layouts 2 to 10 are used for the sensitivity analysis.

Layout number #	D				Gas Pressure STP (Pa)
1					101300.0
2					101300.0
3					101300.0
4					101300.0
5					101300.0
6	1.025	20.0	2.600	1.204	101300.0
7	1.025	20.0	2.600	1.204	101300.0
8	1.025	20.0	2.600	1.204	101300.0
9	1.025	20.0	2.600	1.204	101300.0
10	1.025	20.0	2.600	1.204	101300.0

Use ↑ ↓ → to select cell [Type new value and press RETURN]
R - to repeat column entry - [Esc] to return to main menu

Figure A.13

A.5.4 Particle information

The particle table is shown in Figure A.14. A maximum of 13 sieve sizes can be input. Enter either the percentage passing or percentage retained along with the sieve sizes and particle shape factors. When either the percentage passing or percentage retained columns are completed, push "C" and the remaining column values are automatically calculated.

Should the percentage retained on the sieves be greater or less than 100% by a value of 1%, a warning message will appear.

The percentage retained and percentage passing columns can be reset using ALT R. A further warning message will appear should both these columns contain data when stipulating the calculation operation ("C"). A bubble sort will ensure that the data is in descending order of sieve aperture.

I N P U T P A R T I C L E T A B L E *F1 = HELP*

File in use : C:\RRB\AIRV2_1\DEMO.HTR

Particle variables	*Particle sizes (µm)*	*Percent pass. (%)*	*Percent ret. (%)*	*Shape factor*
1	*16000*	*100.00*	*0.00*	*0.80*
2	*13200*	*98.91*	*1.09*	*0.80*
3	*11200*	*92.60*	*6.31*	*0.80*
4	*9500*	*85.77*	*6.83*	*0.80*
5	*8000*	*71.87*	*13.90*	*0.80*
6	*6700*	*54.25*	*17.62*	*0.80*
7	*4000*	*12.96*	*41.29*	*0.80*
8	*2000*	*0.29*	*12.67*	*0.80*
9	*0*	*0.09*	*0.20*	*0.80*
10	*00000*	*0.00*	*000.00*	*0.80*
11	*00000*	*0.00*	*000.00*	*0.80*
12	*00000*	*0.00*	*000.00*	*0.80*
13	*00000*	*0.00*	*000.00*	*0.80*

=▸ [Alt R] to reset

Use ↑ ↓ → to select cell [Type new value and press RETURN]
[C] Calculate - [R] to repeat column entry - [Esc] to return to main menu

Figure A.14

Figure A.15 shows the help screen available on request.

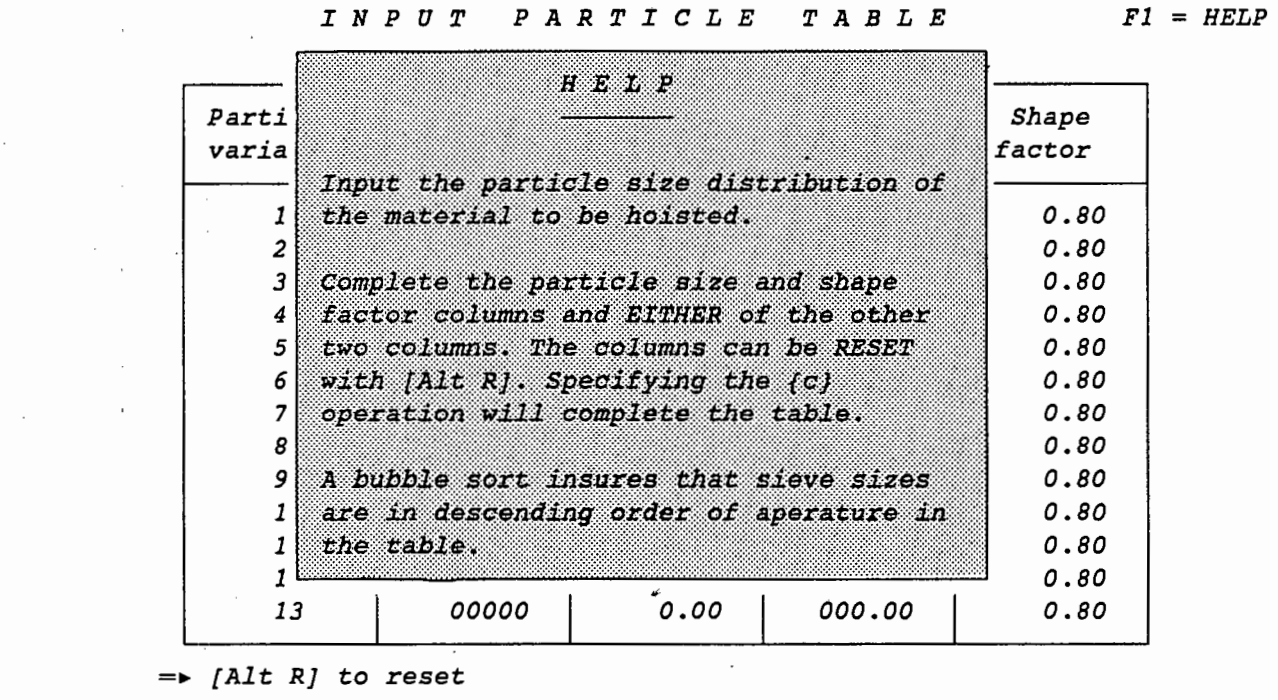

Figure A.15

A.5.5 Concentration information

The solid-liquid concentration table is shown in Figure A.16.

C O N C E N T R A T I O N T A B L E *F1 = HELP*
S O L I D - L I Q U I D
File in use : C:\RRB\AIRV2_1\DEMO.HTR

Layout number #	Delivered concentration by volume Cvd (%)	by weight Cwd (%)	Relative density Sm
1	3.00	7.27	1.0723
2	3.00	7.27	1.0723
3	3.00	7.27	1.0723
4	3.00	7.27	1.0723
5	3.00	7.27	1.0723
6	5.00	11.78	1.1038
7	5.00	11.78	1.1038
8	5.00	11.78	1.1038
9	5.00	11.78	1.1038
10	5.00	11.78	1.1038

=► *[Alt R] to reset*

Use ↑ ↓ → to select cell [Type new value and press RETURN]
[C] Calculate - [R] to repeat column entry - [Esc] to return to main menu

Figure A.16

Referring to the figure, one of the three columns is completed. Pushing "C" results in the calculation of the remaining columns.

For the calculations of the remaining columns, solid (S_s) and liquid (S_l) relative densities from the phase table are required. If these values have not been completed in the phase table, the calculation is not valid. Thus the warning message shown in Figure A.17 appears, giving a summary of the layouts with incomplete information.

The solid-liquid concentrations can either be by weight or by volume. S_m refers to the solid-liquid mixture relative density in the suction pipe.

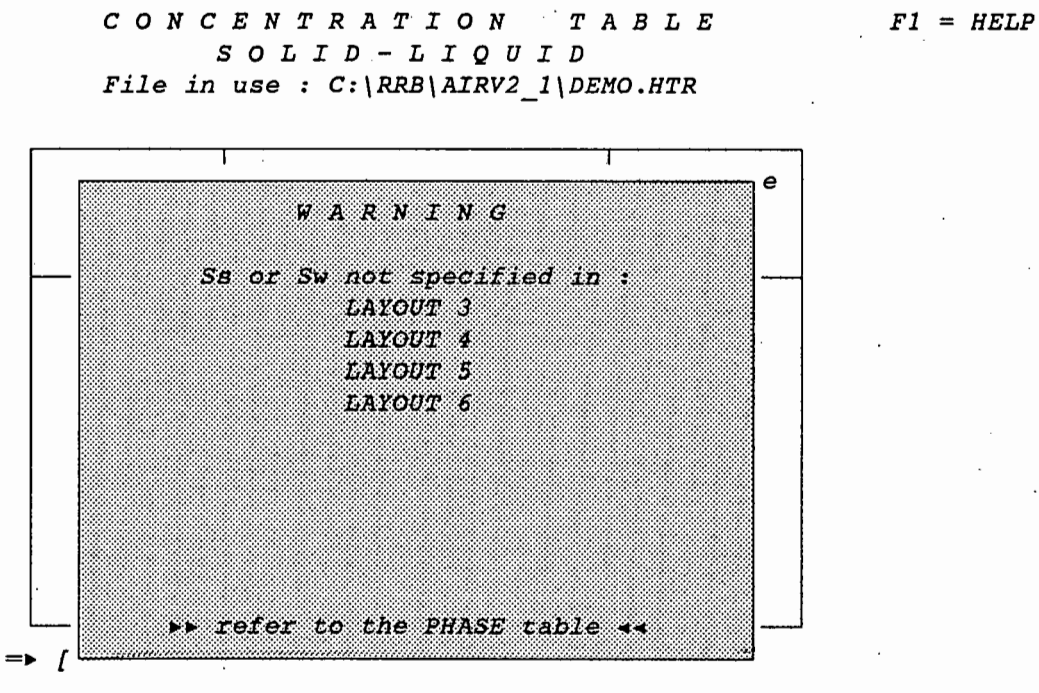

Figure A.17

Should more than one column be completed, a further error message will appear. Figure A.18 shows the help screen available for the table.

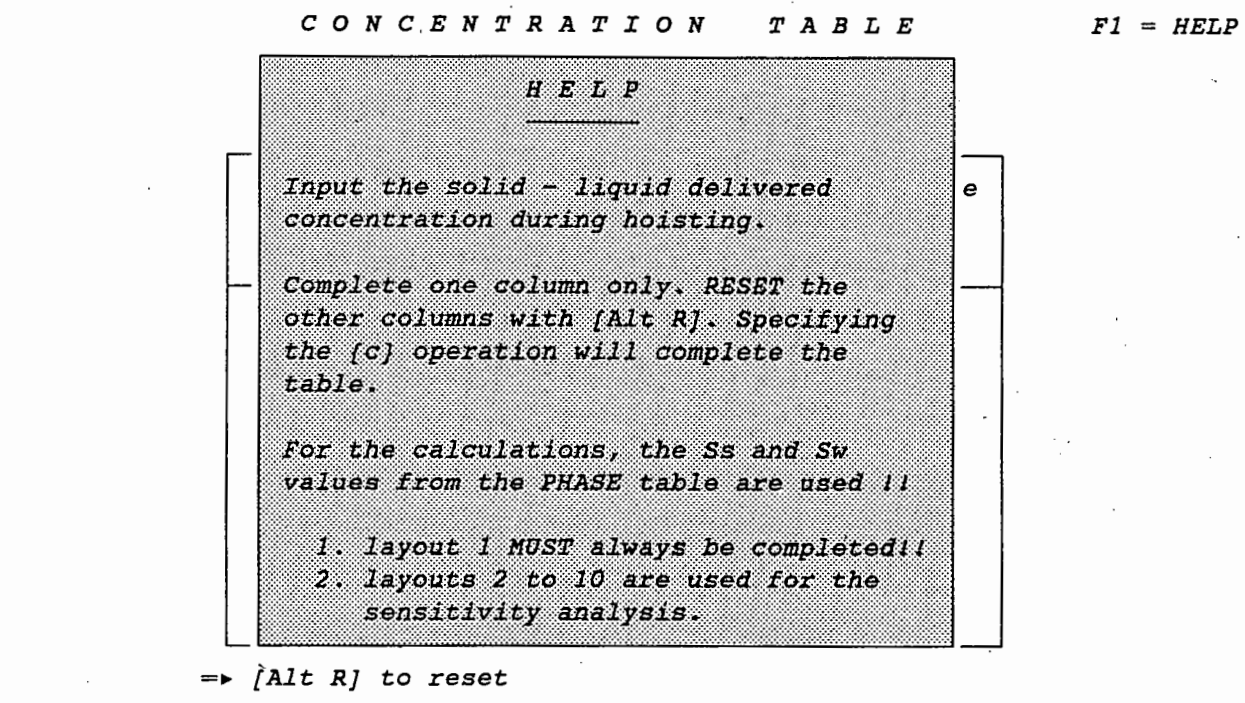

Figure A.18

A.5.6 &

A.5.7 Data points 1 - 20

Should prototype or experimental data be available, a further feature of the "AIRLIFT" is the capability of comparing it to simulated data. The experimental data points are entered into two tables. 1 - 10 are entered in "Data Points 1 - 10" while values 11 - 20 are entered in "Data Points 11 - 20". Figure A.19 shows data Table 1 - 10.

D A T A P O I N T S *F1 = HELP*

File in use : C:\RRB\AIRV2_1\DEMO.HTR

Data Point #	Gas Flow rate STP Qg (l/s)	Solid-Liquid Mixture Flow QmSL (l/s)	Solid-Liquid Delivered Conc. CvdSL (%)
1	100.00	2.00	6.00
2	200.00	3.00	6.00
3	300.00	4.00	6.00
4	0.00	0.00	0.00
5	0.00	0.00	0.00
6	0.00	0.00	0.00
7	0.00	0.00	0.00
8	0.00	0.00	0.00
9	0.00	0.00	0.00
10	0.00	0.00	0.00

Use ↑ ↓ → to select cell [Type new value and press RETURN]
R - to repeat column entry - [Esc] to return to main menu

Figure A.19

If data is present, then the conditions of the system during the data capture are always specified in LAYOUT 1 in all the tables.

Furthermore, the gas flow rate for the FIRST data point must be NON-ZERO if measured data has been input.

Figure A.20 shows the help screen available for the data tables.

D A T A P O I N T S *F1 = HELP*

H E L P

Input field data measured from tests conducted on experimental and prototype airlift pumps.
Test conditions are specified in LAYOUT 1 of the tables.

NOTE: The gas flow rate for the first data point must be NON - ZERO !!

5	*0.00*	*0.00*	*0.00*
6	*0.00*	*0.00*	*0.00*
7	*0.00*	*0.00*	*0.00*
8	*0.00*	*0.00*	*0.00*
9	*0.00*	*0.00*	*0.00*
10	*0.00*	*0.00*	*0.00*

Use ↑ ↓ → to select cell [Type new value and press RETURN]
R - to repeat column entry - [Esc] to return to main menu

Figure A.20

A.6 ANALYSIS OUTPUT OPTIONS

Figure A.21 shows the topic available for "Analysis Output Options" in the main menu.

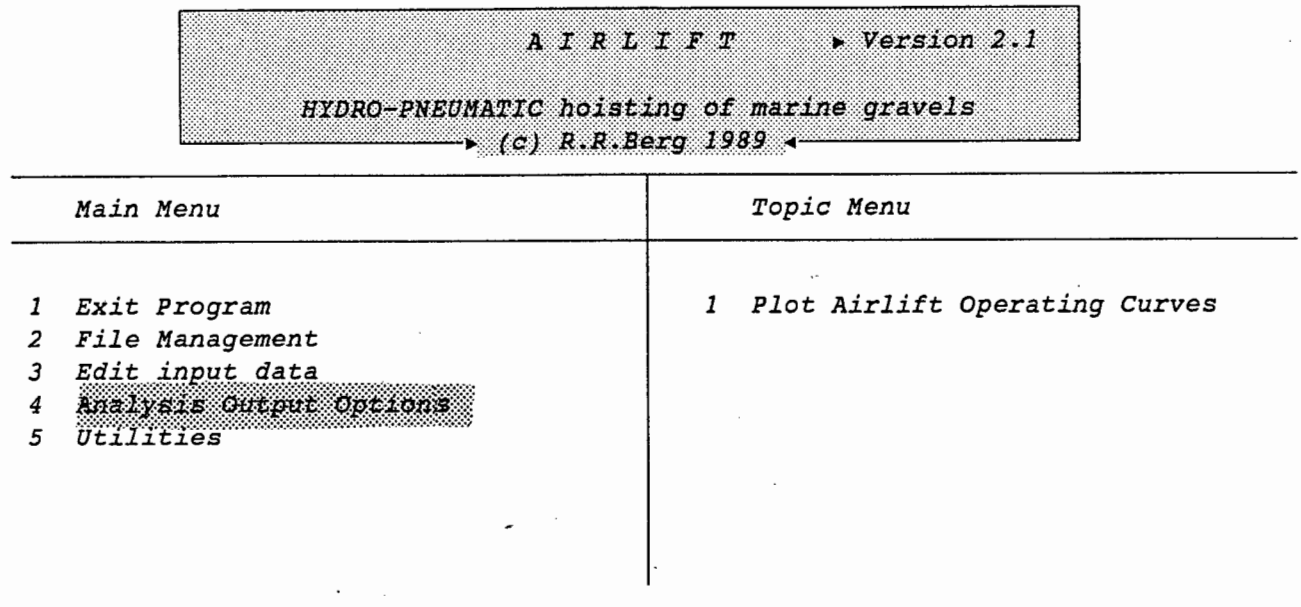

Figure A.21

A.6.1 Plot airlift operating curves

The table for specifying the analysis output is shown in Figure A.22.

Referring to the figure, the table consists of an upper and a lower portion. The F2 key moves the cursor to the lower portion of the table, where the headings for the output graphs are stipulated. The cursor is then returned back to the upper portion by pressing the F1 key.

A N A L Y S I S O U T P U T O P T I O N S *F1 = HELP*

File in use : C:\RRB\AIRV2_1\DEMO.HTR

Edit Keys	Plot Option	(Yes/No)	Analysis & Graph Option	Values
F1 Edit Table	plot DATA	No	X - AXIS	
	plot MODEL	No	Max. QgSTP (l/s)	7000.00
			Inc. QgSTP (l/s)	750.00
F2 Edit Titles			Y - AXIS	
			Max. Qm (l/s)	1200.00
			Max. Qs (l/s)	200.00
↵ yes/no			Max. Ql (l/s)	1500.00
			Max. Ms (kg/s)	300.00
			Max. Vm (m/s)	6.00
	1st. Title	GREEN POINT AIRLIFT RESULTS		
	2nd. Title	Graph 3b: L&M - 12"		
	X Title	GAS FLOW RATE (l/s) STP		
	Y Title	preset to suit graph option		

Use ↑ ↓ → to select cell [Type new value and press RETURN]
[G] - to begin plot - [Esc] to return to main menu

Figure A.22

In the upper portion of the table, the following information is entered :

1. Plot DATA (Yes/No) - "Yes", results in the plotting of the experimentally measured data which was entered in the "Data Points" table (refer Section A.5.6, A.5.7)

2. Plot MODEL (Yes/No) - "Yes", results in the plotting of analysis results calculated using the theoretical model.

Note : "YES" and "NO" are toggled by highlighting either the "YES" or "NO" and pressing "ENTER".

3. Max.Q_gSTP - For the analysis, solid and liquid flow rates are calculated for various input gas flow rates. This item specifies the maximum gas flow rate at standard conditions for the analysis. It also specifies the maximum value on the x-axis during graphing.

4. Inc.Q_gSTP - Specifies the incremental steps from 0 to Max.Q_gSTP (item 3 above) for which output flow rates are calculated. The number of points in the analysis is obtained from

$$\text{Number of analysis points} = \frac{\text{Max.}Q_g\text{STP}}{\text{Inc.}Q_g\text{STP}}$$

Thus if Inc.Q_gSTP is too small, a large number of points are calculated, resulting in a time consuming analysis.

5. Max.Q_m - Specifies the maximum solid-liquid mixture flow rate to be plotted on the y-axis during graphing.

6. Max.Q_s - Specifies the maximum solid VOLUME flow rate to be plotted on the y-axis during graphing

7. Max.Q_l - Specifies the maximum liquid VOLUME flow rate to be plotted on the y-axis during graphing

8. Max.v_m - Specifies the maximum solid-liquid mixture velocity in the suction pipe to be plotted on the y-axis during graphing.

Note :

1. Items 3-9 are entered in the table as disucssed in Section A.5.

2. Items 5-9 are only used in scaling the graphs for the output and can be altered after the analysis.

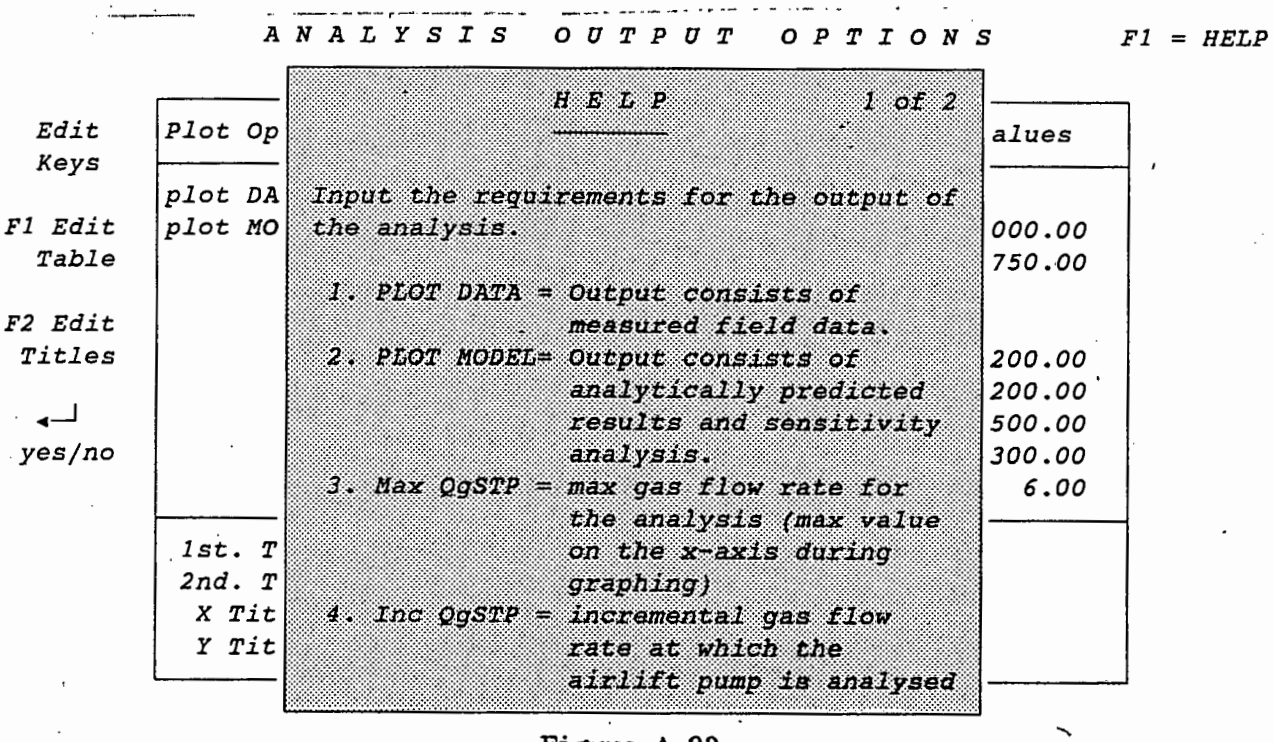

Figure A.23

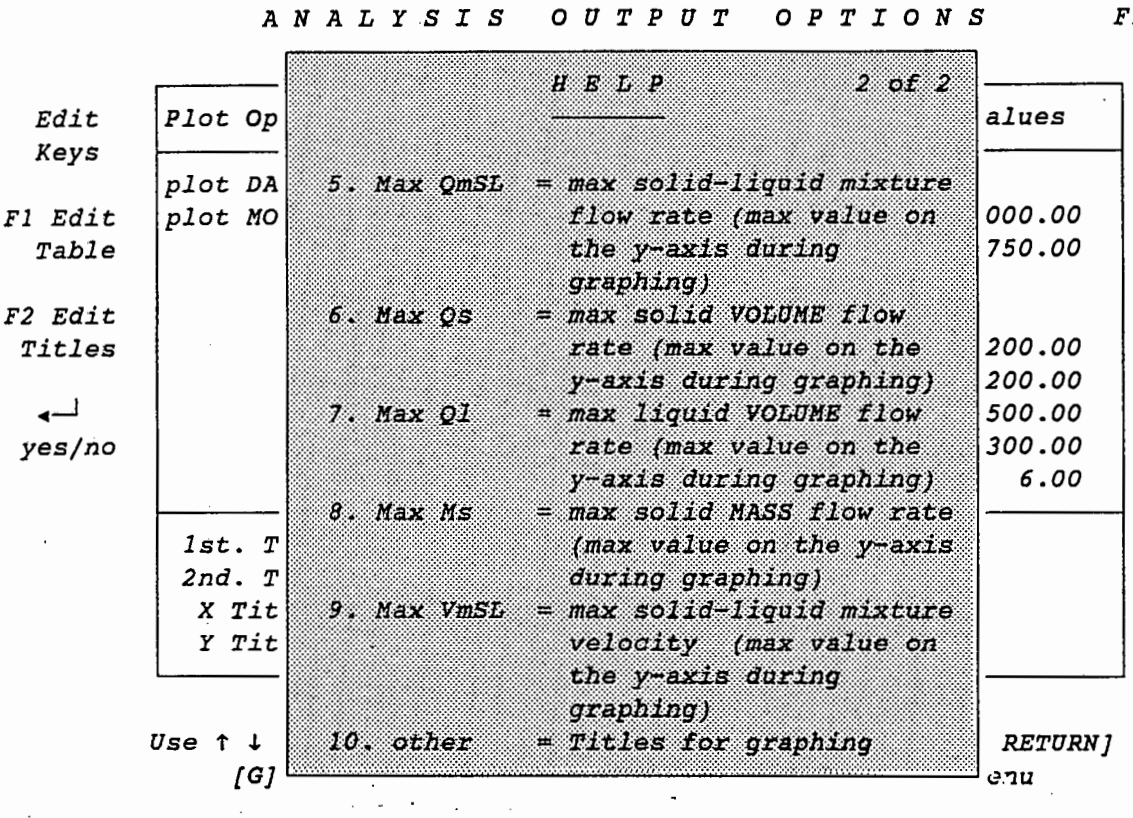

Figure A.23 (continued)

3. *Items 3 and 4 are used to control the number of points calculated in the analysis.*

Two help screens are available by pressing F1 when in the top portion of the table. These are shown in Figure A.23.

When all the required information has been entered, "G" is pressed to start the analysis.

Plotting Data

If only data plots are required, and "Yes" is toggled next to "plot DATA" in Figure A.22, the "available plot options" menu shown in Figure A.24 appears on the screen.

AVAILABLE PLOT OPTIONS			
KEY	OPTION		
F1	QgSTP	vs	QmSL
F2	QgSTP	vs	Ql
F3	QgSTP	vs	Qs
F4	QgSTP	vs	Ms
F5	QgSTP	vs	VmSL
Esc	return to menu		

Figure A.24

Using the F1 to F5 keys, the various graphs available can be viewed. A typical example is shown in Figure A.25. The available options are :

1. Q_gSTP vs Q_mSL → gas flow rate versus solid-liquid mixture flow rate.

2. Q_gSTP vs Q_l → gas flow rate versus liquid flow rate.

3. Q_gSTP vs Q_s → gas flow rate versus solid volume flow rate.

4. Q_gSTP vs M_s → gas flow rate versus solid mass flow rate.

5. Q_gSTP vs V_m → gas flow rate versus solid-liquid mixture velocity in the suction pipe.

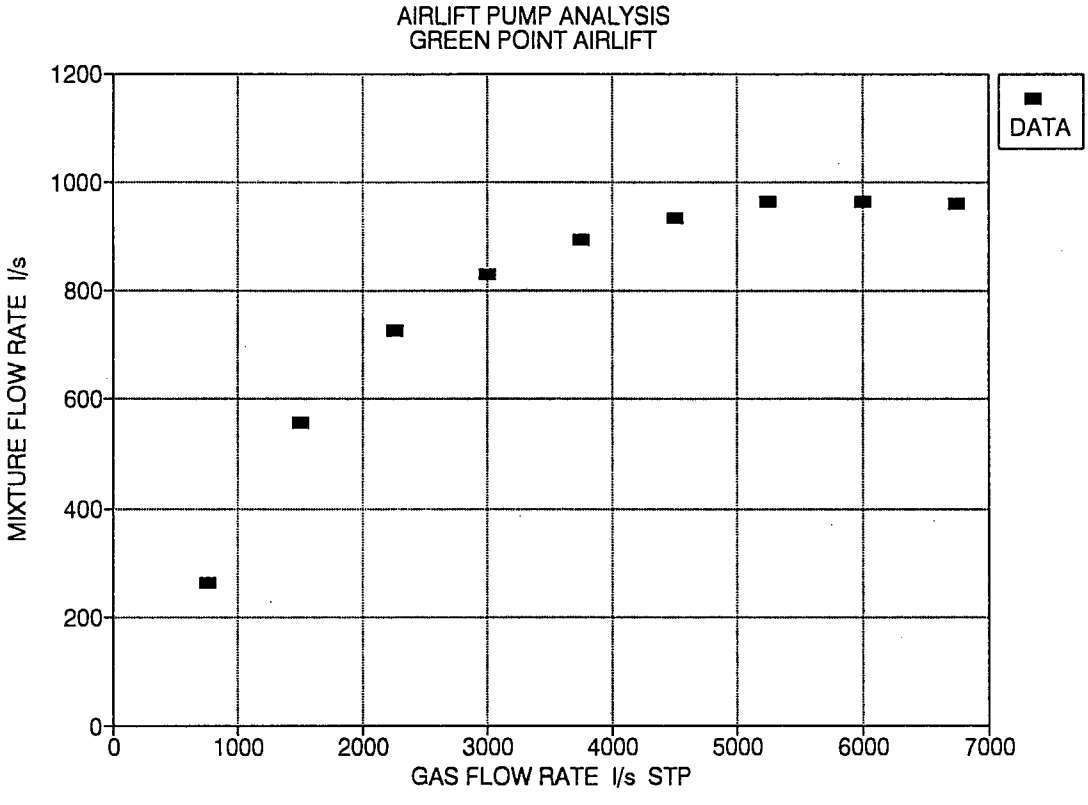

Figure A.25

If no data has been entered in the "Data points" table, an error message will appear and plotting will not continue.

Plotting Model

If only model plots are required, and "Yes" is toggled next to "plot Model" in Figure A.22, the "Analysis Option" screen shown in Figure A.26 will appear. Here the user is prompted to indicate whether the plot is the result of a NEW analysis or of a PREVIOUS analysis.

A N A L Y S I S O P T I O N

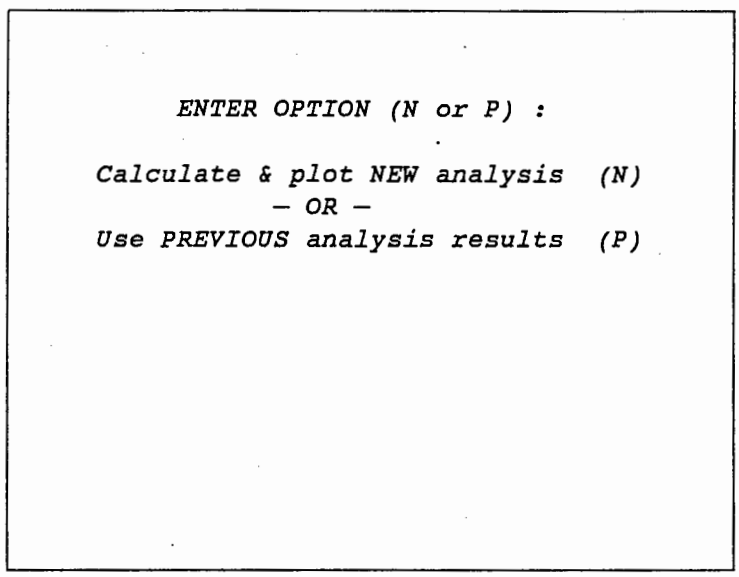

Figure A.26

The "previous analysis" option is available for replotting the most recent analysis. This feature allows return to the "Analysis output option" screen (Figure A.22) for the purpose of changing x and y-axis scales. The analysis can thus be replotted without repeating the calculations.

On choosing the "new analysis" option, all data for the analysis is checked in the "check analysis data" screen shown in Figure A.27.

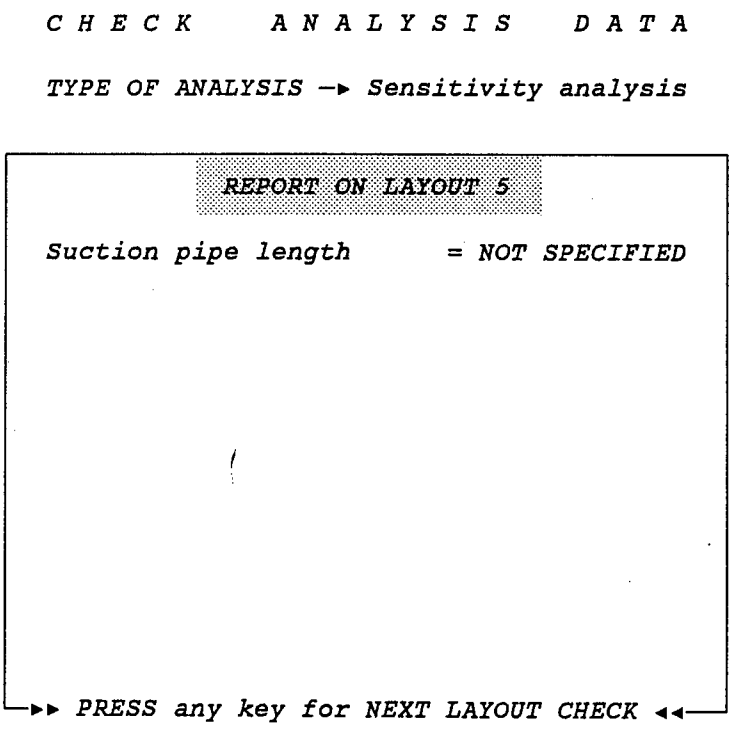

Figure A.27

Each sensitivity layout is checked for missing data. A report on each of the layouts gives a list of the data that has not been specified on previous input tables. The user may be prompted whether the analysis is for two phase flow (clear water) or for three phase flow (water and solids).

Should data be missing, a message will appear indicating that the analysis has been halted, to allow the missing data to be entered.

If all the data is present the analysis can proceed. The number of data points for the analysis is calculated using the Max. Q_gSTP and Inc. Q_gSTP input variables. Should the number of data points exceed 8, a warning will appear and the user is asked to confirm or abort the analysis. This warning is to safeguard excessive calculation.

Having confirmed the number of data points, the user is prompted to input the analysis type. The three options available are shown in Figure A.28.

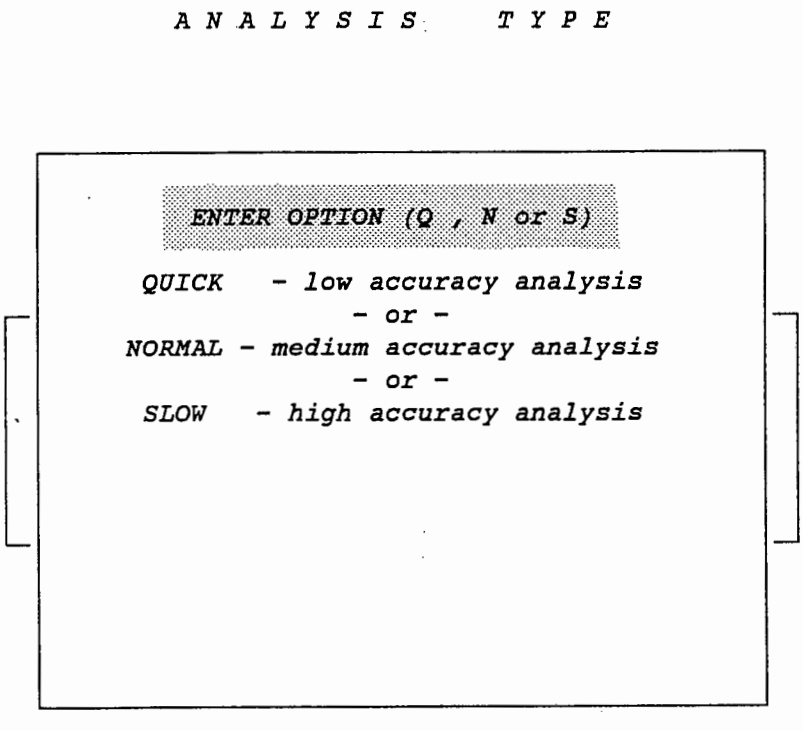

Figure A.28

The analysis type specifies the number of integration steps used to analyse the pressure drop in the delivery pipe. This consequently influences the analysis accuracy.

Quick - The delivery pipe is divided into 3 equal increments for integrating the pressure drop.

Normal - The delivery pipe is divided into 10 equal increments for integrating the pressure drop.

Slow - The pressure drop is evaluated in 1 meter increments up the delivery pipe.

On choosing the desired "Analysis type", the analysis proceeds. While analysing, a "Analysis Report" is given in order to monitor progress. A typical example is given in Figure A.29.

A N A L Y S I S R E P O R T

Layout number	*: 4*	*out of 10*
Analysis point number	*: 8*	*out of 9*
Integration step number	*: 3*	*out of 3*
Iteration loop	*: 5*	
Outlet pressure	*: 128027.*	
Trial flow rate	*: 812.5*	

Figure A.29

Referring to the figure :

Layout number : This item shows the layout which is currently being analysed and the total number of layouts. (Example : In the above figure, a 10 layout sensitivity analysis is being performed).

Analysis point number : This item shows the point that is currently being analysed, and the number of points in each layout. (Example : In the above figure the output flow rates for 9 input gas flow rates are being calculated).

Integration step number : Shown here is the step number while integrating the delivery pipe pressure.

Iteration loop : The iteration loop indicates the number of trial flow rates that have been used in order to satisfy a pressure balance. For the analysis, an initial flow rate is chosen which is corrected according to a pressure balance. (Refer Chapter 4).

Outlet pressure : In order to satisfy the pressure balance mentioned above, the calculated outlet pressure from the analysis must compare to the gas pressure stipulated in section A.5.3 to within certain accuracy. Shown here is the calculated outlet pressure.

Trial flow rate : This item is used to monitor correction of the trial flow rate while satisfying the pressure balance.

On completion of the calculation, the "available plot options" menu shown in Figure A.24 appears on the screen. Using the F1 to F5 keys, the various graphs available can be viewed. A typical example is shown in Figure A.30.

A report on the information used in calculating each of the 10 layouts is available by entering the F1 to F10 keys while viewing a graph.

Figure A.31 shows a typical layout report, giving all information used in the analysis.

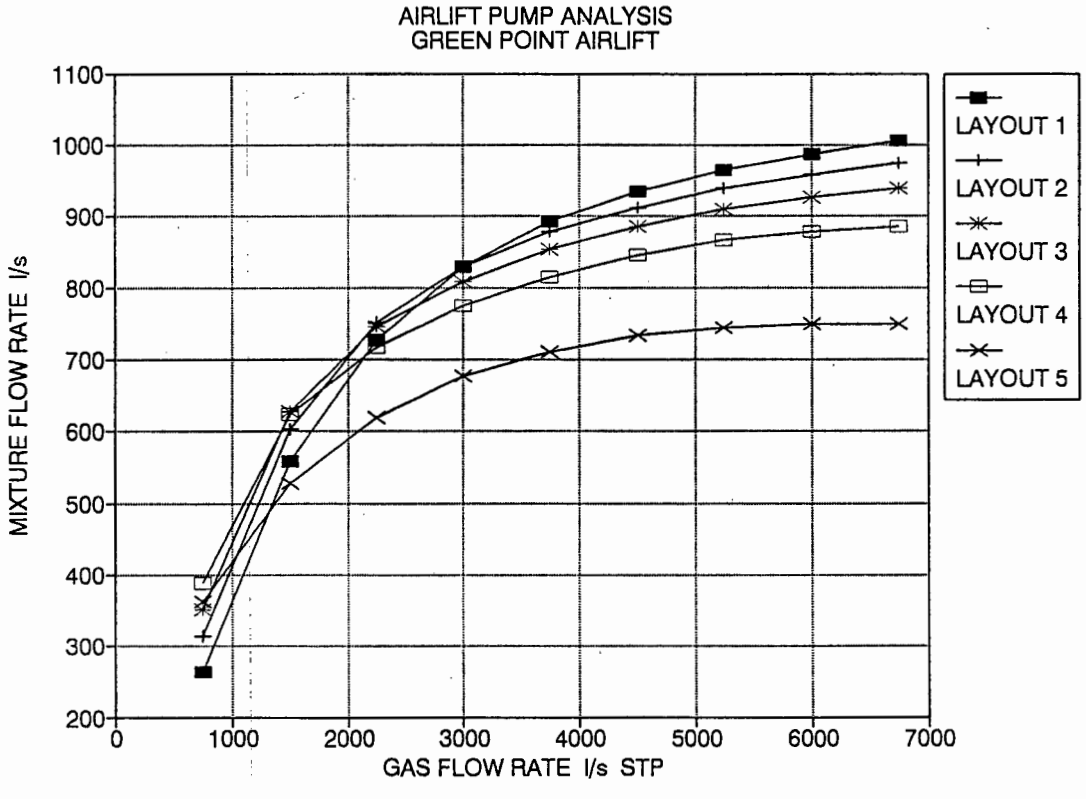

Figure A.30

```
L A Y O U T   R E P O R T

Layout number 1
SYSTEM DATA
   Injection depth              (m) : 150.00
   Lift height                  (m) : 15.00
   Suction pipe length          (m) : 5.00
PIPE DATA
   Delivery pipe diameter      (mm) : 500.00
   Delivery pipe roughness     (µm) : 150.0
   Suction pipe diameter       (mm) : 500.00
   Suction pipe roughness      (µm) : 150.0
PHASE DATA
   Liquid relative density          : 1.025
   Solid relative density           : 2.600
   Gas density           (kg/m^3)   : 1.204
   Delivery outlet pressure  (Pa)   : 101300.0
CONCENTRATION DATA
   Solid-Liquid delivered (vol) %   : 3.00

          ► Any Key - EXIT ◄
```

Figure A.31

A.7 UTILITIES

A.7.1 View PSD curve

This option graphs the particle size distribution specified in "Particle information" table in the "Edit Input Data" Main Menu item.

A.7.2 Export data to Lotus 123

In this option, data can be exported to Lotus 123 and consequently imported into a Lotus spreadsheet for printing and additional plotting.

Note :

When importing files in Lotus, the "NUMBERS" option must be used, in order to assure that each data item is stored in a Lotus cell.

In earlier versions of Lotus 123 the error message "Part of File Missing" might appear. This message can be ignored as all data will be present.

A.8 USEFUL HINTS

When using the program, observe the following rules:

1. Use the screen prompts for information.

2. When an error message appears, press any key to continue.

3. Check that all the input parameters are given in each data file. This requires :

   a. data in all tables for layout 1.

   b. particle size distribution to be input and the percentage retained to be calculated.

APPENDIX B

PARTICLE SIZE DISTRIBUTIONS AND DENSITIES OF TEST MATERIAL

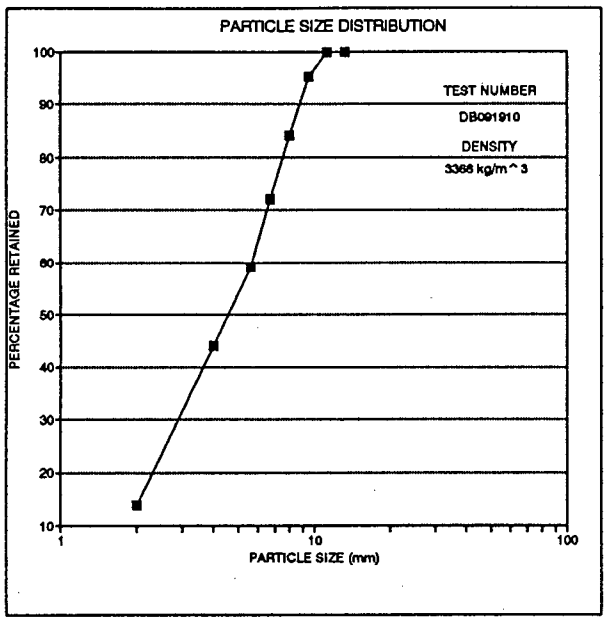
PARTICLE SIZE DISTRIBUTION
TEST NUMBER
DB091910
DENSITY
3368 kg/m^3
PERCENTAGE RETAINED
PARTICLE SIZE (mm)

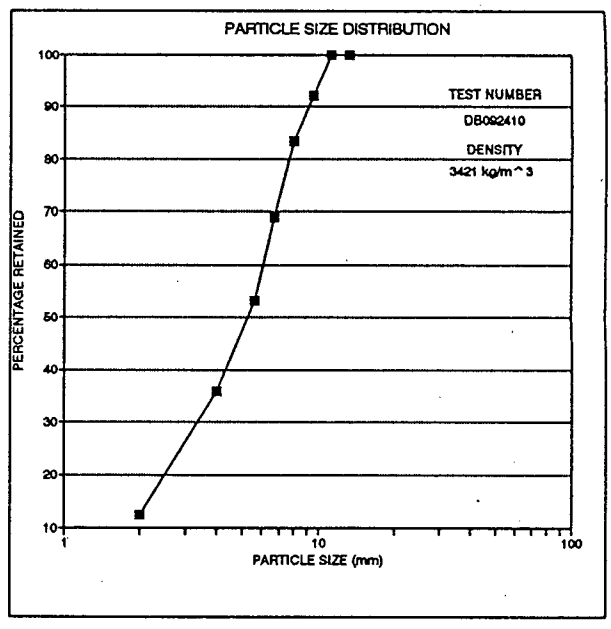
PARTICLE SIZE DISTRIBUTION
TEST NUMBER
DB092410
DENSITY
3421 kg/m^3
PERCENTAGE RETAINED
PARTICLE SIZE (mm)

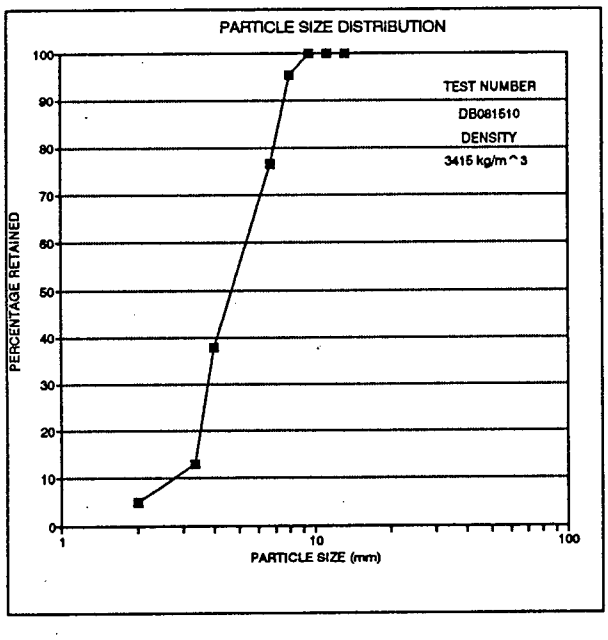
PARTICLE SIZE DISTRIBUTION
TEST NUMBER
DB081510
DENSITY
3415 kg/m^3
PERCENTAGE RETAINED
PARTICLE SIZE (mm)

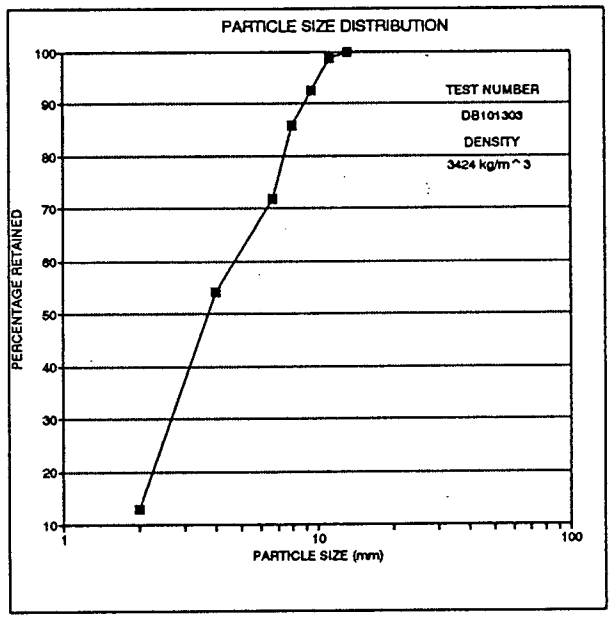
PARTICLE SIZE DISTRIBUTION
TEST NUMBER
DB101303
DENSITY
3424 kg/m^3
PERCENTAGE RETAINED
PARTICLE SIZE (mm)

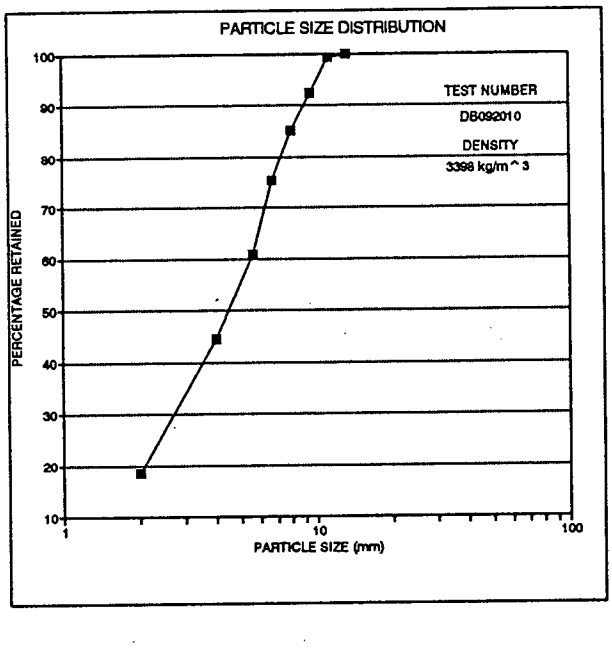
PARTICLE SIZE DISTRIBUTION
TEST NUMBER
DB092010
DENSITY
3398 kg/m^3
PERCENTAGE RETAINED
PARTICLE SIZE (mm)

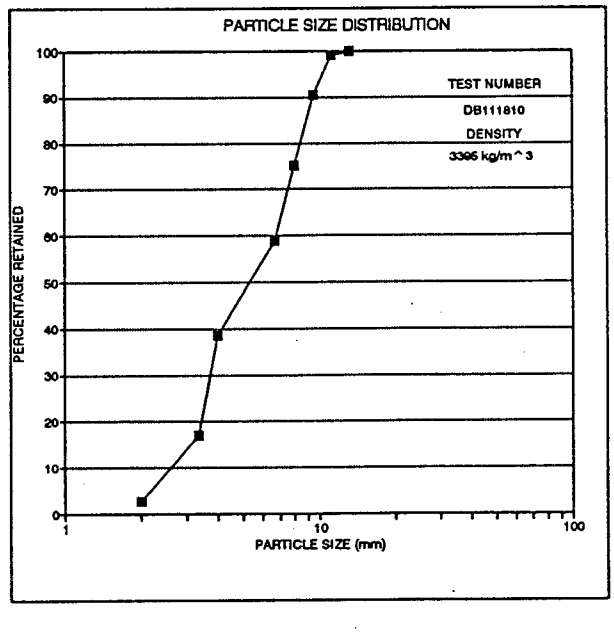
PARTICLE SIZE DISTRIBUTION
TEST NUMBER
DB111810
DENSITY
3396 kg/m^3
PERCENTAGE RETAINED
PARTICLE SIZE (mm)

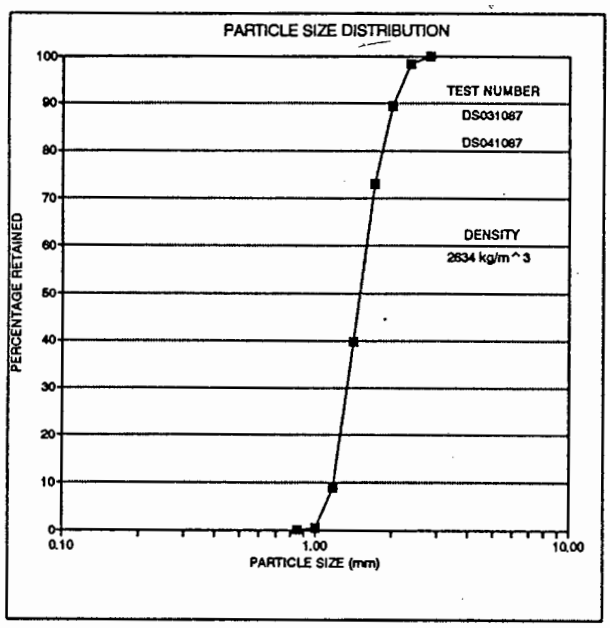
PARTICLE SIZE DISTRIBUTION
TEST NUMBER
DS031087
DS041087
DENSITY
2634 kg/m^3
PERCENTAGE RETAINED
PARTICLE SIZE (mm)
0.10
1.00
10.00

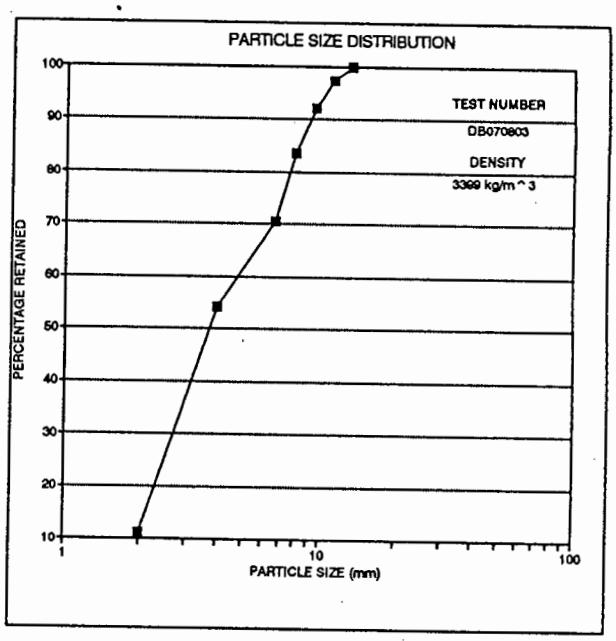
PARTICLE SIZE DISTRIBUTION
TEST NUMBER
DB070803
DENSITY
3369 kg/m^3
PERCENTAGE RETAINED
PARTICLE SIZE (mm)
1
10
100

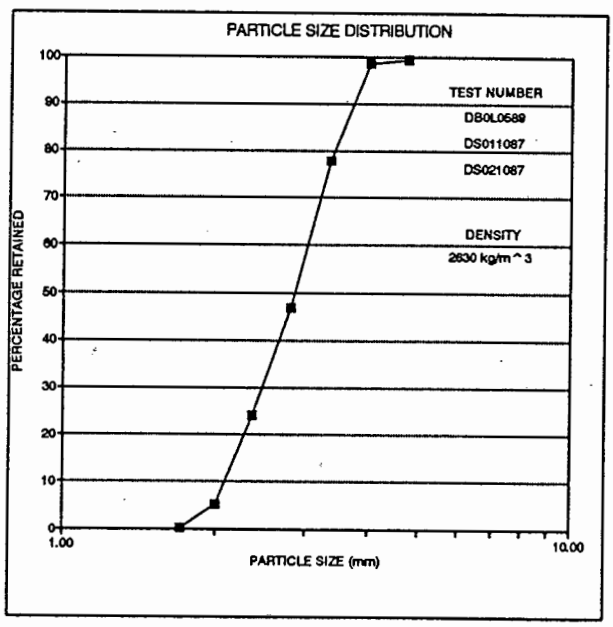
PARTICLE SIZE DISTRIBUTION
TEST NUMBER
DB0L0589
DS011087
DS021087
DENSITY
2630 kg/m^3
PERCENTAGE RETAINED
PARTICLE SIZE (mm)
1.00
10.00

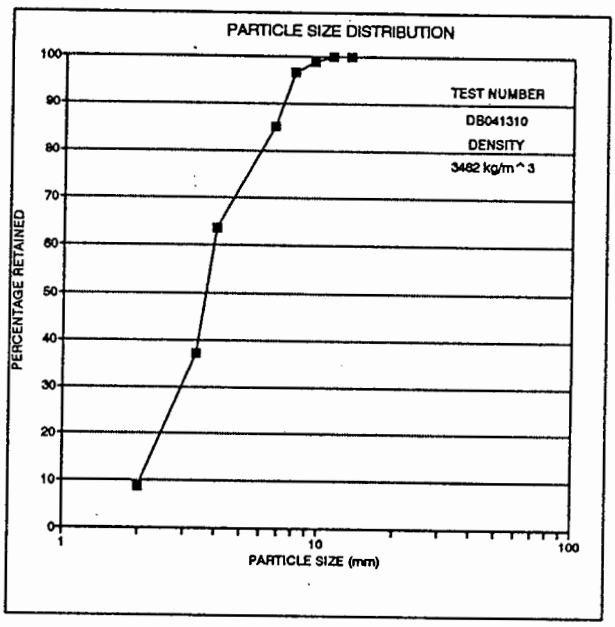
PARTICLE SIZE DISTRIBUTION
TEST NUMBER
DB041310
DENSITY
3482 kg/m^3
PERCENTAGE RETAINED
PARTICLE SIZE (mm)
1
10
100

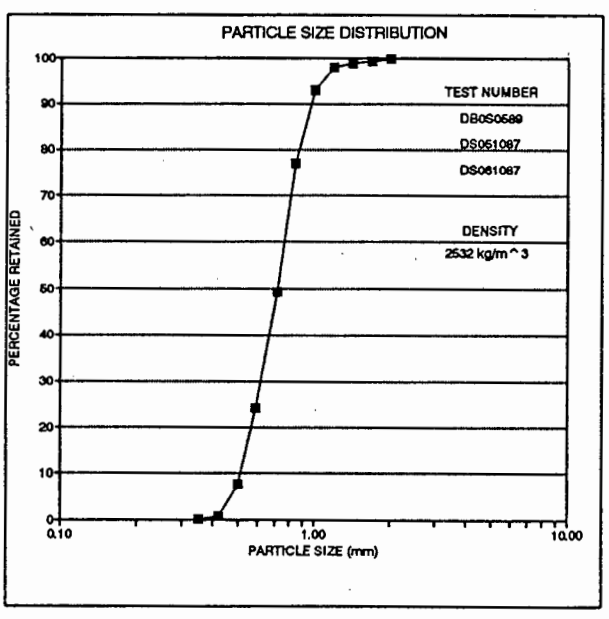
PARTICLE SIZE DISTRIBUTION
TEST NUMBER
DB0S0589
DS051087
DS061087
DENSITY
2532 kg/m^3
PERCENTAGE RETAINED
PARTICLE SIZE (mm)
0.10
1.00
10.00

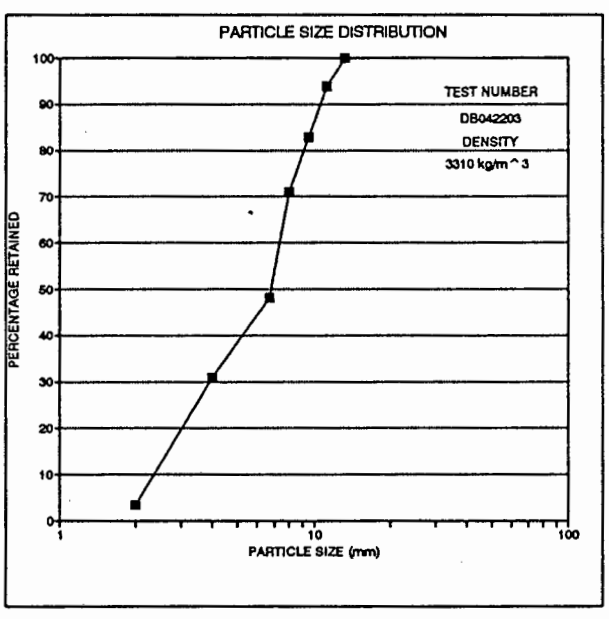
PARTICLE SIZE DISTRIBUTION
TEST NUMBER
DB042203
DENSITY
3310 kg/m^3
PERCENTAGE RETAINED
PARTICLE SIZE (mm)
1
10
100

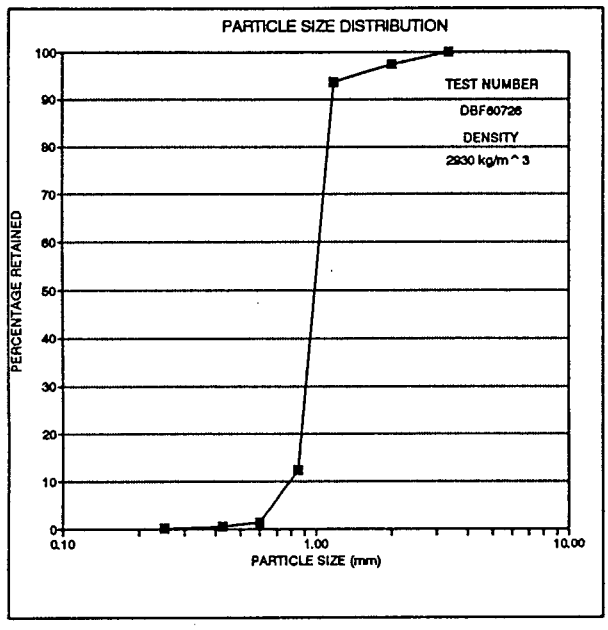
PARTICLE SIZE DISTRIBUTION
TEST NUMBER
DBF60726
DENSITY
2930 kg/m^3
PERCENTAGE RETAINED
PARTICLE SIZE (mm)
0.10
1.00
10.00

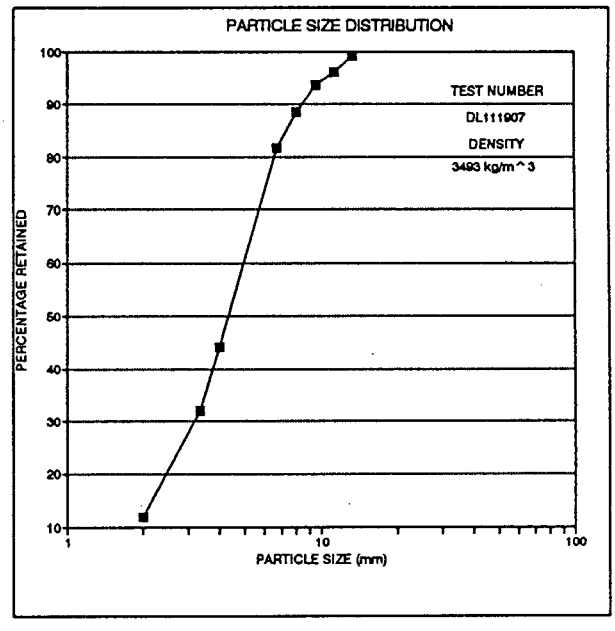
PARTICLE SIZE DISTRIBUTION
TEST NUMBER
DL111907
DENSITY
3493 kg/m^3
PERCENTAGE RETAINED
PARTICLE SIZE (mm)
1
10
100

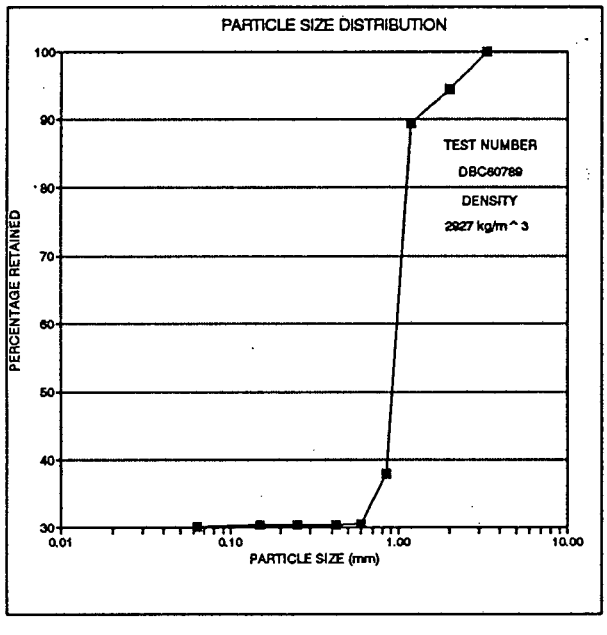
PARTICLE SIZE DISTRIBUTION
TEST NUMBER
DBC60789
DENSITY
2927 kg/m^3
PERCENTAGE RETAINED
PARTICLE SIZE (mm)
0.01
0.10
1.00
10.00

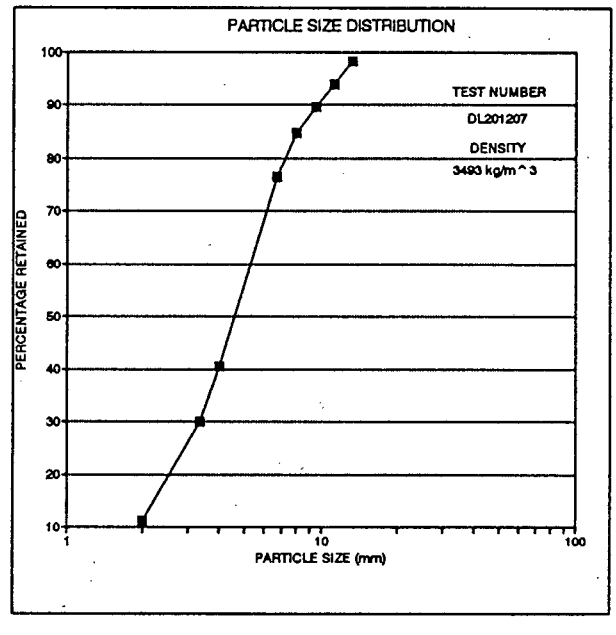
PARTICLE SIZE DISTRIBUTION
TEST NUMBER
DL201207
DENSITY
3493 kg/m^3
PERCENTAGE RETAINED
PARTICLE SIZE (mm)
1
10
100

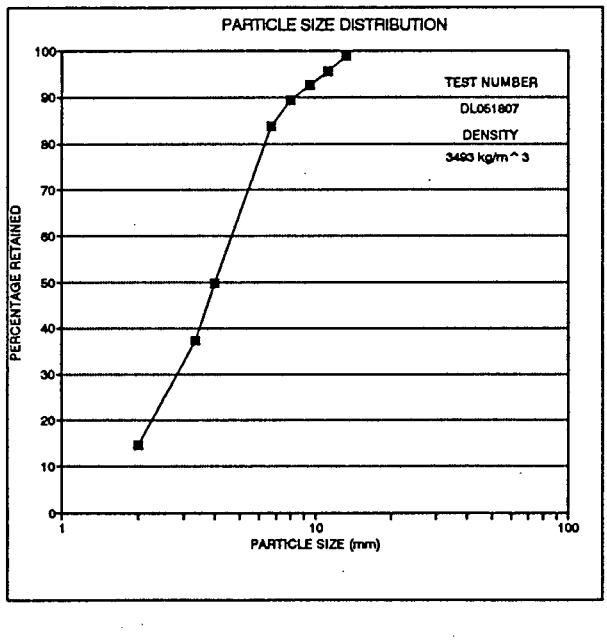
PARTICLE SIZE DISTRIBUTION
TEST NUMBER
DL051807
DENSITY
3493 kg/m^3
PERCENTAGE RETAINED
PARTICLE SIZE (mm)
1
10
100

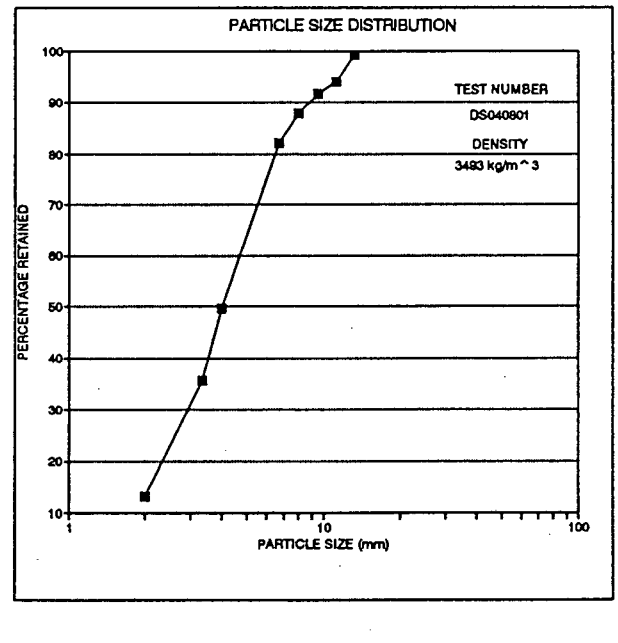
PARTICLE SIZE DISTRIBUTION
TEST NUMBER
DS040801
DENSITY
3493 kg/m^3
PERCENTAGE RETAINED
PARTICLE SIZE (mm)
1
10
100

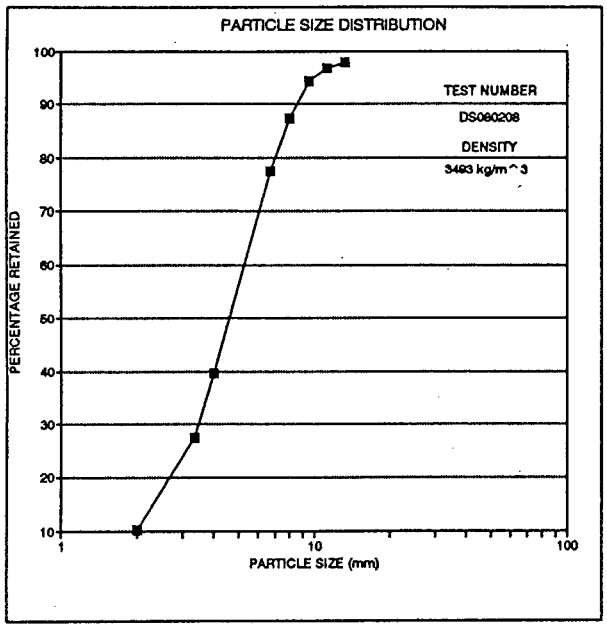
PARTICLE SIZE DISTRIBUTION
TEST NUMBER
DS080208
DENSITY
3493 kg/m^3
PERCENTAGE RETAINED
100
90
80
70
60
50
40
30
20
10
1
10
100
PARTICLE SIZE (mm)

APPENDIX C

PROCEDURE FOR THE CALCULATION OF OUTPUT FLOW RATES FOR A RANGE OF INPUT GAS FLOW RATES

APPENDIX C

PROCEDURE FOR THE CALCULATION OF OUTPUT FLOW RATES FOR A RANGE OF INPUT GAS FLOW RATES

Figure C.1 shows a flow diagram of the procedure used to calculate output flow rates for a range of input gas flow rates. Referring to this figure, along with Figure 4.1, the calculation of output flow rate is achieved in the following manner: for a given input gas flow rate (Q_g^{STP}) and delivered volumetric concentration ($C_{vd}^{s\ell}$) (point B) :

1. A first estimation of output flow rates (Q_ℓ & Q_s) is assumed.

2. The static pressure at the suction inlet (P_C) is calculated using Equation 4.3.

3. The pressure loss in the suction pipe (point C to D) is calculated using Equation 4.5 and consequent Equations 4.6 to 4.27. This pressure loss is subtracted from the static pressure (P_C) in item 2 resulting in pressure P_D.

4. The pressure loss across the gas injector is calculated using Equation 4.29 and consequent Equations 4.30 to 4.32. This pressure loss is subtracted from the absolute pressure obtained in item 3 (P_D) resulting in pressure P_E.

5. For a series of chosen delivery pipe increments, the pressure loss in each increment is calculated using Equation 4.34 and consequent Equations 4.36 to 4.49. These are summed in Equation 4.35. This summed pressure loss is subtracted from the absolute pressure obtained in item 4 (P_E) resulting in pressure P_F.

6. The resulting pressure (P_F) is compared to the outlet pressure (P_A). If it is larger, then the pressure losses evaluated are too low and the assumed output mixture flow rates are increased. Alternatively, if the resulting pressure is smaller than the outlet pressure, then the pressure losses evaluated are too large and the assumed output mixture flow rate is reduced.

7. Items 2 to 6 are repeated until the resultant pressure (P_F) agrees with the outlet pressure (P_A) to within an allowed tolerance.

On agreement, the resulting output flow rates correspond to the given gas input flow rate and the system is in dynamic equilibrium. Consequent repeating of this procedure for a range of gas flow rates yields the airlift pump operating curve.

This procedure is essentially the same as described in Section 4.2. However, allowing calculation in terms of absolute pressure instead of pressure losses permits the outlet pressure to become an input variable. This variable is normally equal to atmospheric pressure.

Figure : C.1
Description : AIRLIFT PUMP CALCULATION PROCEEDURE

Airlift Pump Investigation

GIVEN: QgSTP & CvdSL

ASSUME: Ql & Qs

CALCULATE: Pc

CALCULATE: suction pipe pressure loss [ΔP2]

CALCULATE: Pd = Pc - suction pipe pressure loss

CALCULATE: gas injector pressure loss [ΔP3]

CALCULATE: Pe = Pd - gas injector pressure loss

FOR A SERIES OF DELIVERY PIPE INCREMENTS:
CALCULATE: pressure loss in each delivery pipe increment

CALCULATE: sum of all delivery pipe increment pressure losses[ΔP4]

CALCULATE: Pf = Pe - sum of delivery pipe pressure losses

COMPARE Pf to outlet pressure (Pa)

IF Pf << Pa THEN DECREASE Ql & Qs

IF Pf >> Pa THEN INCREASE Ql & Qs

IF Pf = Pa

OUTPUT
Ql & Qs

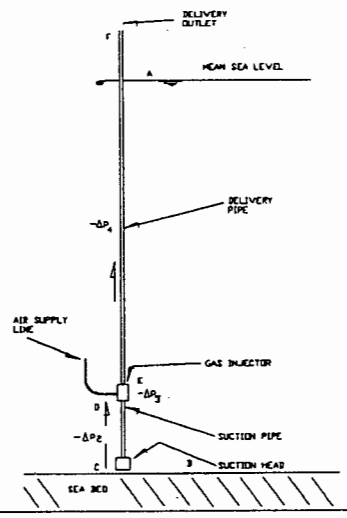

APPENDIX D

TEST DATA

DATA FILE : DL051807

TEST FACILITY : Two phase pipeline test facility

TEST DATE : 1988

TEST MATERIAL : Clear water

APPROX. C_{vd}^{sl} : 5%

PIPELINE DIAMETER : 139,3 mm

Mixture Velocity (m/s)	Total Head Loss (m)	C_{vd}^{sl} (%)	C_{vt}^{sl} (%)
1,843	0,106	3,03	2,92
2,226	0,137	3,79	4,09
2,762	0,162	4,27	4,42
3,074	0,196	5,18	5,58
3,578	0,202	4,85	5,49
4,048	0,231	5,24	6,03
4,451	0,251	5,36	5,98
4,859	0,265	5,35	6,15
5,197	0,278	5,54	6,04

DATA FILE : DL001305

TEST FACILITY : Two phase pipeline test facility

TEST DATE : 1988

TEST MATERIAL : Clear water

APPROX. C_{vd}^{sl} : 0%

PIPELINE DIAMETER : 139,3 mm

Mixture Velocity (m/s)	Total Head Loss (m)	C_{vd}^{sl} (%)	C_{vt}^{sl} (%)
1,490	0,011	0	0
2,075	0,021	0	0
2,606	0,031	0	0
3,116	0,040	0	0
3,512	0,059	0	0
3,906	0,071	0	0
4,341	0,091	0	0
4,884	0,109	0	0
5,226	0,124	0	0
5,675	0,142	0	0
6,127	0,157	0	0

DATA FILE : DL111907

TEST FACILITY : Two phase pipeline test facility

TEST DATE : 1988

TEST MATERIAL : Clear water

APPROX. C_{vd}^{sl} : 10%

PIPELINE DIAMETER : 139,3 mm

Mixture Velocity (m/s)	Total Head Loss (m)	C_{vd}^{sl} (%)	C_{vt}^{sl} (%)
1,972	0,176	5,30	6,15
2,402	0,267	8,28	10,44
2,721	0,289	8,91	10,26
3,010	0,327	10,01	11,84
3,465	0,333	9,93	11,70
3,826	0,370	10,78	12,49
4,508	0,379	10,17	12,32
4,712	0,404	10,87	12,57

DATA FILE : DL201207

TEST FACILITY : Two phase pipeline test facility

TEST DATE : 1988

TEST MATERIAL : Clear water

APPROX. C_{vd}^{sl} : 20%

PIPELINE DIAMETER : 139,3 mm

Mixture Velocity (m/s)	Total Head Loss (m)	C_{vd}^{sl} (%)	C_{vt}^{sl} (%)
2,113	0,313	10,18	11,75
2,298	0,357	11,39	13,27
2,680	0,413	13,57	15,53
3,041	0,451	14,69	16,73
3,515	0,461	14,60	17,01
3,939	0,489	14,94	17,34

DATA FILE : DS001605

TEST FACILITY : Two phase pipeline test facility

TEST DATE : 1988

TEST MATERIAL : Clear water

APPROX. C_{vd}^{sl} : 0%

PIPELINE DIAMETER : 79,715 mm

Mixture Velocity (m/s)	Total Head Loss (m)	C_{vd}^{sl} (%)	C_{vt}^{sl} (%)
1,806	0,034	0	0
2,414	0,062	0	0
3,233	0,112	0	0
3,789	0,142	0	0
4,458	0,209	0	0
5,098	0,259	0	0
6,183	0,361	0	0

DATA FILE : DS040801

TEST FACILITY : Two phase pipeline test facility

TEST DATE : 1988

TEST MATERIAL : Clear water

APPROX. C_{vd}^{sl} : 4%

PIPELINE DIAMETER : 79,715 mm

Mixture Velocity (m/s)	Total Head Loss (m)	C_{vd}^{sl} (%)	C_{vt}^{sl} (%)
1,902	0,068	1,15	0,40
2,359	0,106	1,80	1,50
2,906	0,132	1,77	1,50
3,844	0,228	3,32	2,90
4,465	0,280	3,31	2,70
5,138	0,367	4,59	3,70
5,529	0,407	4,63	3,70

DATA FILE : DS080208

TEST FACILITY : Two phase pipeline test facility

TEST DATE : 1988

TEST MATERIAL : Clear water

APPROX. C_{vd}^{sl} : 8%

PIPELINE DIAMETER : 79,715 mm

Mixture Velocity (m/s)	Total Head Loss (m)	C_{vd}^{sl} (%)	C_{vt}^{sl} (%)
1,890	0,204	5,61	6,9
2,364	0,253	6,84	6,8
2,432	0,290	8,08	8,7
3,083	0,315	7,98	8,4
3,778	0,409	9,95	10,3
4,453	0,445	9,89	10,6
4,892	0,521	11,00	10,6

DATA FILE : VT-15-8s
TEST FACILITY : Settling tube
TEST DATE : 1989
TEST MATERIAL : Glass spheres

Gas *in situ* Volumetric Concentration %	Settling Velocity m/s
0,00	0,84
0,00	0,86
0,00	0,83
0,00	0,81
0,00	0,82
0,00	0,83
14,32	0,86
14,32	1,01
14,32	0,90
14,32	0,86
14,32	0,84
14,32	0,92
14,32	0,92
14,32	0,81
23,85	0,81
23,85	1,10
23,85	0,69
23,85	0,97
23,85	0,97
23,85	0,70
23,85	0,95
23,85	0,84
33,44	0,93
33,44	0,99
33,44	1,24
33,44	0,96
33,44	0,85
33,44	0,81
33,44	1,15
33,44	0,96
41,13	0,68
41,13	0,89
41,13	0,77
41,13	1,01
41,13	0,81
41,13	0,69
41,13	0,84
41,13	0,77
41,13	0,93
41,13	0,89
41,13	0,95
41,13	0,96
45,77	0,77
45,77	0,79
45,77	1,06
45,77	0,90
45,77	0,91
45,77	1,05
45,77	0,72
45,77	0,91
45,77	0,90

Gas *in situ* Volumetric Concentration %	Settling Velocity m/s
53,12	1,03
53,12	0,45
53,12	0,69
53,12	0,56
53,12	0,85
53,12	1,19
53,12	0,50
53,12	0,92
53,12	0,49
53,12	0,71
53,12	0,63
53,12	0,47
55,08	1,00
55,08	1,02
55,08	0,71
55,08	0,77
55,08	0,54
55,08	0,52
55,08	0,67
55,08	0,72
55,08	0,94
55,08	0,82
55,08	0,74
55,08	0,66
57,80	0,88
57,80	1,28
57,80	0,85
57,80	0,97
57,80	1,03
57,80	0,90
57,80	0,95
57,80	0,94
57,80	0,67
57,80	0,59
57,80	0,67
57,80	0,86
57,80	0,67
60,37	1,47
60,37	0,80
60,37	0,80
60,37	0,64
60,37	0,79
60,37	0,93
60,37	0,76
60,37	0,72
60,37	0,61
60,37	0,86
60,37	0,79
60,37	0,77
60,37	0,70
60,37	0,70

DATA FILE : VT-24-5s
TEST FACILITY : Settling tube
TEST DATE : 1989
TEST MATERIAL : Glass spheres

Gas *in situ* Volumetric Concentration %	Settling Velocity m/s
0,00	0,84
0,00	1,01
0,00	0,96
0,00	0,95
0,00	0,96
14,32	1,32
14,32	1,32
14,32	1,11
14,32	1,03
14,32	1,22
14,32	1,32
14,32	1,00
14,32	1,17
23,85	1,40
23,85	0,97
23,85	1,15
23,85	1,01
23,85	1,03
23,85	1,22
23,85	1,17
23,85	1,08
33,44	1,43
33,44	1,42
33,44	1,30
33,44	1,09
33,44	1,10
33,44	1,26
33,44	1,31
33,44	1,26
33,44	1,13
33,44	1,08
41,13	1,30
41,13	1,10
41,13	1,09
41,13	1,09
41,13	1,50
41,13	1,16
41,13	1,28
41,13	1,01
41,13	1,17
41,13	0,98
41,13	1,17
45,77	1,38
45,77	1,28
45,77	1,30
45,77	1,35
45,77	1,17
45,77	1,06
45,77	1,59
45,77	0,82

Gas *in situ* Volumetric Concentration %	Settling Velocity m/s
53,12	1,69
53,12	1,20
53,12	1,15
53,12	1,15
53,12	1,24
53,12	0,63
53,12	1,11
53,12	1,24
53,12	1,05
53,12	1,05
53,12	1,01
53,12	1,11
53,12	0,56
53,12	1,03
55,08	1,12
55,08	1,27
55,08	1,39
55,08	0,99
55,08	0,76
55,08	1,12
55,08	1,17
55,08	1,40
55,08	0,98
55,08	1,05
55,08	1,28
55,08	1,08
55,08	1,23
57,80	1,00
57,80	1,09
57,80	1,18
57,80	1,07
57,80	0,93
57,80	1,03
57,80	1,25
57,80	1,05
57,80	1,45
57,80	1,37
57,80	1,09
57,80	1,03
57,80	1,33
60,37	1,06
60,37	1,19
60,37	1,40
60,37	1,25
60,37	1,11
60,37	1,26
60,37	1,55
60,37	1,53
60,37	1,21
60,37	1,20
60,37	1,28
60,37	1,00
60,37	0,95

DATA FILE : VT-15-8m

TEST FACILITY : Settling tube

TEST DATE : 1989

TEST MATERIAL : Glass spheres

Gas *in situ* Volumetric Concentration %	Settling Velocity m/s
0,00	0,68
0,00	0,69
0,00	0,66
15,50	0,78
15,50	0,75
15,50	0,83
44,50	0,94
44,50	0,88
44,50	0,85
59,20	0,80
59,20	0,92
59,20	0,86

DATA FILE : DB041310

TEST FACILITY : Airlift pump

TEST DATE : 1988

TEST MATERIAL : Marine gravels

APPROX. C_{vd}^{sl} : 1,4%

PIPE DIAMETER : 90 mm NB

PURPOSE : Delivered concentration test

Gas Flow Rate (STP) (l/s)	Mixture Flow Rate (l/s)	Delivered Concentration (%)	Liquid Flow Rate (l/s)	Solid Flow Rate (kg/s)
14,858	3,190	1,7	3,136	0,185
20,256	4,164	1,2	4,114	0,171
25,077	4,512	1,4	4,449	0,216
28,136	4,549	1,2	4,494	0,187
30,163	4,412	1,5	4,346	0,226
34,540	4,093	1,5	4,032	0,210
38,740	4,225	1,6	4,157	0,231
39,678	4,409	1,3	4,352	0,196
44,874	4,174	1,4	4,116	0,200

DATA FILE : DB081510

TEST FACILITY : Airlift pump

TEST DATE : 1988

TEST MATERIAL : Marine gravels

APPROX. $C_{vd}^{s\ell}$: 5%

PIPE DIAMETER : 90 mm NB

PURPOSE : Delivered concentration test

Gas Flow Rate (STP) (ℓ/s)	Mixture Flow Rate (ℓ/s)	Delivered Concentration (%)	Liquid Flow Rate (ℓ/s)	Solid Flow Rate (kg/s)
24,446	2,849	6,0	2,678	0,573
29,866	3,607	5,8	3,398	0,702
39,790	3,888	5,6	3,670	0,730
45,072	3,965	5,1	3,763	0,678
42,237	4,002	5,1	3,798	0,685
34,829	3,796	5,3	3,595	0,675
27,697	3,594	5,5	3,396	0,663
20,421	2,722	5,5	2,572	0,502
17,795	2,676	5,1	2,540	0,458

DATA FILE : DB111810

TEST FACILITY : Airlift pump

TEST DATE : 1988

TEST MATERIAL : Marine gravels

APPROX. C_{vd}^{sl} : 8%

PIPE DIAMETER : 90 mm NB

PURPOSE : Delivered concentration test

Gas Flow Rate (STP) (l/s)	Mixture Flow Rate (l/s)	Delivered Concentration (%)	Liquid Flow Rate (l/s)	Solid Flow Rate (kg/s)
25,032	2,668	8,2	2,449	0,741
28,017	2,773	8,1	2,548	0,760
30,274	2,878	8,9	2,622	0,867
34,701	3,008	8,7	2,746	0,886
37,183	2,799	8,1	2,572	0,767
39,986	3,158	8,0	2,905	0,855
42,735	3,096	8,4	2,836	0,880
44,774	3,083	8,5	2,821	0,887

DATA FILE : DB091910

TEST FACILITY : Airlift pump

TEST DATE : 1988

TEST MATERIAL : Marine gravels

APPROX. C_{vd}^{sl} : 6%

PIPE DIAMETER : 90 mm NB

PURPOSE : Aperture test

Gas Flow Rate (STP) (l/s)	Mixture Flow Rate (l/s)	Delivered Concentration (%)	Liquid Flow Rate (l/s)	Solid Flow Rate (kg/s)
20,421	2,429	6,5	2,271	0,531
24,988	2,921	6,8	2,722	0,669
27,697	3,323	3,9	3,193	0,436
29,679	3,209	6,9	2,988	0,745
34,701	3,468	6,9	3,229	0,805
37,481	3,605	6,1	3,385	0,740
39,986	3,582	6,5	3,349	0,784
42,500	3,611	6,8	3,365	0,827
45,294	3,910	6,0	3,675	0,790

DATA FILE : DB092010

TEST FACILITY : Airlift pump

TEST DATE : 1988

TEST MATERIAL : Marine gravels

APPROX. $C_{vd}^{s\ell}$: 6%

PIPE DIAMETER : 90 mm NB

PURPOSE : Aperture tests

Gas Flow Rate (STP) (ℓ/s)	Mixture Flow Rate (ℓ/s)	Delivered Concentration (%)	Liquid Flow Rate (ℓ/s)	Solid Flow Rate (kg/s)
20,311	2,512	5,7	2,369	0,497
24,537	3,254	6,1	3,056	0,688
28,017	3,474	6,2	3,259	0,747
29,866	3,618	6,1	3,397	0,765
34,861	3,722	6,5	3,480	0,839
37,630	3,870	6,1	3,634	0,819
39,734	3,610	6,3	3,383	0,789
42,892	3,175	6,2	2,978	0,683
45,294	3,728	6,2	3,497	0,802

DATA FILE : DB092410

TEST FACILITY : Airlift pump

TEST DATE : 1988

TEST MATERIAL : Marine gravels

APPROX. $C_{vd}^{s\ell}$: 6%

PIPE DIAMETER : 90 mm NB

PURPOSE : Aperture tests

Gas Flow Rate (STP) (ℓ/s)	Mixture Flow Rate (ℓ/s)	Delivered Concentration (%)	Liquid Flow Rate (ℓ/s)	Solid Flow Rate (kg/s)
19,470	2,702	6,8	2,518	0,629
25,166	3,204	6,4	2,999	0,701
27,857	3,646	6,0	3,427	0,748
29,941	3,678	6,4	3,443	0,805
34,829	3,829	6,1	3,595	0,799
37,481	3,896	6,0	3,662	0,800
39,818	3,679	6,3	3,447	0,793
42,237	3,327	6,2	3,121	0,706
45,294	3,733	6,1	3,505	0,779

DATA FILE : DBF60789

TEST FACILITY : Airlift pump

TEST DATE : 1988

TEST MATERIAL : Marine gravels

APPROX. $C_{vd}^{s\ell}$: 5%

PIPE DIAMETER : 90 mm NB

PURPOSE : Fines tests

Gas Flow Rate (STP) (ℓ/s)	Mixture Flow Rate (ℓ/s)	Delivered Concentration (%)	Liquid Flow Rate (ℓ/s)	Solid Flow Rate (kg/s)
11,663	3,521	0,5	3,503	0,052
13,848	3,917	1,6	3,854	0,184
15,662	3,098	3,2	2,999	0,291
19,867	3,651	5,1	3,465	0,546
20,421	3,363	4,7	3,205	0,464
23,986	3,689	5,4	3,490	0,584
24,809	3,456	4,8	3,290	0,487
29,339	3,802	5,8	3,581	0,647
34,861	3,962	5,1	3,760	0,593
39,311	3,882	5,4	3,672	0,615
43,511	3,985	5,4	3,770	0,631

DATA FILE : DBC60789

TEST FACILITY : Airlift pump

TEST DATE : 1988

TEST MATERIAL : Marine gravels

APPROX. C_{vd}^{sl} : 3,5%

PIPE DIAMETER : 90 mm NB

PURPOSE : Fines tests

Gas Flow Rate (STP) (l/s)	Mixture Flow Rate (l/s)	Delivered Concentration (%)	Liquid Flow Rate (l/s)	Solid Flow Rate (kg/s)
16,494	3,937	2,6	3,835	0,300
29,829	4,412	3,9	4,240	0,504
41,383	4,491	3,8	4,320	0,500
20,692	4,233	2,1	4,144	0,260
35,116	4,461	3,5	4,305	0,457
39,902	4,567	3,1	4,425	0,414
25,298	4,442	3,4	4,291	0,442

DATA FILE : DSO11087

TEST FACILITY : Airlift pump

TEST DATE : 1988

TEST MATERIAL : Quartz

APPROX. $C_{vd}^{s\ell}$: 0,5-5%

PIPE DIAMETER : 40 mm NB

PURPOSE : Operating tests

Gas Flow Rate (STP) (ℓ/s)	Mixture Flow Rate (ℓ/s)	Delivered Concentration (%)	Liquid Flow Rate (ℓ/s)	Solid Flow Rate (kg/s)
0,21	0,34	0,49	0,34	0,004
0,26	0,26	2,22	0,26	0,015
0,33	0,39	1,25	0,39	0,013
0,37	0,41	0,86	0,41	0,009
0,42	0,35	2,61	0,35	0,024
0,54	0,46	1,47	0,46	0,018
0,54	0,46	1,57	0,46	0,019
0,62	0,34	3,53	0,33	0,031
0,76	0,37	2,88	0,36	0,028
0,78	0,35	3,76	0,34	0,035
0,79	0,51	1,71	0,51	0,023
0,98	0,54	2,39	0,53	0,034
1,12	0,58	1,90	0,57	0,029
1,16	0,36	3,82	0,35	0,036
1,37	0,57	2,53	0,56	0,038
1,43	0,37	4,12	0,36	0,040
1,44	0,41	3,53	0,40	0,038
1,60	0,52	2,25	0,51	0,031
1,83	0,44	3,53	0,43	0,041
1,83	0,46	3,57	0,45	0,043
1,86	0,45	3,86	0,44	0,046
1,89	0,58	2,65	0,57	0,040
1,92	0,65	2,65	0,64	0,045
2,22	0,46	3,63	0,45	0,044
2,32	0,59	2,35	0,58	0,037
2,36	0,52	2,43	0,51	0,033
2,81	0,47	3,75	0,46	0,047
2,86	0,54	3,73	0,52	0,053
3,15	0,55	2,39	0,54	0,034
3,26	0,58	2,35	0,57	0,036
3,29	0,46	3,78	0,45	0,046
3,37	0,48	3,82	0,47	0,049
3,60	0,56	2,49	0,55	0,037
3,80	0,52	3,73	0,51	0,052
3,83	0,58	2,49	0,57	0,038

DATA FILE : DSO21087

TEST FACILITY : Airlift pump

TEST DATE : 1988

TEST MATERIAL : Quartz

APPROX. C_{vd}^{sl} : 0,5-5%

PIPE DIAMETER : 40 mm NB

PURPOSE : Operating tests

Gas Flow Rate (STP) (l/s)	Mixture Flow Rate (l/s)	Delivered Concentration (%)	Liquid Flow Rate (l/s)	Solid Flow Rate (kg/s)
0,15	0,36	0,84	0,36	0,008
0,21	0,29	0,74	0,29	0,006
0,26	0,29	2,43	0,29	0,019
0,26	0,38	1,66	0,38	0,016
0,26	0,42	1,23	0,42	0,014
0,42	0,33	2,72	0,33	0,024
0,47	0,49	1,94	0,49	0,025
0,54	0,49	2,21	0,48	0,028
0,78	0,39	3,74	0,38	0,038
0,80	0,56	2,33	0,55	0,034
0,90	0,51	2,56	0,50	0,034
1,14	0,62	2,62	0,61	0,043
1,26	0,48	3,84	0,47	0,049
1,35	0,53	2,90	0,52	0,041
1,38	0,46	4,01	0,45	0,049
1,46	0,56	3,07	0,55	0,046
1,57	0,62	2,54	0,61	0,042
1,72	0,44	4,03	0,43	0,047
1,85	0,51	4,13	0,49	0,055
1,89	0,54	2,80	0,53	0,040
1,98	0,64	3,31	0,62	0,056
2,23	0,51	4,48	0,49	0,060
2,38	0,48	4,50	0,46	0,057
2,75	0,51	4,34	0,49	0,058
3,03	0,65	3,37	0,63	0,057
3,14	0,56	3,35	0,55	0,050
3,24	0,51	4,56	0,49	0,061
3,72	0,65	3,37	0,63	0,057
3,79	0,51	4,58	0,49	0,062
3,84	0,67	3,44	0,65	0,061

DATA FILE : DSO31087

TEST FACILITY : Airlift pump

TEST DATE : 1988

TEST MATERIAL : Quartz

APPROX. $C_{vd}^{s\ell}$: 0,5-5%

PIPE DIAMETER : 40 mm NB

PURPOSE : Operating tests

Gas Flow Rate (STP) (ℓ/s)	Mixture Flow Rate (ℓ/s)	Delivered Concentration (%)	Liquid Flow Rate (ℓ/s)	Solid Flow Rate (kg/s)
0,15	0,26	0,67	0,26	0,004
0,15	0,27	0,31	0,27	0,002
0,26	0,23	1,33	0,23	0,008
0,40	0,45	1,24	0,45	0,014
0,45	0,47	1,79	0,47	0,022
0,56	0,37	2,08	0,37	0,021
0,67	0,49	1,73	0,49	0,022
0,73	0,52	1,51	0,52	0,021
0,96	0,51	1,86	0,51	0,025
0,99	0,44	2,85	0,43	0,033
1,13	0,59	2,49	0,58	0,039
1,19	0,53	1,98	0,52	0,027
1,30	0,46	2,81	0,45	0,034
1,74	0,56	1,96	0,55	0,029
1,82	0,46	2,75	0,45	0,033
2,17	0,46	2,81	0,45	0,034
2,29	0,56	2,16	0,55	0,032
2,91	0,44	2,98	0,43	0,035
3,08	0,56	2,04	0,55	0,030
3,65	0,57	2,08	0,56	0,031

DATA FILE : DSO41087

TEST FACILITY : Airlift pump

TEST DATE : 1988

TEST MATERIAL : Quartz

APPROX. $C_{vd}^{s\ell}$: 0,5-5%

PIPE DIAMETER : 40 mm NB

PURPOSE : Operating tests

Gas Flow Rate (STP) (ℓ/s)	Mixture Flow Rate (ℓ/s)	Delivered Concentration (%)	Liquid Flow Rate (ℓ/s)	Solid Flow Rate (kg/s)
0,15	0,41	1,18	0,41	0,012
0,15	0,25	0,27	0,25	0,001
0,21	0,29	1,27	0,29	0,009
0,33	0,38	2,06	0,38	0,021
0,37	0,49	1,63	0,49	0,021
0,40	0,42	1,57	0,42	0,017
0,54	0,53	1,57	0,53	0,022
0,56	0,42	2,43	0,41	0,026
0,60	0,51	2,00	0,50	0,026
0,72	0,58	1,67	0,58	0,026
0,73	0,48	2,75	0,47	0,035
0,88	0,57	2,25	0,56	0,034
0,93	0,53	2,86	0,52	0,040
1,18	0,59	2,31	0,58	0,036
1,21	0,56	3,00	0,55	0,044
1,56	0,58	3,22	0,57	0,049
1,80	0,60	2,29	0,59	0,036
1,82	0,58	3,27	0,57	0,051
2,39	0,60	2,39	0,59	0,038
2,63	0,58	3,27	0,57	0,051
3,07	0,61	2,35	0,60	0,038
3,57	0,59	3,43	0,57	0,053

DATA FILE : DSO51087
TEST FACILITY : Airlift pump
TEST DATE : 1988
TEST MATERIAL : Quartz
APPROX. $C_{vd}^{s\ell}$: 0,5-5%
PIPE DIAMETER : 40 mm NB
PURPOSE : Operating tests

Gas Flow Rate (STP) (ℓ/s)	Mixture Flow Rate (ℓ/s)	Delivered Concentration (%)	Liquid Flow Rate (ℓ/s)	Solid Flow Rate (kg/s)
0,21	0,16	1,18	0,16	0,005
0,21	0,25	1,00	0,25	0,007
0,21	0,26	0,43	0,26	0,002
0,21	0,28	0,29	0,28	0,002
0,26	0,36	1,00	0,36	0,009
0,33	0,42	0,57	0,42	0,006
0,33	0,49	1,27	0,49	0,015
0,42	0,34	2,39	0,34	0,021
0,45	0,36	1,73	0,36	0,016
0,47	0,42	1,08	0,42	0,011
0,52	0,46	1.02	0,46	0,012
0,52	0,58	1,47	0,58	0,022
0,67	0,46	2,04	0,46	0,024
0,70	0,37	2,63	0,37	0,025
0,70	0,46	1,55	0,46	0,018
0,80	0,62	1,67	0,61	0,026
0,82	0,51	1,33	0,51	0,017
0,93	0,51	2,24	0,50	0,029
0,97	0,47	1,76	0,47	0,021
1,00	0,52	1,31	0,52	0,017
1,01	0,65	1,76	0,64	0,029
1,12	0,44	2,82	0,43	0,031
1,13	0,52	2,31	0,51	0,031
1,20	0,49	1,82	0,49	0,023
1,20	0,67	1,82	0,66	0,031
1,34	0,47	2,90	0,46	0,034
1,47	0,49	2,49	0,48	0,031
1,47	0,54	1,47	0,54	0,020
1,52	0,51	1,76	0,51	0,023
1,62	0,67	1,76	0,66	0,029
1,70	0,49	3,00	0,48	0,037
1,77	0,55	1,53	0,55	0,021
1,83	0,53	2,35	0,52	0,032
2,01	0,49	3,02	0,48	0,038
2,05	0,52	1,86	0,52	0,025
2,22	0,55	1,53	0,55	0,022
2,24	0,65	1,86	0,64	0,031
2,55	0,50	1,86	0,50	0,024
2,79	0,54	2,55	0,53	0,035
2,81	0,67	1,76	0,66	0,029
2,89	0,48	3,00	0,47	0,037
3,10	0,55	1,57	0,55	0,022
3,52	0,55	2,65	0,54	0,037
3,53	0,50	1,86	0,50	0,024
3,63	0,67	1,80	0,66	0,030
3,65	0,48	3,14	0,47	0,038

DATA FILE : DSO61087
TEST FACILITY : Airlift pump
TEST DATE : 1988
TEST MATERIAL : Quartz
APPROX. C_{vd}^{sl} : 0,5-5%
PIPE DIAMETER : 40 mm NB
PURPOSE : Operating tests

Gas Flow Rate (STP) (l/s)	Mixture Flow Rate (l/s)	Delivered Concentration (%)	Liquid Flow Rate (l/s)	Solid Flow Rate (kg/s)
0,21	0,21	1,25	0,21	0,006
0,21	0,21	1,61	0,21	0,008
0,21	0,23	2,06	0,23	0,012
0,21	0,42	0,90	0,42	0,009
0,26	0,21	2,12	0,21	0,011
0,26	0,24	2,35	0,24	0,014
0,33	0,34	2,16	0,34	0,019
0,33	0,41	1,57	0,41	0,016
0,40	0,31	3,24	0,30	0,025
0,40	0,31	0,78	0,31	0,006
0,45	0,53	1.55	0,53	0,021
0,50	0,33	3,92	0,32	0,033
0,52	0,43	2,63	0,42	0,028
0,60	0,57	1,71	0,57	0,025
0,62	0,51	2,49	0,50	0,032
0,65	0,37	3,25	0,36	0,031
0,75	0,36	4,08	0,35	0,037
0,76	0,52	2,69	0,51	0,035
0,80	0,51	3,04	0,50	0,039
0,80	0,62	1,82	0,61	0,028
0,98	0,43	3,78	0,42	0,041
0,98	0,53	2,75	0,52	0,037
1,06	0,50	3,27	0,49	0,042
1,09	0,63	2,06	0,62	0,033
1,10	0,39	4,51	0,38	0,045
1,17	0,46	3,96	0,45	0,047
1,18	0,54	2,76	0,53	0,038
1,36	0,51	3,29	0,50	0,043
1,38	0,46	4,12	0,45	0,049
1,47	0,65	2,25	0,64	0,037
1,50	0,39	4,71	0,38	0,047
1,59	0,55	2,75	0,54	0,038
1,77	0,65	2,25	0,64	0,037
1,87	0,51	3,47	0,50	0,045
2,01	0,46	4,22	0,45	0,050
2,12	0,39	4,80	0,38	0,048
2,54	0,64	2,35	0,63	0,038
2,74	0,48	4,02	0,47	0,049
2,77	0,54	2,94	0,53	0,040
2,88	0,51	3,55	0,50	0,046
3,35	0,40	4,80	0,39	0,049
3,52	0,65	2,35	0,64	0,039
3,63	0,52	3,63	0,51	0,048
3,66	0,51	4,22	0,49	0,054
3,73	0,54	2,84	0,53	0,039

DATA FILE : DB042203

TEST FACILITY : Airlift pump

TEST DATE : 1989

TEST MATERIAL : Marine gravels

APPROX. C_{vd}^{sl} : 4%

PIPE DIAMETER : 90 mm NB

PURPOSE : *In situ* concentration tests

Gas Flow Rate (STP) (l/s)	Gas Flow Rate *in situ* (l/s)	Mixture Flow Rate (l/s)	Delivered Concentration (%)	Gas *in situ* Concentration (%)	Solid *in situ* Concentration (%)
20,475	15,506	3,770	2,1	64,31	0,19
24,079	18,365	3,660	3,8	69,53	0,49
28,314	21,638	3,597	3,4	68,64	0,58
32,184	24,722	3,613	2,9	68,91	0,44
37,600	28,355	3,953	4,0	73,04	0,58
40,498	30,654	4,039	3,3	70,25	0,24
45,796	34,548	3,963	3,3	72,53	0,24

DATA FILE : DB070803

TEST FACILITY : Airlift pump

TEST DATE : 1989

TEST MATERIAL : Marine gravels

APPROX. C_{vd}^{sl} : 6%

PIPE DIAMETER : 90 mm NB

PURPOSE : *In situ* concentration tests

Gas Flow Rate (STP) (l/s)	Gas Flow Rate *in situ* (l/s)	Mixture Flow Rate (l/s)	Delivered Concentration (%)	Gas *in situ* Concentration (%)	Solid *in situ* Concentration (%)
21,276	15,659	2,741	5,0	67,24	1,63
24,741	18,154	3,074	6,5	67,86	1,37
27,373	20,086	3,562	5,9	66,55	0,96
32,201	23,651	3,584	5,9	69,12	0,76
35,668	26,170	3,578	6,0	69,97	0,82
39,537	28,959	3,734	5,9	72,67	0,84
45,060	33,107	3,830	5,8	72,79	0,77

DATA FILE : DB101303

TEST FACILITY : Airlift pump

TEST DATE : 1989

TEST MATERIAL : Marine gravels

APPROX. C_{vd}^{sl} : 8%

PIPE DIAMETER : 90 mm NB

PURPOSE : *In situ* concentration tests

Gas Flow Rate (STP) (l/s)	Gas Flow Rate *in situ* (l/s)	Mixture Flow Rate (l/s)	Delivered Concentration (%)	Gas *in situ* Concentration (%)	Solid *in situ* Concentration (%)
20,475	15,865	2,487	7,0	67,56	2,25
24,355	18,807	2,721	8,0	70,20	1,81
27,957	21,737	2,611	8,3	70,51	2,08
32,597	25,023	3,179	8,0	72,04	1,48
37,362	28,827	2,830	7,8	71,59	1,45
41,127	31,814	2,741	8,0	74,44	1,17
47,727	36,554	3,217	7,3	76,43	1,02

DATA FILE : DB0L0589

TEST FACILITY : Airlift pump

TEST DATE : 1989

TEST MATERIAL : Quartz

APPROX. C_{vd}^{sl} : 4%

PIPE DIAMETER : 50 mm NB

PURPOSE : *In situ* concentration tests

Gas Flow Rate (STP) (l/s)	Gas Flow Rate *in situ* (l/s)	Mixture Flow Rate (l/s)	Delivered Concentration (%)	Gas *in situ* Concentration (%)	Solid *in situ* Concentration (%)
6,656	6,325	0,842	4,16	67,25	0,13
5,692	5,421	0,817	3,87	66,74	-
4,266	4,067	0,732	4,31	66,86	0,12
2,915	2,773	0,702	3,95	61,09	0,08
1,688	1,598	0,632	3,23	53,88	-
0,949	0,892	0,505	2,26	46,45	-
0,592	0,551	0,406	1,24	38,38	-

DATA FILE : DB0S0589

TEST FACILITY : Airlift pump

TEST DATE : 1989

TEST MATERIAL : Quartz

APPROX. C_{vd}^{sl} : 4%

PIPE DIAMETER : 50 mm NB

PURPOSE : *In situ* concentration tests

Gas Flow Rate (STP) (l/s)	Gas Flow Rate *in situ* (l/s)	Mixture Flow Rate (l/s)	Delivered Concentration (%)	Gas *in situ* Concentration (%)	Solid *in situ* Concentration (%)
6,496	6,179	0,755	3,48	67,15	0,29
5,621	5,339	0,757	3,25	66,85	0,29
4,159	3,946	0,760	3,13	63,55	0,21
2,665	2,523	0,717	2,82	59,68	-
1,628	1,536	0,665	2,42	53,29	-
1,049	0,986	0,571	2,10	48,07	-
0,632	0,590	0,474	1,82	41,08	-